Scuola Internazionale Superiore di Studi Avanzati - Trieste

A study of modulation of P2X3 and TRPV1 receptors by the B-type natriuretic peptide and novel synthetic compounds in trigeminal sensory neurons of wild type and migraine-model mice

Department of Neuroscience
SISSA

Thesis submitted for the degree of
"Doctor Philosophiae"

Candidate:
Anna A. Marchenkova

Supervisor:
Prof. Andrea Nistri

SISSA - Via Bonomea 265 - 34136 TRIESTE - ITALY

Table of Contents

Acknowledgements

First of all, I would like to express my sincere gratitude to my supervisor Prof. Andrea Nistri for having given me an opportunity to work in his laboratory, for his kind support, positive attitude and guidance during the years of my PhD. I feel I have improved a lot my skills in experiment planning and interpreting acquired data, presenting results and writing papers.

I would also like to take this opportunity to thank Prof. Olga Balezina and Dr. Aleksandr Gaydukov from Lomonosov Moscow State University, Russia who guided me through my Masters studies and laid a solid foundation for my future research.

I thank all the members (both present and past) of Prof. Nistri's lab for having healthy, friendly and supportive lab environment. Especially, I should mention Dr. Maya Sundukova, who taught me the patch clamp technique, introduced me to the workflow at SISSA and helped me during the first year working in the lab. I am very grateful to Dr. Sandra Vilotti for our fruitful collaboration, for her invaluable contribution to the molecular biology experiments for the current project, which could not be completed without her, for all the insightful ideas and long discussions we have had working together. My thanks also go to Niels Ntamati, who collaborated with us in the beginning of this project, for his valuable contribution to this work.

I would also express my gratitude to my fellow lab members with whom I shared working space during the years of PhD research: Dr. Swathi Hullugundi, for her support and constructive criticism, for helping and advising me about all the experimental procedures; Francesca Eroli, for the friendliness and kind support, and for always willing to assist me in every matter.

I especially like to thank Prof. Elsa Fabbretti, who was always willing to offer her valuable ideas and critical thinking to help advance scientific process. We have had very useful discussions together that always led to new experiments and better understanding of the problem.

I am grateful to all SISSA staff and technicians of Neuroscience Department, SISSA library staff and Student secretariat who have patiently helped and assisted us throughout the period with all imaginable problems.

I would like to thank all my friends who were always very supportive and who made my life during these years so easy, happy and enjoyable. I am extremely thankful to my parents and my whole family for their help and concern, for always being with me and believing in me in spite of the physical distance between us. I cannot fully express my gratitude to my husband Sergey Antopolskiy, who helped me throughout this time in every way possible, including my scientific work, and who has been always there for me no matter what.

Declaration

The work presented in this thesis was carried out at the International School for Advanced Studies (ISAS/SISSA), Trieste, Italy, between November 2011 and October 2015. The data have been published / prepared for publication in the enclosed manuscripts. For the first five listed manuscripts the candidate performed all experimental work and data analysis concerning electrophysiology, contributed to results interpretation, discussion and manuscript preparation.

1. Vilotti S, Marchenkova A, Ntamati N, Nistri A. B-type natriuretic peptide-induced delayed modulation of TRPV1 and P2X3 receptors of mouse trigeminal sensory neurons. PLoS One. 2013 Nov 27;8(11):e81138
2. Marchenkova A, Vilotti S, Fabbretti E, Nistri A. Brain natriuretic peptide constitutively downregulates P2X3 receptors by controlling their phosphorylation state and membrane localization. Mol Pain. 2015 Nov 14;11(1):71
3. Marchenkova A. Inefficient constitutive inhibition of P2X3 receptors by the brain natriuretic peptide system in trigeminal sensory neurons of mouse model of genetic migrain (manuscript in preparation for submission to Molecular Pain)
4. Marchenkova A. Loss of selective inhibition by brain natriuretic peptide over P2X3 receptor mediated excitability of trigeminal ganglion neurons in a mouse model of familial hemiplegic migraine type-1 (manuscript in preparation for submission to Neuroscience)
5. Diego Dal Ben, Anna Marchenkova, Ajiroghene Thomas, Catia Lambertucci, Gabriella Marucci, Andrea Nistri, Rosaria Volpini. Ribose blocked ATP derivatives as new potent antagonists for the purinergic P2X3 receptors (manuscript under revision in Eur J Med Chem)

In the following manuscript the candidate performed part of the experimental work and data analysis concerning electrophysiology, contributed to results interpretation and discussion.

6. Lambertucci C, Sundukova M, Kachare DD, Panmand DS, Dal Ben D, Buccioni M, Marucci G, Marchenkova A, Thomas A, Nistri A, Cristalli G, Volpini R. Evaluation of adenine as scaffold for the development of novel P2X3 receptor antagonists. Eur J Med Chem. 2013 Jul;65:41-50

The current thesis encloses all the above mentioned manuscripts.

List of abbreviations

α,β-meATP	α,β-methylene-adenosine 5'-triphosphate;
ATP	adenosine-5'-triphosphate;
ADP	adenosine-5'-diphosphate;
AMP	adenosine-5'-monophosphate;
ANP	natriuretic peptide type A;
ASICs	acid-sensing ion channels;
BDNF	brain-derived neurotrophic factor;
BK	bradykinin;
BKCa	calcium-activated potassium channel (MaxiK);
BNP	natriuretic peptide type B;
CaMKII	Ca2+/calmodulin kinase II;
cAMP	cyclic adenosine monophosphate;
CACNA1A	calcium channel, voltage-dependent, P/Q type, alpha 1A subunit;
CaV2.1	voltage activated calcium channel 2.1;
CBF	cerebral blood flow;
cGMP	cyclic Guanosine Monophosphate;
CGRP	calcitonin gene related peptide;
CNG	cyclic nucleotide-gated ion channels;
CNP	natriuretic peptide type C;
CNS	central nervous system;
CREB	cAMP response element-binding protein;
CSD	cortical spreading depression;
Csk	C-terminal Src kinase;
DHE	dihydroergotamine;
DRG	dorsal root ganglia;
Epac1	guanine nucleotide exchange factor 1;
FHM-1	Familial Hemiplegic Migraine type 1;
GABA	Gamma-amino butyric acid;
HMGB1	high-mobility group box 1;
5HT	serotonin;
KI	knock-in;
MA	migraine with aura;
MaxiK	calcium-activated potassium channel (BKCa);
MβCD	methyl-β-cyclodextrin;
MO	migraine without aura;
mRNA	messenger ribonucleic acid;
NF-κB	nuclear factor-kappa B;
NPR-A	natriuretic peptide receptor type A;
NPR-B	natriuretic peptide receptor type B;
NPR-C	natriuretic peptide receptor type C;

NGF	nerve growth factor;
NO	nitric oxide;
PACAP	pituitary adenylate cyclase-activating peptide;
Panx1	pannexin 1;
PARs	protease-activated receptors;
PDEs	phosphodiesterases;
P2X	purinergic 2X receptor;
P2Y	purinergic 2Y receptor;
PAG	periaqueductal gray;
PGE2	prostaglandin E2;
PI3K	phosphatidylinositol 3-kinases;
PKA	cAMP-dependent protein kinase A;
PKC	protein kinase C;
PKG	cGMP-dependent protein kinase G;
SCN1A/Nav1.1	Sodium channel voltage-gated type I subunit;
SEM	standard error of the mean;
SP	substance P;
TG	trigeminal ganglia;
TNC	trigeminal nucleus caudalis;
TNFα	tumor necrosis factor alpha;
TRESK	TWIK-related spinal cord potassium channel;
TRP channels	transient receptor potential channels;
TRPA1	transient receptor potential ankyrin Channel 1;
TRPM8	transient receptor potential melastatin 8;
TRPV1	transient receptor potential vanilloid 1;
TRPV4	transient receptor potential vanilloid 4;
WT	wild-type;

Abstract

Background

Trigeminal ganglion (TG) is a key player in processing noxious stimuli. Among many ligand-gated ion channels, trigeminal sensory neurons express on their membranes purinergic P2X3 receptors and capsaicin-sensitive transient receptor potential vanilloid 1 channels (TRPV1). These receptors are thought to be involved in pain transduction and pathophysiology of different pain syndromes, including migraine disorders. P2X3 and TRPV1 channels are continuously regulated by a variety of endogenous modulators, which, upregulating these receptors, can cause sensitization and promote development of pathological pain conditions. Although positive P2X3 and TRPV1 regulators are well studied, not much is known about those which might restrain the activity of these receptors. One candidate for the role of endogenous negative regulator of sensory ganglion activity is the brain natriuretic peptide (BNP). In fact, BNP was recently reported to downregulate inflammatory pain and firing frequency of small neurons in dorsal root ganglia via its receptor NPR-A.

Aims

In order to investigate the role of BNP/NPR-A system in trigeminal ganglion in control conditions and in migraine pathology we used wild-type (WT) mice and transgenic R192Q KI mice of the familial hemiplegic migraine type 1 (FHM1) model. First we characterized BNP and NPR-A expression and functional properties of the BNP/NPR-A pathway in trigeminal ganglions of WT and KI mice. To understand if this pathway can affect the properties of sensory neurons in TG we studied the effects of endogenous and exogenous BNP on P2X3 and TRPV1 receptors responses *in vitro*. Investigating molecular mechanisms underneath P2X3 receptor modulation we carefully examined changes in P2X3 phosphorylation and membrane distribution and considered involvement of particular kinases and phosphatases in this process. Firing activity of the WT and KI trigeminal neurons were also evaluated to find out if the modulatory effects of BNP/NPR-A system on the P2X3 channels are reflected in neuronal excitability.

Additionally, in search for new potent P2X3 antagonists a variety of diaminopurine derivatives as well as several adenosine nucleotide analogues were evaluated on recombinant P2X3 receptors in HEK cells and on native P2X3 receptors of TG sensory neurons.

Results

We found abundant expression of NPR-A in trigeminal ganglion along with low levels of BNP itself; the BNP/NPR-A pathway in both WT and KI neurons proved to be functional. Exogenously applied BNP inhibited TRPV1-mediated responses in WT and KI trigeminal neurons without any changes in the receptor's expression level. On the other hand, P2X3 receptors were not sensitive to additional exogenous BNP, but appeared to be downregulated by the low amount of endogenous BNP already present in WT TG cultures. This negative modulation included P2X3 serine phosphorylation and receptor redistribution to the non-lipid raft membrane compartments. Both mechanisms were dependent on the activity of protein kinase G. Interestingly, in KI mice NPR-A-mediated P2X3 inhibition

could not be seen and receptors remained upregulated, most probably due to the increased activity of P/Q calcium channels and high concentration of calcitonin gene related peptide (CGRP). Considering firing properties of trigeminal neurons, inactivation of BNP/NPR-A system with NPR-A antagonist anantin caused a hyperexcitability phenotype of WT cultures, which was very similar to what is typical for KI neurons. KI cultures remained unaltered, consistent with lack of BNP/NPR-A regulation over P2X3 activity.

Experiments with new diaminopurine compounds and adenosine nucleotide derivatives resulted in molecules which showed antagonistic behavior towards P2X3 receptors with IC_{50} values in low micromolar and nanomolar range, respectively.

Conclusion

The main result of the present study is the identification of BNP/NPR-A pathway as an intrinsic negative modulatory system for P2X3 and TRPV1 receptors activity in sensory neurons of mouse trigeminal ganglion and related neuronal excitability. However, in a mouse FHM1 migraine model BNP/NPR-A lacked the inhibitory effect on P2X3 receptors due to the overall amount of activation these receptors undergo in KI neurons.

Modifications of diaminopurine and adenosine scaffold could serve as a promising strategy in search for new potent antagonists of P2X3 receptors.

Introduction

1. P2X3 receptors

1.1. ATP receptors

Nowadays the notion that ATP is not only a principal energy source and component of nucleic acids inside the cell, but also a signaling molecule and a genuine neurotransmitter is widely accepted [1]. ATP was first reported to be released from sensory nerves by Pamela Holton [2,3] and then this idea was further developed by Geoffrey Burnstock [4]. Later on, ATP was shown to cause neuronal depolarization in rat dorsal horn neurons [5], to activate inward cation currents in mammalian sensory neurons [6] and to act like a mediator during synaptic transmission in the peripheral and central nervous systems [7–9]. ATP is released from a variety of cell types in physiological and pathophysiological conditions in response to mechanical tissue injury, hypoxia, and inflammation [1]. After being released ATP usually undergoes rapid breakdown by the ecto-nucleotidase 5'-triphosphate diphosphohydrolase (NTPDase) enzyme family to ADP, ANP and adenosine [10] (Fig. 1).

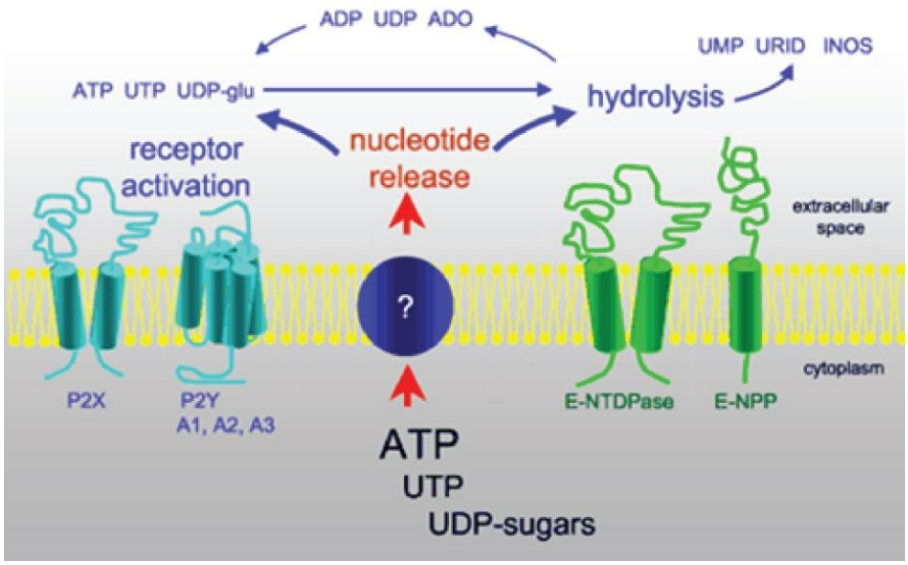

Figure 1. Interplay of released nucleotides, nucleotide metabolism, and activity of P2Y, P2X, and adenosine receptors. Released ATP, UTP, and UDP-glucose activate P2Y2, P2Y4, P2Y11, or P2Y14 receptors and ATP activates all P2X receptors. E-NTPDases generate ADP and UDP, transiently providing agonists for P2Y1 and P2Y6 receptor activation, respectively [10].

Nucleotide action is mediated by a large group of cell surface receptors divided into two main families: metabotropic P2Y receptors that work through coupling with G-proteins, and ionotropic P2X receptors that form an ion permeable pore upon agonist binding. The time scale of purinergic receptor activation and subsequent effects vary from milliseconds to

minutes [11], likewise, receptor ATP sensitivity has a wide range: from nanomolar in the case of P2Y receptors, to hundreds of micromolar for P2X7 receptors [12].

1.2 P2X receptor structure

P2X receptors were cloned in 1994 and showed to possess an unique structure, different from other known ligand-gated channels [13,14]. This was further supported when the crystal structure of zebrafish P2X4 receptor in closed [15] and open [16] states were reported. Even though the transmembrane (TM) topologies of P2X receptors are similar to acid sensing ion channels (ASICs), epithelial sodium channels (ENaCs), and degenerin channels (DEGs), their primary amino acid sequences have little in common [15]. Seven subunits of P2X receptors are encoded in the mammalian genome and form homomeric and heteromeric complexes [17–21]. Each subunit contains two hydrophobic transmembrane segments (TM1 and TM2) separated by a glycosylated and disulfide-rich extracellular domain (Fig. 2; [13,14]). The extracellular domain forms binding sites for ATP, competitive antagonists and modulatory metal ions, whereas the transmembrane domains form a non-selective cation channel, permeable for sodium, potassium and calcium [22]. Systematic analysis by Egan and Khakh showed that P2X channels seem to have relatively high calcium permeability that can be even larger than the one of acetylcholine-, serotonin or glutamate-gated channels [23]. Moreover, P2X receptors can mediate Ca2+ influx at resting or low membrane potential when other Ca2+ sources (like high Ca2+ -permeable NMDA receptors) are not active [24,25]. In some cells, P2X channels are also permeable to anions. Specific properties of various P2X receptors are summarized in Table 1.

P2X receptors are present in virtually all mammalian tissues and mediate a variety of responses such as synaptic transmission, smooth muscle contraction, platelet aggregation, activation of macrophages, cell proliferation and cell death, pain and taste sensation [21,24,26–28].

Table 1: Properties of P2X receptors [29]

	NC-IUPHAR subunit nomenclature						
	P2X1	P2X2	P2X3	P2X4	P2X5	P2X6	P2X7
Molecular properties							
Gene name	P2RX1	P2RX2	P2RX3	P2RX4	P2RX5	P2RX6	P2RX7
Human chromosome location	17p13.3	12q24.33	11q12	12q24.32	17p13.3	22q11.21	12q24
Protein length (amino acids)	399	472	393	389	455	379	595
C tail length (amino acids)	45	119	53	31	96	26	239
Membrane expression	Good	Good	Good	Good	Poor	No expression in most cases	Good
Desensitization (complete in)	Fast (< 1 s)	Slow (> 20 s)	Fast (< 1 s)	Slow (> 20 s)	Slow (> 20 s)	–	Slow (> 20s)
Pore "dilation"	No	Yes	No	Yes	–	–	Yes
P_{Ca}/P_{Na}^{a}	4.8	2.8	1.2	4.2	1.5	–	–
Fractional Ca ^{2b} current (%)	12.4	5.7	2.7	11	4.5	–	4.6
Conductance (pS)	18	19–21	Unresolvable	9	–	–	–
Activation-dependent endocytosis	Yes	No	–	Yes	–	–	–
Physiology and pathophysiology							
Major cellular expression	Smooth muscle	Neurons	Pain sensing neurons	Microglia	Skeletal muscle	Broad expression	Immune cells
Major role	Neuroeffector transmission	Taste, pre- and post-synaptic responses	Bladder reflexes, chronic pain, taste	Vascular remodeling, neuropathic pain	–	–	Bone reabsorption, chronic pain

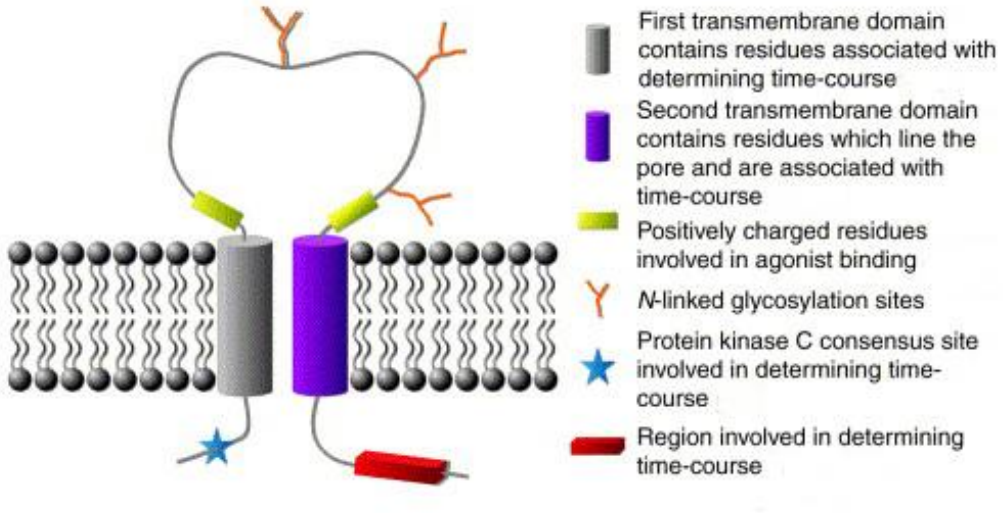

Figure 2. Structure of P2X3 receptors (adapted from [30])

1.3 P2X3 receptors in pain pathways

ATP-activated P2X receptors and in particular P2X3 receptors are widely accepted to play an important role in nociception [24,26,31,32]. Studies on role of P2X receptors in pain started with early observations that ATP evokes pain in humans when applied to blisters [33]. Investigations considering P2X receptor distribution within the tissues and their localisation to pain relevant neuronal structures showed almost unique P2X3 receptor distribution to nociceptive neurons of small and medium somatic size [18,34,34–37], suggesting their particular importance in pain pathways among all P2X receptors (Fig. 3). In particular, P2X3 receptors are predominantly expressed on C- and Aδ-fibers and their cell bodies of primary afferent neurons in most tissues [32,38] and also on their central projections to the spinal cord and brainstem (Fig. 3; [36]).

P2X3 is often coexpressed with capsaicin-sensitive TRPV1 channels and isolectin B4, further supporting the involvement of P2X3 receptors in pain [18,37,39].

P2X3 knockout mice offered further evidence for the role of these receptors in nociception, showing reduced mechanical allodynia [40,41,41].

Considering their fast desensitization and slow recovery, the importance of homomeric P2X3 receptors is most often regarded in relation to chronic rather than acute pain conditions [32].

1.3.1 P2X3 receptors in inflammatory and neuropathic pain

During inflammation high concentrations of extracellular ATP at the site of tissue injury, originated from damaged cells as well as from non-damaged endothelial cells have been measured in humans and animals [42,43]. Selective P2X3 antagonists or prior depletion of P2X3 receptor expression by intrathecal antisense oligonucleotides were shown to reduce chronic neuropathic and inflammatory pain as well as prevent or reduce mechanical hyperalgesia and allodynia in neuropathic pain models [44–48], providing strong evidence for the involvement of P2X3 receptors in the development of inflammatory pain. Further support came from

experiments on P2X3 KO mice [41,49]. Inflammation was proved to enhance P2X3 receptor expression in TG and DRG neurons [50,51]. Neuropeptides such as CGRP along with inflammatory factors released within the inflamed tissue were observed to further sensitise P2X3 receptors leading to hyperalgesia [31,52,53].

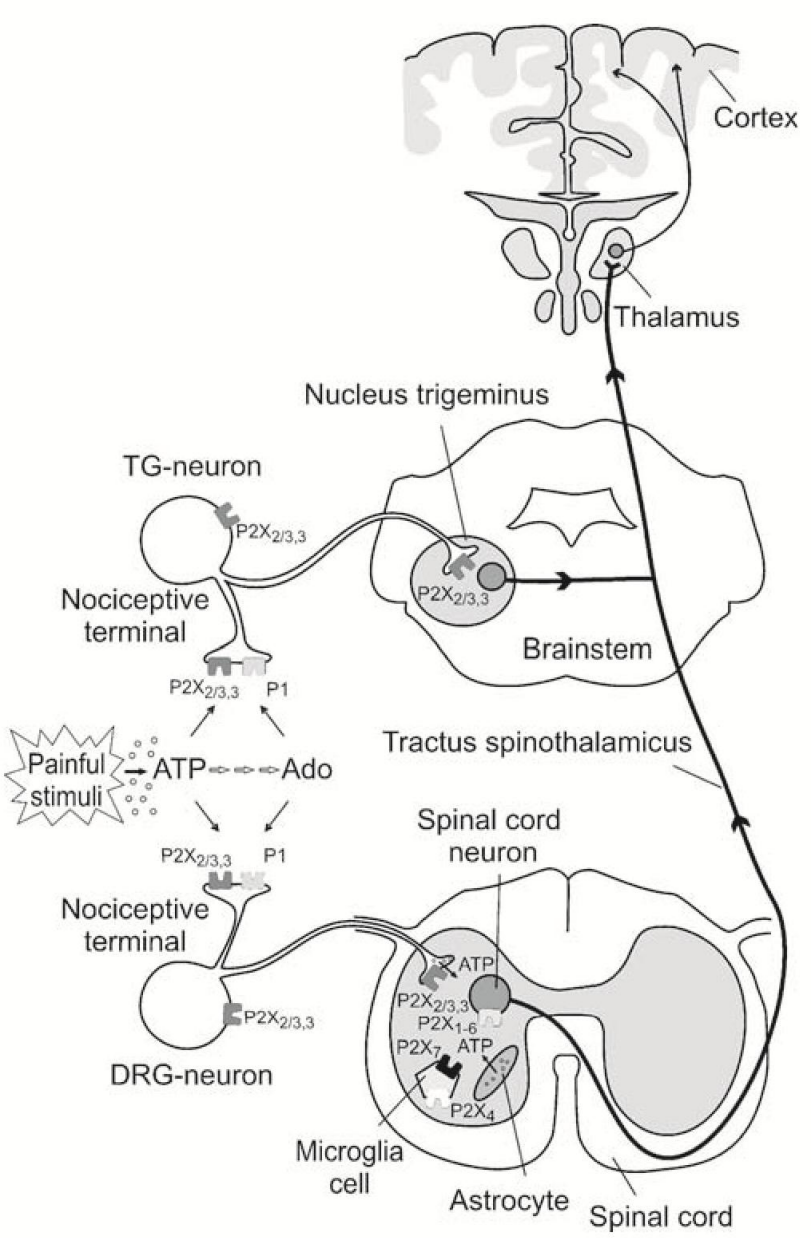

Figure 3. P2X receptors in pain pathways (adapted from [32]). ATP is released by nociceptive stimuli from primary afferent neurons or from damaged neuronal or non-neuronal cells in peripheral tissue and can stimulate P2X2/3,3 receptors localized on nociceptive terminals of sensory ganglia (TG, DRG) neurons. The signal is then projected to the spinal cord and brainstem and through the thalamus to the cortex. Ado – adenosine, DRG – dorsal root ganglion, TG – trigeminal ganglion.

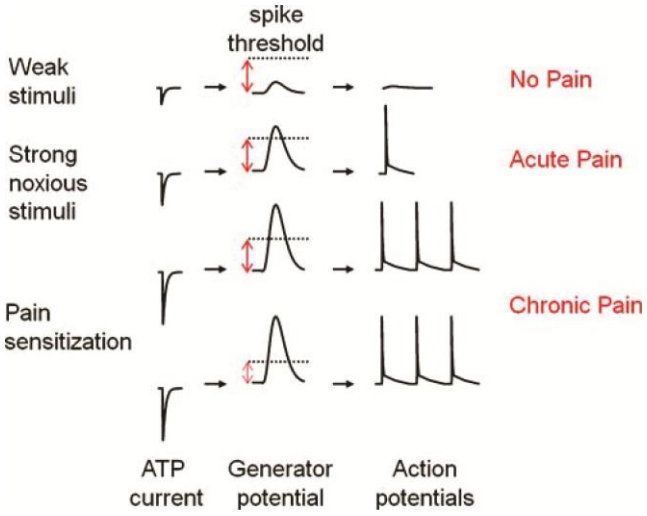

Figure 4. P2X3 in pain sensitization (adapted from [52]) If the noxious stimulus is weak (top row), the ATP membrane current is small and cannot produce a generator potential large enough to reach the threshold for spike firing and pain signal. A strong stimulus (middle row) can, however, evoke an ATP receptor current large enough to induce generator potential that reaches firing threshold and thus elicits pain. When there is pain sensitization (bottom rows) due to pathological processes, the ATP receptor current is proposed to be very large even for modest stimuli: the resulting increase in generator potential may allow repetitive firing and stronger pain signals.

Experimental models include sensitisation of the peripheral or central pain processing to mimic certain aspects of chronic pain conditions [54]. During inflammatory and neuropathic pain nociceptors become sensitized and could be activated even by sub-threshold stimuli (Fig. 4). Recent experiments on chemically-induced colitis in rats show that P2X3 receptors mediate visceral hypersensitivity via different mechanisms of sensitization [55]. Likewise, in a rat model of lumbar disc herniation persistent pain hypersensitivity was associated with increased P2X3 expression and was partially reversed by the P2X3 antagonist A317491 [56]. P2X3 expression and function upregulation in DRG was also shown in relation to chronic pancreatic pain [57] and neuropathic pain in diabetic rats [58].

The particularly high expression of P2X3 receptors by the majority of sensory neurons in TG [59] provides the molecular substrate for P2X3-mediated trigeminal pain including migraine pain [52]. Experimental models of trigeminal and migraine pain showed P2X3 receptor upregulation via different mechanisms, including enhanced membrane expression and trafficking of these receptors, changes in phosphorylation state and receptor membrane distribution [60–62].

1.3.2 P2X3 receptors in migraine pain

Accumulating evidence suggests that P2X3 receptors play an important role in trigeminal and migraine pain [32,63–65]. The high expression of P2X3 receptors by the vast majority of trigeminal sensory neurons [59] provides the molecular substrate for P2X3-mediated trigeminal pain including migraine [52]. Experiments on R192Q CACNA mouse migraine model in vitro

show upregulation of P2X3 currents [64] and P2X3-mediated firing activity of TG neurons [66]. Sensitization of P2X3 receptors during migraine headache could be caused by neuropeptides and inflammatory mediators released in TG after activation of trigeminal afferents [31,52,53]. A well-known migraine mediator CGRP [67–69], increases P2X3 receptor membrane level in vitro by enhancing receptor transcription and trafficking from intracellular compartments and facilitates P2X3 receptor recovery from desensitisation [52,60], contributing to the elevated P2X3 receptor function. Furthermore, most neurons coexpress P2X3 and CGRP receptors in TG [50], a phenomenon that can facilitate P2X3 modulation by CGRP.

A clinical study found higher levels of nerve growth factor (NGF) in the cerebrospinal fluid of patients with chronic headache, supporting its involvement in chronic head pain [70]. NGF was shown to enhance P2X3 activity in trigeminal neurons [59] and neutralization of endogenous NGF downregulated P2X3 currents and their recovery from desensitization via a PKC-dependent pathway [71].

Data obtained with well-established anti-migraine drugs further support the role of P2X3 receptors in migraine pain. Thus, naproxen, a popular anti-headache analgesic, directly inhibits P2X3 receptors by facilitating receptor desensitization, an effect enhanced in the presence of the algogen nerve growth factor [72], the level of which is elevated in patients with chronic migraine [73]. Another study found that dihydroergotamine (DHE), an ergot alkaloid derivative used extensively in the acute migraine treatment, supresses ATP-mediated sensitization of trigeminal neurons via downregulation of P2X3 receptors [74].

1.4 Modulation of P2X3 receptors

A summary of known modulators of P2X3 receptors is in Tables 2, 3; some of them will be discussed further in more details.

Table 2. Pain Mediators Upregulating P2X3 Receptors (adapted from [31]).

Pain Mediator	Effect	References
NGF	Potentiation *via* PKC phosphorylation	D'Arco *et al*. 2007
CGRP	Potentiation *via* enhanced trafficking and gene expression	Fabbretti *et al*. 2006 Simonetti *et al*. 2008
PGE2	Potentiation *via* Epac, PKA, PKC	Wang *et al*. 2007
Bradykinin	Neuro-glia crosstalk facilitation	Ceruti *et al*. 2011
BDNF	Enhanced gene expression	Simonetti *et al*. 2008
GABA acting on $GABA_A$, $GABA_B$ receptors	Occlusion	Sokolova *et al*. 2001 Toulmé *et al*. 2007 Sokolova *et al*. 2003

Table 3. Cell Signaling Effectors on P2X3 Receptors (adapted from [31]).

Modulator	Effect	References
PKC	Potentiation	Paukert *et al*. 2001 D'Arco *et al*. 2007
Tubulin	Trafficking	Chaumont *et al*. 2004
Csk	Inhibition	D'Arco *et al*. 2009
CaMKII	Trafficking; Potentiation	Nair *et al*. 2010 Xu *et al*. 2004
Cdk5	Potentiation	Nair *et al*. 2010
Early endosome Lamp1 Rab5 Rab7	Trafficking	Chen *et al*. 2012 Vacca *et al*. 2009 Ceruti *et al*. 2011
Calcineurin	Potentiation	Nair *et al*. 2010
TNFα	Potentiation	Oliveira *et al*. 2010
PKA Epac	Potentiation	Wang *et al*. 2007
Ubiquitin	Trafficking	Vacca *et al*. 2009
Lipid rafts	Trafficking	Vacca *et al*. 2009 Gnanasekeran *et al*. 2011
CREB, C/EBPβ, Ret	Upregulation; potentiation	Simonetti *et al*. 2008 Ugarte *et al*. 2012 Franck *et al*. 2011

1.4.1 P2X3 Synthesis

Changing the amount of receptor protein can be one of the mechanisms to modulate its activity. De novo expression of P2X3 receptors in distinct neuronal subpopulations can underlie persistent enhancement of ATP mediated activity in sensory neurons during chronic and neuropathic pain conditions [56,57,75]. CGRP promotes P2X3 receptor expression via a BDNF-dependent mechanism, CaMKII activation and phosphorylation of CREB transcription factor [76] (Fig. 5). Recent evidence indicates that Runx1 and C/EBPβ transcription factors also can directly up-regulate P2X3 gene transcription in DRG [77], while Ret is a critical regulator of several pain-related ion channels and receptors, including P2X3 receptors [78]. Recent evidence suggests that P2X3 expression can be positively regulated by p2x3r gene promoter DNA demethylation and enhanced interaction with p65, an active form of nuclear factor-kappa B (NF-κB), contributing to cancer and neuropathic pain in rats [58,79]. Another study shows enhanced P2X3 receptor synthesis in chronic neuropathic pain injury probably via intermedin-dependent phosphorylation of p38 and ERK1/2 [80].

1.4.2 P2X3 trafficking

With the development of imaging and biochemical experimental methods to track ion channels, it had become clear that membrane receptors undergo constant surface diffusion and trafficking. A conserved site responsible for P2X receptor surface expression and receptor trafficking has been identified in the cytoplasmic C-terminus, that for P2X3 subunits comprises residues 353-357, YKAKK [81]. Enhancing surface abundance of pain-facilitating receptors, including P2X3 receptors, even without changes in their total expression level, in nociceptors and dorsal horn neurons is an important mechanism underpinning chronic pain states (Ma 2014). Inflammation, tissue damage or pain mediators facilitate P2X3 cell surface trafficking in primary sensory neurons to amplify pain intensity and duration [82]. Conversely, in other brain regions the same pathological conditions could lead to decreased P2X3 delivery to the membrane. Thus, in the model of neuropathic pain in diabetic rats decreased P2X3 membrane expression in PAG led to mechanical allodynia, most likely by impairing the descending inhibitory system in modulating pain transmission [83].

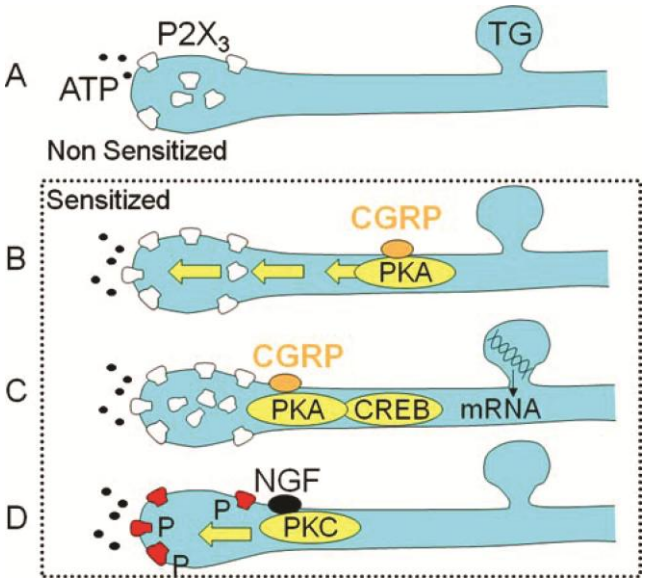

Figure 5. Molecular mechanisms regulating P2X3 receptors of trigeminal neurons (TG) in basal conditions (nonsensitized, A) and in a migraine pain model (sensitized, B–D), when pain mediators such as CGRP (B, C) or NGF (D) are released (adapted from [52]). A, ATP-gated P2X3 receptors are expressed intracellularly and on the neuronal membrane of trigeminal neurons at rest. B, CGRP stimulates trafficking of P2X3 receptors from intracellular stores to the cell membrane via PKA- and PKC-dependent mechanisms. C, CGRP triggers new P2X3 gene expression to support long-lasting upregulation of P2X3 receptor function. D, NGF induces rapid and reversible upregulation of P2X3 receptor function through their PKC-dependent phosphorylation.

The molecular mechanisms to speed up P2X3 membrane delivery can vary for different cell types. Thus, in DRG it relies on CaMKII, whereas in TG increased membrane expression of P2X3 is related to PKC and PKA activity that in turn is modulated by CGRP [52,84,85] (Fig. 5).

The level of functional receptors expressed on the cell surface is temperature- and agonist-dependent [31]. Agonist stimulation rapidly increases the number of P2X3 on the membrane as well as augments receptor endocytosis accompanied by preferential targeting of the receptors to late endosomes/lysosomes, with subsequent degradation [86]. Likewise, the protein kinase CASK stabilizes P2X3 receptors on the membrane and decreases their internalization and degradation [87]. Experiments show that retrograde trafficking of P2X3 receptors along DRG neuronal processes relies on the activity of the GTPase family proteins, Rab5 and Rab7 [88]. A recent study describes the mechanism of ATP-induced membrane delivery of the P2X3 receptors in DRG as a CaMKIIα and caveolin-1-dependent process. CaMKIIα binds to the P2X3 N-terminus and phosphorylates Thr388 on C terminus responsible for P2X3 interaction with caveolin-1 (Fig. 6; [89]).

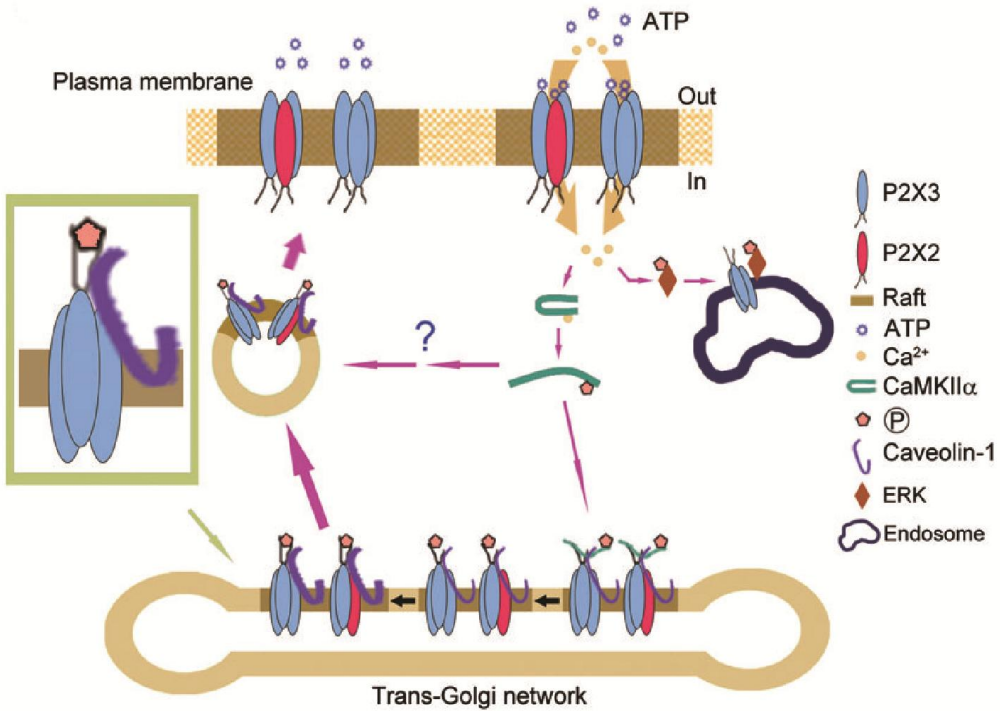

Figure 6. A schematic diagram showing the ATP-induced membrane delivery of the P2X3 and P2X2/3 receptors (adapted from [89]). Extracellular ATP binds to and activates the P2X3 receptors present on the cell membrane in the soma and the nerve terminal of DRG neurons. Ca2+ influx via the P2X3 receptor not only phosphorylates ERK to form a 'signaling endosome' but also activates CaMKIIα, which binds to the N terminus of the P2X3 receptor and phosphorylates Thr388 in the C terminus. Thr388 phosphorylation of the P2X3 receptor enhances its binding to caveolin-1, leading to the promotion of forward trafficking and membrane insertion of the P2X3 receptor. CaMKIIα is dispensable in forward transport of the P2X3 receptor after Thr388 phosphorylation. Furthermore, this regulated trafficking of the P2X3 receptor also drives the membrane delivery of the assembled P2X2 receptor and enhances the P2X3 receptor-mediated response.

1.4.3 Lipid rafts in control of P2X3 function

Growing evidence indicates that ligand-gated receptor clustering and localization to particular membrane regions is one of the key factors to regulate their function [90–92]. P2X3 receptors were shown to be unevenly distributed within the membrane, showing their association with so called lipid rafts – membrane microdomains rich in cholesterol and sphingolipids [93–95]. Preferential localization of P2X3 receptors to lipid rafts in sensory neurons of migraine-model mice is associated with a large gain of function that is promptly lost following disruption of membrane cholesterol [94]. Lipid rafts were also shown to regulate P2X3 receptor trafficking and agonist-binding dependent endocytosis [86].

Lipid rafts can affect P2X3 receptors in a number of different ways, from direct lipid-protein interaction to indirect mechanisms. Thus, phosphoinositides can regulate P2X3 activity by interacting with their C-terminal domain [96]. On the other hand, lipid rafts can create a specific membrane microenvironment and facilitate P2X3 modulation by the protein kinase CASK, known to upregulate P2X3 receptors and usually found in a complex with P2X3 receptors in trigeminal sensory neurons [87,97].

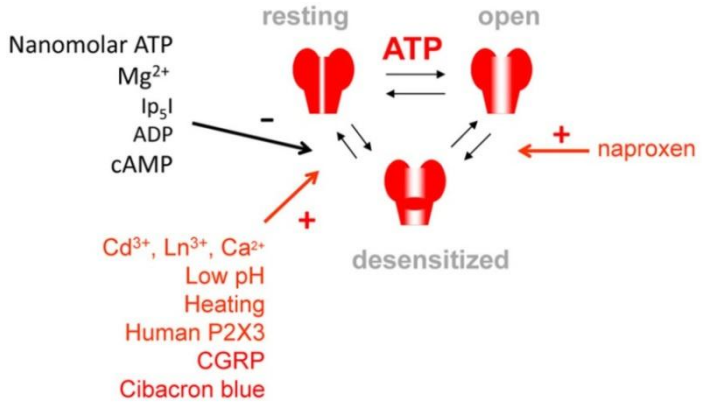

Figure 7. A simplified kinetic scheme for P2X3 receptor operation indicating resting, open and desensitized receptor states (adapted from [63]). Note multiple factors accelerating (+, red arrow) or retarding (-, black arrow) recovery from desensitization, while naproxen promotes desensitization onset. Factors accelerating recovery are expected to facilitate ATP signaling via P2X3 receptor activity, whereas factors retarding recovery (or promoting desensitization onset) could provide the anti-nociceptive effect.

1.4.4 Desensitization

Desensitization is a general phenomenon which can be observed in most membrane receptor types and implies a loss of receptor responsiveness which develops with the continuous presence of the agonist. P2X3 receptors are characterized by very fast (ms range) desensitization onset and slow (min range) recovery from desensitization [21,98]. Desensitization is an important process to limit P2X3 receptor-mediated responses [63]. Desensitization onset of P2X3 receptors is accelerated by increased agonist concentration [99] and remarkably insensitive to the temperature changes [100]. Low pH slows down

desensitization development [101] that might contribute to the development of migraine pain, during which acidic conditions could potentially originate [102,103]. Likewise, experiments with *Xenopus* oocytes showed a decrease in heteromeric P2X2/3 receptor channel desensitization after treatment with inflammatory mediators substance P and bradykinin [104]. Conversely, the analgesic naproxen speeds up the desensitization onset of recombinant P2X3 receptors expressed in HEK cells [72] (Fig. 7).

Recovery from desensitization of P2X3 receptors is an agonist-specific process [99]. Unlike desensitization onset, recovery from desensitization is highly temperature dependent [100] and facilitated by cibacron blue [105], extracellular Ca2+ [106], low pH, or CGRP [60]. The independent modulation of desensitization onset and recovery suggests that they are likely to have different determinants [63].

1.4.5 P2X3 phosphorylation/dephosphorylation

A number of kinases are involved directly or indirectly in P2X3 modulation [31] (Fig. 8). A highly conserved T-X-K motif (residues 12-14 TTK in P2X3) for PKC-mediated phosphorylation is present in the intracellular N-terminus of P2X3 receptors [107], and is likely to mediate NGF-dependent potentiation [71]. It has been shown that substance P and bradykinin as well as PKC activators augment P2X3 receptor currents via PKC-dependent phosphorylation of the receptor N-terminal domain, although some reports argue that PKC-mediated upregulation does not require direct P2X3 receptor phosphorylation [108,109].

D'Arco et al. [110] demonstrated that P2X3 receptor function is constitutively inhibited by phosphorylation of its C-terminal tyrosine-393 by the C-terminal Src inhibitory kinase (Csk). Cyclin-dependent kinase 5 (Cdk5) involved in pain signaling [111] was shown to downregulate P2X3 receptors by increasing their serine phosphorylation [62], whereas the phosphatase calcineurin and activated CaMKII opposed this action [64]. Moreover, a specific phosphorylation site on P2X3 receptor C terminus was identified for CaMKIIα, namely the Thr388, which is crucial for ATP-induced receptor delivery to the membrane (Fig. 6; [89]).

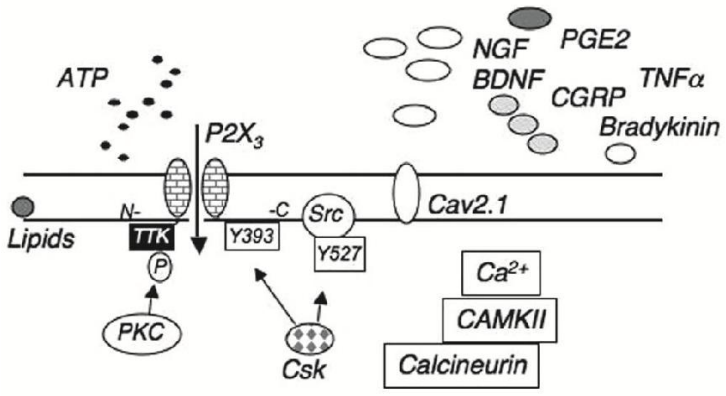

Figure 8. Schematic representation of cell signaling effectors and intracellular modulators known to act on P2X3 receptors (adapted from [31]).

Another important P2X3 modulator is the inflammatory mediator, PGE2, that largely increases ATP currents by stimulating PKA and PKCε dependent P2X3 phosphorylation [112]. A critical role in this process is played by the cAMP-responsive guanine nucleotide exchange factor 1 (Epac1), since it biases the intracellular kinase activity toward PKCε to phosphorylate P2X3 receptors [112].

1.5 P2X3 receptor antagonists

In the last decades P2X3 and P2X2/3 ion channels have received strong interest by research groups and pharmaceutical companies for development of new therapeutic strategies to treat P2X3-related pathologies [45,113,114]. Synapses formed by involvement of P2X3 subunits in the spinal cord or in the brainstem are suggested to play a role in enhancing the release of glutamate at this first sensory synapse, and therefore provide an ideal subject to amplify neuronal responses by sensitization. Expression of P2X3 subunit-containing receptors is very limited and is mostly restricted to small and medium nociceptive sensory neurons in the dorsal root, trigeminal and nodose ganglia [32]. Considering that, P2X3 subunit antagonists may offer a lower likelihood of adverse effects if used therapeutically. Data from studies on P2X3 knock-out mice are also useful for identifying potential side effects of a future P2X3 antagonising drug, most probable being hypogeusia and urinary hyporeflexia [49,115].

According to the review of patent literature a considerable number of the of potential therapeutic uses could be proposed for compounds with P2X3 antagonist properties [113]. Most important therapeutic fields for the P2X3 antagonists include genitourinary diseases such as urinary incontinence, overactive bladder/dysuria and benign prostate hyperplasia. Furthermore, P2X3 antagonists could be potentially used for treating respiratory disorders such as asthma, bronchospasm and chronic obstructive pulmonary disease. Other relevant areas disease targets may include sleep disorders and epilepsies as well as various acute and chronic pain conditions such as neuropathic and inflammatory pain disorders, tissue injury pain, headache and migraine.

Differently from agonists, most of which are derivatives of the natural P2X agonist ATP, P2X receptor antagonists belong to different chemical classes [114]. Until recently, only nonselective P2X antagonists, such as PPADS (4-[(*E*)-diazenyl]benzene-1,3-disulfonic acid) suramin, were available as tools for pharmacological animal studies and *in vivo* pain models (Fig. 9). However, they show weak P2X3 antagonist activity with IC_{50} values in the micromolar range (with the exception of NF110, which displays nanomolar activity at rat receptors) and not favourable pharmacokinetic properties due to the presence of several charged groups [114]. Modification of the natural ligand ATP led to the discovery of competitive P2X receptor antagonist TNP-ATP (Fig. 9; [47]), which, although not selective, showed high potency at P2X1, P2X3 (IC_{50} of 0.006 μM and 0.001 μM, respectively), and heteromeric P2X2/3 receptors.

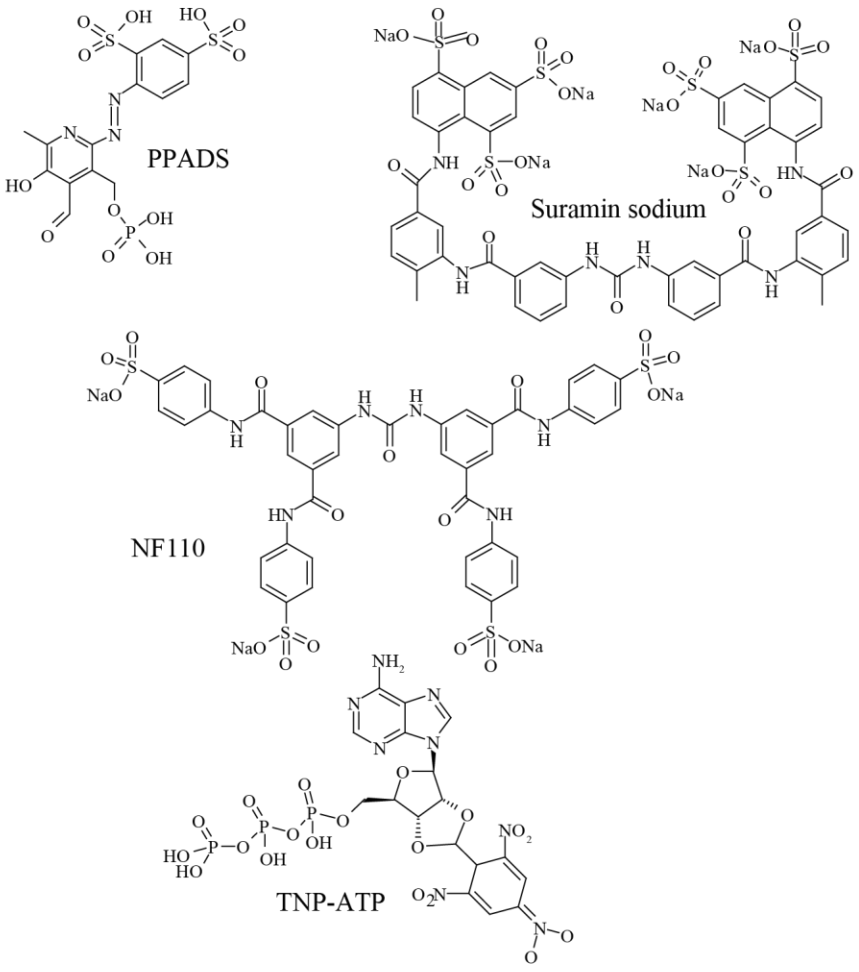

Figure 9. P2X antagonists: PPADS, suramin, NF110, TNP-ATP (adapted from [113]).

Several pharmacological companies proposed and patented a variety of molecules with P2X3 antagonist properties, with the three main compound families dominating the patent literature (Fig. 10; [113]). More than 50 patent applications have been published in the field of small-molecule P2X3 and P2X2/3 receptor antagonists, with most active companies being Roche, Merk, Evotec, Shionogi and AstraZeneca [113]. Compound A-317491 (Fig. 11) designed by Abbot was the earliest non-nucleotide small molecule with nanomolar affinity for blocking P2X3 and/or P2X2/3 receptors [46]. However, because of the poor bioavailability and the competitive mechanism of action [46,47,116], A-317491 could not serve as a lead compound or a starting point for any chemical program.

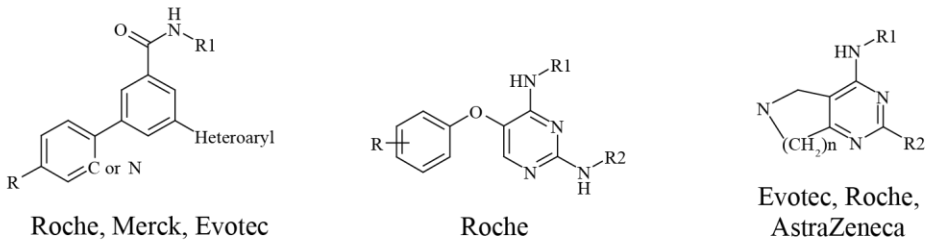

Figure 10. P2X3 antagonist compound families used by different pharmacological companies (adapted from [113]).

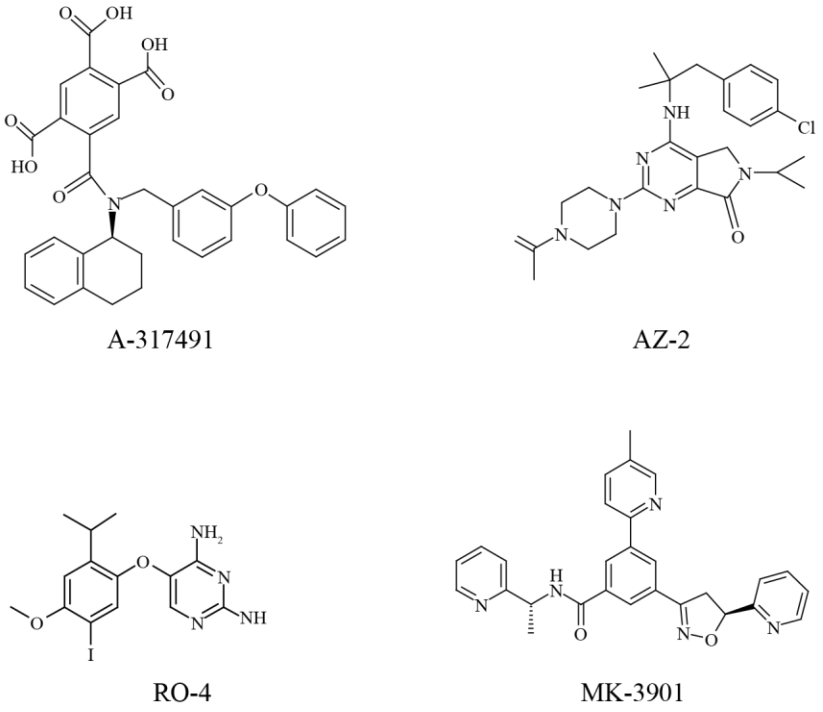

Figure 11. P2X3 antagonist developed by Abbot (A-317491), AstraZeneca (AZ-2), Roche (RO-4) and Merck (MK-3901) (adapted from [113]).

The common structural features of several promising compounds produced by Roche, Merck and Evotec are three aryl and/or hetaryl moieties and a carboxamide function in meta arrangement on the central ring of the molecule (Fig. 10). Most of these compounds show high P2X3 antagonist activity (IC_{50} values in the nanomolar range) and drug-like properties [113]. The compound showing the highest level of selectivity (approximately 570-fold) for P2X3 over P2X2/3 is AZ-2 (Fig. 11) produced by AstraZeneca (P2X3 IC_{50} = 15 nM; P2X2/3 IC_{50} = 8579 nM). AZ-2 was proved to act only peripherally and demonstrated analgesic effect in a rat Freund's complete adjuvant-induced inflammatory pain model [117]. Roche has been the most active in the field of P2X3 antagonists. In the early research in this field their favorite scaffold was the diaminopyrimidine ring, various modifications of which

(like RO-3, RO-4, RO-51) were reported as promising P2X3 inhibitors [118,119]. A dual P2X3 and P2X2/3 allosteric antagonist RO-4 (Fig. 11) is known as AF-353 and has recently been shown to have a favorable pharmacokinetic profile with reasonable oral bioavailability and high brain penetrability [118]. Substitution of the diaminopyridine scaffold with diaminopurine led to molecules which maintained the antagonistic bchavior [120]. Another group of P2X3 antagonists from Roche consists of carboxamide derivatives. The company's first carboxamide derivative, RO-85 [121] has a modest P2X3 IC_{50} value (398 nM), but this was the first compound reported to be selective over P2X2/3 receptors. One of the most promising compounds produced by Merk is MK-3901 (Fig. 11), which, however, does not fulfill the requirements of drug-likeness, containing too many aromatic and heteroaromatic rings [113].
Apart from synthetic molecules, several natural compounds have been reported to exhibit antagonist properties for P2X3 receptors. Recently, scientists from Nanchang University published that the known isoflavone, puerarin (Fig. 12) was useful for treating P2X3 receptor-mediated acute pain and other nervous system diseases [113]. Additionally, compounds emodin and resveratrol (Fig. 12) were claimed to have P2X3 inhibitory properties and have been proposed for the treatment of neuropathic and chronic pain [113].

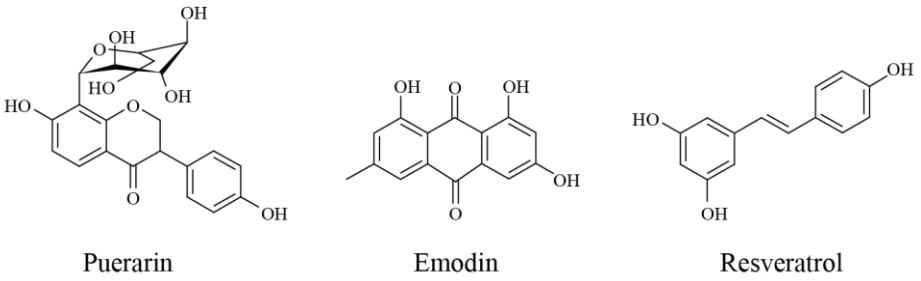

Figure 12. Natural products with P2X3 antagonist activity (adapted from [113]).

So far, the most advanced reported P2X3 antagonist is R-1646 known as AF-219 (structure undisclosed), developed by Afferent Pharmaceuticals (licensed from Roche in 2009). AF-219 is the only compound that has been in clinical development (Phase II) for the treatment of chronic cough, osteoarthritis of the knee and bladder pain syndrome [113]. In fact, further Phase II studies are currently ongoing in order to prove the applicability of P2X3 antagonists for treatment other pathologies like knee osteoarthritis and interstitial cystitis/bladder pain [113]. The results of these clinical studies will clarify the therapeutic potential of P2X3 antagonists. Supposing that the outcome of these trials is positive, terapeutic applications of AF-219 and P2X3 antagonists in general may be further extended. Considerable amount of data on various available P2X3 antagonists together with the recently published crystal structure of sebrafish P2X4 receptor [15,16] and, hopefully, future availability of the P2X3 structure itself, will help to develop new potent and selective molecules with P2X3 antagonist activity.

2. Transient receptor potential vanilloid 1 (TRPV1)

2.1 TRP receptors superfamily

The mammalian TRP channel superfamily consists of 28 members subdivided into 6 subfamilies according to their primary amino acid sequence homology [122]: TRPC (canonical, 7 members), TRPV (vanilloid, 6 members), TRPM (melastatin, 8 members), TRPA (ankyrin, 1 member), TRPP (polycystin, 3 members) and TRPML (mucolipin, 3 members). TRP receptors share a common structure, which consists of six transmembrane domains (S1–6), S5 and S6, and intracellularly located NH2 and COOH termini which regulate channel assembly and channel function [123]. The number of ankyrin repeats, coiled-coil regions, a TRP signature motif and other domains differentiate TRP subfamilies. Complete TRP channels are composed of four pore-forming subunits that may assemble as homo- or hetero-tetramers [123]. Upon activation, TRP channels form a cation permeable pore, mediating an inward cationic current, that produces membrane depolarization and the opening of voltage gated ion channels and hence in a large series of intracellular events that eventually lead to specific cell responses [122,123]. Each individual TRP channel can be activated by a large series of disparate exogenous and endogenous stimuli of both physical and chemical nature.

TRP channels are expressed in almost every tissue and cell type and play an important role in the regulation of various cell functions. Currently, significant effort is devoted to understanding the physiology of TRP channels and their relationship to human diseases [122].

2.2 TRPV1 activation and structure

The transient receptor potential vanilloid 1 (TRPV1) channel was first identified by its responsiveness to capsaicin, a vanilloid derived from chili peppers that elicits a hot burning sensation [124]. Apart from capsaicin, TRPV1 is directly activated by high temperatures (>42°C) [125] and potentiated by low pH conditions that originate during inflammation and injury [126]. Therefore, TRPV1 can act as a polymodal nociceptor integrating multiple forms of noxious stimuli [127].

TRPV1 is expressed by approximately 30-50% of small- and medium-sized sensory neurons in TG and DRG [39,128], predominantly peptidergic C-fiber nociceptors [129]. As all TRP receptors, TRPV1 is a nonselective cation channel with six transmembrane domains, a pore loop region between the S5 and S6 segments, and six ankyrin repeats at the N terminal (Fig. 13) [130,131]. Recent single-particle cryo-EM structural analyses revealed the TRPV1 architecture as a tetramer with a radial symmetry around the central ion pore [132] (fig. 14).

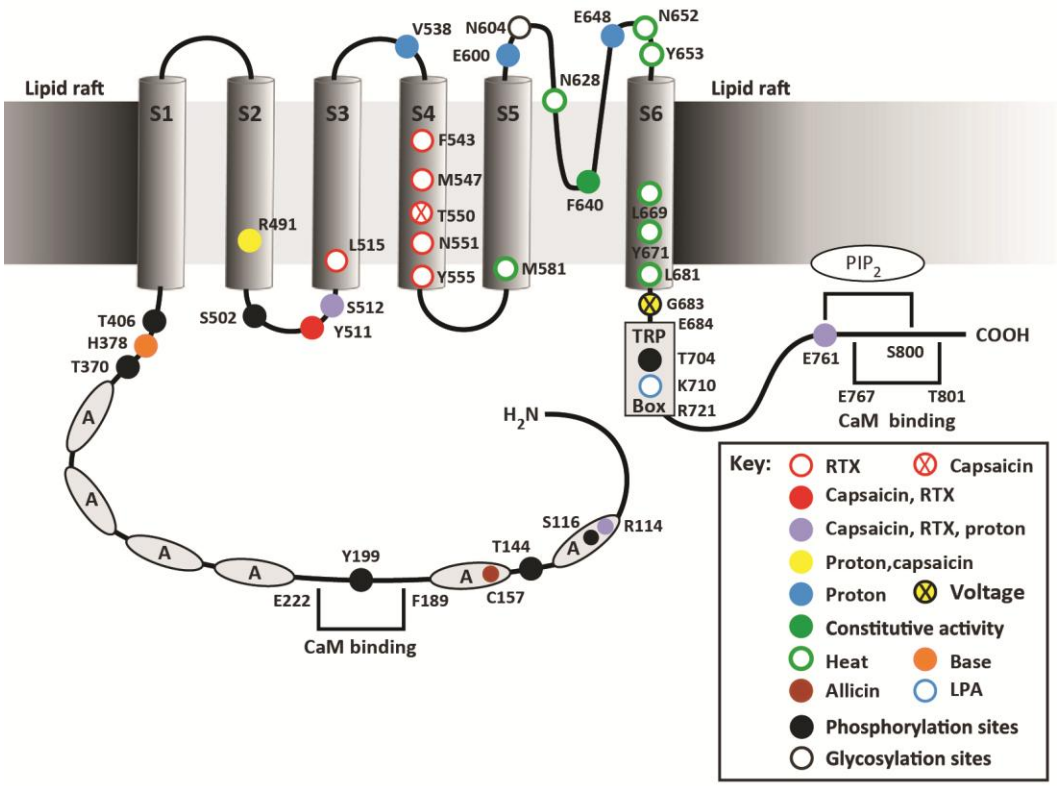

Figure 13. Schematic structure of TRPV1 channel illustrating residues that are involved in channel activation and regulation (adapted from [131]). TRP – transient receptor potential domain conserved for TRP channels required for PIP2 activation; PIP2 – phosphatidylinositol 4,5-bisphosphate; black circles – phosphorylation sites involved in sensitizing actions of PKC and PKA.

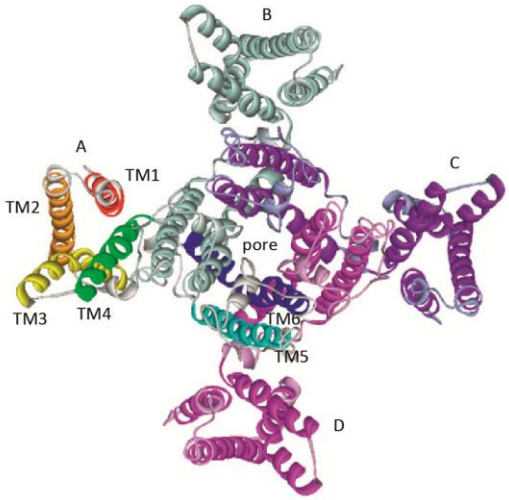

Figure 14. Tetrameric architecture of the rat transient receptor potential vanilloid type 1 (rTRPV1) homology model viewed from the extracellular side (adapted from [131]). The four monomers (A, B, C, D) are arranged so that their loop between transmembrane (TM) domains TM5 and TM6 form a central position.

Vanilloid agonists pass through the plasma membrane to act from at an intracellular side of TRPV1 binding to a hydrophobic pocket composed of the transmembrane domains S3 and S4 [131,133]. TRPV1 proton sensitivity relies on the residues in the pore helix and in the S3-S4 region [134] as well as on the residue E648 between the selectivity filter and S6, whereas E600 mediates the ability of protons to potentiate the activity of other TRPV1 agonists [126]. TRPV1 is intrinsically temperature sensitive and C-terminal region, pore forming region and N-terminal region are implicated in this process, and recently it has been found that PKCβII is also required for TRPV1 thermal sensitivity [135–139].

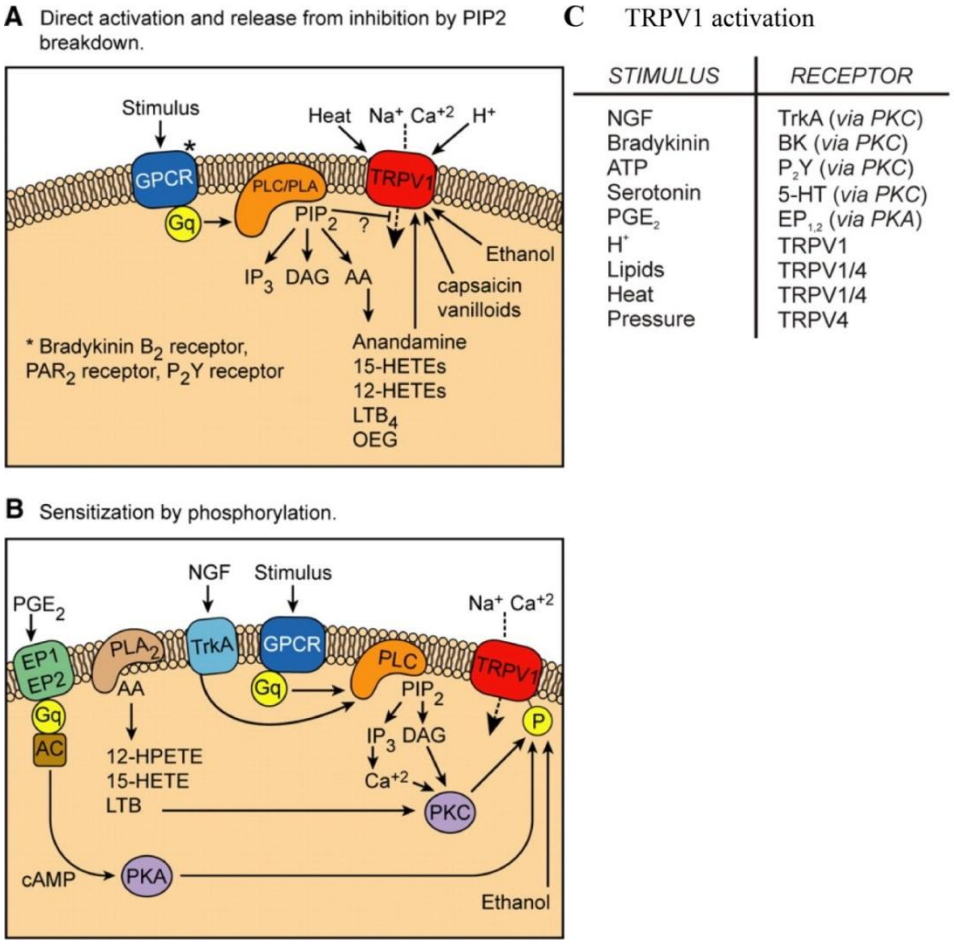

Figure 15. TRPV activation by neuropeptides and inflammatory mediators (adapted from [122]).

Owing to the smaller number of charged amino acids in the voltage sensor domain, TRPV1 was shown to be weakly voltage-dependent [124,131]. Nevertheless, capsaicin and high temperatures shift this voltage dependence toward physiological relevant potentials, indicating that TRPV1 could operate as a voltage-gated cation channel [140].

2.3 TRPV1 modulation

TRPV1 activity is modulated via various second messenger signaling pathways by a range of proalgesic and proinflammatory agents including NGF, bradykinin, lipids, prostaglandins and ATP (Fig. 15) [127,129]. Activation of GPCRs by bradykinin or prostaglandins initiates intracellular pathways for phosphorylation-induced sensitization/activation of TRPV1 channel, thus forming an indirect activation [131]. Similar indirect positive modulation is under the effect of NGF [60,141–143]. PI3K promotes trafficking of TRPV1 to the plasma membrane [144]. Endogenous lipid ligands such as endocannabinoids, lipoxygenase metabolites, or LPA are also released intracellularly, inducing a direct activation of TRPV1.

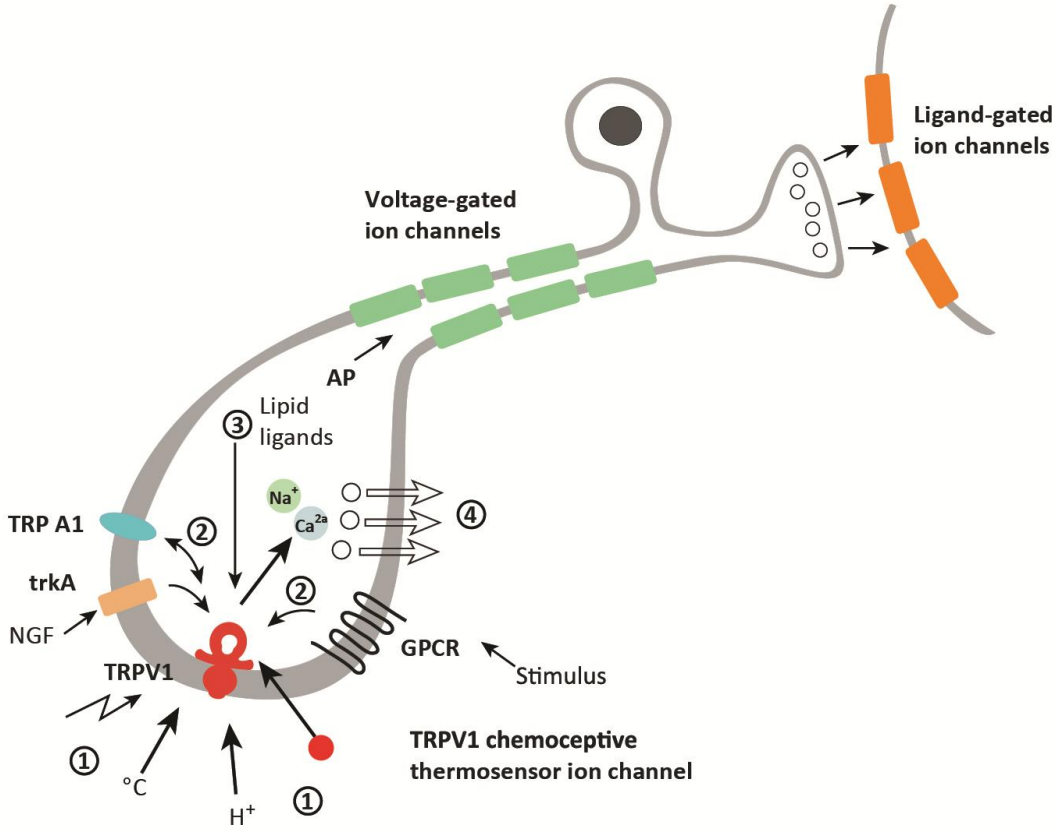

Figure 16. Complex operational features of the TRPV1 channel on the nociceptive nerve ending of the primary afferent neuron (adapted from [131]). 1, Exogenous (e.g., capsaicin) or endogenous (lipoxygenase products, H+) chemical agents as well as physical interventions (noxious heat, depolarizing voltage) trigger channel opening. 2, PKA, PKC, phospholipase C pathways induce TRPV1 sensitization; dephosphorylation of the channel induces desensitization. 3, Intracellularly released lipophilic ligands (e.g., anandamide, lysophosphatidic acid or lipoxygenase metabolites) could act directly on TRPV1. 4, Influx of Ca2+ through the activated channel induces release of sensory neuropeptides from the nerve endings. AP: axonal action potentials, mediated by voltage-gated channels (green) transmit information to the spinal dorsal horn or brainstem where synaptic ligand-gated channels (orange) are activated by the released neurotransmitter.

Activation of other GPCR receptors, mediated by opioids, cannabinoids, and somatostatin, lead not to activation, but to inhibition of TRPV1 signals [131]. One way to modulate functioning of TRPV1 receptor is to target its phosphorylation state (Fig. 15). Regulation of TRPV1 by phosphorylation has been shown to contribute to its ability to respond to noxious stimuli, whereas dephosphorylation led to receptor desensitization following activation [124]. Figure 16 summarizes multiple functions of the TRPV1 chemoceptive thermosensor ion channel.

2.4 TRPV1 in pain conditions

Preferential expression of TRPV1 on peripheral nociceptors [39,128], its ability to sense noxious stimuli and become potentiated by various neuropeptides and inflammatory agents involved in pain conditions, have made TRPV1 one of the major targets for pain-related research [124,131,145,146]. Currently, a pivotal role of TRPV1 receptors in nociception and development of various pathological pain states is well recognized [124,131].

TRPV1 channels have become a promising target for high throughput screening (HTS) for analgesics that either block the function of the receptor or utilize the lasting loss of function of nociceptors which ensues after application of high doses of capsaicin. However, side effects such as hyperthermia and impaired noxious heat sensation (burn risk) were the main obstacles discovered in preclinical studies and clinical trials of TRPV1 antagonists. [131].

2.4.1 Inflammatory pain

There is growing evidence showing a strong link between TRPV1 receptors and inflammatory pain [124]. TRPV1 knockout mice exhibit reduced nociceptive behavior in various models of inflammation. Likewise, antagonists of TRPV1 receptors were shown to act as analgesics in inflammation models [147,148]. Human studies reported an increase in TRPV1 immunoreactive fibers in inflamed skin that correlates with inflammatory hyperalgesia [149]. Furthermore, TRPV1 receptors are associated with the pain from inflammatory diseases of the gastrointestinal tract [150–153].

2.4.2 Neuropathic pain

TRPV1 expression increases following nerve injury, whereas TRPV1 antagonists reduce thermal and mechanical hypersensitivity [154,155]. Additionally, desensitization of TRPV1 receptors with capsaicin or resiniferatoxin has been shown to relieve osteoarthritic pain, and nerve injury-induced heat sensitivity, further supporting the idea of the importance of TRPV1 in the development of neuropathic and inflammatory pain states [156–159].

2.4.3 TRPV1 in migraine

Numerous studies focussed on the role of TRPV1 in the generation and pathophysiology of migraine [65]. A two-stage genetic association study found that single nucleotide polymorphisms in the TRPV1 gene contribute to the genetic susceptibility to migraine in a Spanish population, but how these channel mutations may contribute to migraine is not clear

[160]. An immunohistological study found that nerve fibers in the dura mater express TRPV1 [161]. In line with that observation, approximately 24% of dural afferents express TRPV1 [162]. Application of capsaicin to the rat dura produces behavioral responses consistent with headache [163,164], and sumatriptan, a well-known antimigraine drug, inhibits TRPV1 channels [165] as well as attenuates the positive modulation of TRPV1-mediated behavioral responses by 5HT [166].

Bolus injections of capsaicin induce dural vessel dilation through TRPV1-mediated release of CGRP, which plays an important role in the generation of migraine headache [167]. Another well-known inducer of headache, ethanol, is able to stimulate TRPV1 on primary afferent neurons, promoting neurogenic inflammation and CGRP-mediated coronary dilation [168]. Endogenous or exogenous mediators of inflammation have been shown to either activate TRPV1 directly or lower its activation threshold [65,169]. Thus, numerous mechanisms exist by which dural TRPV1 receptors may be activated and sensitized following meningeal inflammation, but which of these actually occurs either before or during migraine headache is not clear [169].

Multiple TRPV1-targeted therapies have been developed to potentially treat migraine, some of which showed to be partially effective, although not side effect-free, leaving the question of the efficacy of TRPV1-based therapy open [65,169].

3. B-type natriuretic peptide system

3.1 Natriuretic peptide family

Natriuretic peptides (NPs) comprise the structurally related atrial, brain, and C-type natriuretic peptides (ANP, BNP, and CNP, respectively) which principally mediate natriuretic, diuretic, vasorelaxant, and antimitogenic responses, by reducing blood pressure and maintaining fluid volume homeostasis [170–172]. ANP, BNP, and CNP are expressed as pro-hormones and are proteolytically processed to form the mature peptides. The three peptides share a similar structure (Fig. 17) consisting of two cysteine residues flanking a 17- residue disulfide-linked ring that is essential for biological activity [170].

3.1.1. Atrial natriuretic peptide (ANP)

The gene encoding for ANP (NPPA) is localized on chromosome 1p36.2 in humans and on chromosome 4 in mice [173]. ANP knockout mice show marked hypertensive state [174], highlighting the critical role of this peptide in regulating blood pressure, inducing natriuresis and diuresis in the kidney [175]. Like the other two natriuretic peptide genes, NPPA contains three exons and its mRNA is translated into a preprohormone that needs to be sequentially processed in order to generate the mature peptide. In humans, a 151 aminoacid-long preproANP is cleaved off from its amino-terminal signal sequence to yield a 126-aminoacid proANP. This form is the one predominantly found stored inside the atrial myocardial secretory granules [176]. The prohormone is then converted to its carboxy-terminal 28-aminoacid active form, via exocytosis by a transmembrane serine protease corin, [177], which is

crucial for correct ANP processing [178]. Interestingly, ANP aminoacid sequence of ANP is highly conserved, being almost identical across various mammalian species [179,180].
ANP is mainly synthesized in the heart, mostly in the atria, and secreted into the circulation in response the atrial walls stretch. The major molecular form of circulating ANP is a 28-aminoacid peptide with a ring structure formed by an intramolecular disulphide link (Fig. 17). Among extracardiac tissues that also express ANP are kidney, lung and the central nervous system [181], although ANP expression there is much lower than in the heart.

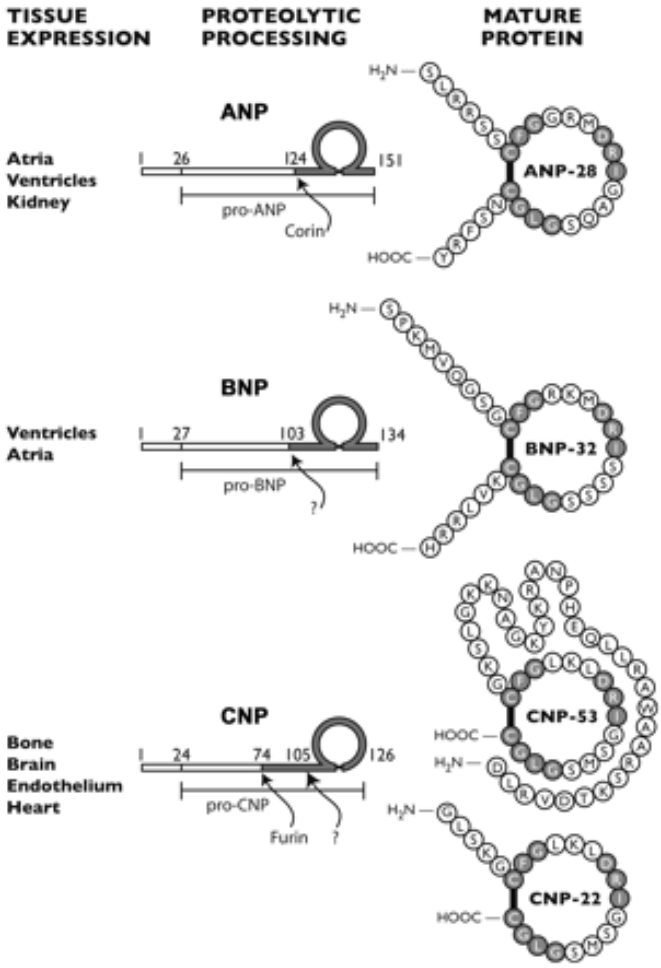

Figure 17. Natriuretic peptides structure and tissue expression (adapted from [182]). Representation of the polypeptide precursors of ANP, BNP and CNP and their aminoacidic length in human. Their proteolytic processing by corin and/or furin leads to the production of the respective active peptides. The disulfide link generating the conserved ring structure is shown in black, and invariant residues are highlighted in grey.

3.1.2. B-type (brain) natriuretic peptide (BNP)

BNP was first purified in 1988 from porcine brain extracts [183], but not long after that it was shown that the highest concentrations of BNP could be found in the heart and its secretion highly increased when ventricles undergo cardiac stress [184,185], making BNP a good biomarker of the heart pathophysiological state. For this reason, "B-type" rather than "brain" natriuretic peptide is the denomination considered more appropriate when referring to this hormone.

The BNP gene (NPPB) is located on human chromosome 1p36.2 and mouse chromosome 4maps, close to NPPA [186]. Knockout of NPPB causes animals to develop pressure-sensitive ventricular fibrosis while being normotensive [187]. Thus, unlike ANB, BNP does not have a crucial role in the regulation of blood pressure and is considered as an antifibrotic factor that plays a role in ventricular remodelling and as an important biomarker for heart failure or myocardial infarction [188].

BNP expression is suggested to undergo dynamical changes, depending on the physiological and pathophysiological conditions, and to have a distinct regulation from that of ANP. Thus, BNP half-life in the plasma can be as much as 10 times longer than that of ANP [189,190].

In humans, NPPB transcript is translated into a 134-aminoacid preproBNP, which subsequently generates a 108 aminoacids-long proBNP after its amino-terminal signal peptide removal. An additional cleavage by proteases such as corin or furin results into an inactive amino-terminal 76-residue fragment and the biologically active carboxy-terminal BNP, which is the predominant circulating BNP form (Fig. 17) [191]. While ANP structure has been shown to be relatively unchanged among species, the aminoacid sequence of BNP is less conserved and the length of the fully processed peptide can vary from 26 aminoacids in the pig, to 32 aminoacids in man and 45 aminoacids in the rat and mouse [183,192,193].

Both proBNP and BNP can be found circulating in the plasma following heart failure, with their ratio being influenced by the type of failure: the proBNP/BNP ratio appears to be higher in case of ventricular overload or decompensated heart failure compared to failures caused by atrial overload. This is consistent with the finding that both forms of the peptide are stored in the heart, with the proBNP being dominant in ventricular tissue while BNP is dominant in atrial tissue [194].

The heart represents the main source of BNP. Despite being normally more expressed in the atrium, during heart failure BNP increases dramatically almost exclusively in the ventricles, making it the the main source of total cardiac and circulating BNP [184,195]. Extra-cardiac expression of BNP is up to 1 – 2 orders of magnitude lower than that in the heart, but it is extended to a variety of tissues, including kidney, lung, small intestine, striated muscle and nervous system [196].

3.1.3. C-type natriuretic peptide (CNP)

CNP was first identified in porcine brain extracts by Sudoh and colleagues in 1990 [197]. Based on structural similarity it was included into the natriuretic peptide family (Fig. 17), though its sodium-excretion properties are actually low or hardly detectable [182,198].

Evolutionary studies suggest that ANP and BNP may have evolved from CNP gene duplication events, making it the most ancient and, interestingly, the most conserved in the family [199].

The CNP gene (NPPC) is localized on chromosome 2 in human and on chromosome 1 in mouse [200]. Its disruption was reported to yield normotensive mice with impaired endochondral ossification, which results in severe dwarfism and early death [201]. These observations may be explained by CNP ability to regulate the proliferation of chondrocytes, where it is abundantly expressed and operates in an autocrine fashion [202].

NPPC mRNA is translated to preproCNP, a 126-aminoacid long precursor that, after the signal peptide removal, generates a 103-aminoacid proBNP. Further processing of proBNP can yield two forms of the mature peptide: CNP-53 and CNP-22. Two forms of CNP have different tissue distribution, but show similar, if not identical, functions [203]. In general, CNP-53 is the predominant BNP form in most tissues, whereas CNP-22 is more abundant in plasma and cerebrospinal fluid [204,205].

Overall, CNP is most expressed in the central nervous system [206]. Other sites of expression include cartilage, bone, and vascular endothelium and, to a lower extent, also heart [172,182]. CNP is expressed in cardiac fibroblasts and not in myocytes, emphasizing the distinctly different expression profile of this peptide compared to ANP and BNP.

3.2 Natriuretic peptide receptors

For three natriuretic peptides three receptor subtypes have been identified (Fig. 18): namely, NP receptor-A (NPR-A), NP receptor-B (NPR-B), and NP receptor-C (NPR-C). Both NPR-A and NPR-B are membrane-bound receptors, containing an extracellular ligand-binding domain, a single transmembrane spanning region and intracellular kinase homologous domain (KHD) and guanylyl cyclase (GC) catalytic domain [170,171,182,207]. ANP and BNP activate NPR-A, and CNP activates NPR-B that leads to the production of second messenger cGMP. The cGMP in turn can activate cGMP-dependent protein kinase G (PKG) and subsequent cellular signaling cascades [172,208]. All three natriuretic peptides indiscriminately bind to NPR-C, which contains only a short intracellular fragment with no GC activity and is considered to clear NPs through receptor-mediated internalization and degradation [209,210].

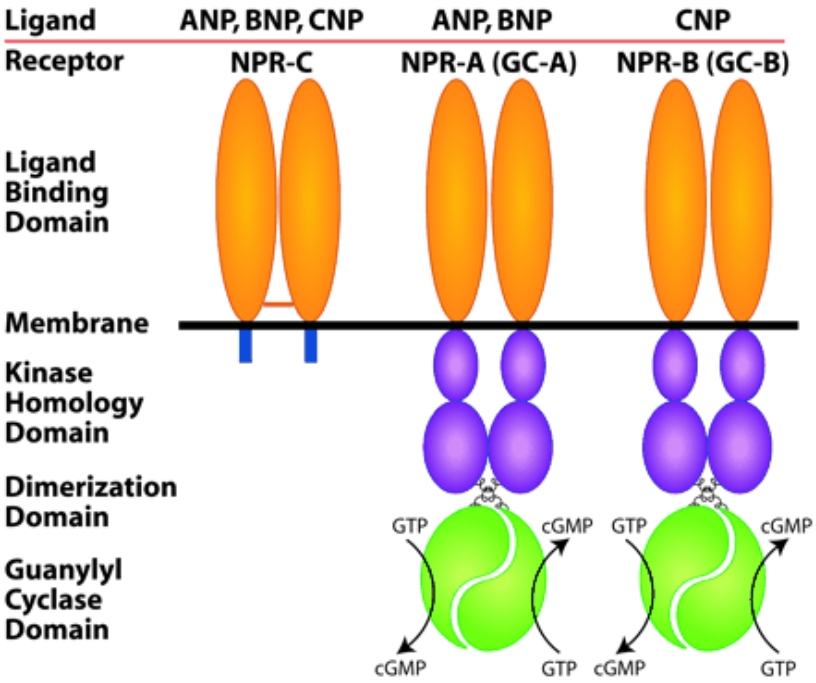

Figure 18. Natriuretic peptide receptor topology and ligand preferences (adapted from [182]). Natriuretic peptides bind three types of receptors with different selectivity, as indicated by the figure. NPR-C contains an intermolecular disulphide bond, indicated by the red horizontal line, but has a short intracellular domain with no intrinsic enzymatic activity. In contrast, NPR-A and NPR-B contain intracellular kinase homology, dimerization and carboxy-terminal guanylate cyclase domains.

3.2.1 Natriuretic peptide receptor type A (NPR-A)

NPR-A (or GC-A) is the main receptor for ANP and BNP. Studies of NPR-A activation revealed that ANP stimulates the receptor equally or more than BNP, while CNP has a much lower potency [172,182]

NPR-A expression was observed in a variety of tissues, including kidney, adrenal and adipose tissues, lung, nervous system and endocardial endothelium [182]. NPR-A receptor is coded by a gene NPR1 localized on chromosome 1q21-22 in human, and on chromosome 3 in mouse. Disruption of the gene generates animals that develop high blood pressure and cardiac hypertrophy [211]. Similar symptoms were observed also in humans displaying a rare mutation in NPR1 promoter that causes it to decrease dramatically its expression [212], confirming the important roles exerted by its agonists in the regulation of blood pressure and heart integrity.

The NPR-A receptor consists of three parts: an extracellular domain (ECD), a single transmembrane domain and an intracellular domain (ICD). The amino-terminal ECD, which binds the ligand, shows less sequence homology with NPR-B [171] that probably accounts for the different binding affinity to the natriuretic peptides showed by the two receptors. The ICD is composed of regulatory kinase homologous domain (KHD), dimerization domain and carboxy-terminal guanylate cyclase domain (GCD) [172].

NPR-A could be preassembled on the membrane as a homodimer or homotetramer, even prior to ligand binding [213,214], although the oligomerisation process is ligand-dependent and speeds up upon ligand binding [172]. It should be noted that the activation of the receptor requires simultaneous binding of its agonist to the ECD and of ATP to a glycine-rich binding site located in the KHD [215]. ATP increases ligand-dependent GC activity of NPR-A, but the exact mechanism of its action is debatable [172,216]. It is suggested that the KHD, which has no intrinsic kinase activity, acts by repressing the receptor's basal activity. This repression may then be relieved by the conformational change induced by ATP and the extracellular agonist [217,218]. Additionally, under basal conditions N-terminal end of KHD is phosphorylated on four serine and two threonine residues that is essential for NPR-A ligand-dependent GC activity. Dephosphorylated upon prolonged agonist binding is, thus, responsible for the receptor desensitization [219,220] (Fig. 19).

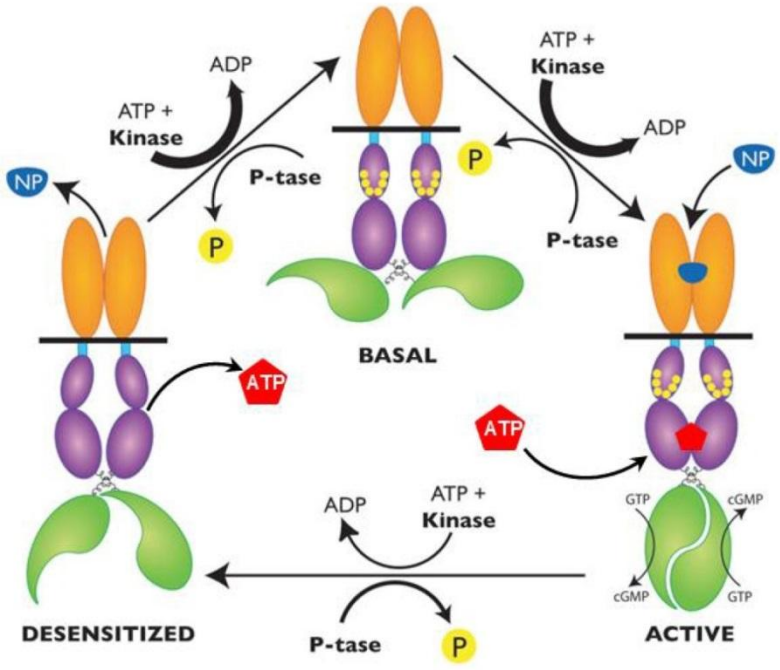

Figure 19. Hypothetical model for NPR-A (and NPR-B) activation and desensitization (adapted from [182]). NPR-A and NPR-B are proposed to exist in basal, active and desensitized states. In the basal state, receptors are phosphorylated on several residues of the KHD (yellow dots). Simultaneous natriuretic peptide (blue) and ATP (red) binding promotes the functional activation of the GCD (green), whereas prolonged ligand exposure stimulates receptor dephosphorylation and consequent desensitization. Ligand release and re-phosphorylation return the receptors to the basal state.

The exact molecular mechanism through which extracellular binding of the ligand is translated into the activation of the NPR-A intracellular catalytic domain (GCD) is still poorly understood. It was shown that natriuretic peptide and ATP binding can dramatically

increase GCD's affinity for its substrate, GTP [221]. The resulting increase in the conversion of GTP to cGMP can, thus, be considered as an indicator of receptor activation. The increased intracellular cGMP levels may ultimately mediate biological functions through the activation of several cGMP-dependent effectors (see section 4.3).

After NPR-A activation, signal transduction may be terminated by three mechanisms. One is the enzymatic degradation of natriuretic peptides mediated by the neutral endopeptidase neprilysin [222]. Another one is the aforementioned dephosphorylation-dependent receptor desensitization. The last mechanism includes ligand-induced receptor internalization and degradation, though there is some controversy as to whether such a phenomenon indeed occurs [223,224].

The receptor can be pharmacologically and specifically blocked by anantin, a bacterial 1.9 kDa peptide isolated from S. coerulescens that binds NPR-A as a competitive antagonist and prevents its GC activation [225].

3.3 Main NPR-A effectors

Natriuretic peptides (mainly ANP and BNP) upon binding to the NPR-A promote CG activity and cGMP production. Thus, cGMP represents the major intracellular second messenger through which natriuretic peptides elicit their physiological responses.

There are three main cGMP binding proteins that could act as the NPRs effectors: the cGMP-dependent protein kinases, the cGMP-binding phosphodiesterases (PDEs) and the cyclic nucleotide-gated ion channels (CNG) (Fig. 20) [182].

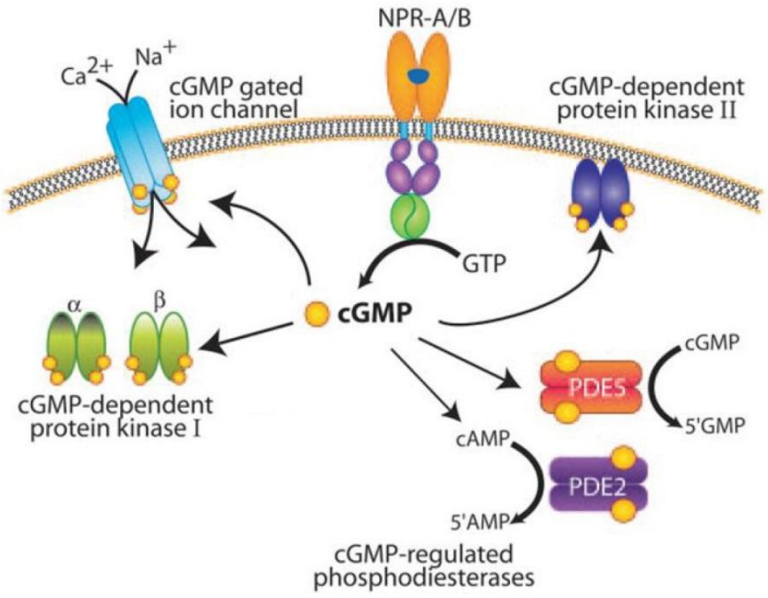

Figure 20. Main cGMP effectors. Illustration of the main classes of cGMP-regulated proteins, which may mediate biological effects of NPR-A and NPR-B activation (adapted from [182]).

3.3.1. Protein kinase G

The cGMP-dependent kinases are all termed protein kinase G (PKG) and are the best studied cGMP effectors. They are homodimeric proteins composed of three domains. The amino-terminal homodimerization domain interacts with protein substrates and also suppresses basal kinase activity. The regulatory domain activates the enzyme upon cGMP binding, and a kinase domain catalyses phosphotransferase reaction on serine and threonine residues of target proteins. Two different genes have been identified for this kinase. The PKGI gene produces two splice variants differing in their amino-termini, denominated PKGIα and PKGIβ. Both are mostly cytosolic and are found in platelets, smooth muscle, cardiomyocytes and nervous system. Their absence in mouse causes a lack of cGMP-dependent vasorelaxation, resulting in severe vascular and intestinal dysfunctions [226]. PKGII instead produces a myristoylated form of the kinase that is mostly membrane bound [227]. This gene is highly expressed in the intestine, kidney, nervous system, cartilage and bone, and its deletion yields animals with dwarfism, due to impaired chondrocyte differentiation and impaired ossification [228,229].

The substrates of PKG comprise an extremely large variety of proteins which, upon phosphorylation, may then become enzymatically active, inactive, or generally undergo a structural and functional change. Moreover, PKG signaling may branch out and cross-talk with further signaling pathways through phosphorylation-dependent activation of other biologically important protein kinases, including protein kinase A (PKA), protein kinase B (PKB, also known as Akt) and the extracellular signal-regulated kinase 1/2 (ERK1/2) [230–232].

3.3.2. Phosphodiesterases (PDEs)

Cyclic nucleotide PDEs are enzymes that break the phosphodiester bond of cAMP and cGMP, converting them into the inactive AMP and GMP, respectively. Therefore, they represent important regulators of the intracellular levels of these second messengers and of the respective signaling cascades.

Up to now, eleven genes for PDEs have been identified, encoding for at least 25 different proteins in mammals [233]. They differ in their substrate specificity (cAMP, cGMP or both), and in how they are activated or inhibited. For instance, the isoforms that selectively hydrolyze cGMP are PDE5, -6 and -9, whereas PDE1, -2, -3, -10 and -11 can degrade both cyclic nucleotides. Some of these may be allosterically regulated by cGMP itself, which is, thus, able to modulate its own degradation, via PDE5, as well as that of cAMP, through PDE2 [234].

3.3.3. Cyclic nucleotide-gated ion channels

Cyclic nucleotide-gated ion channels represent a third potential effector of cGMP. They constitute a family of tetrameric nonselective cationic channels activated by intracellular cAMP or cGMP [235]. In both human and mouse, subunits are coded by 6 different genes, which are divided in two subfamilies, CNGA and CNGB, according to their sequence relationships [236]. However, despite the fact that NPR-A (or -B) GC activity could

theoretically lead to the opening of CNG channels, very few studies have suggested an actual direct link between these channels and a specific natriuretic peptide function [237,238].

3.4. Natriuretic peptides in the nervous system

The natriuretic peptide system is generally considered in relation to blood pressure and volume homeostasis regulation, since this is the first and most obvious function that was described. However, the natriuretic peptide system, and BNP with its receptor NPR-A in particular, has been associated with various functions apart from the regulation of the cardiovascular system [172]. Supporting the idea of multiple functions, natriuretic peptides and their receptors were found in a variety of tissues in animals and humans [171,182]. For the purposes of this thesis, I will focus on the physiological role natriuretic peptide system can play in the nervous system.

3.4.1. Central nervous system

All three natriuretic peptides are expressed in the central nervous system (CNS), although at different levels. For instance, CNP is the most highly expressed natriuretic peptide in the CNS, whereas BNP is rarer than CNP but generally more abundant than ANP [237,239,240]. BNP and CNP show a similar distribution throughout many CNS regions, (and their overall distribution tends to be complementary to that of ANP, with some exceptions where expression of all three peptides overlaps, like in the hypothalamus, retina and the cerebral cortex [182].

Binding and functional studies suggest that NPR-A, NPR-B and NPR-C are predominantly expressed by glial cells [241–244]. However, neuronal expression of the NPRs has also been reported, particularly in the hypothalamus, brainstem and retina [245,246].

Elements of the natriuretic peptide system start being expressed in CNS from the earliest stages of embryonal development [247], suggests a possible role in modulating the cell differentiation in the developing brain and spinal cord [248]. In vitro studies suggest that this modulation may consist in an antiproliferative action, through DNA synthesis inhibition, probably driving cells towards terminal differentiation [249,250].

Various workers have shown that NPR signaling can modulate neurotransmitter uptake and release, including noradrenaline [251–253], vasopressin and oxytocin [254,255]. ANP was also shown to modulate synaptic transmission from osmoreceptor afferents to the supraoptic nucleus in the hypothalamus, reducing their postsynaptic responsiveness [256]. Natriuretic peptides may alter synaptic transmission also in the retina, where NPR-A activation can suppress GABAA currents in bipolar cells, whereas NPR-B can reduce AMPA-mediated transmission in amacrine cells [246,257]. Furthermore, it was reported recently that NPR-A inhibits glutamatergic release in the projections between the epithalamus and the midbrain, enhancing stress-induced analgesia, through a PDE-mediated suppression of cAMP signaling [258].

Additionally, several studies have shown that cGMP might protect neurons against excitotoxicity and oxidative stress [259,260]. Given that cortical spreading depression, which is suggested to contribute to neuroprotection against ischemia [261,262], is followed by an increase

in cortical ANP expression and cGMP levels [263], it would not be surprising that the natriuretic peptide system might have a neuroprotective role in the CNS. One example is NPR-A protection against NMDA-induced neurotoxicity in the rat retina [264]. This effect is supposedly caused by an enhancement of dopaminergic signaling, however the precise mechanisms through which it leads to actual neuroprotection remains unclear.

3.4.2. Peripheral nervous system

Compared to the wealth of information regarding the effects of natriuretic peptides in the CNS, fewer studies have investigated their physiological role in the peripheral nervous system. Nonetheless, the fact that ANP-induced hypotension is usually not followed by the expected reflex tachycardia or increased sympathetic activity, and that this hypotension is attenuated by vagotomy, indicates that ANP may somehow interact with the autonomic nervous system [265]. A study on in vitro vagal-sinoatrial transmission has proposed that CNP may potentiate bradycardia by increasing vagal acetylcholine release in a NPR-B- and PKA-dependent manner [266]. A similar bradycardic effect had been reported earlier in vivo, although it was attributed to ANP [267], strengthening the hint that NPRs are expressed in the autonomic nervous system.

Autoradiographic and in situ hybridization analyses revealed an early (E10.5) expression of NPRs in dorsal root ganglia (DRG) and cranial ganglia [248,268]. In contrast to the embryonal CNS, where NPR signaling has antiproliferative effects, it was shown to stimulate DNA synthesis in Schwann cells and promote sensory neuron survival. Furthermore, natriuretic peptides were reported to have an important role in guiding axonal outgrowth and branching from DRG neurons toward their target in the spinal cord [269].

3.5 Natriuretic peptides in nociception

More recently, evidence has supported a potential involvement of the natriuretic peptide system in the modulation of sensory neuron nociceptive transmission [270]. In 2010 Zhang et al showed that BNP and NPR-A are both expressed in the rat DRG, and their signaling attenuates inflammatory pain through a mechanism that involves large-conductance Ca2+-activated K+ (BKCa) channels and PKG [271] (Fig. 21). Another study showed that also NPR-C is present in DRG, where it colocalizes with transient receptor vanilloid-1 (TRPV1) channels. Here, however, NPR-C activation by CNP displays the opposite effect, enhancing thermal hyperalgesia in a protein Gβɣ-, TRPV1- and PKC-dependent fashion, appearing as a positive modulator of chronic pain [272].

These results indicate the coexistence of functional NPRs in sensory neurons that exhibit contrasting effects on pain transduction, and could play an important role not only under normal conditions but also during pathological pain states. Apart from DRG, the trigeminal ganglion (TG) is another important player in the pain transduction and development of different pain-associated conditions. While all NPRs have been identified in the brainstem trigeminal nuclei [273–275], few studies investigated the presence and possible role of the natriuretic peptides system in TG. For instance, ANP was reported to be expressed in TG

[276,277], and one study suggested the presence of BNP in porcine TG neurons innervating arteries of the Circle of Willis. Yet, the question of whether natriuretic peptides and their receptors are involved in the modulation of trigeminal pain states at the TG level remains to be answered.

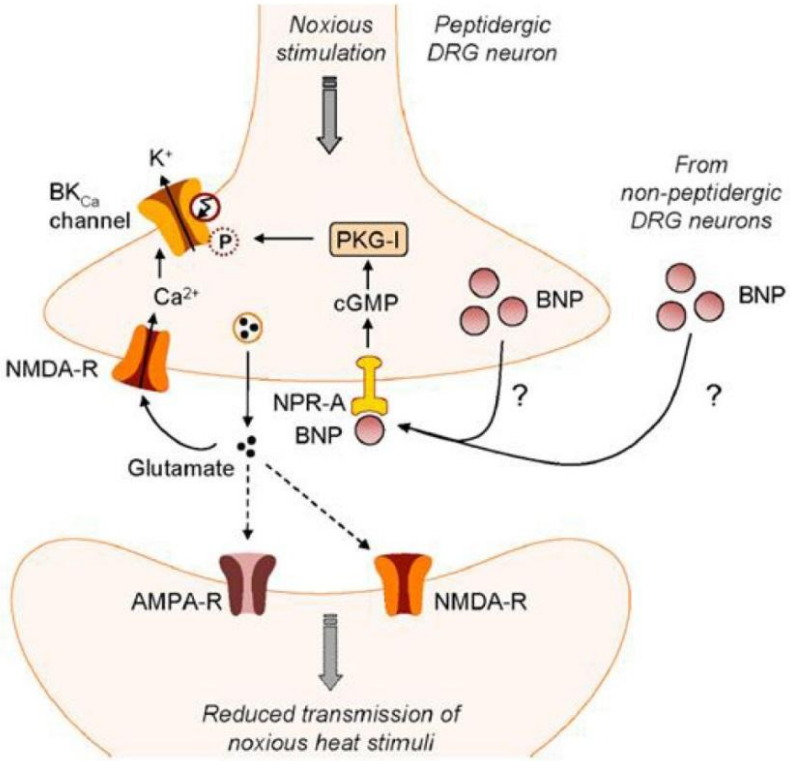

Figure 21. BNP modulation of nociceptive transmission in murine DRG (adapted from [270]). Activation of the BNP/NPR-A pathway leads to the PKG-I-mediated phosphorylation of BKCa channels, which, in the presence of high intracellular Ca2+ levels, may suppress the transmission of noxious heat stimuli in peptidergic DRG neurons. The exact release mechanism of BNP is unclear.

4. Excitability of trigeminal neurons

Primary sensory neurons, including trigeminal neurons, constitute the first link in the chain of neurons making up somatosensory pathways. They encode their responses to received stimuli as a series of action potentials. Under normal circumstances, trigeminal neurons are relatively quiescent, but they produce highly modulated series of action potentials when stimulated, conveying information about the sensory stimuli to the higher brain regions [278]. In some pathological conditions, however, primary sensory neurons can become hyperexcitable and can give rise to unprovoked spontaneous action potential activity or bursting which can contribute to chronic pain [279–281]. Chronic pain is characterized by enhanced sensory neurotransmission that underlies increased sensitivity to noxious stimuli and the perception of non-noxious stimuli as painful [282]. Therefore, excitability and firing

properties of sensory neurons including those in TG are aspects of greatest interest as they are the major determinants of the encoding capacity and transduction properties of the neuron. Heterogeneous firing properties have been reported in a number of studies on adult rat and mouse TG neurons [66,283].

Trigeminal neurons in culture express diverse voltage gated and ligand gated ion channels and a wide array of metabotropic receptors which collectively control neuronal excitability. Studies in trigeminal ganglion neurons show that their functional properties correlate with distinct electrophysiological phenotypes. Catacuzzeno et al [283] have identified three distinct firing patterns among trigeminal neurons of adult mice having biophysical and pharmacological properties influenced by different low-threshold K+ currents, namely slow-inactivating (Ik), fast inactivating transient (IA) and slow-inactivating transient (ID)currents. In rat trigeminal neurons, low threshold TTX-resistant sodium currents mostly mediated by NaV1.9 channels are also observed [284]. Multiple types of high voltage activated and low voltage activated Ca2+ channels [285–287] are known to be expressed by trigeminal neurons.

Activation of ATP-gated P2X3 channels and capsaicin-sensitive TRPV1 channels, expressed on the membranes of trigeminal sensory neurons, also invokes firing activity that is conveyed to higher brain regions and then is interpreted as pain [66,282]. Thus, brief firing responses could be invoked in trigeminal neurons by activation of P2X3 channels while neurons activated by the pungent compound capsaicin in nociceptors have been found to exhibit more sustained firing [66,282,288]. In acutely dissociated neurons in vitro, action potentials are close to true membrane action potentials; they usually include a stump of axon as well as varying amounts of proximal dendrites, but the remaining processes are usually short enough that the whole membrane surface can be considered isopotential, even during spikes [289]. The main characteristics of a neuron are its electro responsive and membrane properties which include input resistance, rheobase, capacitance and voltage threshold for spike generation.

Input resistance represents the resistance exhibited by the neuron or a cell for a change in membrane potential caused by injected current, and depends on the open membrane channels in the neuron. **Rheobase** is a measure of excitability and is defined as the minimal strength of an electrical current injected (of indefinite duration) for generation of an action potential in a neuron. Rheobase depends on resting membrane potential, input resistance and the voltage threshold [290]. The **capacitance** of an excitable cell membrane is affected by the processes of the neuron and influences the shape and speed of membrane potential changes including action potentials [290]. **Voltage threshold** for spike generation is usually measured in mV and is defined as the amount of depolarization required to generate an action potential. Voltage sensitivity of sodium channels primarily dictates the voltage threshold [290]. The spike threshold can be determined using a phase plane plot with the time derivative of the voltage (dV/dt) versus the voltage. On the plot threshold for action potential is the voltage at which dV/dt suddenly increases.

5. Migraine

Migraine is a common, disabling, and undertreated episodic brain disorder with a complicated and not fully understood pathophysiology [65,291]. It is characterized by recurrent headache attacks with associated autonomic symptoms. Intensity of headache varies from moderate to severe pain, causing prolonged incapacitation. Migraine is one of the most common disabling brain disorders and it affects according to different sources approximately 11- 20% of people at some point in their lives [292–294]. The annual costs of diagnosing and treating migraines to American employers are estimated to be over $1 billion per year for direct costs, and $13 billion per year for indirect costs that are due to reduced productivity, reduced ability to do household work, and high likelihood of adverse consequences in relationships between migraines and other family members [292,295,296]. The prevalence of migraine was estimated to be around 17-18 % in women and 5-8% in men [296,297].

5.1 Classification of migraine

Migraine comprises a group of disorders which differ considerably in their clinical symptoms, origins and pathophysiology. In addition, migraine-like conditions can mimic stroke, seizure or epilepsy [298,299]. All this adds up to make a complex classification of migraine headaches.

A full spectrum of migraine includes migraine without aura, migraine with aura, and migraine-related conditions.

Migraine without aura (MO) affects approximately one third of all migraine sufferers. It is an idiopathic, recurring headache disorder with attacks usually lasting 4 to 72 hours if untreated. Typically migraine headache is unilateral and is accompanied by a characteristic pattern of other symptoms such as nausea, vomiting, photophobia and phonophobia in various combinations. Not all features are present in every attack or in every patient [298].

Migraine with aura (MA) is similar to MO but it is also characterized by the presence of so called aura – a complex of neurologic symptoms that usually occurs at or just before the onset of a migraine headache [300]. Approximately 20 to 30% of migraineurs experience aura, which most often includes visual phenomena, but it may involve somatosensory or motor phenomena, as well as language or brainstem disturbances [300].

Migraine-related conditions. The diagnosis of migraine-related condition is based on a transient sign or symptom in the absence of conventional visual aura. The headache may or may not be present [299].

5.2 The stages of migraine

A typical migraine attack can be divided into four phases: the premonitory phase (or prodrome), the aura, the ictus, and the resolution phase (postdrome) [301].

1. **Prodrome** occurs from hours to a day or two before the aura in 60% of migraineurs and may include symptoms such as fatigue, difficulty in concentrating, neck stiffness, sensitivity to light or sound, nausea, blurred vision, yawning, and pallor [301].

2. The **aura** usually develops over a period of 5 to 20 minutes and lasts less than an hour; the most common aura is the visual aura that may include simple flashes, specks or more complicated hallucinations [298].
3. The **headache** is unilateral and is aggravated by head movement or physical activity; 85% of patients describe it as throbbing. The onset is usually gradual and the attack lasts 4 to 72 hours, but it may be completely absent as well [298].
4. Headache phase is followed by a phase known as **postdrome** when patients suffer from head tenderness, fatigue and mood changes [301,302].

5.3 Migraine pathophysiology

Migraine is a complex disorder that includes a variety of pathological conditions with different clinical profiles and undetermined causes. Unravelling the pathophysiological mechanisms underlying migraine headache proved to be a challenging task that is yet to be completed. However, years of investigations were able to shed light upon several mechanisms that might contribute to the migraine pathophysiological profile [303].
Nowadays migraine is most often described as a neurovascular disorder, since its symptoms arise from a combination of vascular and neurological events occurring in the cranial meninges [304]. Phenomena like cortical spreading depression (CSD), activation of the trigeminovascular system, neurogenic inflammation (leading to changes in the meningeal vasculature) are thought to be the key events in the development of migraine pain [305], although the exact interaction between these processes is not completely clear [303].

5.3.1 Migraine theories

The vascular theory and the neurogenic theory are two independent theories that were proposed to explain migraine etiology.

Vascular theory

The vascular theory was first introduced by Thomas Willis and then advanced by Graham and Wolff, postulating migraine as a vascular event mediated by initial intracranial vasoconstriction followed by rebound vasodilation [306,307]. This was consistent with the notion of "throbbing" pain during migraine attacks and with the fact that vasoconstrictors such as ergotamine, triptans (serotonin receptor agonists) and calcitonin gene-related peptide (CGRP) agonists diminish migraine symptoms [308,309]. Because the vasodilator nitroglycerin was observed to induce headache, this result was taken as a confirmation of vascular migraine theory [310].
However, there is evidence that does not support a vascular theory as the primary cause for migraine [311,312]. Amin et al. (2013) have shown that vasodilation itself is not the cause of peripheral and central pain pathways [313]. Vasodilation remains linked to migraine attacks and can promote migraine via accompanied release of neuropeptides and proinflammatory substances from trigeminal afferents in the meninges [314]. It was demonstrated that electrical and mechanical stimulation of dural vasculature produced head pain in awake patients

undergoing craniotomy, whereas stimulation of non-vascular areas of the dura induced no pain [315,316]. This is consistent with the notion that the dural innervation is nociceptive largely due to unmyelinated C-fibers and thinly myelinated Aδ fibers coming from the trigeminal ganglion and C1-3 dorsal root ganglia [311,317–319]. Moreover, sensory nerves in trigeminal and upper cervical ganglia closely follow meningeal blood vessels but not non-vascular areas of the dura [315].

Neurogenic theory

The alternative neurogenic theory explains migraine as a disorder of the brain in which any vascular events are caused by dysfunction of neuronal networks [314]. Indeed, some of the migraine symptoms could not be described only in terms of vasodilation [320]. Currently the neurogenic theory implies activation and sensitisation of the trigeminovascular system and a phenomenon of cortical spreading depression that underlies aural symptoms in migrainers [314,320].

Clearly neither theory can account for the entire cascade of events associated with a migraine attack and it is likely that both theories contribute to a more complex neurovascular model that describes migraine pathophysiology as the interaction between vascular and neurogenic mechanisms [303].

5.3.2 The trigeminovascular system

The trigeminovascular system consists of the trigeminal nerve and trigeminal sensory afferents innervating extra- and intra- cranial meningeal blood vessels and the brain stem [321]. The trigeminal nerve contains both sensory and motor components. The sensory component conveys thermal and tactile sensations from the face and forehead and is thought to play an integral role in regulating vascular tone and pain transduction including migraine pain and other headache conditions [303]. The cell bodies that give rise to the trigeminal sensory fibers are pseudo-unipolar neurons localized in the trigeminal ganglion.

Upon activation of perivascular trigeminal afferents, the signal is first conveyed from the trigeminal ganglion to neurons in the trigeminocervical complex via CGRP that serves as the main neuromodulator [322] and then to the thalamus [323,324] and finally to the cortex where the awareness of the pain originates. The pain signal is modulated through extensive connections with brainstem regions such as the periaqueductal gray and the locus coeruleus [323] (Fig. 22).

Activation of the trigeminovascular system during migraine is thought to initiate the release of a variety of chemical components from trigeminal sensory nerve endings [325,326]. Trigeminal pain fibers contain vasoactive neuropeptides such as substance P (SP), calcitonin gene-related peptide (CGRP), neurokinin A and pituitary adenylate cyclase-activating peptide (PACAP) that released in the extracellular compartment lead to neurogenic inflammation around vascular structures in the meninges and, thus, head pain [53,327–330]. However, the neurogenic inflammation hypothesis does not explain what causes the initial activation of meningeal nociceptors to trigger migraine pain.

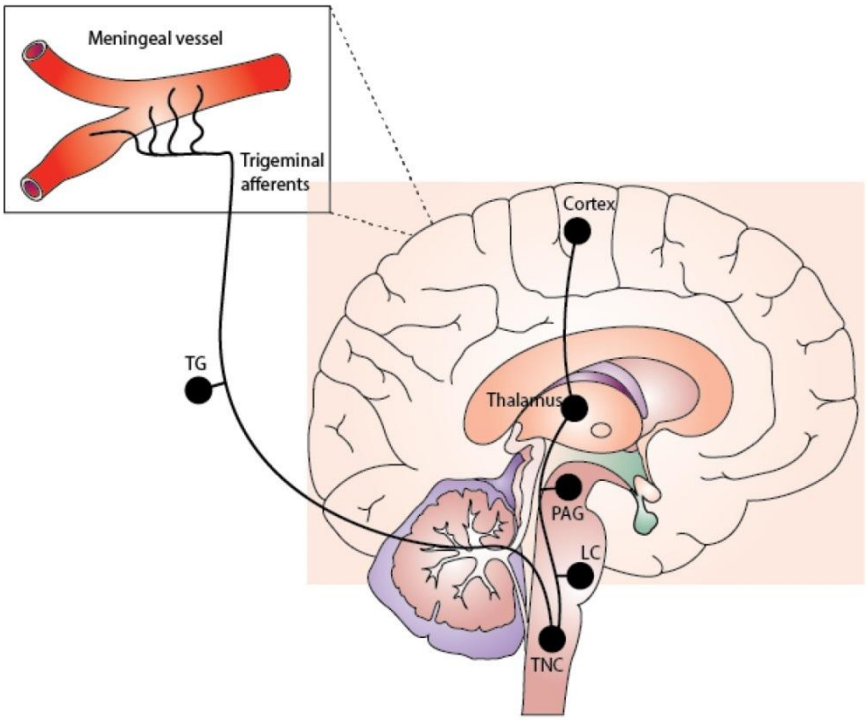

Figure 22. Migraine headache is caused by activation of the trigeminovascular system (adapted from [331]). TG = trigeminal ganglion; PAG = periaqueductal gray; LC = locus coeruleus; TNC = trigeminal nucleus caudalis.

5.3.3 Cortical spreading depression

Activation of meningeal nociceptors is considered to be a key process from which pain signals originate during a migraine attack. Nevertheles, it remains unclear what serves as a trigger for such an activation. Recent studies suggest that initial activation of trigeminal nociceptors could be caused by the process of cortical spreading depression (CSD).

CSD, first observed by Leão in 1944 [332,333], may be described as a short-lasting, intense wave of neuronal and glial depolarisation that spreads at a rate of approximately 2–4 mm/min over the cerebral cortex. This depolarisation wave is accompanied by disruption of ionic gradients (Ca^{2+}, Na+, K+), followed by long-lasting inhibition of spontaneous and evoked neuronal activity [334,335] (Fig. 23). This is accompanied by localized changes in blood flow that spread through the cortex at a similar rate. In migraineurs, cerebral blood flow studies demonstrate a wave of oligoemia that precedes the aura and progresses with the rate comparable to the rate of CSD [336–338]. At the present time, CSD is regarded as the electrophysiological substrate of migraine aura [336,337,339]. Since the aura often precedes the onset of headache by 20-30 min, it was postulated that CSD may stimulate the initial activation of meningeal nociceptors. In fact, CSD may activate and sensitize the trigeminovascular system, starting a series of neural, vascular and inflammatory events that result in pain [340] (Fig. 24).

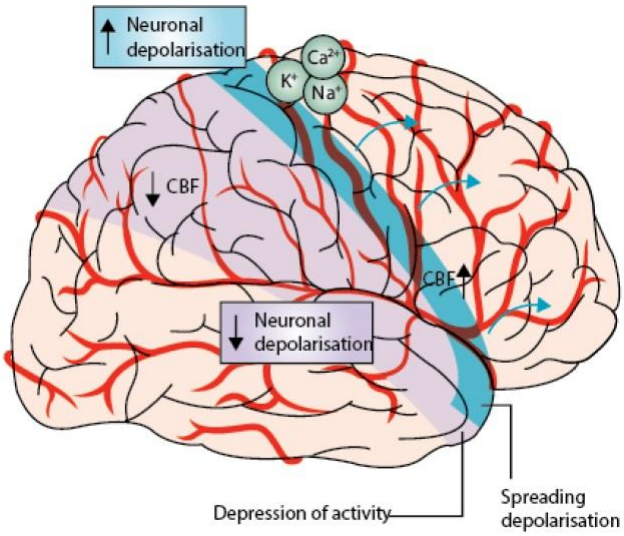

Figure 23. Cortical spreading depression (adapted from [331]). CBF – cerebral blood flow

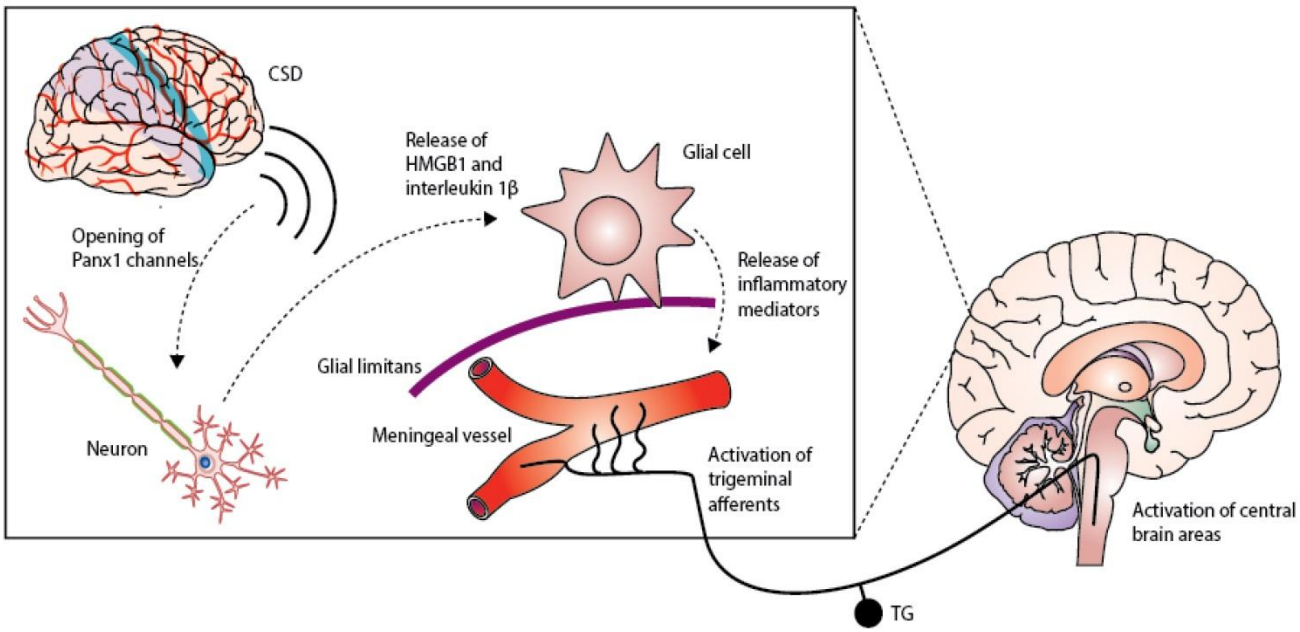

Figure 24. Cortical spreading depression might activate the trigeminovascular system (adapted from [331]). CSD – cortical spreading depression; TG – trigeminal ganglion; HMGB1 – high-mobility group box 1; Panx1 – pannexin 1.

Experiments in rats have shown that evoked cortical spreading depression might persistently activate first nociceptors within the trigeminal ganglion which innervate the meninges [341] and second (central) trigeminovascular neurons. [340,342].

A recent study has shown that CSD caused Pannexin1 megachannel opening and caspase-1 activation that in turn can turn on parenchymal inflammatory pathways and may provide the stimulus for sustained trigeminal activation and longlasting pain [343]. The CSD hypothesis assumes that agents such as potassium ions, hydrogen ions, and glutamate largely released extracellularly during CSD in the cortex, diffuse through the overlying meninges to activate meningeal nociceptors and induce neurogenic inflammation in the dura [344–346]. Thus, if confirmed in human studies, CSD might not only cause the migraine aura, but also trigger the mechanisms underlying the migraine headache and associated symptoms [331].

5.3.4 Neuronal sensitization

Sensitization is a process by which primary sensory neuron afferents in peripheral nervous system and central synapses become hypersensitive to nociceptive and innocous stimuli [347–350]. Thus, neurons show a reduction in their activation threshold [349,351–354], and increased responses to supra-threshold stimuli [347,355–357]. Peripheral and central sensitization is thought to underlie neuropathic and chronic pain, including allodynia, hyperalgesia and spontaneous pain [348].

Peripheral sensitization

Symptoms of peripheral sensitization during migraine include throbbing headache and its aggravation during routine physical activities that increase intracranial pressure such as coughing and bending over [303,358,359]. Intracranial hypersensitivity involves sensitization of nociceptors that innervate the meninges, implying that the trigeminovascular system plays an important role in the process of peripheral sensitization during migraine attack [65].

Peripheral sensitization is supported by enhanced release of neurotransmitters and inflammatory peptides from primary afferents to spinal synapses after injury and inflammation [360]. Bradykinin, histamine, serotonin (5HT), and prostaglandin E2, (PGE2) cause mechanical sensitization and increase the excitability of somatic [361] and meningeal nociceptors [349,350]. Inflammatory mediators such as interleukins 1, 6 and 8 (IL-1, IL-6, IL-8) and tumor necrosis factor α (TNFα) exert their effects through the endogenous release of eicosanoids and sympathetic amines [362,363]. Acidic pH and proteases were shown to induce inflammation within the meninges through protease-activated receptors (PARs) [364] triggering headache or migraine in patients [365]. Existing evidence suggest that CSD might sensitize meningeal nociceptors indirectly, triggering the release of CGRP and SP which in turn cause the release of inflammatory mediators such as histamine, 5HT, BK, TNFα and nitric oxide from mast cells, macrophages and other immune cells [366–368].

Inflammatory mediators modulate the activity of ion channels on nociceptors, therefore contributing to the spontaneous activity of sensory fibers to complete a pathological cycle of hyper-responsiveness [348,369,370]. Purinergic receptors, acid-sensing ion channels and TRPV1 channels are modulated by inflammatory mediators [65]. Experiments in sensory ganglion cultures show that the development of a neuroinflammatory profile facilitates the release of endogenous mediators (including ATP and cytokines) to reinforce inflammatory cell

activation and to constitutively potentiate ATP-gated P2X3 receptors amplifying nociceptive signaling [348].

Central sensitization

Central sensitization is a condition in which nociceptive neurons in the dorsal horn of the spinal cord exhibit increased excitability, increased synaptic strength, and enlargement of their receptive fields [371,372]. Like peripheral sensitization, central sensitization is induced by released neurotransmitters and inflammatory factors. Animal models and human studies provide direct evidence that symptoms of central sensitization in somatosensory pain pathways contribute to post-injury pain hypersensitivity [373–378] that arises from increased responsiveness of dorsal horn nociceptors. Clinically, central sensitization is manifested as decreased pain threshold and exaggerated pain response even outside the original pain site. In migraineurs, symptoms of central sensitization are often expressed as allodynia, when patients become sensitive to otherwise innocuous stimuli [379–383]. This involves the sensitization of nociceptive trigeminovascular neurons of the medullary dorsal horn that receive converging sensory input from the dura and the skin [384,385].

Overall, although migraine headache has been intensely investigated for decades, there are still many questions concerning its origins and pathophysiology that remain unanswered and require future research. Figure 25 shows a schematic representation of pathophysiology of headache as proposed by Pietrobon and Striessnig ([386].

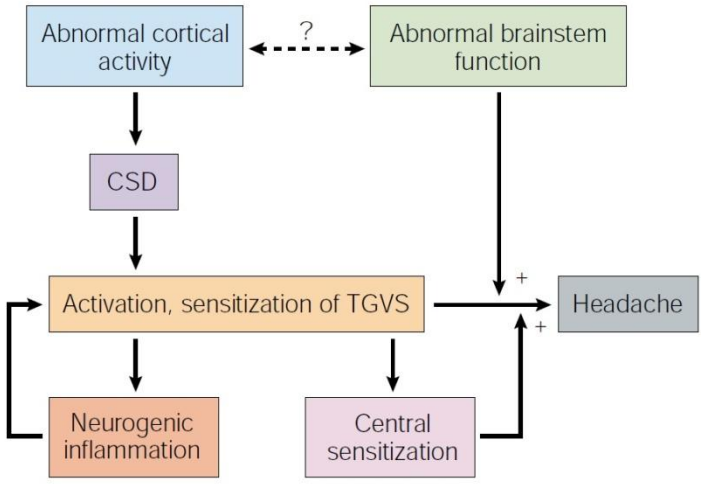

Figure 25. Schematic representation of pathophysiology of headache (adapted from [386]).

5.3.5 Migraine as a channelopathy

Ion channels are pore-forming transmembrane proteins that allow the transmembrane flow of ions. Ion channels are essential components of every living cell, even considering not excitable ones, and are vitally important for proper signaling and cell function. No wonder

that alterations and dysfunctions in ion channels functioning are expected to lay at the origins of a variety of known disease.

Throughout the years, migraine disorders are often considered as channelopathies, since more and more channels malfunctions are shown to contribute to the development of these pathologies [65].

Mutations in several ion channels have been shown to underlie particular migraine pathologies. Mutations in the CACNA1A gene, encoding the α1 subunit of P/Q voltage-gated calcium channel Cav2.1, and SCNA1A, encoding α1 subunit of the voltage-gated sodium channel Nav1.1, have been linked to familial hemiplegic migraine types 1 and 2 (FHM 1 and 2), respectively [387–389]. Recently, another susceptibility gene responsible for the potassium channel subfamily K member 18 (KCNK18), which encodes a two-pore domain potassium channel (K2P), TRESK, was linked to inherited migraine with aura [390,391] although further work could not validate that the aura or the migraine attacks in these patients are directly related to dysfunction of TRESK [65].

Apart from these particular mutations that are usually linked to relatively rare migraine types, there is growing evidence that the dysfunction of a variety of ion channels is involved in the process of migraine development.

Acid-Sensing Ion Channels (ASICs)

The ASIC family consists of 4 members, ASIC1-4, with several splice variants [392]; they are proton-activated voltage-insensitive cationic channels [393] that are widely expressed in the central [394,395] and peripheral nervous system [396]. Approximately 80% of dural afferents show immunolabeling for ASIC3 [397,398] and their expression is found in most trigeminal neurons. ASIC3 have been proposed as a sensor of decreased extracellular pH within the dura [384]. Considering the ASICs pH sensitivity and their high expression in dural afferents, it is possible that even small pH changes can activate ASIC-positive neurons [65]. That could be an important contribution to the migraine headache during which low pH conditions could potentially arise: for example, CSD is shown to be accompanied by ischemia [102] which could induce a pH drop in the dura. Furthermore, experiments demonstrate that low pH elicits migraine-related pain behavior in awake animals through the activation of ASICs [103], and increases CGRP release in TG neurons [397] that might result in neurogenic inflammation and headache progression. In accordance with this view, the non-specific blocker of ASICs amiloride was shown to block CSD and inhibit trigeminal activation through an ASIC1-dependent mechanism in a preclinical study [399]. Overall, these data provide support for the idea of ASIC involvement in the pathophysiology and initiation of migraine.

Transient Receptor Potential (TRP) Channels in migraine

TRP channels are a group of cation ion channels that respond to a variety of stimuli, including heat, changes in osmolarity and pH, and various natural products [65,400]. The 28 mammalian TRP channels can be divided into 6 subgroups based on their primary amino acid sequences. 3 of 6 subgroups include channels that are considered to be involved in

migraine pathophysiology: transient receptor potential channel ankyrin (TRPA), transient receptor potential channel melastin (TRPM) and transient receptor potential channel vanilloid (TRPV) [65].

Transient Receptor Potential Ankyrin Channel 1 (TRPA1) is expressed on sensory neurons [401] including dural afferents [402] and has an established role in pain transduction [403]. Recently TRPA1 has been also proposes to play a role in migraine pathophysiology. Thus, studies on rodents demonstrated that umbellulone (an agent known to trigger headache) evokes nociceptive behavior, meningeal vasodilation, and CGRP release through activation of TRPA1 [404]. Moreower, many identified TRPA1 agonists (like formaldehyde, ammonium chloride, cigarette smoke, and umbellulone) are chemical irritants, and they have long been known to trigger migraine headache in susceptible individuals [404–406].

Transient Receptor Potential Melastatin 8 (TRPM8) is activated by low temperatures (<26°C) and chemical cooling agents, including menthol and icilin. Until now the strongest evidence for a role of TRPM8 in migraine comes from three separate genome-wide association analyses, all of which identified that a TRPM8 gene variant (2q37.1, rs10166942) is associated with increased susceptibility to common migraine [407–409]. However, it is still to be identified how this gene variant alters channel expression or function if at all, and prove its causal relation to migraine [65].

Transient Receptor Potential Cation Channel V4 (TRPV4) is a mechanosensitive channel that is thought to be responsible for the trigeminal nociceptors activation by osmolarity changes. In awake animals dural application of hypotonic solutions acting on TRPV4 resulted in migraine related pain behavior, although the endogenous mechanism remains unclear [65]. There is no evidence for osmolarity changes before or during a migraine attack. Nevertheless, TRPV4 might be activated by mechanical stimulation (sudden intracranial pressure changes due to head jolts or rotation, breath holding, sneezing, coughing, etc). It is noteworthy that mechanosensitivity is most probably elevated during migraine attack, since mechanical stimulation such as rapid head movements and coughing can worsen headache pain in migraine patients [379]. One possible basis for such symptoms as well as for the throbbing pain sensation of migraine headache could be sensitization of TRPV4 [65], followed the release of inflammatory mediators in the meninges.

Transient Receptor Potential Cation Channel V1 (TRPV1)

The structure and function of TRPV1 channel and its relation to migraine pathophysiology were addressed in details in the section 2 of the introduction.

P2X Channels

ATP-activated P2X receptors and P2X3 receptors in particular have been widely implicated in pain conditions including migraine headache [31,65]. The structure and function of P2X3 channel and its relation to migraine pathophysiology were addressed in details in the section 1 of the introduction.

Calcium-Activated Potassium (BKCa or MaxiK) Channel

Large conductance calcium-activated potassium channels BKCa are widely expressed in the brain, including sensory neurons, both in soma, dendrites, and axonal terminals [410]. BKCa decrease presynaptic Ca2+ influx by narrowing the presynaptic action potential upon activation, resulting in reduced neurotransmitter release [411]. Thus, they might play an important role in modulation of pain transmission from the peripheral to the higher centers of CNS [65]. It was shown that activation of MaxiK channels can depress neuronal firing and presumably release of neurotransmitters from trigeminal neurons [412]. Mice with sensory neuron-specific knockout of MaxiK channels exhibited increased inflammatory, but not acute or neuropathic pain, suggesting their role in inflammatory pain conditions [413].

5.4 Migraine genetics

Insights into the genetic basis of migraine have come from different angles. First, linkage studies in family pedigrees in which inheritance of migraine is apparent have been used to identify genomic regions, and even particular genes, responsible for migraine susceptibility. Second, studies of migraine pathophysiology have led to proposals of candidate genes potentially involved in migraine [303].

Unbiased genome-wide association studies (GWAS) [407,408,414] and subsequent meta-analysis [414] have identified 13 migraine-associated variants pointing to genes that cluster in pathways for glutamatergic neurotransmission, synaptic development and plasticity, pain sensing, metalloproteinases, and vasculature and metabolism (Table 4).

5.5 Familial Hemiplegic Migraine

5.5.1 Classification and genetics

Familial hemiplegic migraine (FHM), a rare autosomal dominantly inherited subtype of migraine with aura, was first described by Clarke in 1910 in a UK family of 4 generations. Since then it has been the object of much interest by geneticists researching migraine [387], and it has led to FHM being the most extensively studied model for migraine [331]. FHM attacks typically include hemiparesis (half-side motor weakness) during the aura phase [415], but are otherwise indistinguishable from common forms of migraine and can be provoked by similar triggering factors; in two-third of FHM patients hemiplegic attacks might alternate with episodes of migraine without motor weakness [416,417]. The stronger genetic component and major phenotypic overlap of FHM with MA have made FHM an advantageous model to study the mechanisms of headache and aura [418].

Three causative genes have been identified for FHM: CACNA1A, ATP1A2 and SCNA1A, each gene associated with one of three familial forms of hemiplegic migraine, referred to as FHM1, FHM2, and FHM3, respectively (Table 5) [419]. All three genes encode ion-homoeostasis-regulating proteins that control neuronal activity via modulation of the availability of glutamate at synaptic terminals [331]. Although FHM-causing mutations target different genes, encoding proteins that are involved in different molecular pathways,

Table 4. Susceptibility genes for migraine with or without aura identified in genome-wide association studies (adapted from [331]).

	Chromosomal region	Gene	Description	Migraine subtype*	Study population	GWAS reference†
Glutamatergic neurotransmission						
rs1835740	8q22·1	*MTDH/AEG-1*	Astrocyte elevated gene-1 downregulates EAAT1/2, the main glutamate transporter in the brain	Migraine with aura	Clinic-based	Anttila and colleagues
rs11172113	12q13	*LRP1*	Lipoprotein receptor 1 interacts with glutamate (NMDA) receptors on neurons and modulates synaptic transmission	Migraine without aura	Population-based or clinic-based	Chasman and colleagues,Freilinger and colleagues,and Antilla and colleagues
rs3790455	1q22	*MEF2D*	Neuronal activity-dependent activation of the TF MEF2D restricts glutamatergic excitatory synapses	All migraine; migraine without aura	Population-based or clinic-based	Freilinger and colleagues and Antilla and colleagues
Synapse development and plasticity						
rs6478241	9q33	*ASTN2*	Member of astrotactin gene family involved in development of laminar structure of the cortex	All migraine	Clinic-based	Freilinger and colleagues and Antilla and colleagues
rs13208321	6q16	*FHL5*	Transcription factor regulating cAMP responsive CREM/CREB proteins that influence synaptic plasticity	Migraine without aura	Population-based or clinic-based	Antilla and colleagues
Pain sensing						
rs10166942	2q37	*TRPM8*	Member of the TRP superfamily acting as a sensor for cold pain, expressed in sensory neurons (mostly dorsal root ganglion neurons)	Migraine without aura	Population-based or clinic-based	Chasman and colleagues,Freilinger and colleagues,and Antilla and colleagues
Metalloproteinases						
rs10504861	8q21	near*MMP16*	Metalloproteinases remodel the extracellular matrix; the protein encoded by MMP16 also cleaves lipoprotein receptor	Migraine without aura	Population-based or clinic-based	Antilla and colleagues
rs10915437	1p36	near*AJAP1*	AJAP1 is involved in metalloproteinase activity structuring extracellular matrix	All migraine	Clinic-based	Antilla and colleagues
rs12134493	1p13	near*TSPAN2*	Member of the tetraspanin family, a cell surface protein implicated in cell motility and metalloproteinase activity	All migrain	Population-based or clinic-based	Antilla and colleagues
rs7640543	3p24	near*TGFBR2*	Serine-threonine kinase regulating cell differentiation and extracellular matrix production	All migraine	Clinic-based	Freilinger and colleagues and Antilla and colleagues
Vasculature and metabolism						
rs4379368	7p14	*C7orf10*	Mutations in this gene have been found in mild symptomatic forms of glutaric aciduria type III	Migraine without aura	Population-based or clinic-based	Antilla and colleagues
rs2651899	1p36	*PRDM16*	Transcription factor involved in brown fat development	All migraine	Population-based or clinic-based	Chasman and colleagues and Antilla and colleagues
rs9349379	6p24	*PHACTR1*	Phosphatase and actin regulator 1 promotes synapse morphology and is implicated in endothelial cell lining	Migraine without aura	Population-based or clinic-based	Freilinger and colleagues and Antilla and colleagues

For each pathway, the SNPs with the lowest p value mentioned in the initial GWAS are listed. *When applicable, associations specific for migraine with aura or migraine without aura are mentioned; associations to both types of migraine or which could not be linked to a specific subtype are referred to as all migraine. SNP=single nucleotide polymorphism. GWAS=genome-wide association studies. EAAT1/2=excitatory aminoacid transporters 1/2. CREM/CREB=cAMP response element/binding protein. TRP=transient receptor potential, TF=transcriptor factor.

clinically the phenotypes of the three FHMs are nearly identical. The seemingly diverging mechanisms ultimately converge and lead to the same neuronal profile: increased glutamate concentration in the synaptic cleft (Fig. 26). That in turn induces cerebral hyperexcitability and enhances susceptibility to cortical spreading depression [331]. FHM1 Cav2.1 CACNA1A gain-of-function mutations cause increased neuronal release of glutamate, while FHM2 Na+/K+-ATPase ATP1A2 loss-of-function mutations diminish glial cell reuptake of glutamate from the synaptic cleft. FHM3 NaV1.1 SCN1A loss-of-function mutations are predicted to cause increased activity of glutamatergic excitatory neurons via decreased GABAergic interneuronal inhibition [331,420,421].

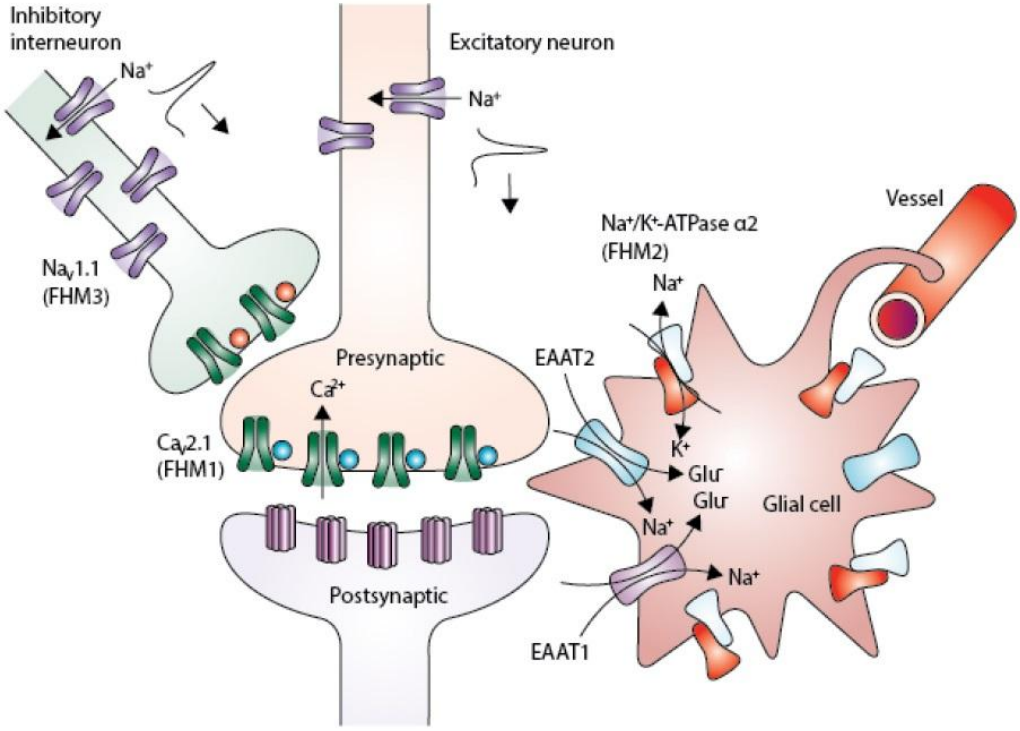

Figure 26. A common pathway for the effects of mutations in FHM genes (adapted from [331])
FHM – familial hemiplegic migraine; EAAT1 – excitatory amino acid transporter 1; EAAT2 – excitatory amino acid transporter 2.

Table 5. Familial Hemiplegic Migraine and Defective Genes Identified (adapted from [303]).

	Gene	Chromosome Location	Protein
FHM1 (MIM141500)	*CACNA1A*	19p13	Pore-forming α1 subunit of neuronal Ca2.1(P/Q type) voltage-gated calcium channels
FHM2 (MIM609634)	*ATP1A2*	1q23	Catalytic α2 subunit of a glial and neuronal sodium-potassium pump
FHM3 (MIM602481)	*SCN1A*	2q24	Pore forming α1 subunit of neuronal Na1.1 voltage-gated sodium channels

5.5.2 FHM1 pathophysiology

FHM1 is caused by missense mutations in the CACNA1A gene on chromosome 19p13 that encodes the pore-forming α1 subunit of neuronal voltage-gated P/Q-type (Cav2.1) calcium channel (Fig. 27) [387,422]. These channels are widely expressed at presynaptic terminals throughout the mammalian nervous system [423] and trigger neurotransmitter release in CNS synapses in response to neuronal excitation [424]. Cav2.1 channels are expressed in all brain structures that have been implicated in the pathogenesis of migraine, including the cerebral cortex, the trigeminal ganglia, and brainstem nuclei involved in the central control of nociception [386]. Cav2.1 channels were also found at somatodendritic membranes, where they can modulate neuronal excitability [425,426]. Fifteen different missense mutations in the CACNA1A gene have been associated with FHM. Some mutations cause pure FHM, whereas other add neurological symptoms such as ataxia or coma to the typical FHM profile [303,331].

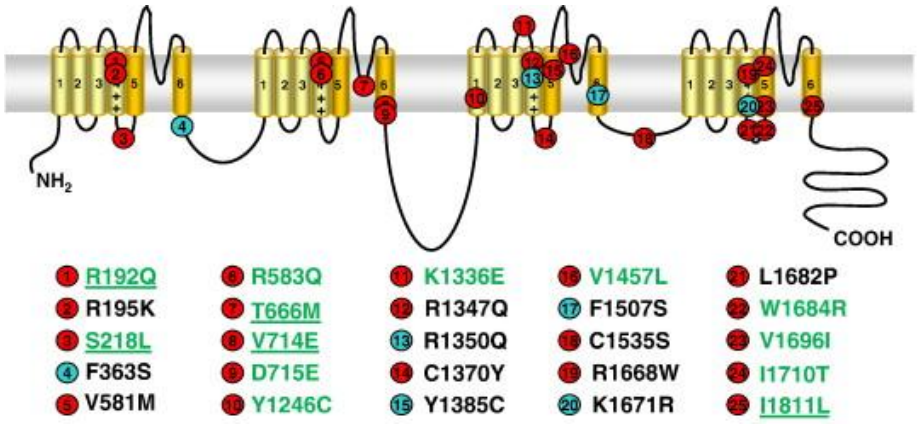

Figure 27. Mutations of α1 subunit of P/Q-type voltage gated calcium channel responsible for FHM-1 (adapted from [389]).

Mutant FHM1 Cav2.1 channels show gain-of-function because of increased probability of being open and shifted activation to lower voltages [427–431]. Thus, FHM1 neurons expressing Cav2.1 channels possess higher basal calcium concentration [432]. Not all neurons carrying Cav2.1 channels are equally affected by FHM1 mutations. Experiments on autapses and brain slices reveal that, while Cav2.1 channel-mediated excitatory neurotransmission in FHM1 neurons is enhanced due to increased glutamate release, Cav2.1 channel-mediated inhibitory neurotransmission at cortical interneuronal synapses is apparently unaltered [433]. As a result, the final effect of FHM1 mutations is enhanced glutamatergic excitatory activity without apparent compensatory GABA-ergic interneuronal inhibition (Fig. 28).

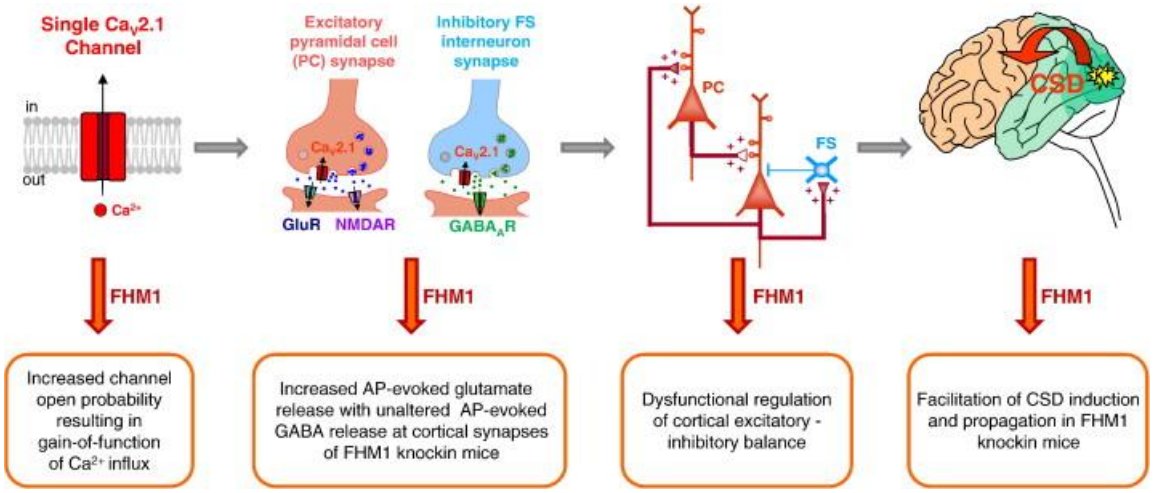

Figure 28. Functional alterations in the cerebral cortex of a familial hemiplegic migraine type 1 (FHM1) knockin mouse model (adapted from [389]).

Another important feature of FHM1 mice is their higher susceptibility to cortical spreading depression as a result of higher glutamate release [331,433]. Indeed, experiments show lower threshold for in vivo induction of cortical spreading depression by KCl application or cortical electrical stimulation in FHM1 mice, along with increased frequency and propagation velocity of cortical spreading depression (van den [429,430,434].

In the trigeminal ganglion, analysis of the P/Q-type Ca current in small TG neurons from adult R192Q KI mice showed gain-of-function only of the Cav2.1 channels in capsaicin-insensitive TG neurons expressing T-type Ca channels (CI-T neurons), but not of capsaicin-sensitive TG neurons (CS neurons) that innervate the dura [435] (Fig. 29).

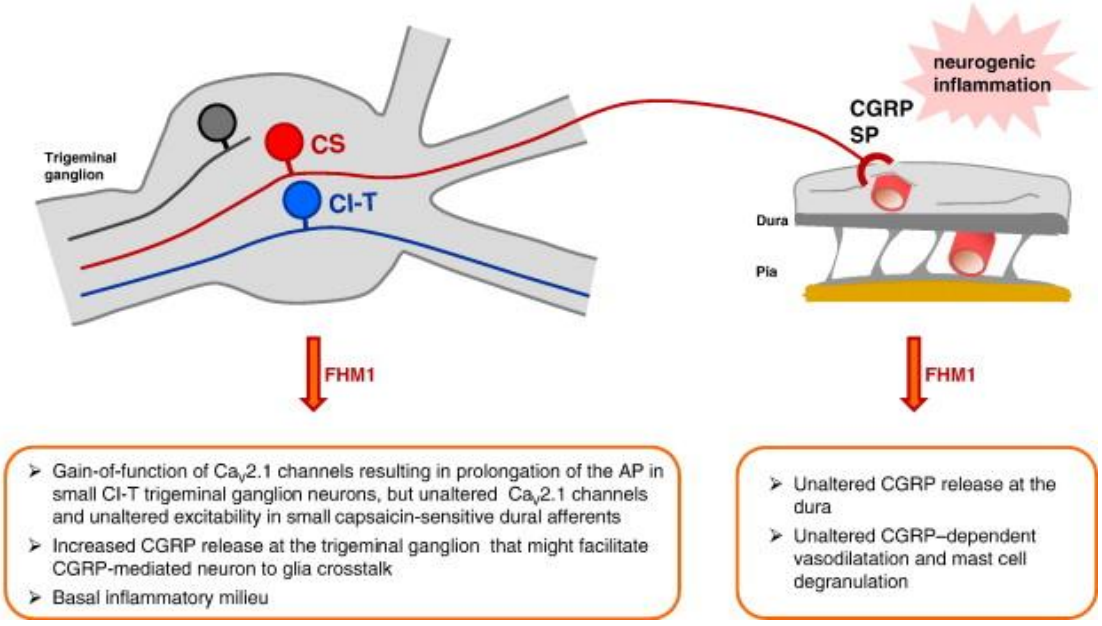

Figure 29. Functional alterations in trigeminal ganglion neurons of an FHM1 knockin mouse model (adapted from [389]).

Investigations into the actual intracellular Ca2 levels demonstrated that a significant number of KI neurons display substantially larger Ca2 transients inhibited by the selective blocker ω–agatoxin, suggesting upregulated Cav2.1 channels (Nair et al 2010). The FHM1 mutation increases evoked CGRP release from intact trigeminal ganglia [435] and cultured TG neurons [436]. Elevated CGRP levels in R192Q KI migraine-model TG in turn was reported to upregulate P2X3 receptors (Fig. 30) via increased gene expression and trafficking through PKA/PKC dependent mechanism [31,60,64]. Additionally, enhanced P2X3 currents were associated with decreased serine phosphorylation, higher immunoreactivity for active phosphorylated CaMKII in R192Q KI mice compared to WT [64] and higher neuronal excitability in response to P2X3 receptor activation [66]. CGRP is also an important messenger in the neuron-neuron and neuron-satellite glial cells crosstalk; it increases expression of inflammatory genes and release of inflammatory mediators from satellite glial cells, that in turn can sensitise TG neurons and further activate glial cells, maintaining an inflammatory milieu in TG [68,389,437,438]. Experiments with TG cell cultures reveal enhanced basal release of TNFα and stronger basal activation of macrophages in R192Q KI trigeminal neurons [439,440]. On the basis of these findings, it has been suggested that FHM1 mutations create a basal inflammatory milieu within the trigeminal ganglion and facilitate peripheral sensitization contributing to the development of pathological profile typical for FHM1 [64,389,439,440].

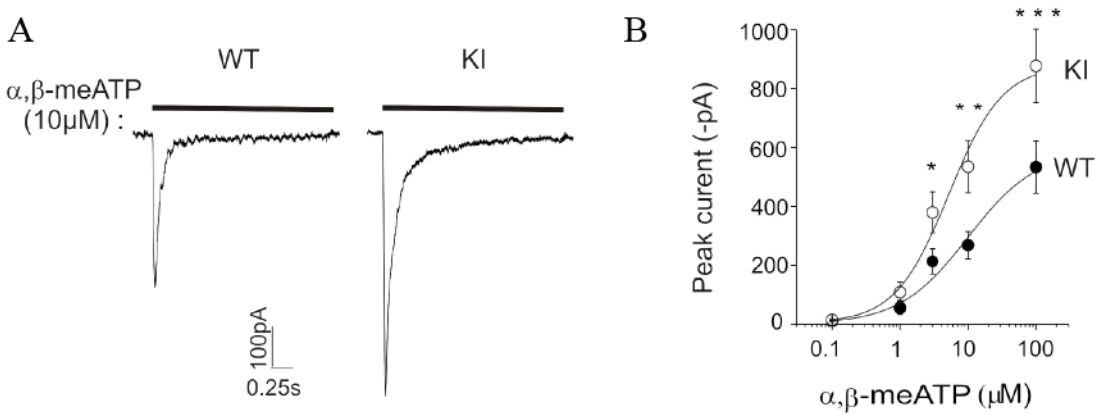

Figure 30. Upregulated P2X3 currents in R192Q KI trigeminal neurons in culture (adapted from [64]). A, Representative traces of αβ-meATP-induced responses of WT and KI neurons. B, Plot showing P2X3 current amplitudes in response to different α,β-meATP in WT and KI neurons.

5.5.3 FHM1 as a model for common migraine

Genetically modified mice have been engineered based on mutations in the three specific genes responsible for FHM with the goal to shed light on the pathophysiology of common migraine [303,331]. Despite the large number of mutations characterized at each FHM locus, only a small fraction of mutations have been studied in genetically altered mice given the expense and time involved in generating modified animals [303].

FHM1 has been used as a model to identify possible pathways for the more common forms of migraine with aura and migraine without aura. The question remains whether and to what extent mechanisms identified for FHM1 are also involved in non-hemiplegic migraine. Migraine is phenotypically and genetically heterogeneous and no single variant can explain the entire underlying genetic component across different families and populations [303]. However, there is growing, albeit circumstantial, evidence that FHM-like mechanisms might also be involved in patients with non-hemiplegic migraine with aura or non-hemiplegic migraine without aura, including evidence obtain from humans. Among them are the phenomenon of enhanced cortical spreading depression susceptibility of transgenic FHM1 mice, increased glutamatergic neurotransmission and cerebral hyperexcitability [331]. Moreover, resemblance of FHM1 clinical profile to that of common migraine is another reason to support the idea of potential similarity between the mechanisms underlying these pathologies.

Two common FHM1 mutations in the CACNA1A gene have been introduced in knock-in mice: R192Q [429,433] and S218L [430,441]. While both mutations cause gain-of-function of P/Q-type Ca2+ channel, the phenotype of S218L mutation is more extreme than R192Q and mice exhibit symptoms of cerebellar ataxia, seizure and head trauma and in particular increased sensitivity to CSD [430].

R192Q KI mouse model of FHM1

The FHM1 mouse model used in the present study is based on the KI R192Q mutation in theCACNA1A gene and was first introduced by van den Maagdenberg et al. in 2004 [429]. Functional analysis revealed a pure gain-of-function effect on P/Q type Ca2+ channel current and increased action potential-evoked Ca2+ influx and glutamate release [431] in R192Q KI mice. Moreover, R192Q mutation reduces threshold and increases propagation velocity of cortical spreading depression [421,429]. Chanda et al [442] recently reported pain like symptoms similar to episodic attacks of migraine in R192Q KI mice.

Further investigation of the R192Q mouse phenotype and its deviations from the WT phenotype may explain the underlying mechanism for the increased susceptibility of the migraine brain for CSD and aura and in general for migraine pathophysiology, thereby providing new directions for future therapy.

Aims of the study

Trigeminal sensory neurons play a crucial role in nociception, processing and transducing noxious stimuli from periphery to higher brain regions under normal conditions as well as in pathological pain states including migraine [303,323,324]. A variety of neuromodulators control different aspects of trigeminal neurons' functioning [349,350,361]. In particular, many of them regulate activity of certain membrane ion channels, involved in nociception, such as ATP-gated P2X3 receptors and capsaicin-sensitive TRPV1 receptors [65,348,369,370]. That in turn can cause changes in neuronal excitability [66,348]. Most known modulators of P2X3 and TRPV1 receptors positively affect these receptors activity and very little is known about their negative regulation. However, recent evidence brought to light natriuretic peptides as potential regulators of sensory neuron nociceptive transmission [270]. Brain natriuretic peptide in particular was suggested to play an inhibitory role in inflammatory pain [271]. Collectively these data prompted the present project to investigate the following aspects of BNP system in sensory trigeminal cultures of WT mice and transgenic R192Q KI mice of the familial hemiplegic migraine type 1 model:

- Expression of BNP and its receptor NPR-A in trigeminal cultures *in vivo* and *in vitro* and functional properties of BNP/NPR-A pathway in WT and KI mice
- Effects of endogenous and exogenous BNP on P2X3 and TRPV1 receptors activity in WT and KI trigeminal neurons
- Molecular mechanisms underlying BNP/NPR-A-dependent modulation of P2X3 receptors, in particular in terms of receptor's membrane distribution and serine phosphorylation in WT mice
- Effects of BNP/NPR-A system on the excitability of small to medium sized trigeminal sensory neurons in WT and KI
- Evaluation of new synthetic compounds as potential P2X3 antagonists on recombinant P2X3 receptors in HEK cells and native P2X3 receptors of trigeminal neurons

Methods and results

1. B-type natriuretic peptide-induced delayed modulation of TRPV1 and P2X3 receptors of mouse trigeminal sensory neurons.

OPEN ACCESS Freely available online

PLOS ONE

B-Type Natriuretic Peptide-Induced Delayed Modulation of TRPV1 and P2X3 Receptors of Mouse Trigeminal Sensory Neurons

Sandra Vilotti[☒], **Anna Marchenkova**[☒], **Niels Ntamati, Andrea Nistri***

Neuroscience Department, International School for Advanced Studies (SISSA), Trieste, Italy

Abstract

Important pain transducers of noxious stimuli are small- and medium-diameter sensory neurons that express transient receptor vanilloid-1 (TRPV1) channels and/or adenosine triphosphate (ATP)-gated P2X3 receptors whose activity is upregulated by endogenous neuropeptides in acute and chronic pain models. Little is known about the role of endogenous modulators in restraining the expression and function of TRPV1 and P2X3 receptors. In dorsal root ganglia, evidence supports the involvement of the natriuretic peptide system in the modulation of nociceptive transmission especially via the B-type natriuretic peptide (BNP) that activates the natriuretic peptide receptor-A (NPR-A) to downregulate sensory neuron excitability. Since the role of BNP in trigeminal ganglia (TG) is unclear, we investigated the expression of BNP in mouse TG in situ or in primary cultures and its effect on P2X3 and TRPV1 receptors of patch-clamped cultured neurons. Against scant expression of BNP, almost all neurons expressed NPR-A at membrane level. While BNP rapidly increased cGMP production and Akt kinase phosphorylation, there was no early change in passive neuronal properties or responses to capsaicin, α,β-meATP or GABA. Nonetheless, 24 h application of BNP depressed TRPV1 mediated currents (an effect blocked by the NPR-A antagonist anantin) without changing responses to α,β-meATP or GABA. Anantin alone decreased basal cGMP production and enhanced control α,β-meATP-evoked responses, implying constitutive regulation of P2X3 receptors by ambient BNP. These data suggest a slow modulatory action by BNP on TRPV1 and P2X3 receptors outlining the role of this peptide as a negative regulator of trigeminal sensory neuron excitability to nociceptive stimuli.

Citation: Vilotti S, Marchenkova A, Ntamati N, Nistri A (2013) B-Type Natriuretic Peptide-Induced Delayed Modulation of TRPV1 and P2X3 Receptors of Mouse Trigeminal Sensory Neurons. PLoS ONE 8(11): e81138. doi:10.1371/journal.pone.0081138

Editor: Steven Barnes, Dalhousie University, Canada

Received July 1, 2013; **Accepted** October 18, 2013; **Published** November 27, 2013

Funding: The financial support of Telethon-Italy (Grant no. GGP10082) is gratefully acknowledged. This work was also supported by the TransReg grant (MINA) from the Friuli Venezia Giulia Region and by the Cariplo Foundation Grant no. 2011-0505. The funders had no role in study design, data collection and analysis, decision to publish, or preparation of the manuscript.

Competing interests: The authors have declared that no competing interests exist.

* E-mail: nistri@sissa.it

☒ These authors contributed equally to this work.

Introduction

Sensory inputs, including painful and tissue-damaging stimuli, are conveyed from the periphery to the central nervous system through primary afferent neurons located in the trigeminal ganglia (TG) and dorsal root ganglia (DRG). Small- and medium-diameter sensory neurons (nociceptors) express, amongst a range of membrane proteins detecting noxious stimuli, capsaicin (and heat)-sensitive transient receptor potential vanilloid-1 (TRPV1) channels and/or adenosine triphosphate (ATP)-gated P2X3 subunit-containing receptors [1,2] to transduce pain. In particular, several studies have demonstrated TRPV1 to be essential for the development of inflammatory thermal pain conditions [3–5]. Among ATP-gated P2X receptors, the P2X3 receptors are almost exclusively expressed by sensory ganglion neurons [6,7] and have been implicated in craniofacial pain [8,9], including migraine [10]. The activity of TRPV1 and P2X3 receptors is known to be upregulated by endogenous peptides, like bradykinin, CGRP or substance P [11–15], and trophic factors like NGF and BDNF [16–18]. Thus, the functional action of such modulators is manifested as sensitization of these receptors, thereby contributing to lowering pain threshold and to triggering pain, especially of chronic nature. In this sense, their role on trigeminal sensory neurons as facilitators of migraine pain has been proposed [14,19–21]. As recently reviewed [22,23], clinical studies have confirmed that P2X3 and TRPV1 receptors mediate pain induced by distinct stimuli in man.

Less is known about the potential role of endogenous modulators in restraining the expression and function of TRPV1 and P2X3 receptors. Recent evidence supports a potential involvement of the natriuretic peptide system in the modulation

of sensory neuron nociceptive transmission [24–27]. Natriuretic peptides (NPs) are a family of structurally related paracrine factors, namely atrial NP (ANP), B-type NP (BNP), also known as brain natriuretic peptide, and C-type NP (CNP) [28]. ANP administration does not affect sensitivity to radiant heat [29] or mechanical allodynia [26,27], while CNP is proposed as a positive modulator of chronic pain [24]. Conversely, microarray gene profiling has indicated that chronic pain enhances BNP and its natriuretic peptide receptor-A (NPR-A) in rat DRG. Moreover, BNP application reduces the excitability of DRG nociceptors and the hyperalgesic response in a rat model of inflammatory pain. This led to the suggestion that BNP may play an inhibitory role in chronic pain [25]. BNP acts through binding to NPR-A, which is a guanylyl cyclase receptor (also sensitive to ANP), and increases intracellular cGMP levels [30,31].

While all NPRs have been identified in brainstem trigeminal nuclei [32–34], little is known about the possible role of the natriuretic peptide system at TG level where nociceptive signals are transduced [35–37]. A recent clinical report has shown that BNP levels are raised in the jugular vein blood during a migraine attack [38]. We have developed an in vitro model system using primary cultures of mouse TG to investigate the cellular mechanisms regulating the expression and function of P2X3 and TRPV1 receptors [18,39]. Hence, the present study was initiated to characterize BNP and NPR-A expression in the mouse TG and to examine whether the BNP/NPR-A system may modulate TRPV1 and P2X3 nociceptor activity.

Results

BNP and NPR-A are expressed *in vivo* in adult mouse TG

Gene expression of BNP and its receptor NPR-A investigated by RT-PCR indicated weakly positive BNP and strongly positive NPR-A bands of the expected size (199 bp and 200 bp respectively; Figure 1 A). We next examined with Western blot analysis if NPR-A protein was synthesized. The NPR-A antibody recognized a single band of the expected size (approximately 140 kDa) in mouse TG homogenates, corresponding to the NPR-A protein. Conversely, BNP expression was below detection. Thus, BNP expression was evaluated by ELISA assay. Mouse BNP concentrations in tissue extracts from entire TG and in the serum were 1.12 ± 0.34 pg/mg protein and 185.2 ± 47 pg/ml, respectively (n=6 mice). Western blot analysis confirmed that NPR-A receptor was synthesized both in adult (P30) and in younger (P12) animal TG (Figure 1 B). Thus, the properties of this peptide could be investigated with younger tissues as well, a convenient preparation for primary culture studies.

The distribution of NPR-A and BNP in mouse TG was further examined by immunohistochemistry. We found that NPR-A was expressed in most neurons, as shown by co-localization with β-tubulin III (Figure 1 C). NPR-A immunoreactivity could not be detected in other cell types. Further observations (Figure S1 A) confirmed that the NPR-A staining appeared colocalized with TRPV1 and P2X3 immunopositive neurons. Unlike the data concerning its receptor, BNP immunopositive cells were few and scattered elements, in which the peptide staining appeared as small perinuclear granules (0.9 ± 0.4% of total ganglion cells, n=3) (Figure 1 D). The few BNP-immunoreactive cells seldom showed neuron-like morphology.

Characterization of BNP and NPR-A in TG primary cultures

In order to examine the characteristics of BNP effects on TG cells, we used TG primary cultures as previously reported [18,39]. Consistent with our results from tissue sections, double immunostaining for NPR-A and the neuronal marker β-tubulin III showed that *in vitro* the receptor was expressed exclusively by neurons (Figure 2 A). Figure 2 B summarizes the distribution of NPR-A immunoreactivity in relation to the neuronal cell body size which was the highest in neurons with somatic diameter between 12 and 25 μm, consistent with the higher prevalence of small and medium sized neurons in TG [18]. Systematic cell counting indicated that the vast majority of β-tubulin III-positive cells expressed NPR-A (91.3 ± 1.1%, n=10), confirming the extensive colocalization of the two proteins already observed *in vivo*. Western blot analysis with biotinylation method validated the expression and membrane localization of NPR-A (Figure 2 C).

Immunocytochemistry revealed the scant presence of BNP-positive cells also in TG primary cultures, as they accounted for only 2.0 ± 0.2% of the total cell population in our cultures (n=12). The morphology of these cells appeared prevalently non-neuronal (Figure 2 D, left), although rare neuron-like cells were observed as well (Figure 2 D, right). We also estimated (with ELISA assay) the concentration of BNP in primary cultures and in their medium that was found to be 1.1±0.4 pg/mg and 4.9±2.6 ng/ml, respectively (n=8 mice).

Functional assays of NPR-A

We sought to understand whether the large expression of membrane bound NPR-A was actually indicative of a functional receptor system. To this end, since activation of NPR-A by ANP and BNP has been shown to increase intracellular cGMP production [40], we investigated if application of BNP to mouse TG cultures could increase intracellular cGMP production, as determined by ELISA. Figure 3 A shows that application of 100 or 500 ng/ml BNP (compared to the vehicle control treatment) increase the mean cGMP levels in a concentration- and time-related fashion. In fact, the cGMP rise was already detectable after 5 min and reached its peak after 30 min with a late (1 h) decline. The greatest increment was observed after 30 min application of 500 ng/ml BNP. Even 100 ng/ml BNP was sufficient to activate the NPR-A mediated pathways by significantly increasing cGMP by almost 2-fold compared to basal levels. This effect was prevented by the application of 500 nM anantin, a specific antagonist of NPR-A [41,42], that completely inhibited the elevation of cGMP levels. A lower anantin concentration (100 nM) failed to produce significant antagonism of BNP-elicited rise in cGMP (Figure 3 A). It is noteworthy that anantin (500 nM) per se significantly decreased the basal level of cGMP.

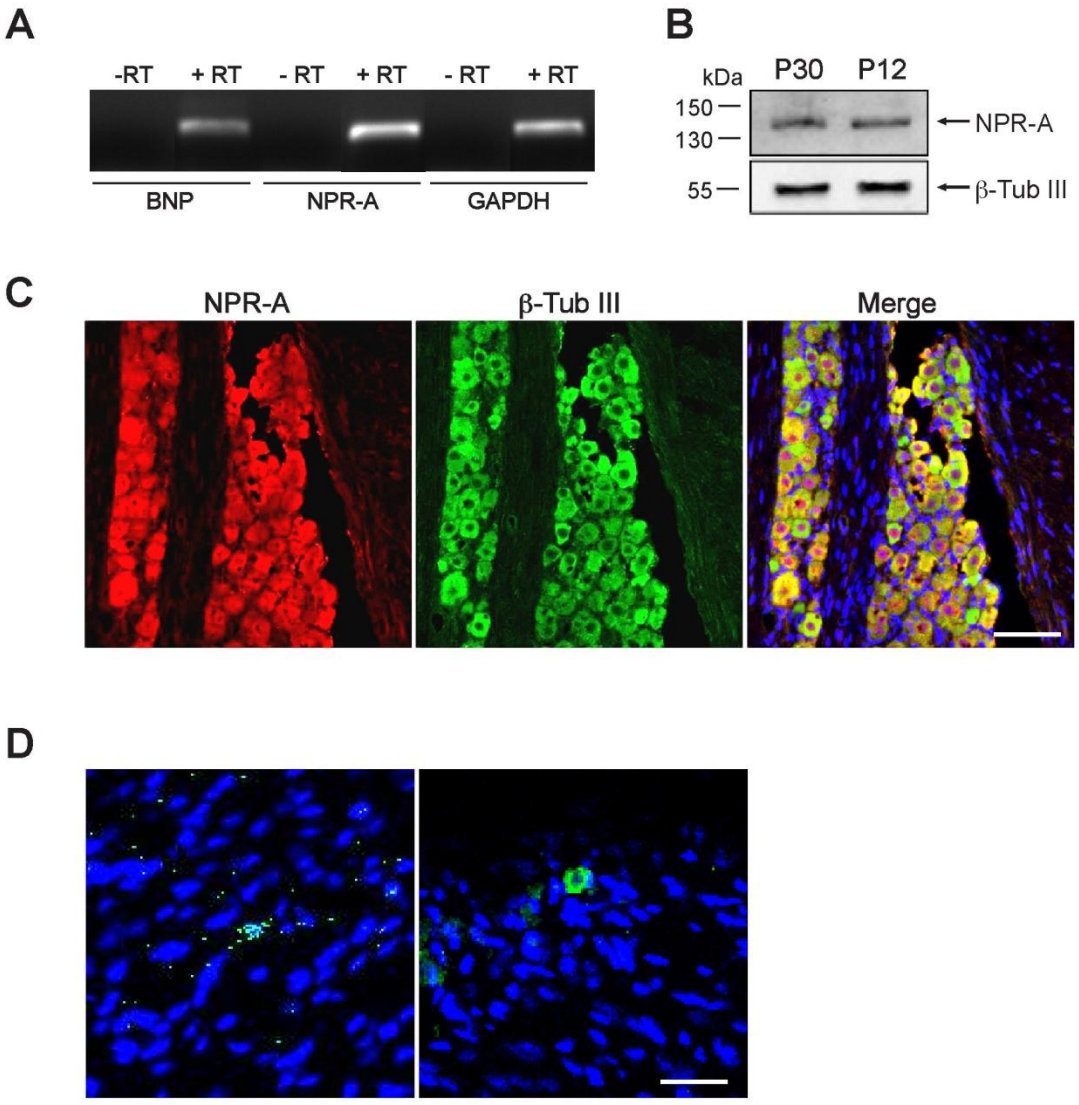

Figure 1. Expression of BNP and NPR-A in adult mouse TG *in vivo*. A, PCR products (amplified with 40 cycles) identified by ethidium bromide staining show RT-PCR amplification of BNP and NPR-A mRNA (+RT), as well as of the housekeeping gene GAPDH. Negative control reactions for retrotranscription (-RT) do not show any bands. B, Chemiluminescence image of Western blot showing protein expression of NPR-A in TG from P30 and P12 mice. β-Tubulin III was used as a loading control. C, Example of confocal microscopy images showing the widespread colocalization of immunostaining for NPR-A (red) and β-tubulin III (green). Cell nuclei are visualized with DAPI staining (blue). Scale bar, 100 μm. D, Representative confocal images of longitudinal sections of adult TG. Immunohistochemistry reveals BNP-immunoreactive granules around few nuclei (DAPI). Among these cells, most possess non-neuronal morphology (left panel); neuron-like cells are rarely immunostained (right panel). Scale bar, 30 μm.
doi: 10.1371/journal.pone.0081138.g001

One important intracellular effect of NPR-A activation is phosphorylation of Akt that occurs downstream of cGMP synthesis [43]. We tested whether this phenomenon could be also observed in TG cultures. Figure 3 B shows that after 10 or 30 min application of 500 ng/ml BNP, there was a significant increase in Akt phosphorylation, an effect fully blocked by 500

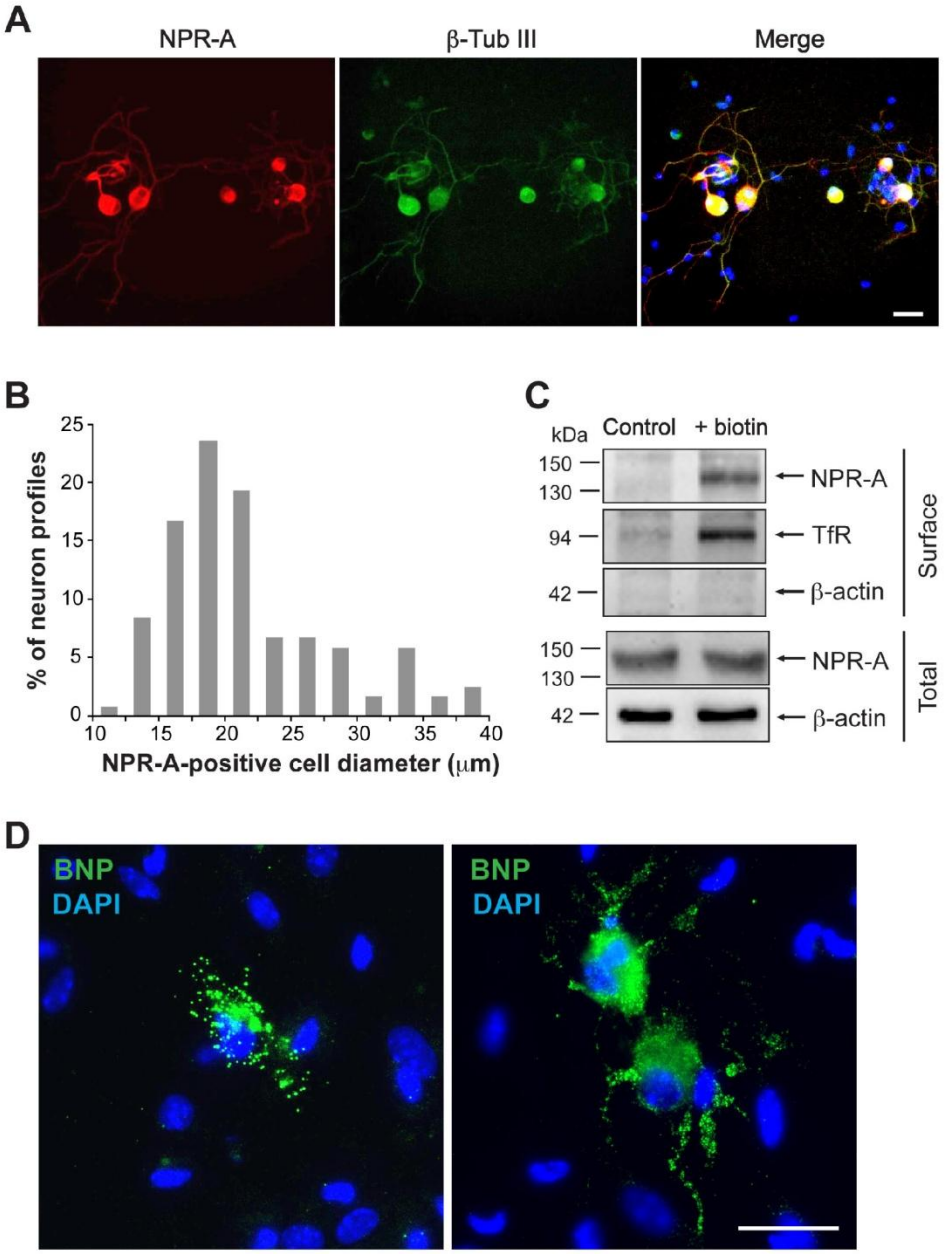

Figure 2. BNP and NPR-A are expressed in mouse TG cultures. A, Immunocytochemical analysis of NPR-A (red) and β-tubulin (green) in mouse TG culture. Nuclei are visualized with DAPI (blue). Merge image (right) indicates extensive co-staining. Scale bar, 30 μm. B, Somatic size distribution of NPR-A-positive TG neurons. Data represent 119 NPR-A-positive neurons from 4 independent experiments. C, Example of Western immunoblotting (representative of three experiments) showing the surface (obtained after membrane biotinylation) and total expression of NPR-A in TG culture. β-Actin was used as loadingcontrol of the total extract. TfR is the marker for correct biotinylation. D, Immunostaining for BNP (green) is mostly restricted to few cells with non-neuronal morphology that display perinuclear immunoreactive granules (left panel). More rarely, some neuron-like cells are also stained for BNP with granules extending along their processes (right panel). Nuclei are visualized with DAPI staining (blue). Scale bar, 30 μm.

doi: 10.1371/journal.pone.0081138.g002

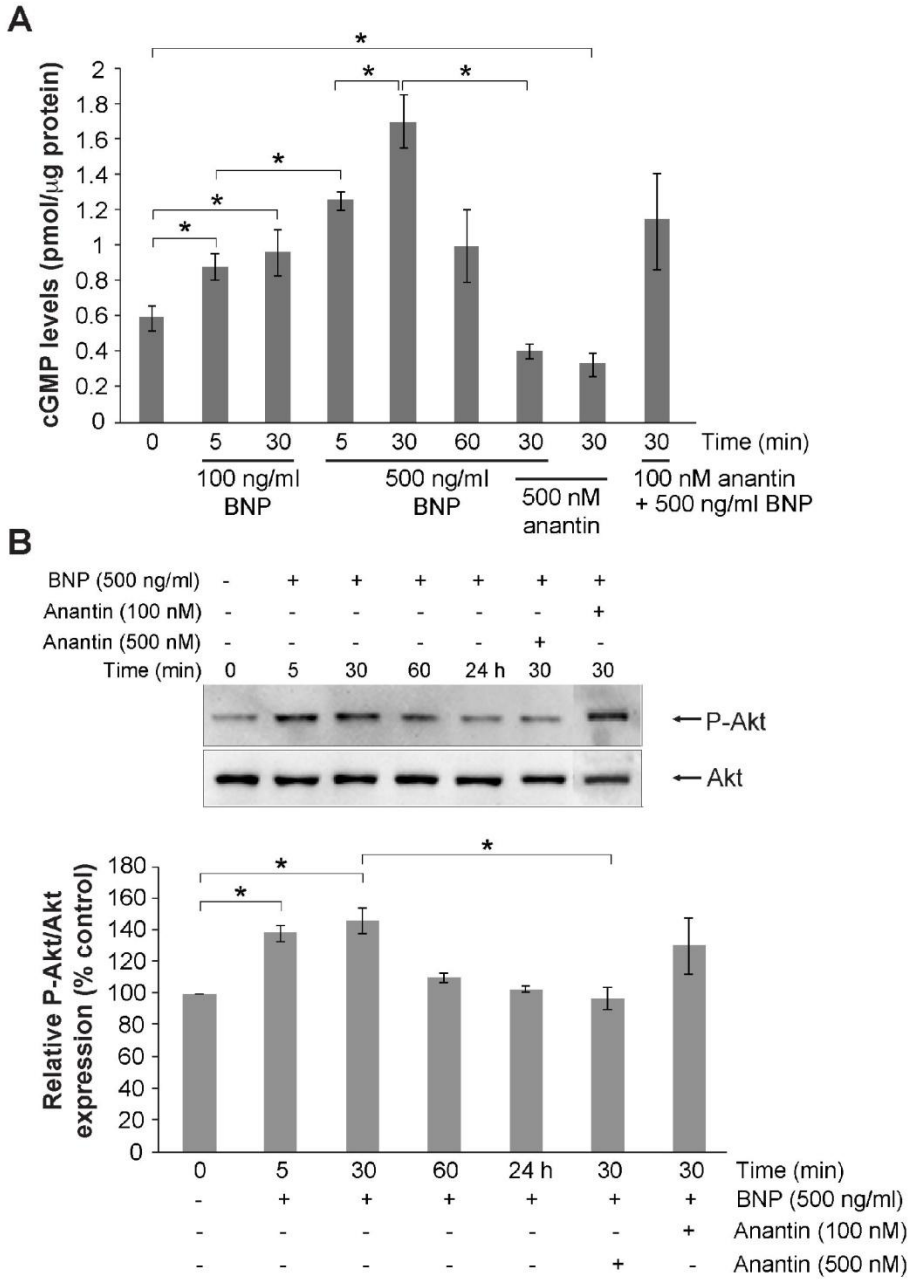

Figure 3. cGMP production by mouse TG cultures. A, ELISA-based quantification of intracellular cGMP in primary cultures from P12 mice. Cultures were treated with BNP (100 or 500 ng/ml for 5, 10 or 30 min) and/or anantin (100 and 500 nM, 30 min), or treated with vehicle (indicated as 0). Note large rise in cGMP that declines at 60 min; anantin alone (500 nM) decreases basal cGMP. Data were normalized to the total protein content in each sample and are presented as mean value ± SEM (n=3). *p≤0.05. B (top), example of western blot of Akt phosphorylation induced by BNP (500 ng/ml) applied alone or together with anantin (100 and 500 nM) for various times as indicated. Bottom histograms quantify these data from at least 3 experiments, demonstrating early and transient increment in P-Akt expression.

doi: 10.1371/journal.pone.0081138.g003

nM anantin, yet insensitive to 100 nM antagonist concentration. It was of interest that the increment in Akt phosphorylation was not sustained as it declined at 30 min and disappeared 24 h later (Figure 3 B).

These experiments, thus, demonstrated that functional NPR-A receptors were found in TG cultures despite the poor expression of BNP. We wondered if activation of these receptors could be translated into changes in the activity of ligand-gated neuronal channels considered to be important transducers of nociceptive signals. For this purpose, we studied how BNP application could affect electrophysiological responses mediated by P2X3 or TRPV1 channels.

Effect of BNP on P2X3 and TRPV1 receptors

Patch clamp experiments were run to test whether short or long term application of 100 ng/ml BNP could change responses evoked by α,β-meATP (10 μM) or capsaicin (1 μM) to activate P2X3 or TRPV1 receptors, respectively [18]. As a reference, we also tested the inward, Cl^- mediated currents generated by GABA (10 μM) via activation of $GABA_A$ receptors [44,45]. Only one concentration of BNP (100 ng/ml) was used for electrophysiological experiments, since we had shown it to be sufficient to activate NPR-A-mediated pathways and to increase significantly cGMP levels (Figure 3 A); the same BNP concentration was also used in previous studies, showing its effectiveness on DRG neurons [25].

Figure 4 A shows that continuous superfusion with BNP (100 ng/ml for 10 min) did not change sample responses to these three ligands. Furthermore, BNP did not change cell input resistance (528±50 MΩ in control versus 552±57 MΩ in the presence of BNP; n=28) or baseline current (84±15 versus 79±11 pA before and after BNP, respectively; n= 28). Preincubating cultures for 2 h with 100 ng/ml BNP also failed to alter the responses mediated by P2X3, $GABA_A$ or TRPV1 receptors (Figure 4 B). Nonetheless, 24 h application of 100 ng/ml BNP significantly and selectively depressed the currents evoked by 1 μM capsaicin (Figure 5 A, see arrows). This effect was also observed for other capsaicin concentrations (0.1 μM, 0.5 and 5 μM; see Figure 5 B) as the dose/response plot was shifted downwards after chronic application of BNP.

We next explored whether this slow action by BNP could be attributed to the consequence of NPR-A receptor activation followed by a rather slow series of events culminating in TRPV1 channel modulation. Should this hypothesis be correct, the effects of BNP ought to be suppressed by the selective antagonist of NPR-A anantin [32,41,42]. Thus, we first validated the use of anantin, that, when applied alone at 500 nM (to ensure a complete blockage of NPR-A; Figure 3 A, B), did not change control responses to capsaicin α,β-meATP. Figure S1 B shows that preapplication of anantin (500 nM; 10 min) failed to change P2X3 receptor responses. Likewise, responses evoked by capsaicin (1 μM) were 11.9±4.3 pA/pF (n=6), a value not significantly different from the one observed after anantin (9.5±5.1 pA/pF, n=4), suggesting no direct channel modulation by anantin.

Figure 5 C shows that the inhibitory effect on TRPV1 receptors seen after 24 h application of BNP was fully prevented by concomitant administration of 500 nM anantin (that per se had no effect on capsaicin-induced responses even when chronically applied). No significant change in P2X3 receptor-mediated currents was present after 24 h BNP application (Figure 5 D). It was, however, interesting to observe that anantin (500 nM; 24 h) per se enhanced responses to α,β-meATP (10 μM), that were almost twice (196 %) their controls (Figure 5 E). This effect was detected at various agonist concentrations as the α,β-meATP dose-response curve was shifted leftwards without significant change in the maximum response amplitude (Figure 5 F). When anantin plus BNP were continuously co-applied for 24 h, the potentiation of the P2X3 receptor currents persisted (Figure 5 E). Figure 5 G shows that 24 h application of BNP (100 ng/ml) or anantin (500 nM) did not change the expression level of either TRPV1 or P2X3 receptors. Finally, we did not find any change in GABA-mediated currents after applying BNP, or anantin, or their combination (Figure 5 H, I).

Although short-term BNP and/or anantin application was sufficient to produce fast changes in cGMP levels or Akt phosphorylation, modulation of TRPV1 or P2X3 currents appeared only after 24 h of BNP and/or anantin exposure. Thus, we wondered if even a short BNP or anantin treatment could trigger a very delayed receptor modulation. For this, we applied BNP (100 ng/ml) or anantin (500 nM) for 1 h only and, after overnight wash, patch-clamping was performed. With this protocol, the effects of BNP and anantin on TRPV1 or P2X3 currents were no longer observed (Figure S2).

Discussion

The principal result of our study is the novel demonstration of widespread expression of functional NPR-A receptors in mouse TG neurons (against a modest expression of BNP), and their ability to modulate TRPV1 and P2X3 receptor activity with a characteristically delayed timecourse. Thus, these data outline a new downregulation by the BNP system of the two major nociceptive signal transducers [1-5] of TG sensory neurons.

The influence of the natriuretic peptide system on nociception has only recently come to light. A study by Zhang and colleagues [25] has shown, in control conditions, high levels of BNP and low expression of NPR-A in the rat DRG. In our experiments with *in vivo* and *in vitro* mouse TG tissue, we found a different phenomenon, namely low BNP presence and almost universal neuronal expression of NPR-A, that, with biotinylation experiments, was demonstrated to be localized at membrane level.

The cellular distribution of BNP and NPR-A was well preserved *in vitro*, indicating that TG cultures could represent a suitable model to explore the BNP mode of action. It is noteworthy that, while the NPR-A expression was exclusively neuronal and included virtually all somatic sizes, the expression of BNP could be detected in a few non-neuronal cells, alluding to a role of this peptide in the growing family of neuropeptides involved in neuron/non-neuronal cell crosstalk at ganglion level [19,20]. The scant occurrence of BNP immunopositive cells could not be attributed to an artifact of the histological procedure as lack of signal was noted even with freshly frozen sections of the trigeminal ganglion. Some

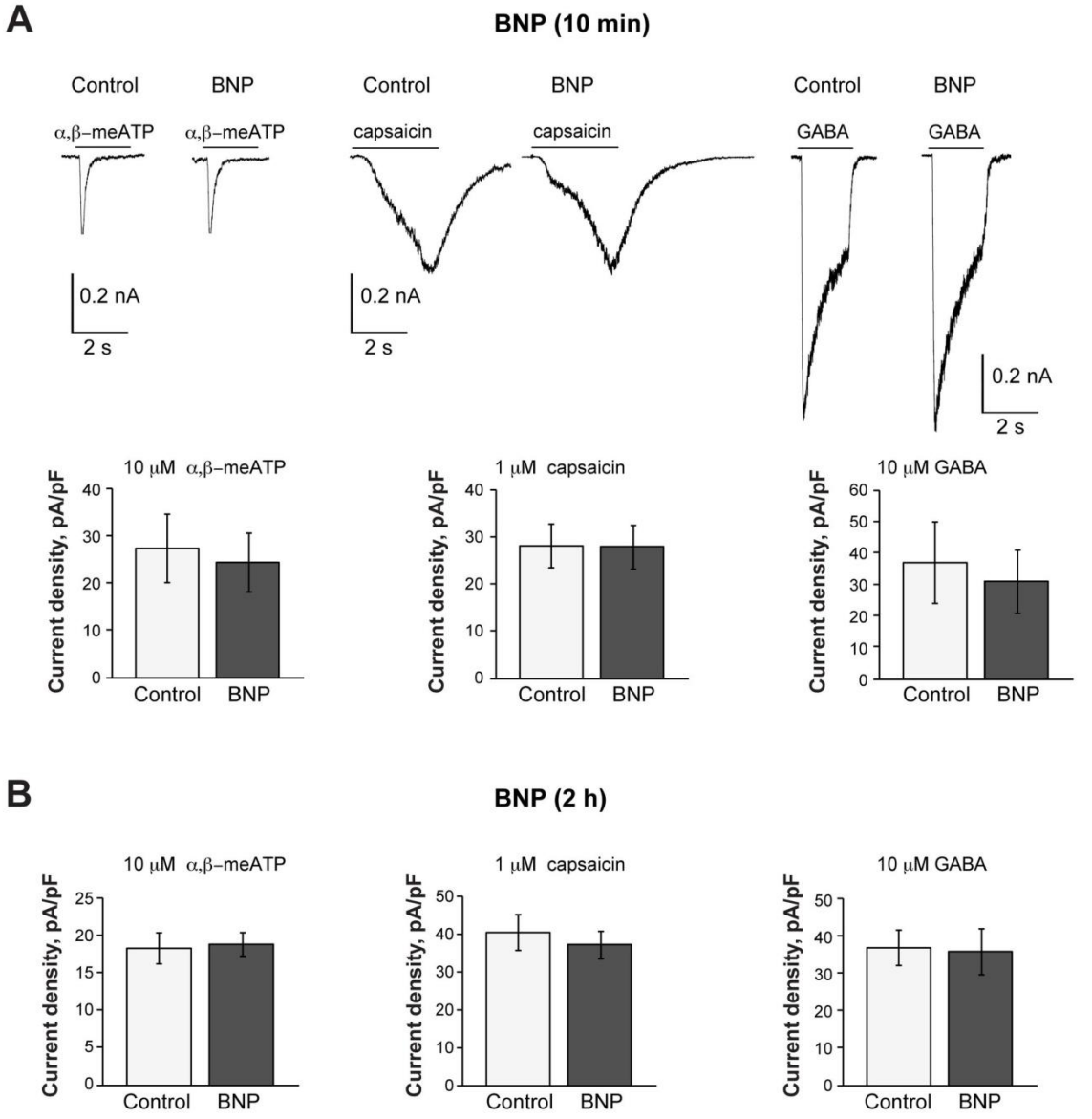

Figure 4. Ten min or 2 h BNP application does not affect capsaicin-, α,β-meATP- or GABA-mediated responses. A, Representative traces of currents induced by pulse application of α,β-meATP (10 μM, 2 s), capsaicin (1 μM, 3 s), or GABA (10 μM, 2 s) to TG neurons in control conditions or after application of BNP (100 ng/ml, 10 min) to the same cells. Histograms show average current density values of P2X3, TRPV1 or GABA-mediated responses (n=12, 12, 11, respectively). B, Histograms show average current density values of P2X3, TRPV1 or GABA-mediated responses in control conditions (n=52, 73, 123, respectively) or after 2 h application of 100 ng/ml BNP (n=42, 53, 119).

doi: 10.1371/journal.pone.0081138.g004

neuropeptides, like vasoactive intestinal polypeptide, galanin and NPY, are normally expressed at low or undetectable levels in sensory neurons and a specific stimulus is required for these peptides to be upregulated [46]. In keeping with this view, the concentration of BNP in ganglia in situ or in primary cultures was low, yet clearly detectable even in the extracellular

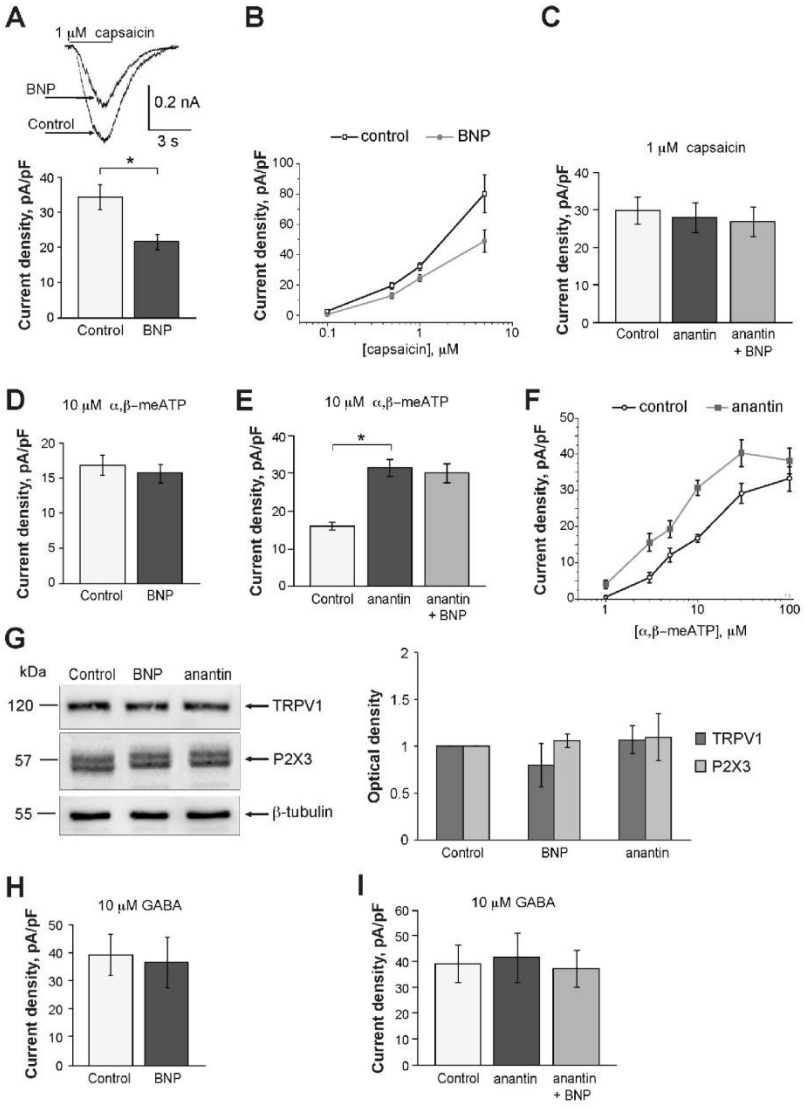

Figure 5. Changes in current responses produced by capsaicin, α,β-meATP or GABA following 24 h BNP application. A, Histograms show average current density values of TRPV1-mediated responses induced by 1 μM capsaicin in TG neurons under control conditions or after 24 h application of BNP (100 ng/ml); n=151 and 109 for control and after application of BNP, respectively; *p= 0.00014. Inset shows an example of superimposed currents of one neuron in control and after BNP treatment. B, Dose-response curves for capsaicin mediated currents in control and after 24 h BNP treatment (100 ng/ml); *p<0.035; n≥ 15 for each agonist concentration. C, Histograms summarize average current density values of the responses to 1 μM capsaicin in control conditions, after 24 h application of 500 nM anantin, or anantin plus 100 ng/ml BNP (n=53, 50, 43, respectively). D, E, Histograms show average current density values of P2X3-mediated currents in control conditions and after 24 h application of BNP (100 ng/ml); n=74 and 76, respectively. Anantin alone significantly increases these values compared to control, an effect not reversed by co-application with BNP (n=69, 63, 64, respectively); *p<0.0001. F, Dose-response curves for α,β-meATP mediated currents in control and after 24 h exposure to 500 nM anantin ; *p<0.035; n≥14 for each agonist concentration. G, Western blot analysis of TRPV1 or P2X3 receptor expression 24 h after applying BNP (100 ng/ml) or anantin (500 nM); data are from 3 experiments. H, I, Histograms show no change in GABA-mediated responses after 24 h application of BNP (100 ng/ml; n=25 and 27, respectively). Likewise, there is no change after application of anantin alone, or with BNP (n=73, 73, or 86, respectively).

doi: 10.1371/journal.pone.0081138.g005

medium of the primary cultures where it is expected to be concentrated by the lack of continuous blood circulation. It seems feasible that certain stimuli (yet to be identified) might raise BNP levels to become more functionally relevant for modulation of ganglion neurons.

The application of exogenous BNP rapidly evoked a large increase in cGMP level, a canonical effector of BNP [28], that peaked at about 30 min and then declined. This phenomenon was fully inhibited by the selective NPR-A antagonist anantin. Downstream of NPR-A activation and cGMP production is phosphorylation of Akt [40], an intracellular kinase targeting multiple pathways in cell signalling [47]. In accordance with this notion, BNP significantly enhanced Akt phosphorylation, an effect of transient nature (like the cGMP increment) as it was lost after 1 h.

The relatively quick onset of biochemical effects of BNP and the widespread neuronal expression of its receptor might have suggested an early change in the activity of the receptors like TRPV1 and P2X3 on nociceptors. Nevertheless, we found no significant change in neuronal currents induced by capsaicin, α,β-meATP, or GABA when BNP was applied for up to 2 h. Likewise, in the presence of BNP, there was no change in neuronal input resistance or baseline current, implying that the peptide produced neither a rapid alteration in background conductances regulating neuronal excitability nor a direct change in membrane permeability. We suggest that the relatively fast onset of biochemical effects evoked by BNP against lack of early electrophysiological action indicates a complex intracellular signalling system that triggers comparatively slow modifications in neuronal activity. This phenomenon would be compatible with a role of BNP in controlling chronic rather than acute pain. It is worth mentioning that, in rat DRG neurons, BNP rapidly enhances the activation of voltage-dependent potassium channels only when extracellular glutamate is persistently increased [25].

Despite the waning of BNP-induced rise of cGMP level and Akt phosphorylation following prolonged exposure, 24 h application of the peptide significantly depressed the currents evoked by capsaicin and shifted downwards the dose/response plot, suggesting systematic inhibition of TRPV1 receptor activity. This effect was prevented by anantin that per se did not change TRPV1 receptor responses. The same BNP application protocol had no effect on P2X3 receptor responses (or those mediated by GABA). Nonetheless, chronic anantin administration per se significantly augmented currents induced by various concentrations of α,β-meATP, with a lateral shift of the dose/response plot that did not change its maximum. This finding suggested that there was ambient release of BNP sufficient to inhibit P2X3 receptors, a notion fully compatible with the ELISA assay of this peptide in culture. This suggestion is also supported by the decreased cGMP level observed in the presence of anantin alone. When the NPR-A receptors were blocked by anantin (500 nM) with consequent facilitation of P2X3 receptor activity, co-applied BNP could not reverse this phenomenon. It is noteworthy that short application of anantin (or BNP) per se did not rapidly alter currents evoked by capsaicin or α,β-meATP. Furthermore, testing neurons 24 h after a short application of anantin or BNP failed to detect any receptor modulation. Overall, these findings are consistent with the view that modulation of the responses to capsaicin or α,β-meATP was a rather delayed consequence of NPR-A receptor occupation rather than a direct interaction of anantin with TRPV1 or P2X3 channels. The observed phenomenon that a NPR-A blocker could slowly enhance P2X3 receptor activity is reminiscent of a well-known process formerly described for TRPV1 receptors that are constitutively inhibited by phospholipids such as PIP2: when PIP2 hydrolysis is suppressed, TRPV1 function is slowly augmented [48].

Although the present report did not explore the molecular mechanisms linking NPR-A activation to TRPV1 and P2X3 receptor changes, a few clues might emerge by comparing the present data with former studies of sensory ganglion modulators. While further investigations are necessary to identify the precise reason whereby the modulation by BNP of TRPV1 and P2X3 receptors occurred so late, it is worth noting that, on trigeminal ganglia, modulation of P2X3 receptors by other peptides such as CGRP [20,39], bradykinin [48,49], or NGF deprivation [50] is typically slow in onset and persistent as multiple intracellular cascades are believed to be involved. Likewise, modulation of TRPV1 receptor function by growth factors (NGF, GDNF; [51]) or the cytokine TNF-α is also slow [52]. Since after 24 h exposure to BNP or anantin there was no change in the expression of TRPV1 or P2X3 protein in ganglion cell lysates, a possible target for BNP modulation is hypothesised to be the turnover process of these receptors [53,54] which might have shifted the balance between receptor compartments at membrane and cytosol level with consequent reduction in membrane current responses.

It is also emphasized that the strong expression of NPR-A by TG neurons (despite the poor presence of BNP) would make the TG particularly sensitive to circulating BNP released by a variety of peripheral tissues under physiological and pathological conditions [28]. Hence, the NPR-A system might represent a slow regulator of sensory excitability.

While in vivo experiments using trigeminal pain conditions will be necessary to establish the functional outcome of NPR-A activity, our data suggest that BNP/NPR-A signaling could have antinociceptive functions. Conversely, NPR-C receptors are present in DRG (and colocalized with TRPV1 channels) and are activated by CNP to enhance thermal hyperalgesia in a protein G βγ- and PKC-dependent fashion [24]. These results indicate the coexistence of functional NPRs in DRG that exhibit contrasting effects in pain transduction.

Trigeminal sensory neurons constitute the peripheral component of the so-called trigeminovascular system, an important pain complex thought to play a central role in primary headache syndromes, such as migraine [55,56]. Several neuropeptides contribute to the development of migraine pain: for example, CGRP increases the expression and the membrane targeting of P2X3 receptors [19,20,39], and bradykinin upregulates TRPV1 channels [57]. These mediators have the common ability to alter both neuronal and vascular function, a property shared by natriuretic peptides, which modulate nociceptive transmission at DRG level [24,25]. Since migraine patients display higher proBNP serum levels compared to healthy subjects [38], these data together with the

present findings indicate the desirability for future studies to address the potential involvement of the natriuretic peptide system in migraine pathophysiology.

Methods

All experiments involving the use of mice and the procedures followed therein were approved by the Scuola Internazionale Superiore di Studi Avanzati (SISSA) ethics committee and are in accordance with the European Union guidelines. Animals were maintained in accordance with the guidelines of the Italian Animal Welfare Act.

Preparations of mouse trigeminal ganglia and immunostaining

Primary cultures of P12 mouse trigeminal ganglia were prepared as described previously [18,39] and used 24 h after plating.

For immunohistochemistry, mice were deeply anesthetized with intraperitoneal injection of urethane (0.3 ml of 1 g/ml; Sigma, Milan, Italy) and perfused transcardially with phosphate buffer solution followed by 4% paraformaldehyde. Trigeminal ganglia were removed, postfixed for 1 h at room temperature and cryoprotected overnight in 30% sucrose at 4°C. Each immunohistochemistry experiment was performed on an average of 5 cryostat-cut serial longitudinal slices (14 µm-thick) sampled every ~70 µm, and thus covering the entire ganglion. Samples were incubated in a blocking solution containing 5% bovine serum albumin, 1% fetal bovine serum and 0.1% Triton X-100 in phosphate saline buffer for 2 h at room temperature, and immunostained with primary (for 16 h at 4°C) and secondary antibodies (2 h at room temperature). Antibodies against NPR-A (1:1000; Abcam, Cambridge, UK), BNP (1:100; Phoenix Pharmaceuticals, Burlingame, CA, USA) and β-tubulin III (1:1000; Sigma) were used. The specificity of the NPR-A antibody used in this study has been previously validated [25]. Secondary antibodies conjugated with Alexa Fluor-488 or Alexa Fluor-594 were purchased from Invitrogen (1:500; Milan, Italy). Nuclei were counterstained with DAPI (Sigma). The scant immunostaining for BNP led us to check whether this phenomenon could be attributed to a fixation artifact. Thus, we cut, with a cryostat, freshly frozen ganglia (14 µm sections) and processed them for BNP immunoreactivity using the blocking solution indicated above. Even in this case, BNP signals were absent or very rare. Double immunofluorescence experiments were performed using Zenon Technology: the anti-NPR-A antibody was labeled with Zenon Alexa-594 rabbit IgG labeling reagent as per manufacturers' instructions (Invitrogen). Images from whole ganglion sections were visualized with Leica confocal microscope (Leica TCS SP2, Wetzlar, Germany) or a Zeiss Axioskop fluorescence microscope (Zurich, Switzerland). Similar procedures were used for fluorescence immunostaining of cultured mouse TG neurons [18,58]. MetaMorph software (Molecular Devices, Downingtown, PA, USA) was employed for data analysis.

Western blot

Western blot analysis was performed according to the methods previously reported [58,59]. Cells were lysed in buffer solution (2% n-octyl-beta-D-glucopyranoside, contaning 1% Nonidet P-40, 10 mM Tris pH 7.5, 150 mM NaCl plus protease inhibitors mixture; Complete, Roche Applied Science, Basel, Switzerland) and immunoblotted with rabbit anti-NPR-A (1:1000, Abcam), anti-β-tubulin III (1:2000; Sigma) or anti-β-actin (1:3000, Sigma) antibodies. For Akt phosphorylation assays, cells were lysed in phosphate buffer solution containing 0.1% SDS, 1% sodium deoxycholate, and 1% triton X-100, and immunoblotted with anti-phospho-Akt Ser473 (1:1000; Cell Signaling, Danvers, MA, USA), anti-Akt (1:1000; Cell Signaling) or anti-β-actin-HRP (1:3000; Sigma). Signals were detected with the enhanced chemiluminescence light system ECL (Amersham Biosciences, Piscataway, NJ, USA) and recorded by the digital imaging system Alliance 4.7 (UVITEC, Cambridge, UK). Quantification of the optical density of the bands was performed with ImageJ software plug-in (Rasband, W.S., ImageJ, US National Institutes of Health, Bethesda, MD, USA, http://imagej.nih.gov/ij/, 1997-2012).

Biotinylation of surface expressed receptors

For biotinylation experiments, cells were incubated with 1 mg/ml EZ-Sulfo-NHS-LC-biotin (Pierce, Rockford, IL, USA) as previously described [39,60]. Pull-down of biotinylated proteins was obtained with Streptavidin agarose resin (Pierce) for 2 h at 4°C according to the manufacturer's instructions. Samples were processed for Western immunoblotting using antibodies against the NPR-A receptor (1:1000). Biotinylation experiments resulted to be free of intracellular protein contaminants (as shown by lack of signal for β-actin). Positive control for biotinylation assay was obtained by checking the surface expression of the transferrin receptor detected with an antibody purchased from Santa Cruz Biotechnology (1:1000, Heidelberg, Germany). For control of correct gel loading, the expression of β-actin in the intracellular fraction was checked.

RNA isolation, reverse transcription and RT-PCR

Total RNA was extracted from mouse intact TG tissue samples using Trizol reagent (Invitrogen) according to the manufacturer's instruction. All RNA samples were subjected to DNase I treatment (Ambion, Monza, Italy). A total of 1 µg of RNA was subjected to retrotranscription using iScript cDNA synthesis kit (BioRad, Hercules, CA, USA) and RT–PCR was carried out using SYBR green fluorescence dye (2× iQ5 SYBR Green supermix, BioRad) as described previously [61]. Specific primer sets for NPR-A [62], BNP [63], GAPDH [64] and β-actin [65] were previously described.

Assay for intracellular cGMP production in TG cultures

Quantification of BNP-induced intracellular cGMP production in mouse TG cultures was performed using a direct ELISA kit (MBL International Corporation, Woburn, MA, USA) following the instructions of the manufacturer. Briefly, cultures were lysed in 0.1 M HCl and subjected to determination of intracellular cGMP concentration. The protein concentrations in

cell lysates were determined by the BCA method (Sigma). Intracellular cGMP concentrations were expressed as pmol of cGMP per µg of protein. Three independent experimental replicates were generated from three different batches of mouse TG cultures.

Serum sampling and ELISA assay for BNP

Blood was sampled from the retro-orbital sinus of mice, immediately transferred to chilled microtubes on ice for 30 min and centrifuged at 10,000 *g* at 4°C for 10 min. Culture medium was collected from TG cultures 24 h after plating and centrifuged at 10,000 *g* at 4°C for 10 min. From the same cultures, cells were lysed in 0.1 M HCl and centrifuged at 10,000 *g* at 4°C for 10 min. Protein concentrations in cell lysates were determined by the BCA method (Sigma). Tissue and medium samples were immediately used for ELISA assay to determine BNP concentrations following the instructions of the manufacturer (Abnova, Hidelberg, Germany). All samples were run in triplicate and values averaged.

Electrophysiology and data analysis

Electrophysiology experiments were performed according to the methods previously reported [17,18]. Briefly, after 24 h in culture, TG neurons were superfused continuously (3 mL/min) with physiological solution containing (in mM): 152 NaCl, 5 KCl, 1 $MgCl_2$, 2 $CaCl_2$, 10 glucose, and 10 HEPES (pH adjusted to 7.4 with NaOH). Cells were patch-clamped in the whole-cell configuration using pipettes with a resistance of 3-4 M⍰ when filled with the following solution (in mM): 140 KCl, 0.5 $CaCl_2$, 2 $MgCl_2$, 2 Mg_2ATP_3, 2 GTP, 10 HEPES, and 10 EGTA (pH adjusted to 7.2 with KOH). Recordings were performed from small and medium size neurons that mostly express TRPV1 and/or P2X3 receptors [17,18]. Cells were held at -65 mV; membrane currents were filtered at 1 kHz and acquired by means of a DigiData 1200 interface and pClamp 8.2 software (Molecular Devices, Sunnyvale, CA, USA). To obtain stable and reproducible P2X3 receptor currents, its synthetic agonist α,β-methylene-adenosine-5'-triphosphate (α,β-meATP; Sigma) at the concentration of 10 µM that elicits near-maximal responses [58,64,66] was applied (for 2 s) using a fast superfusion system (Rapid Solution Changer RSC-200; BioLogic Science Instruments, Claix, France). α,β-meATP at 1, 3, 5, 30 and 100 µM concentrations was additionally studied to obtain dose-response curves in control and experimental conditions. In line with previous reports [17,58], capsaicin (Sigma) was applied at the concentration of 1 µM (3 s) to evoke reproducible inward currents. Additionally concentrations 0.1, 0.5, 5 and 10 µM were included to obtain capsaicin dose-response curves under control conditions and after the treatment. GABA (10 µM) was applied with 2 s pulses [45]. Peak current amplitudes were divided by the cell slow capacitance to express responses as current density values.

For patch clamp experiments, various protocols were used to test the effect of BNP on these ligand-gated channels. In a series of experiments, BNP was continuously superfused (starting 10 min prior to the agonist pulses) at 100 ng/ml concentration while agonist responses were repeatedly tested. In other experiments, TG cultures were incubated with BNP solution (100 ng/ml) for 2 or 24 h; after washing out the peptide, cells were immediately patch-clamped and tested for their responsiveness to the agonists. In the third type of the protocol BNP was applied for 1 h and, after wash out, cells were incubated for 23 h in the usual medium before the experiment. A similar approach was employed for the NPR-A antagonist anantin (500 nM) applied either alone or together with BNP.

Chemicals and reagents

Purified recombinant mouse BNP was purchased from Phoenix Pharmaceuticals; the specific NPR-A antagonist anantin was from US Biologicals (Salem, MA, USA). BNP and anantin were dissolved in distilled water as the datasheet suggested. BNP was applied at the dose of 100 ng/ml, as previously performed for sensory ganglia [25], and 500 ng/ml. Anantin was applied at the dose of 100 nM and 500 nM as previously reported [67].

To inhibit NPR-A receptor activity, we used anantin since, to the best of our knowledge, it is the only specific and selective NPR-A antagonist [41–43], devoid of agonistic activities [68], unlike commercially-available antagonists which are not selective on NPR subtypes [69–72], and which may also possess agonistic activities [73].

Statistical analysis

Data were collected from at least three independent experiments, and are expressed as mean ± standard error of the mean (SEM), where *n* indicates the number of independent experiments or the number of investigated cells, as indicated in figure legends. Statistical analysis was performed using the Student's *t*-test or the Mann-Whitney rank sum test, after the software-directed choice of parametric or non-parametric data, respectively (Sigma Plot and Systat Software Inc., San Jose, CA, USA). A p value of ≤ 0.05 was accepted as indicative of a statistically significant difference.

Supporting Information

Figure S1. Co-localization of NPR-A with TRPV1 and P2X3 receptors, and lack of acute NPR-A block on P2X3 receptor responses. A, Example of confocal microscopy images showing the colocalization of immunostaining for NPR-A (red) and TRPV1 or P2X3 (green). Cell nuclei are visualized with DAPI staining (blue). Scale bar, 30 µm. B, Representative traces of currents induced by pulse application of α,β-meATP (10 µM, 2 s) to TG neurons in control conditions or after application of anantin (500 nM, 10 min) to the same cells. Histograms show average current density values of P2X3-mediated currents (n=18).
(TIF)

Figure S2. 1 h BNP or anantin application has no effect on capsaicin-, α,β-meATP- or GABA-mediated responses recorded 23 h later. Histograms show average current density values of P2X3, TRPV1 or GABA-mediated responses in control conditions (n=40, 58, 82, respectively) or 23 h after 1 h

application of 100 ng/ml BNP (n=32, 66, 98) or 500 nM anantin (n=39, 38, 64).
(TIF)

Author Contributions

Conceived and designed the experiments: SV AM NN AN. Performed the experiments: SV AM NN. Analyzed the data: SV AM NN. Wrote the manuscript: SV AM NN AN.

References

1. Julius D, Basbaum AI (2001) Molecular mechanisms of nociception. Nature 413: 203–210. doi:10.1038/35093019. PubMed: 11557989.
2. North RA (2003) The P2X3 subunit: a molecular target in pain therapeutics. Curr Opin Investig Drugs 4: 833–840. PubMed: 14619405.
3. Caterina MJ, Leffler A, Malmberg AB, Martin WJ, Trafton J et al. (2000) Impaired nociception and pain sensation in mice lacking the capsaicin receptor. Science 288: 306–313. doi:10.1126/science.288.5464.306. PubMed: 10764638.
4. Davis JB, Gray J, Gunthorpe MJ, Hatcher JP, Davey PT et al. (2000) Vanilloid receptor-1 is essential for inflammatory thermal hyperalgesia. Nature 405: 183–187. doi:10.1038/35012076. PubMed: 10821274.
5. Gavva NR, Tamir R, Qu Y, Klionsky L, Zhang TJ, et al. (2005) AMG 9810 [(E)-3-(4-t-butylphenyl)-N-(2,3-dihydrobenzo[b][1,4] dioxin-6-yl)acrylamide], a novel vanilloid receptor 1 (TRPV1) antagonist with antihyperalgesic properties. J Pharmacol Exp Ther 313: 474–484.
6. Vulchanova L, Riedl MS, Shuster SJ, Buell G, Surprenant A et al. (1997) Immunohistochemical study of the P2X2 and P2X3 receptor subunits in rat and monkey sensory neurons and their central terminals. Neuropharmacology 36: 1229–1242. doi:10.1016/S0028-3908(97)00126-3. PubMed: 9364478.
7. Llewellyn-Smith IJ, Burnstock G (1998) Ultrastructural localization of P2X3 receptors in rat sensory neurons. Neuroreport 9: 2545–2550. doi:10.1097/00001756-199808030-00022. PubMed: 9721930.
8. Yang Z, Cao Y, Wang Y, Luo W, Hua X et al. (2009) Behavioural responses and expression of P2X3 receptor in trigeminal ganglion after experimental tooth movement in rats. Arch Oral Biol 54: 63–70. doi:10.1016/j.archoralbio.2008.09.003. PubMed: 18945422.
9. Oliveira MCG, Parada CA, Veiga MCFA, Rodrigues LR, Barros SP et al. (2005) Evidence for the involvement of endogenous ATP and P2X receptors in TMJ pain. Eur J Pain 9: 87–93. doi:10.1016/j.ejpain.2004.04.006. PubMed: 15629879.
10. Fabbretti E, Nistri A (2012) Regulation of P2X3 receptor structure and function. CNS Neurol Disord Drug Targets 11: 687–698. doi:10.2174/187152712803581029. PubMed: 22963434.
11. Premkumar LS, Abooj M (2013) TRP channels and analgesia. Life Sci 92: 415–424. doi:10.1016/j.lfs.2012.08.010. PubMed: 22910182.
12. Park CK, Bae JH, Kim HY, Jo HJ, Kim YH et al. (2010) Substance P sensitizes P2X3 in nociceptive trigeminal neurons. J Dent Res 89: 1154–1159. doi:10.1177/0022034510377094. PubMed: 20651096.
13. Giniatullin R, Nistri A, Fabbretti E (2008) Molecular mechanisms of sensitization of pain-transducing P2X3 receptors by the migraine mediators CGRP and NGF. Mol Neurobiol 37: 83–90. doi:10.1007/s12035-008-8020-5. PubMed: 18459072.
14. Simonetti M, Giniatullin R, Fabbretti E (2008) Mechanisms mediating the enhanced gene transcription of P2X3 receptor by calcitonin gene-related peptide in trigeminal sensory neurons. J Biol Chem 283: 18743–18752. doi:10.1074/jbc.M800296200. PubMed: 18460469.
15. Tang H-B, Li Y-S, Miyano K, Nakata Y (2008) Phosphorylation of TRPV1 by neurokinin-1 receptor agonist exaggerates the capsaicin-mediated substance P release from cultured rat dorsal root ganglion neurons. Neuropharmacology 55: 1405–1411. doi:10.1016/j.neuropharm.2008.08.037. PubMed: 18809416.
16. Bonnington JK, McNaughton PA (2003) Signalling pathways involved in the sensitisation of mouse nociceptive neurones by nerve growth factor. J Physiol 551: 433–446. doi:10.1113/jphysiol.2003.039990. PubMed: 12815188.
17. Hullugundi SK, Ferrari MD, van den Maagdenberg AMJM, Nistri A (2013) The mechanism of functional up-regulation of P2X3 receptors of trigeminal sensory neurons in a genetic mouse model of familial hemiplegic migraine type 1 (FHM-1). PLOS ONE 8: e60677. doi:10.1371/journal.pone.0060677. PubMed: 23577145.
18. Simonetti M, Fabbro A, D'Arco M, Zweyer M, Nistri A et al. (2006) Comparison of P2X and TRPV1 receptors in ganglia or primary culture of trigeminal neurons and their modulation by NGF or serotonin. Mol Pain 2: 11. doi:10.1186/1744-8069-2-11. PubMed: 16566843.
19. Messlinger K, Fischer MJM, Lennerz JK (2011) Neuropeptide effects in the trigeminal system: pathophysiology and clinical relevance in migraine. Keio J Med 60: 82–89. doi:10.2302/kjm.60.82. PubMed: 21979827.
20. Ceruti S, Villa G, Fumagalli M, Colombo L, Magni G et al. (2011) Calcitonin gene-related peptide-mediated enhancement of purinergic neuron/glia communication by the algogenic factor bradykinin in mouse trigeminal ganglia from wild-type and R192Q Cav2.1 Knock-in mice: implications for basic mechanisms of migraine pain. J Neurosci 31: 3638–3649. doi:10.1523/JNEUROSCI.6440-10.2011. PubMed: 21389219.
21. Capuano A, De Corato A, Lisi L, Tringali G, Navarra P et al. (2009) Proinflammatory-activated trigeminal satellite cells promote neuronal sensitization: relevance for migraine pathology. Mol Pain 5: 43. doi:10.1186/1744-8069-5-43. PubMed: 19660121.
22. Burnstock G (2013) Purinergic mechanisms and pain-An update. Eur J Pharmacol.
23. Benemei S, De Cesaris F, Fusi C, Rossi E, Lupi C et al. (2013) TRPA1 and other TRP channels in migraine. J Headache Pain 14: 71. doi:10.1186/1129-2377-14-71. PubMed: 23941062.
24. Loo L, Shepherd AJ, Mickle AD, Lorca RA, Shutov LP et al. (2012) The C-type natriuretic peptide induces thermal hyperalgesia through a noncanonical Gβγ-dependent modulation of TRPV1 channel. J Neurosci 32: 11942–11955. doi:10.1523/JNEUROSCI.1330-12.2012. PubMed: 22933780.
25. Zhang F-X, Liu X-J, Gong L-Q, Yao J-R, Li K-C et al. (2010) Inhibition of inflammatory pain by activating B-type natriuretic peptide signal pathway in nociceptive sensory neurons. J Neurosci 30: 10927–10938. doi:10.1523/JNEUROSCI.0657-10.2010. PubMed: 20702721.
26. Heine S, Michalakis S, Kallenborn-Gerhardt W, Lu R, Lim H-Y et al. (2011) CNGA3: a target of spinal nitric oxide/cGMP signaling and modulator of inflammatory pain hypersensitivity. J Neurosci 31: 11184–11192. doi:10.1523/JNEUROSCI.6159-10.2011. PubMed: 21813679.
27. Schmidtko A, Gao W, König P, Heine S, Motterlini R et al. (2008) cGMP produced by NO-sensitive guanylyl cyclase essentially contributes to inflammatory and neuropathic pain by using targets different from cGMP-dependent protein kinase I. J Neurosci 28: 8568–8576. doi:10.1523/JNEUROSCI.2128-08.2008. PubMed: 18716216.
28. Potter LR, Yoder AR, Flora DR, Antos LK, Dickey DM (2009) Natriuretic peptides: their structures, receptors, physiologic functions and therapeutic applications. Handb Exp Pharmacol: 341–366. PubMed: 19089336.
29. Azarov AV, Szabó G, Telegdy G (1992) Effects of atrial natriuretic peptide on acute and chronic effects of morphine. Pharmacol Biochem Behav 43: 193–197. doi:10.1016/0091-3057(92)90657-2. PubMed: 1409804.
30. Misono KS (2002) Natriuretic peptide receptor: structure and signaling. Mol Cell Biochem 230: 49–60. doi:10.1023/A:1014257621362. PubMed: 11952096.
31. Hofmann F, Feil R, Kleppisch T, Schlossmann J (2006) Function of cGMP-dependent protein kinases as revealed by gene deletion. Physiol Rev 86: 1–23. doi:10.1152/physrev.00015.2005. PubMed: 16371594.
32. Abdelalim EM, Tooyama I (2011) Mapping of NPR-B immunoreactivity in the brainstem of Macaca fascicularis. Brain Struct Funct 216: 387–402. doi:10.1007/s00429-011-0313-1. PubMed: 21455797.
33. Abdelalim EM, Masuda C, Bellier JP, Saito A, Yamamoto S et al. (2008) Distribution of natriuretic peptide receptor-C immunoreactivity in the rat brainstem and its relationship to cholinergic and catecholaminergic neurons. Neuroscience 155: 192–202. doi:10.1016/j.neuroscience.2008.05.020. PubMed: 18571869.
34. Abdelalim EM, Osman AHK, Takada T, Torii R, Tooyama I (2007) Immunohistochemical mapping of natriuretic peptide receptor-A in the brainstem of Macaca fascicularis. Neuroscience 145: 1087–1096. doi:10.1016/j.neuroscience.2006.12.062. PubMed: 17293051.
35. Nohr D, Weihe E, Zentel HJ, Arendt RM (1989) Atrial natriuretic factor-like immunoreactivity in spinal cord and in primary sensory neurons of spinal and trigeminal ganglia of guinea-pig: correlation with tachykinin immunoreactivity. Cell Tissue Res 258: 387–392. PubMed: 2531038.
36. Spencer SE, Kibbe MR, Hurley KM, Needleman P, Saper CB (1991) Origin of porcine brain natriuretic peptide-like immunoreactive

innervation of the middle cerebral artery in the rat. Neurosci Lett 128: 217–220. doi:10.1016/0304-3940(91)90264-T. PubMed: 1834966.
37. Puri V, Cui L, Liverman CS, Roby KF, Klein RM et al. (2005) Ovarian steroids regulate neuropeptides in the trigeminal ganglion. Neuropeptides 39: 409–417. doi:10.1016/j.npep.2005.04.002. PubMed: 15936815.
38. Uzar E, Evliyaoglu O, Yucel Y, Ugur Cevik M, Acar A et al. (2011) Serum cytokine and pro-brain natriuretic peptide (BNP) levels in patients with migraine. Eur Rev Med Pharmacol Sci 15: 1111–1116. PubMed: 22165670.
39. Fabbretti E, D'Arco M, Fabbro A, Simonetti M, Nistri A et al. (2006) Delayed upregulation of ATP P2X3 receptors of trigeminal sensory neurons by calcitonin gene-related peptide. J Neurosci 26: 6163–6171. doi:10.1523/JNEUROSCI.0647-06.2006. PubMed: 16763024.
40. Pandey KN (2005) Biology of natriuretic peptides and their receptors. Peptides 26: 901–932. doi:10.1016/j.peptides.2004.09.024. PubMed: 15911062.
41. Nachshon S, Zamir O, Matsuda Y, Zamir N (1995) Effects of ANP receptor antagonists on ANP secretion from adult rat cultured atrial myocytes. Am J Physiol 268: E428–E432. PubMed: 7900789.
42. El-Ayoubi R, Menaouar A, Gutkowska J, Mukaddam-Daher S (2005) Urinary responses to acute moxonidine are inhibited by natriuretic peptide receptor antagonist. Br J Pharmacol 145: 50–56. doi:10.1038/sj.bjp.0706146. PubMed: 15700025.
43. Abdelalim EM, Tooyama I (2011) NPR-A regulates self-renewal and pluripotency of embryonic stem cells. Cell Death. Drosophila Inf Service 2: e127.
44. Nistri A, Constanti A (1979) Pharmacological characterization of different types of GABA and glutamate receptors in vertebrates and invertebrates. Prog Neurobiol 13: 117–235. doi:10.1016/0301-0082(79)90016-9. PubMed: 227014.
45. Fabbro A, Nistri A (2004) Chronic NGF treatment of rat nociceptive DRG neurons in culture facilitates desensitization and deactivation of $GABA_A$ receptor-mediated currents. Br J Pharmacol 142: 425–434. doi:10.1038/sj.bjp.0705813. PubMed: 15148248.
46. Hökfelt T, Broberger C, Xu ZQ, Sergeyev V, Ubink R et al. (2000) Neuropeptides--an overview. Neuropharmacology 39: 1337–1356. doi:10.1016/S0028-3908(00)00010-1. PubMed: 10818251.
47. Brazil DP, Hemmings BA (2001) Ten years of protein kinase B signalling: a hard Akt to follow. Trends Biochem Sci 26: 657–664. doi:10.1016/S0968-0004(01)01958-2. PubMed: 11701324.
48. Chuang HH, Prescott ED, Kong H, Shields S, Jordt SE et al. (2001) Bradykinin and nerve growth factor release the capsaicin receptor from PtdIns(4,5)P2-mediated inhibition. Nature 411: 957–962. doi:10.1038/35082088. PubMed: 11418861.
49. Ceruti S, Fumagalli M, Villa G, Verderio C, Abbracchio MP (2008) Purinoceptor-mediated calcium signaling in primary neuron-glia trigeminal cultures. Cell Calcium 43: 576–590. doi:10.1016/j.ceca.2007.10.003. PubMed: 18031810.
50. D'Arco M, Giniatullin R, Simonetti M, Fabbro A, Nair A et al. (2007) Neutralization of nerve growth factor induces plasticity of ATP-sensitive P2X3 receptors of nociceptive trigeminal ganglion neurons. J Neurosci 27: 8190–8201. doi:10.1523/JNEUROSCI.0713-07.2007. PubMed: 17670966.
51. Ciobanu C, Reid G, Babes A (2009) Acute and chronic effects of neurotrophic factors BDNF and GDNF on responses mediated by thermo-sensitive TRP channels in cultured rat dorsal root ganglion neurons. Brain Res 1284: 54–67. doi:10.1016/j.brainres.2009.06.014. PubMed: 19524560.
52. Spicarova D, Palecek J (2010) Tumor necrosis factor alpha sensitizes spinal cord TRPV1 receptors to the endogenous agonist N-oleoyldopamine. J Neuroinflammation 7: 49. doi:10.1186/1742-2094-7-49. PubMed: 20796308.
53. Vacca F, Giustizieri M, Ciotti MT, Mercuri NB, Volonté C (2009) Rapid constitutive and ligand-activated endocytic trafficking of P2X receptor. J Neurochem 109: 1031–1041. doi:10.1111/j.1471-4159.2009.06029.x. PubMed: 19519775.
54. Shimizu T, Shibata M, Toriumi H, Iwashita T, Funakubo M et al. (2012) Reduction of TRPV1 expression in the trigeminal system by botulinum neurotoxin type-A. Neurobiol Dis 48: 367–378. doi:10.1016/j.nbd.2012.07.010. PubMed: 22820141.
55. May A, Goadsby PJ (1999) The trigeminovascular system in humans: pathophysiologic implications for primary headache syndromes of the neural influences on the cerebral circulation. J Cereb Blood Flow Metab 19: 115–127. PubMed: 10027765.
56. Moskowitz MA (1984) The neurobiology of vascular head pain. Ann Neurol 16: 157–168. doi:10.1002/ana.410160202. PubMed: 6206779.
57. Fischer MJM, Leffler A, Niedermirtl F, Kistner K, Eberhardt M et al. (2010) The general anesthetic propofol excites nociceptors by activating TRPV1 and TRPA1 rather than $GABA_A$ receptors. J Biol Chem 285: 34781–34792. doi:10.1074/jbc.M110.143958. PubMed: 20826794.
58. Nair A, Simonetti M, Fabbretti E, Nistri A (2010) The Cdk5 kinase downregulates ATP-gated ionotropic P2X3 receptor function via serine phosphorylation. Cell Mol Neurobiol 30: 505–509. doi:10.1007/s10571-009-9483-2. PubMed: 19960242.
59. D'Arco M, Giniatullin R, Leone V, Carloni P, Birsa N et al. (2009) The C-terminal Src inhibitory kinase (Csk)-mediated tyrosine phosphorylation is a novel molecular mechanism to limit P2X3 receptor function in mouse sensory neurons. J Biol Chem 284: 21393–21401. doi:10.1074/jbc.M109.023051. PubMed: 19509283.
60. Sundukova M, Vilotti S, Abbate R, Fabbretti E, Nistri A (2012) Functional differences between ATP-gated human and rat P2X3 receptors are caused by critical residues of the intracellular C-terminal domain. J Neurochem 122: 557–567. doi:10.1111/j.1471-4159.2012.07810.x. PubMed: 22639984.
61. Franceschini A, Vilotti S, Ferrari MD, van den Maagdenberg AMJM, Nistri A et al. (2013) TNFα levels and macrophages expression reflect an inflammatory potential of trigeminal ganglia in a mouse model of familial hemiplegic migraine. PLOS ONE 8: e52394. doi:10.1371/journal.pone.0052394. PubMed: 23326332.
62. Christoffersen C, Bartels ED, Nielsen LB (2006) Heart specific up-regulation of genes for B-type and C-type natriuretic peptide receptors in diabetic mice. Eur J Clin Invest 36: 69–75. doi:10.1111/j.1365-2362.2006.01596.x. PubMed: 16436087.
63. Nielsen LB, Bartels ED, Bollano E (2002) Overexpression of apolipoprotein B in the heart impedes cardiac triglyceride accumulation and development of cardiac dysfunction in diabetic mice. J Biol Chem 277: 27014–27020. doi:10.1074/jbc.M203458200. PubMed: 12015323.
64. Franceschini A, Nair A, Bele T, van den Maagdenberg AM, Nistri A et al. (2012) Functional crosstalk in culture between macrophages and trigeminal sensory neurons of a mouse genetic model of migraine. BMC Neurosci 13: 143. doi:10.1186/1471-2202-13-S1-P143. PubMed: 23171280.
65. Zucchelli S, Vilotti S, Calligaris R, Lavina ZS, Biagioli M et al. (2009) Aggresome-forming TTRAP mediates pro-apoptotic properties of Parkinson's disease-associated DJ-1 missense mutations. Cell Death Differ 16: 428–438. doi:10.1038/cdd.2008.169. PubMed: 19023331.
66. Franceschini A, Hullugundi SK, van den Maagdenberg AMJM, Nistri A, Fabbretti E (2013) Effects of LPS on P2X3 receptors of trigeminal sensory neurons and macrophages from mice expressing the R192Q Cacna1a gene mutation of familial hemiplegic migraine-1. Purinergic Signal 9: 7–13. doi:10.1007/s11302-012-9328-1. PubMed: 22836594.
67. Yu Y-C, Cao L-H, Yang X-L (2006) Modulation by brain natriuretic peptide of GABA receptors on rat retinal ON-type bipolar cells. J Neurosci 26: 696–707. doi:10.1523/JNEUROSCI.3653-05.2006. PubMed: 16407567.
68. Weber W, Fischli W, Hochuli E, Kupfer E, Weibel EK (1991) Anantin--a peptide antagonist of the atrial natriuretic factor (ANF). I. Producing organism, fermentation, isolation and biological activity. J Antibiot (Tokyo) 44: 164–171. doi:10.7164/antibiotics.44.164. PubMed: 1849131.
69. Lonardo G, Cerbai E, Casini S, Giunti G, Bonacchi M et al. (2004) Atrial natriuretic peptide modulates the hyperpolarization-activated current (If) in human atrial myocytes. Cardiovasc Res 63: 528–536. doi:10.1016/j.cardiores.2004.03.004. PubMed: 15276478.
70. Medvedev A, Crumeyrolle-Arias M, Cardona A, Sandler M, Glover V (2005) Natriuretic peptide interaction with [3H]isatin binding sites in rat brain. Brain Res 1042: 119–124. doi:10.1016/j.brainres.2005.02.051. PubMed: 15854583.
71. Potter LR, Abbey-Hosch S, Dickey DM (2006) Natriuretic peptides, their receptors, and cyclic guanosine monophosphate-dependent signaling functions. Endocr Rev 27: 47–72. PubMed: 16291870.
72. Katoli P, Sharif NA, Sule A, Dimitrijevich SD (2010) NPR-B natriuretic peptide receptors in human corneal epithelium: mRNA, immunohistochemistochemical, protein, and biochemical pharmacology studies. Mol Vis 16: 1241–1252. PubMed: 20664698.
73. Endlich K, Steinhausen M (1997) Natriuretic peptide receptors mediate different responses in rat renal microvessels. Kidney Int 52: 202–207. doi:10.1038/ki.1997.320. PubMed: 9211363.

2. Brain natriuretic peptide constitutively downregulates P2X3 receptors by controlling their phosphorylation state and membrane localization

Marchenkova et al. Mol Pain (2015) 11:71
DOI 10.1186/s12990-015-0074-6

MOLECULAR PAIN

RESEARCH Open Access

Brain natriuretic peptide constitutively downregulates P2X3 receptors by controlling their phosphorylation state and membrane localization

Anna Marchenkova[1†], Sandra Vilotti[1†], Elsa Fabbretti[2] and Andrea Nistri[1*]

Abstract

Background: ATP-gated P2X3 receptors are important transducers of nociceptive stimuli and are almost exclusively expressed by sensory ganglion neurons. In mouse trigeminal ganglion (TG), P2X3 receptor function is unexpectedly enhanced by pharmacological block of natriuretic peptide receptor-A (NPR-A), outlining a potential inhibitory role of endogenous natriuretic peptides in nociception mediated by P2X3 receptors. Lack of change in P2X3 protein expression indicates a complex modulation whose mechanisms for downregulating P2X3 receptor function remain unclear.

Results: To clarify this process in mouse TG cultures, we suppressed NPR-A signaling with either siRNA of the endogenous agonist BNP, or the NPR-A blocker anantin. Thus, we investigated changes in P2X3 receptor distribution in the lipid raft membrane compartment, their phosphorylation state, as well as their function with patch clamping. Delayed onset of P2X3 desensitization was one mechanism for the anantin-induced enhancement of P2X3 activity. Anantin application caused preferential P2X3 receptor redistribution to the lipid raft compartment and decreased P2X3 serine phosphorylation, two phenomena that were not interdependent. An inhibitor of cGMP-dependent protein kinase and siRNA-mediated knockdown of BNP mimicked the effect of anantin.

Conclusions: We demonstrated that in mouse trigeminal neurons endogenous BNP acts on NPR-A receptors to determine constitutive depression of P2X3 receptor function. Tonic inhibition of P2X3 receptor activity by BNP/NPR-A/PKG pathways occurs via two distinct mechanisms: P2X3 serine phosphorylation and receptor redistribution to non-raft membrane compartments. This novel mechanism of receptor control might be a target for future studies aiming at decreasing dysregulated P2X3 receptor activity in chronic pain.

Keywords: Trigeminal ganglia, ATP, Pain, Purinergic receptor, Purinergic signaling, Lipid raft, Protein kinase G (PKG), Sensory neuron

Background

P2X3 receptors are trimeric cation channels gated by extracellular ATP, almost exclusively expressed by the majority of sensory ganglion neurons [1, 2], and important transducers of nociceptive stimuli [3, 4]. Even though the P2X3 receptor desensitizes rapidly (and, thus, self-limits its function), it can elicit fast, strong sensory neuron depolarization and firing which are actually enhanced in pathological pain states [4–8]. Certain endogenous modulators can upregulate P2X3 channels via multiple signaling pathways that alter their rate of synthesis, trafficking [9–11], phosphorylation state [10, 12–15], and receptor desensitization [10, 15, 16]. In particular, a major role is played by the neuropeptide calcitonin gene-related peptide (CGRP) that persistently enhances P2X3 receptor activity and, thereby, contributes to the development of algogenic syndromes in

*Correspondence: nistri@sissa.it
†Anna Marchenkova and Sandra Vilotti contributed equally
[1] Neuroscience Department, International School for Advanced Studies (SISSA), Via Bonomea 265, 34136 Trieste, Italy
Full list of author information is available at the end of the article

inflammation [17–19], chronic and neuropathic pain [10, 20], and migraine headache [21, 22]. It is, however, conceivable that endogenous substances may serve as negative regulators of P2X3 receptors under basal conditions. Their dysfunction might actually contribute to pain sensitization, a notion that could potentially paved the way to design novel analgesic drugs.

One candidate for the role of endogenous negative regulator of sensory ganglion activity is the brain natriuretic peptide (BNP). In fact, BNP downregulates inflammatory pain as well as firing frequency of small neurons in dorsal root ganglia (DRG; [9, 23]). BNP is one of the three structurally related paracrine factors belonging to natriuretic peptides family [24]. This peptide is a potent agonist on NPR-A receptors [24, 25] abundantly expressed by DRG CGRP-containing neurons [9] and trigeminal ganglion (TG) neurons [26] in which BNP-dependent NPR-A activation increases cGMP production [26, 27]. It is suggested that this system plays a constitutive inhibitory role in nociception mediated by P2X3 receptors because sustained pharmacological block of NPR-A strongly enhances P2X3 receptor mediated responses [26].

The molecular mechanism underlying the NPR-A dependent inhibition of TG P2X3 receptor function remains unclear. Our previous data indicate that NPR-A antagonism does not interfere with P2X3 expression [26], outlining a subtle process of P2X3 modulation. Potential targets might be the fine balance between phosphorylation and dephosphorylation controlling channel structure and function [3, 10, 13, 14, 28] or the differential distribution of P2X3 receptor between cholesterol-rich raft and non-raft membrane compartments [29–32].

The aims of the present study were to clarify the mechanisms and dynamics of BNP mediated constitutive regulation of P2X3 receptor function. Thus, we investigated changes in P2X3 receptor compartmentalization and phosphorylation state, and the role of certain intermediate steps in this process. To this end, BNP siRNA or the selective NPR-A blocker anantin were used to suppress NPR-A signaling and to evaluate any alteration in P2X3 receptor membrane distribution and phosphorylation state. Our results indicated multiple processes through which BNP-dependent NPR-A activity controlled P2X3 receptors.

Results

Unmasking tonic inhibition of P2X3 receptors by BNP

To support constitutive inhibition of P2X3 receptor activity by endogenous BNP in mouse TG neurons, the present study looked for changes in P2X3 receptor function after siRNA of BNP and compared this effect with the action of the pharmacological antagonist anantin.

Following BNP siRNA (48 h), no BNP (measured with the standard ELISA assay) could be detected in the culture medium, while in control conditions BNP was clearly detectable (4.7 ± 1.5 ng/ml), consistent with our previous report [26]. Furthermore, even if immunoreactive cells for BNP are just a few in cultured or in situ trigeminal ganglia ([26]; see top panels in Fig. 1a), after 48 h siRNA immunohistochemical staining did not demonstrate any BNP immunopositive cells in TG culture (Fig. 1a, bottom panels). P2X3 receptor mediated currents elicited by the selective P2X3 agonist α,β-methylene-ATP (α,β-meATP) [33] were next investigated using trigeminal sensory neurons (see experimental protocols schematized in Fig. 1b, bottom panels). Thus, BNP siRNA yielded larger amplitude responses that were similar to those recorded after anantin application (as exemplified in the records of Fig. 1b, left). When anantin was applied over a background of siRNA BNP, no further upregulation of P2X3 receptor function was observed, as seen from the histograms (Fig. 1b, right) and representative current traces (Fig. 1b, left). In addition, after siRNA BNP, 2 h application of BNP (100 mg/ml) depressed P2X3 receptor currents back to the untreated control level (Fig. 1b, right). These data, thus, validate that sustained block of NPR-A receptors with anantin and suppression of endogenous BNP synthesis evoked similar potentiation of P2X3 receptor activity. It is also noteworthy that a significant decrease in P2X3 receptor function was observed with BNP after siRNA, unmasking an inhibitory effect of this peptide that had not been previously detected.

Dynamic modulation of P2X3 receptor function by the NPR-A blocker anantin

We next explored the timecourse of anantin potentiation of P2X3 activity, as this approach can cast light on the dynamics of the NPR-A modulatory action. Figure 2a shows examples of α,β-meATP (10 μM, 2 s)-induced P2X3 currents (Fig. 2a, upper panel) along with their mean current density values at various times of anantin treatment (Fig. 2a, lower panel). In fact, a significant increase in P2X3 currents was observed after 1 h of anantin (500 nM) application and remained at a stable plateau for longer (up to 24 h) exposures. Dose–response curves for α,β-meATP mediated currents in control and after 24 h exposure to 500 nM anantin were previously described [26], showing that this potentiation occurred throughout the agonist concentration range. Anantin (500 nM, 3 h) did not change cell input resistance (820 ± 57 MΩ in control versus 811 ± 58 MΩ after anantin treatment) or the baseline current (36 ± 5.7 pA in control versus 41 ± 9.1 pA after anantin treatment), indicating that anantin caused no significant change in background conductances that might have accounted

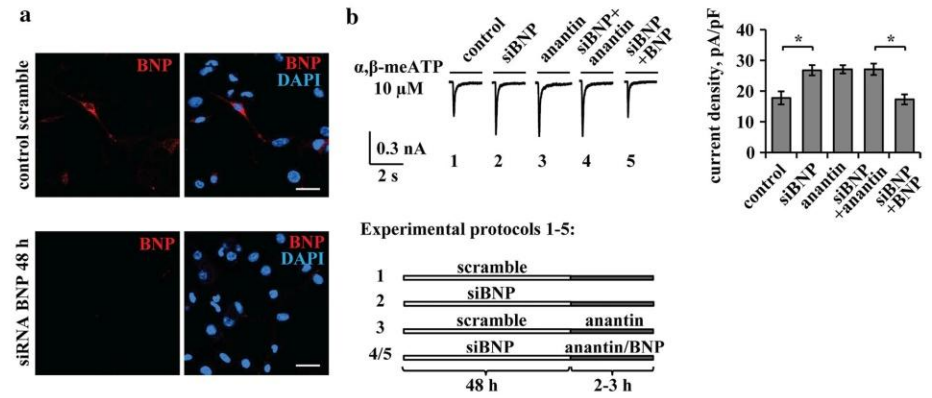

Fig. 1 Effects of BNP siRNA. **a** Representative immunocytochemical examples of endogenous BNP expression in mouse TG cultures in control (*upper panels*) and after BNP siRNA (*lower panels*). Nuclei are visualized with DAPI (*blue*); *scale bar* = 20 μm. **b** Representative current traces show α,β-meATP (10 μM, 2 s)-evoked P2X3 responses in control, after 48 h of siBNP, anantin application (500 nM, 2–3 h), or after a combination of siBNP treatment with application of anantin or BNP (100 ng/ml, 2–3 h). The scheme at the *bottom* describes aforementioned experimental protocols. Histograms show average P2X3 current density values (n = 33, 33, 40, 32, 33, respectively; *p < 0.05, Kruskal–Wallis test). Note that effects of BNP silencing and anantin application are not additive and statistically indistinguishable; BNP applied after siBNP depresses P2X3 currents to the control level

for a broad, non-selective rise in neuronal membrane responses. We also studied whether the effect of anantin was reversible on washout: Fig. 2b illustrates that 5 h wash with standard physiological solution restored P2X3 current values to control level.

Because desensitization is an important process to limit P2X3 receptor-mediated responses [10, 15, 33], we investigated if anantin might have impaired P2X3 desensitization. Figure 2c, (left panel) shows averaged P2X3 currents (scaled and superimposed to aid comparison) in control solution or after anantin application (1 h). P2X3 currents normally decay with a bi-exponential time course [33], corresponding to the fast and slow components of P2X3 desensitization (τ_1 and τ_2; see also Fig. 2c, left) [34]. A total number of 161 currents was analyzed (85 in control and 76 after anantin application collected from several separate experiments) with peak amplitudes varying from 250 to 800 pA. Figure 2c shows a small, albeit significant, increase in τ_1 values after anantin application compared to the control without statistically significant alteration in τ_2 values (Fig. 2c, right; $p < 0.05$, Mann–Whitney rank sum test). Thus, retarding the onset of desensitization appeared to be one mechanism for the anantin-induced enhancement of P2X3 activity.

Changes in extracellular CGRP do not affect anantin mediated P2X3 upregulation

CGRP is a powerful positive regulator of P2X3 function via complex signaling involving neurons and non-neuronal cells [28, 35–38]. We wondered if anantin might act by facilitating the action of ambient CGRP in trigeminal cultures [38]. Pretreatment with the selective CGRP receptor antagonist peptide CGRP 8-37 (1 μM, overnight; see the protocol scheme in Fig. 3a, right) per se did not modify P2X3 activity in accordance with our previous data [39] (Fig. 3a, left). Anantin retained its enhancing action on P2X3 currents even after CGRP 8-37 pretreatment (Fig. 3a, left).

We also studied whether the effects of CGRP and anantin were additive in upregulating P2X3 receptor currents. To address this issue, on the basis that the effect of anantin was manifested already at 1 h (Fig. 2a), we first applied this antagonist (500 nM) for 1 h and then together with CGRP (1 μM) for further 2 h when the action of CGRP is known to be reliably expressed [9]. With this protocol (Fig. 3b, right), the increase in P2X3 activity was the same as with either agent applied in isolation (histogram in Fig. 3b, left), indicating lack of additivity.

Anantin promotes P2X3 localization to lipid rafts

In previous experiments we observed how the differential localization of P2X3 receptors to lipid raft and non-raft membrane compartments of sensory neurons is an important process to characterize the efficiency of P2X3 signaling [29, 31, 32, 34]. Thus, using anantin we tested if the P2X3 receptor membrane distribution was dependent on the BNP/NPR-A system. In accordance with our former report [34], we obtained lipid raft (flotillin-labeled) and non-raft membrane preparations from control and treated cultures and tested them

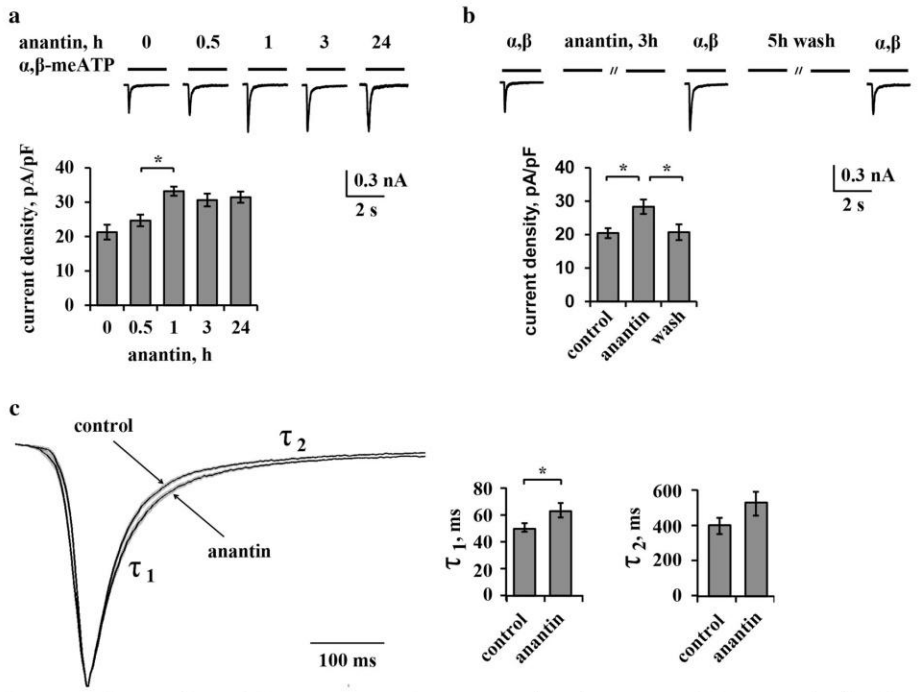

Fig. 2 Time-course of anantin effects on P2X3 receptor currents. **a** Histograms together with representative P2X3 currents induced by α,β-meATP (10 μM, 2 s) show time-course of anantin (500 nM) effects on P2X3 currents. Anantin significantly increases mean P2X3 current density values after 1 h treatment already (n = 44, 30, 40, 40 for control, 1, 3 and 24 h treatment, respectively; *p < 0.05, Kruskal–Wallis test). **b** Representative traces obtained using α,β-meATP (10 μM, 2 s) show P2X3 current amplitudes in control, after 3 h anantin treatment (500 nM) and after 3 h anantin application followed by 5 h wash with standard physiological solution. Histograms show average P2X3 current density values in control, anantin and wash out conditions (n = 42, 40, 33, respectively; *p < 0.05, Kruskal–Wallis test). Note that 5 h wash abolishes anantin effects on P2X3 current density. **c** Superimposed average traces of scaled P2X3 currents (shown as mean; sem is within the trace thickness), in control and after anantin treatment (n = 67, 76, respectively, Mann–Whitney rank sum test). Note no significant change in the current onset and slowing down of the decay after anantin application; τ_1, τ_2 are the fast and slow components of P2X3 current desensitization dynamics. Histograms show mean values for τ_1 and τ_2 desensitization constants of P2X3 receptor currents in control and after 500 nM anantin application (n = 67, 76, respectively; *p < 0.05, Mann–Whitney rank sum test)

with Western immunoblotting as exemplified in Fig. 4a. Hence, a significant increase in the amount of immunopurified P2X3 receptors associated with the lipid raft compartment (R) vs the non-raft compartment (NR) was observed following 24 h anantin application (Fig. 4b, see examples in upper panel and data analysis at the bottom; middle panels show total lysates; n = 4, p < 0.05, Kruskal–Wallis test). It is noteworthy that, after anantin, there was no change in P2X3 receptor expression in total lysate samples that contained a broad assembly of membrane and intracellular P2X3 receptors with different degree of maturation (lower panel in Fig. 4a; see also [9, 12]). Consistent with previously reported data [34], the cholesterol-depleting agent MβCD (10 mM, 30 min treatment) disrupted lipid rafts almost completely (see loss of flotillin labelling in Fig. 4a, upper panel) and shifted a significant fraction of P2X3 receptors to the non-raft compartment, while the total amount of receptors remained constant (Fig. 4a, middle panel). Applying MβCD during the last 30 min of anantin administration blocked the anantin effect on P2X3 membrane distribution: thus, most P2X3 receptors were redistributed from lipid rafts to the non-raft membrane compartment (Fig. 4a, examples in upper panels and data analysis at the bottom).

Forty-eight hours after siBNP, we observed effects statistically indistinguishable from those of anantin per se

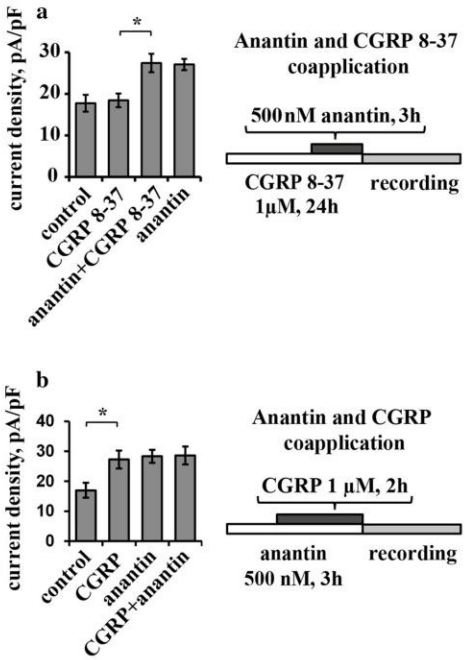

Fig. 3 Anantin-mediated changes of P2X3 currents are not CGRP-dependent. **a** Histogram shows mean current density values of P2X3 receptors in control and after application of CGRP 8-37 (1 μM, overnight), anantin (500 nM, 3 h), or their combination (n = 44, 40, 50, 43, respectively; *p < 0.05, Kruskal–Wallis test). Pretreatment with CGRP 8-37 has no influence on anantin-mediated enhancement of P2X3 current density values, suggesting that this effect is not mediated via CGRP release. Scheme on the right describes experimental protocol of anantin and CGRP 8-37 coapplication. **b** Histograms compare mean current density values of P2X3 receptors in control and after application of CGRP (1 μM, 3 h), anantin (500 nM, 2 h) or their combination (n = 42, 40, 34, 33, respectively; *p < 0.05, Kruskal–Wallis test). Adding CGRP to the anantin treatment does not further increase P2X3 currents. Scheme on the *right* describes experimental protocol of anantin and CGRP co-application

in terms of localization of P2X3 receptors to the lipid raft membrane fraction (Fig. 4b, examples in upper panels and data analysis at the bottom). This phenomenon was unchanged by adding anantin during the last 3 h of silencing, while there was no alteration in the total lysate expression of P2X3 receptor protein (Fig. 4b, middle panels).

Electrophysiological recordings of α,β-meATP (10 μM, 2 s) induced P2X3 currents showed decreased peak amplitudes after MβCD treatment ($p < 0.05$, Fig. 4c, right), similar to previous data [34]. Data from this set of experiments are presented as peak current amplitudes and not as current density values, since MβCD treatment affects cell capacitance by depleting the cholesterol content of the cell membrane and, thus, its dielectric component (Fig. 4c, histograms on the left). After combined anantin and MβCD treatment, P2X3 current values were the same as in the control conditions (Fig. 4c, left and right). This result suggested that the combined administration enabled potentiation by anantin despite MβCD even though it could not reach the level observed with anantin alone (Fig. 4c, left and right).

NPR-A receptors modulate P2X3 serine phosphorylation

Previous reports have indicated that the efficiency of P2X3 receptors depends on their phosphorylation state, concerning in particular their serine or tyrosine residues [12, 13]. To look for mechanisms through which the BNP system may modulate P2X3 function, we checked if anantin affected P2X3 serine or tyrosine phosphorylation by screening immunoprecipitated membrane P2X3 receptors with antibodies against the corresponding phosphorylated residues.

Figure 5a shows Western blot analysis of the serine phosphorylation (pSer) level in immunopurified membrane P2X3 receptors in control or anantin-treated cultures. The data revealed a significant reduction ($n = 4$ experiments, $p < 0.05$, Mann–Whitney rank sum test) of serine P2X3 phosphorylation (revealed as a single band; [13, 40]) following 1 h (Fig. 5a, examples in upper panels and data analysis on the right) or 24 h anantin application (Fig. 5c, examples in upper panels and data analysis on the right), in analogy to the upregulation of P2X3 currents (Fig. 2a). By comparison, P2X3 tyrosine phosphorylation (pTyr) remained unaltered (Fig. 5b).

Silencing BNP for 48 h (with or without later application of anantin) produced a reduction of P2X3 serine phosphorylation similar to the effect of anantin alone (Fig. 5d, examples in upper panels and data analysis on the right). Thus, inactivation of the NPR-A pathway by either blocking the receptors with anantin or exhausting cultures of endogenous BNP caused similar effects, confirming the idea of tonic regulation of P2X3 receptors activity by BNP via NPR-A.

Because calcineurin, CdK5, or CaMKII are known intracellular regulators of P2X3 receptor activity via changes in receptor phosphorylation [11, 13, 40, 41], we investigated whether blocking these enzymes might have effects analogous to those of anantin, and/or interact with the anantin potentiating action.

Figure 6a (left) shows mean values of P2X3 current density in cells treated for 30 min with the calcineurin inhibitor FK-506 (5 μM), that increased P2X3 currents without altering pSer P2X3, as previously

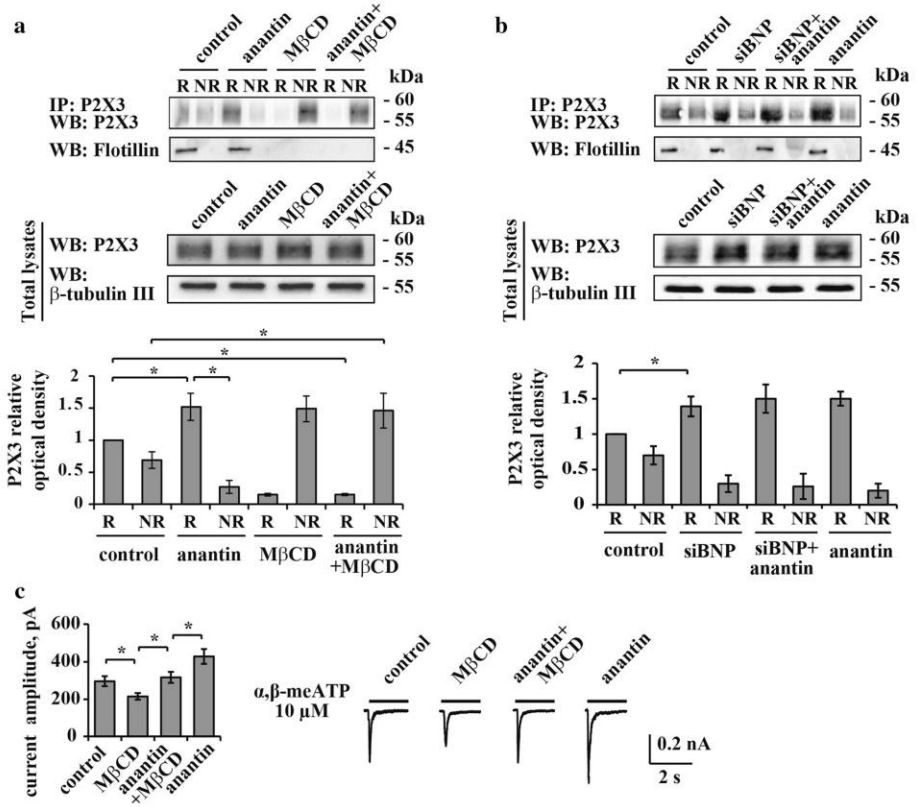

Fig. 4 Anantin facilitates P2X3 localization to lipid rafts. **a** *Top panel* is a representative example of Western immunoblotting showing the amount of P2X3 receptors in raft (*R*) and non-raft (*NR*) membrane fractions in control and after treatment with anantin (500 nM, 24 h), MβCD (10 mM, 30 min) or their combination; flotillin bands indicate lipid raft membrane fractions. *Lower panel* shows total amount of P2X3 receptors for each experimental condition; β-tubulin was used as loading control of the total extract. Histograms at the bottom quantify mean P2X3 relative optical density values in lipid raft and non-raft membrane fractions (n = 4; *p < 0.05, Kruskal–Wallis test). Anantin relocates P2X3 receptors from non-raft to lipid raft membrane compartments, while MβCD abolishes anantin effect. **b** *Top panel* is a representative example of Western immunoblotting showing the amount of P2X3 receptors in raft and non-raft membrane fractions in control and after treatment with anantin (500 nM, 2–3 h), siRNA BNP (48 h), or their combination; flotillin bands indicate raft membrane fractions. Lower panel shows total amount of P2X3 receptors in each experimental condition; β-tubulin was used as loading control of the total extract. Histograms at the *bottom* quantify P2X3 relative optical density in lipid raft and non-raft membrane fractions according to the used treatment (n = 4; *p < 0.05, Kruskal–Wallis test). **c** Histograms show mean P2X3 current amplitude values in control and after application of MβCD (10 mM, 30 min), anantin (500 nM, 2–3 h), or their combination (n = 47, 58, 40, 61; *p < 0.05, Kruskal–Wallis test). Representative current traces of P2X3 receptors evoked by α,β-meATP (10 μM, 2 s) for each experimental condition are shown on the *right*. MβCD per se decreases P2X3 current density, whereas MβCD co-application with anantin returns current density values to control level

reported [40]. Co-application of FK-506 together with anantin did not interfere with the effects of anantin on P2X3 receptors (Fig. 6a, b). Although Cdk5 is a negative modulator of P2X3 receptor activity [13], unchanged effects of anantin were also observed when we used 48 h Cdk5 siRNA treatment (Fig. 6c, d). Likewise, while CaMKII is reported to control P2X3 serine phosphorylation in TG neurons [40], the CaMKII antagonist KN-93 did not influence subsequent anantin effects on P2X3 receptors (Fig. 6e, f). In summary, the basal Ser phosphorylation of P2X3 receptors was under the distinct control of NPR-A receptors without apparently involving calcineurin, CdK5 or CaMKII.

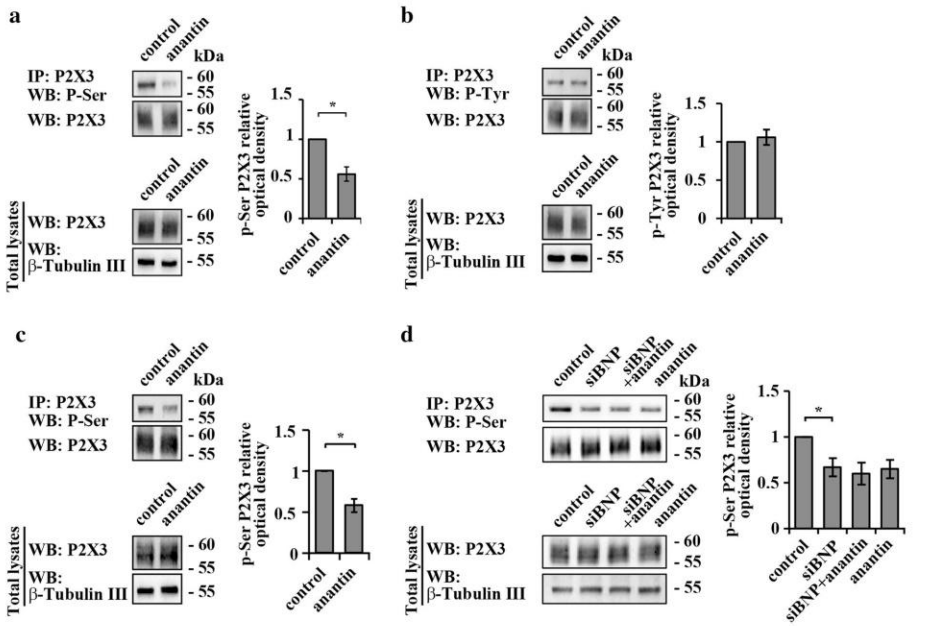

Fig. 5 Anantin increases P2X3 serine phosphorylation. **a** Western immunoblotting shows the amount of P2X3 pSer and total amount of P2X3 receptors in control and after 1 h anantin (500 nM) application. β-tubulin was used as loading control of the total extract. Histograms on the *right* show statistically lower P2X3 pSer (relative optical density value) after anantin application compared to control (n = 4; *p < 0.05, Mann–Whitney rank sum test). **b** Representative example of Western immunoblotting, showing the amount of P2X3 pTyr and total amount of P2X3 receptors in control and after anantin application; β-tubulin used as loading control of the total extract. P2X3 pTyr does not change as shown in the plot on the *right*, summarizing pTyr P2X3 relative optical density in control and after anantin treatment. **c** Western immunoblotting shows the amount of P2X3 pSer and total amount of P2X3 receptors in control and after prolonged anantin application (500 nM, 24 h) (n = 3; *p < 0.05, Mann–Whitney rank sum test). β-tubulin used as loading control of the total extract. Note that anantin effects after 24 h or 1 h of treatment (panels **c** and **a**, respectively) are virtually indistinguishable. **d** Representative example of Western immunoblotting showing the amount of P2X3 pSer in control and after treatment with anantin (500 nM, 2–3 h), siRNA BNP (24 h), or their combination (n = 4); β-tubulin is used as loading control of the total extract. Histograms on the right quantify P2X3 pSer (relative optical density) according to the treatment (n = 4; *p < 0.05, Kruskal–Wallis test)

P2X3 serine phosphorylation and receptor membrane distribution

We next explored how the preferential lipid raft localization of P2X3 receptors and the decrease in P2X3 pSer were inter-related. Thus, we tested if lipid raft depletion with MβCD affected P2X3 pSer levels following anantin application.

Figure 7a shows a representative example of Western blot analysis of P2X3 pSer levels in control or after application of anantin, MβCD or their combination. MβCD per se did not change basal P2X3 pSer level and did not influence the anantin-induced decrease in P2X3 pSer (Fig. 7a, upper panels and diagram at the bottom). Furthermore, there was no significant difference in the level of pSer of P2X3 receptors between raft and non-raft domains despite varying experimental conditions (Fig. 7b, upper panels and diagram at the bottom). Indeed, anantin produced an analogous two-fold reduction in P2X3 pSer in both compartments, regardless of the presence of MβCD.

Relying on these findings, it seems likely that P2X3 serine phosphorylation and receptor distribution between lipid rafts and non-raft membrane compartments were two separate processes targeted by the BNP/NPR-A pathway to regulate P2X3 receptor activity.

NPR-A pathway is PKG dependent

Since NPR-A activation by BNP produces a rapid increase in cGMP level [25, 26, 42], one important downstream effector of this activity is the kinase PKG [9, 43–45]. We, therefore, inquired whether PKG might regulate P2X3 pSer and/or receptor distribution at membrane level.

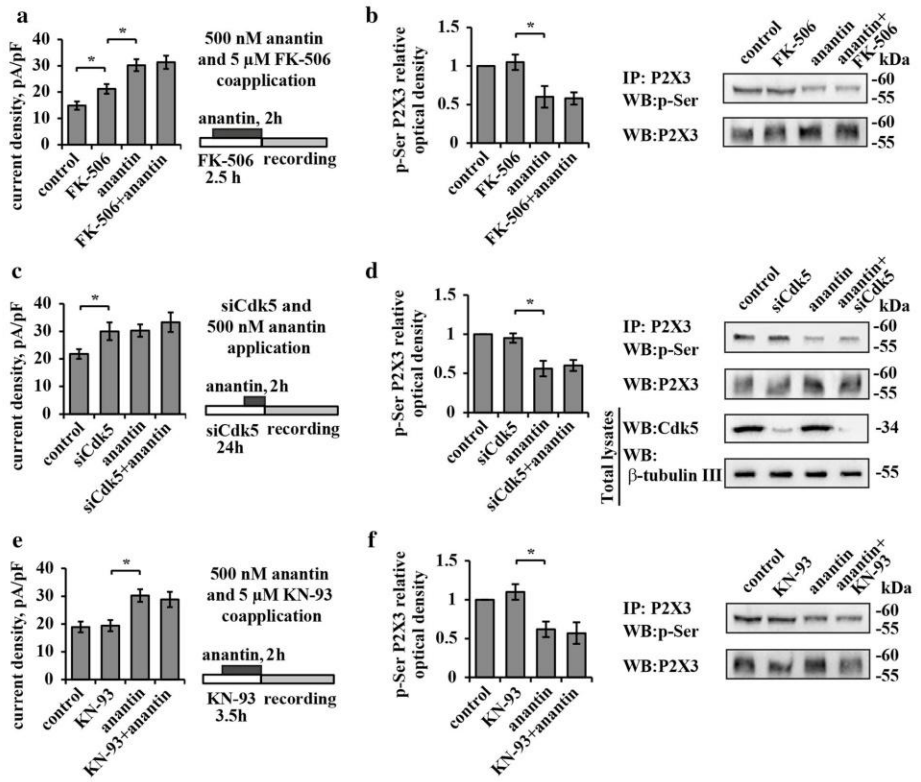

Fig. 6 Anantin effects do not depend on the activity of CaMKII, Cdk5 kinase or the phosphatase calcineurin. **a** *Bar* plot summarizes means of P2X3 current density values in control and after application of calcineurin inhibitor FK-506 (5 μM, 2.5 h), anantin (500 nM, 2 h) or their combination (n = 37, 36, 40, 31, respectively; *p < 0.05, Kruskal–Wallis test). Scheme on the *right* describes experimental protocol of anantin and FK-506 coapplication. FK-506 pretreatment does not prevent anantin-induced increase of P2X3 current density values. **b** Representative example of Western immunoblotting (*right*) and the histogram (*left*), summarizing P2X3 pSer relative optical density values in control, after application of anantin (500 nM, 2 h), FK-506 (5 μM, 2.5 h), or their combination (n = 3; *p < 0.05, Kruskal–Wallis test). **c** Histograms show mean current density values of P2X3 receptors in control, after 24 h Cdk5 silencing with small interfering RNAs, after anantin application (500 nM, 3 h), or after a combination of those two treatments (n = 32, 31, 40, 30, respectively; *p < 0.05, Kruskal–Wallis test). Scheme on the *right* describes experimental protocol of combined siCdk5 and anantin treatments. Cdk5 RNA silencing does not prevent anantin from upregulating P2X3 receptor activity. **d** Representative example of Western immunoblotting (*right*) and histogram (*left*), summarizing P2X3 pSer (relative optical density values) in control, after application of anantin, 24 h siCdk5, or a combination of these treatments (n = 3; *p < 0.05, Kruskal–Wallis test); β-tubulin used as loading control of the total extract. **e** Histograms compare mean current density values of P2X3 receptors in control and after application of CaMKII inhibitor KN-93 (5 μM, 3.5 h), anantin (500 nM, 2 h), or their combination (n = 29, 26, 40, 28, respectively; *p < 0.05, Kruskal–Wallis test). Scheme on the *right* describes experimental protocol of anantin and KN-93 coapplication. KN-93 does not influence anantin-mediated increase in P2X3 current density. **f** Representative example of Western immunoblotting (*right*) and histograms (*left*), summarizing P2X3 pSer (relative optical density values) in control and after application of anantin (500 nM, 2 h), KN-93 (5 μM, 3.5 h), or KN-93 together with anantin (n = 3; *p < 0.05, Kruskal–Wallis test)

Figure 8a shows that 2 h application of KT 5823 (1 μM), that is reported to be a selective PKG inhibitor at this concentration [46, 47], significantly increased control P2X3 current density values (Fig. 8a, middle and right), therefore mimicking the anantin action without any additive effect when co-applied with it. Likewise, KT 5823 produced anantin-like effects on both P2X3 phosphorylation (Fig. 8b) and receptor distribution to raft/non raft membrane fractions (Fig. 8c), with no additivity when co-applied together with anantin. Hence, it is suggested that PKG, operating as an early gateway of the BNP/NPR-A mediated molecular cascade, regulated P2X3

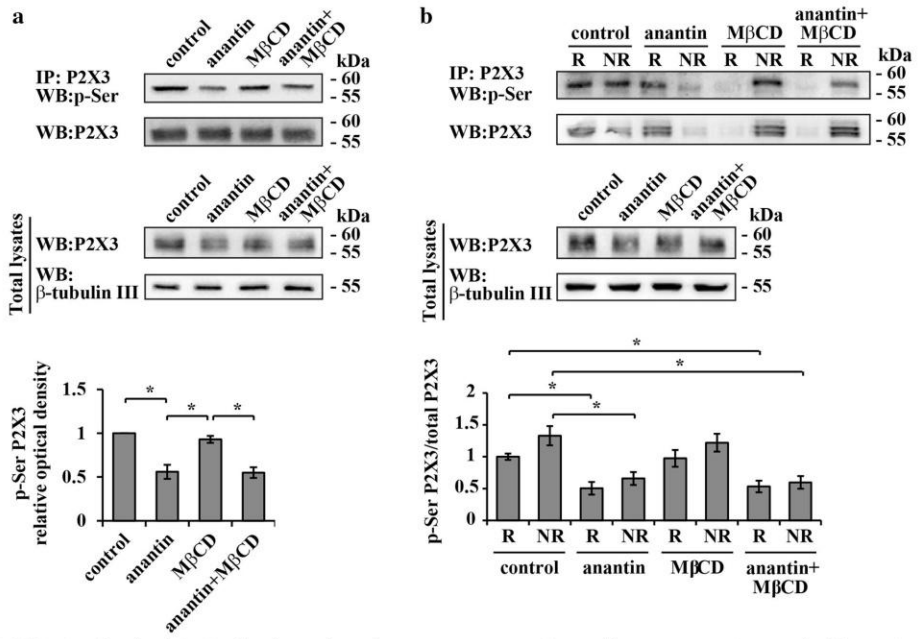

Fig. 7 P2X3 serine phosphorylation in raft and non-raft membrane compartments. **a** *Top panel* shows representative example of Western immunoblotting with P2X3 pSer and anti-P2X3 receptor antibodies, summarizing the amount of P2X3 receptors in control and after application of anantin (500 nM, 2–3 h), MβCD (10 mM, 30 min), or their combination. *Lower panel* shows total P2X3 receptor amount for each experimental condition; β-tubulin used as loading control of the total extract. Histograms at the *bottom* quantify P2X3 pSer (relative optical density values) for each experimental condition ($n = 4$; $^*p < 0.05$, Kruskal–Wallis test). Note that anantin effect on P2X3 pSer level is not influenced by MβCD. **b** *Top panel* shows representative example of Western immunoblotting with P2X3 pSer and P2X3 anti-P2X3 receptor antibodies, summarizing the amount of P2X3 receptors in lipid raft (*R*) and non-raft (*NR*) membrane compartments in control and after application of anantin (500 nM, 2–3 h), MβCD (10 mM, 30 min), or their combination. *Lower panel* shows total P2X3 receptor amount for each experimental condition; β-tubulin used as loading control of the total extract. Histograms at the *bottom* quantify the ratio between P2X3 pSer and total P2X3 in lipid raft and non-raft membrane fractions for each experimental condition ($n = 4$; $^*p < 0.05$, Kruskal–Wallis test). Note that anantin reduces P2X3 pSer equally in both raft and non-raft membrane fractions and this effect is not influenced by MβCD

pSer and receptor distribution within the membrane compartments.

Discussion

The novel result of the present study is the demonstration that constitutive activation of NPR-A by endogenous BNP inhibited P2X3 receptor activity in mouse trigeminal neurons. This process required two distinct modulatory mechanisms: P2X3 serine phosphorylation and receptor distribution to non-raft membrane compartments. This is the first observation of an intrinsic process that may functionally restrain inappropriate activation of pain-sensing P2X3 receptors, and it raises the possibility that chronic pain, at least at the level of the trigeminal territory, might originate from dysfunction of endogenous negative regulators.

Negative control by BNP over P2X3 receptors

A difficulty in demonstrating this role of NPR-A receptors (and of its ligand BNP) was the experimental need to block them to reveal their contribution to P2X3 receptor activity. Thus, one important finding of the present work is that, once background BNP had been depleted by siRNA, we could demonstrate that exogenous BNP inhibited P2X3 function. Because depletion of BNP by siRNA had a basal facilitatory effect on P2X3 receptors, we propose that NPR-A receptors needed background levels of BNP to exert their effect rather than being simply activated even in the absence of their natural ligand. Consistent with that notion, the ambient concentration of BNP in TG cultures was rather low, yet clearly detectable even in the extracellular medium [26] and apparently sufficient to regulate P2X3 receptors. Furthermore, the effects of

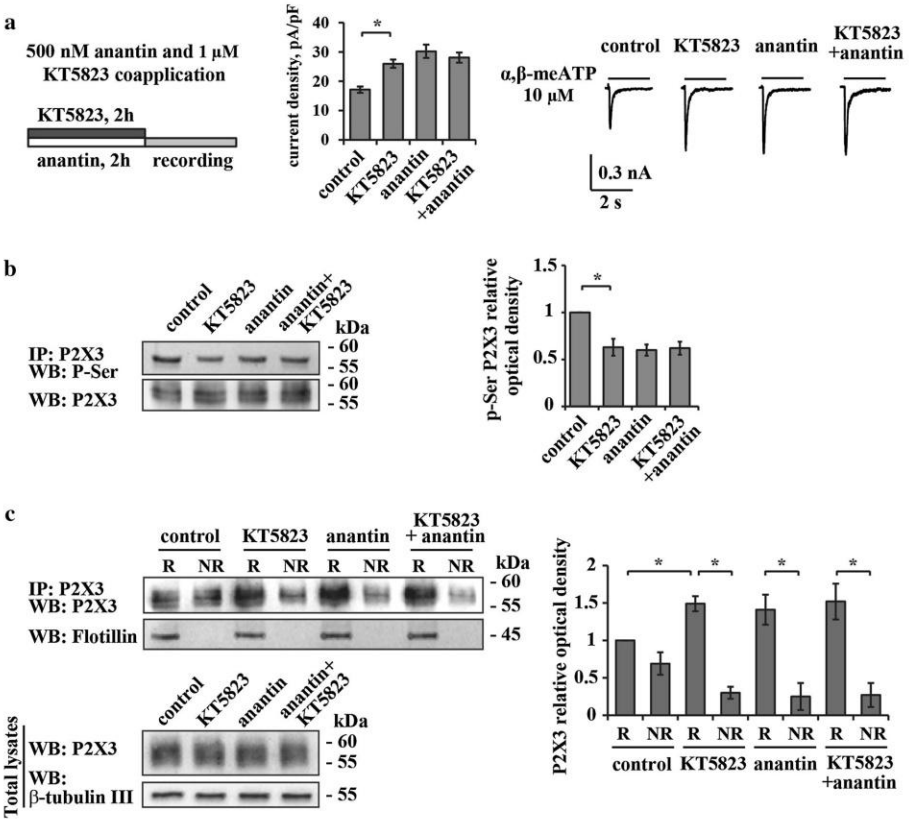

Fig. 8 Effects of the PKG inhibitor KT 5823. **a** Scheme on the *left* describes the protocol of anantin (500 nM, 2 h) and the selective PKG inhibitor KT 5823 (1 μM, 2 h) co-application. Histograms (*middle*) show mean P2X3 current density values in control and after application of KT 5823 (1 μM, 2 h), anantin (500 nM, 2 h), or their combination (n = 33, 30, 40, 34, respectively; *p < 0.05, Kruskal–Wallis test). Representative current traces of P2X3 receptors for each experimental condition are shown on the right and were evoked by 2 s pulses of 10 μM α,β-meATP. KT 5823 produces anantin-like effect on P2X3 currents and shows no additivity when co-applied with anantin. **b** Representative example of Western immunoblotting with P2X3 pSer and P2X3 anti-P2X3 receptor antibodies (*left*) shows the amount of P2X3 receptors in control and after application of KT 5823 (1 μM, 2 h), anantin (500 nM, 2 h) or their combination; histogram on the right quantifies P2X3 pSer (relative optical density values) for each experimental condition (n = 3; *p < 0.05, Kruskal–Wallis test). Note that KT 5823 is as efficient as anantin in lowering the amount of P2X3 pSer. **c** Representative example of Western immunoblotting (on the *left*) and the histograms (on the *right*) summarize the amount of P2X3 receptors and P2X3 pSer in lipid rafts and non-raft membrane fractions in control and after application of KT 5823 (1 μM, 2 h), anantin (500 nM, 2–3 h), or their combination (n = 3; *p < 0.05, Kruskal–Wallis test). KT 5823 acts like anantin, causing P2X3 receptors redistribution to the lipid raft membrane compartment

siBNP seem to suggest that BNP itself rather than other related natriuretic peptides was responsible for the modulation of P2X3 receptors. Our interpretation is that, since basal levels of BNP constitutively depressed P2X3 receptors, unmasking this phenomenon required blocking BNP or its receptor. The synthetic agonist α,β-meATP is selective for P2X3 receptor subunit and can, therefore, activate heteromeric P2X2/3 receptors as well [48–50] with their characteristic slow plateau current. While colocalization of P2X2 and P2X3 subunits has been previously reported in a number of mouse TG neurons, the contribution by P2X2/3 receptors to membrane currents is relatively small in view of the fact that slow-desensitizing responses are only detected in a minority of these cells [51]. Their small number precluded a systematic evaluation of BNP/NPR-A inhibition on heteromeric P2X2/3 receptors.

The process responsible for the enhanced currents seen after suppressing the BNP/NPR-A system with either anantin or siBNP remains incompletely understood. One contribution was likely to originate from the delayed onset of P2X3 receptor desensitization, an important parameter that controls current amplitude and pain signaling [15]. In the present work monitoring the dynamics of the anantin action showed that BNP/NPR-A system regulated P2X3 receptors almost in all-or-none fashion because there was no gradual modulation of P2X3 currents: in fact, 30 min anantin application was insufficient to affect P2X3 currents, whereas 1 h treatment produced P2X3 receptor upregulation as strong as the one after 24 h, yet these effects were fully reversible on washout.

Because the effects of BNP/NPR-A system inactivation largely resembled the action of CGRP, a well-known positive P2X3 receptor modulator [9], we wondered if the BNP/NPR-A pathway might act by opposing the facilitatory role of CGRP [9, 35–38]. However, simultaneous block of NPR-A and CGRP receptors did not prevent full expression of the potentiating action by anantin, suggesting independence of the BNP/NPR-A system from ambient CGRP.

BNP signaling relies on P2X3 receptor compartmentalization

Our former studies have reported higher peak amplitudes and slower desensitization time of P2X3 receptors when they are preferentially localized to lipid raft membrane compartments [34], a result similar to what we detected after anantin treatment. The lipid raft structure is highly mobile [52, 53], and potentially adaptable to accommodate redistribution of P2X3 receptors on the time scale seen after inactivation of the BNP/NPR-A system. In accordance with this notion, after anantin or siBNP, the number of P2X3 receptors localized to lipid raft membranes increased significantly without changes in the global receptor level, and this redistribution was completely abolished by disrupting lipid rafts with MβCD. It is, however, noteworthy that, even after application of MβCD (that had made P2X3 currents smaller), anantin or siBNP could retain a moderate degree of enhancing activity. Since the total number of P2X3 receptors had not changed, it is suggested that enhancement of P2X3 amplitudes could be partly, but not entirely, explained by the preferential P2X3 receptors localization to lipid raft membrane fraction. This proposal implied the existence of an additional mechanism, apart from receptor redistribution, employed by the BNP/NPR-A system to regulate P2X3 receptor function.

Changes in P2X3 phosphorylation state evoked by BNP/NPR-A block

As phosphorylation/dephosphorylation is one of the most common ways of altering receptor functions, for P2X3 receptors such a crucial regulatory role is often played by serine and tyrosine residues [5, 12, 13, 54, 55]. In our experiments anantin application or siBNP significantly reduced the amount of P2X3 serine phosphorylation (with no change in tyrosine phosphorylation), a phenomenon shown before to associated to larger P2X3 currents [13]. Disrupting lipid rafts with MβCD did not affect pSer or its decline after anantin application, suggesting that membrane compartmentalization and receptor phosphorylation were distinct phenomena.

Our working hypothesis is that there are two distinct branches of the BNP/NPR-A pathway targeting P2X3 receptors. One regulates receptor distribution between lipid rafts and non-raft membrane compartments, the other one controls P2X3 serine phosphorylation level. Further investigations are required to unravel the details of the molecular cascade starting from NPR-A activation and resulting in depressed P2X3 currents.

Intracellular pathways linking NPR-A receptors to P2X3 receptors

In search for intermediate steps of the P2X3 modulating NPR-A pathway, we examined the involvement of kinases such as Cdk5 and CaMKII, and of the phosphatase calcineurin, all previously shown to play a role in P2X3 modulation [13, 40]. However, experiments with CaMKII or calcineurin antagonists, or siCdk5 indicated that these enzymes did not play a significant role in the NPR-A modulation of P2X3 pSer or current size.

Notwithstanding the elucidation of the intermediate factors controlling P2X3 receptors via NPR-A activity, our study examined the contribution by PKG as a downstream step after BNP/NPR-A activation. Our previous work has reported early changes in cGMP levels evoked by BNP [26] that would be expected to activate PKG, a family of intracellular kinases that regulate multiple intracellular targets [56–58]. Because KT 5823, used to inhibit PKG, mirrored the effects of anantin or siBNP, it seems that PKG activity was, indeed, a critical gateway to modulate P2X3 receptors. Using the ScanProsite tool (http://prosite.expasy.org/cgi-bin/prosite/ScanView.cgi?scanfile=432156126103.scan.gz), we could not identify apparent consensus sites for the kinase activity on mouse P2X3 receptors. It appears, therefore, unlikely that PKG would directly phosphorylate discrete sites in the intracellular domains of the P2X3 receptors.

Figure 9 illustrates our proposal that the operation of P2X3 receptors under normal conditions is controlled

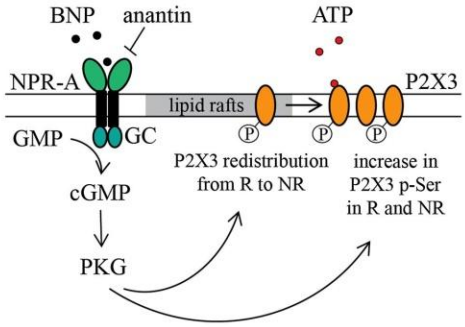

Fig. 9 The scheme of BNP/NPR-A dependent downregulation of P2X3 receptors. ATP (*open circles, red*) and BNP (*filled circles*) are extracellular ligands for P2X3 and NPR-A receptors, respectively. P2X3 receptors are localized to lipid raft (*R*) and non-raft (*NR*) membrane compartments. When P2X3 receptors are in *NR*, they show less efficient signaling. BNP by activating NPR-A receptors of sensory neurons activates guanylyn cyclase (*GC*) to increase intracellular cGMP and activate PKG. The latter indirectly regulates, in a negative fashion, P2X3 function by determining their localization to the non-raft domains and by facilitating their pSer

by the constitutively active NPR-A pathway due to ambient BNP. In our diagram, the basal level of BNP, which is partly produced in TG and mainly supplied to the tissue with the blood flow [24], constantly downregulates P2X3 receptors, elevating their agonist threshold [26]. Hence, BNP via PKG activation mediated by NPR-A receptors would help to localize P2X3 receptors to non-lipid raft membrane compartments, to control their serine phosphorylation state, and to speed up their desensitization without impairing the ability to respond to the natural agonist ATP.

While our scheme includes a P2X3 inhibitory role of BNP via guanylate cyclase and cGMP production, any interaction between P2X3 receptors and other guanylate cyclase activators like nitric oxide (NO) remains unclear. NO donors such as glyceryl trinitrate (GTN) are used as models to induce trigeminal pain and delayed migraine [59]. Former studies show that GTN is effective only when given systemically [60] and that its migraine-provoking activity is dependent on CGRP [61, 62]. This process is, however, incompletely understood because CGRP antagonists do not block GTN headache [63]. Since activation of P2X3 receptors is known to trigger membrane translocation of the NO synthetic enzyme and NO production [64], it is possible to speculate that P2X3 receptor activity is an upstream event to NO-evoked cGMP synthesis and pain [65]. Thus, ongoing P2X3 inhibition by BNP via neuronal NPR-A receptors might be a primary mechanism for controlling the threshold to trigeminal nociception regulated by a complex mix of soluble factors.

The inhibitory role of the BNP/NPR-A system via PKG activity appears to be present also in DRG in which BNP (when co-applied with glutamate) depresses the excitability of a subgroup of sensory neurons in a model of inflammatory pain [27]. In this study, BNP reduced the firing frequency of DRG neurons via intracellular signaling leading to activation of large-conductance Ca^{2+}-activated K^+ channels (BK_{Ca} channels). Future investigations are necessary to explore whether P2X3 receptors, that are expressed by 40 % DRG neurons [66], are also a target for the inhibitory action by BNP.

Conclusions

In conclusion, the present data outline BNP as the first inhibitory neuropeptide to constitutively depress the P2X3 receptor function. The process appears to be NPR-A and PKG dependent and it involves P2X3 serine phosphorylation and receptor redistribution to the non-raft membrane compartments (Fig. 9). This suggestion will have to be studied in the framework of complex mechanisms responsible for acute or chronic nociception at trigeminal sensory ganglion level. In particular, pharmacological or genetic interference with the BNP/NPRA system in vivo and its effects on allodynia or hyperalgesia would significantly enhance the impact of the current results.

Methods

Animals and TG primary culture preparations

All animal procedures were conducted in accordance with the guidelines of the Italian Animal Welfare Act and regulations of animal welfare. All treatment protocols were approved by the Scuola Internazionale Superiore di Studi Avanzati (SISSA) ethics committee and are in accordance with the European Union guidelines. Trigeminal ganglion primary cultures were obtained from animals at the age of P12-14 as described previously [51] and employed after 24 or 48 h from plating.

Chemicals and treatments

A range of validated chemicals were used to uncover molecular mechanisms underlying the main biochemical and electrophysiological observations. The specific NPR-A receptor antagonist anantin (US Biologicals, Salem, MA, USA), the CGRP receptor antagonist CGRP 8-37 (Sigma-Aldrich, Milan, Italy), and the cholesterol depleting agent methyl-β-cyclodextrin (MβCD, Sigma) were dissolved in sterile water and applied to the cell cultures medium. Anantin was applied for 30 min–24 h at the concentration of 500 nM to ensure full block of NPR-A receptors [26, 67]. CGRP 8–37 was applied in

1 μM concentration to effectively block CGRP receptors [39, 68–70]. MβCD (10 mM) was applied for 30 min in accordance with previous reports [34, 71, 72]. We also applied 5 μM FK-506 (dissolved in DMSO), a well-known immunosuppressant drug that induces persistent pain in humans [73, 74] and acts by inhibiting the Ca^{2+}-dependent phosphatase calcineurin [75]. KN-93 (5 μM) was used to block the activity of calcium calmodulin mediated kinase II (CaMKII) in accordance with previous studies [40]. KT 5823 (1 μM; Sigma) was used to inhibit PKG [46, 47].

BNP and cyclin-dependent kinase 5 (Cdk5) silencing

Cultured mouse trigeminal neurons were transfected with specific siRNA BNP (siBNP) oligonucleotides (Sigma), or siCdk5 oligonucleotide (ThermoFisher Scientific, Milan, Italy) using the DharmaFECT transfection reagent (Dharmacon, Lafayette, CO, USA). As control ("scramble"), cells were transfected with siGLO RISC-Free siRNA (Dharmacon). The BNP siRNA and control siRNA were transfected at a final concentration of 100 nM for 24 h in triplicate for each treatment. At 48 h post-transfection, BNP knockdown was confirmed by immunostaining and Elisa assay. A pool of two different oligonucleotide sequences were used to knockdown BNP (NM_008726) expression, as previously published [76]: BNP siRNA-1: sense 5′-CCCAGAGAC AGCUCUUGAATT-3′ with antisense 5′-UUCAAGA GCUGUCUCUGGGTT-3′, and BNP siRNA-2: sense 5′-GGCACAAGAUAGACCGGAUTT-3′ with antisense 5′-AUCCGGUCUAUCUUGUGCCTT-3′. To knockdown Cdk5 expression (NM_007668.3), siCdk5 or control siRNA sequences were transfected at a final concentration of 100 nM. Twenty-four hours after silencing, cells were used for protein expression and patch clamping experiments. Efficiency of Cdk5 silencing was tested with Western blot.

Immunocytochemistry

Forty-eight hours after siRNA-treatment, primary cultures from P12-P14 mouse TG were fixed in 4 % paraformaldehyde and immunofluorescence was carried out as previously described [26]. Polyclonal antibody against BNP (G-011-23; 1:100) was from Phoenix Pharmaceuticals (Burlingame, CA, USA). Secondary antibody conjugated with Alexa Fluor-594 was purchased from Invitrogen (1:500; Milan, Italy). Nuclei were counterstained with DAPI (Sigma). Images were obtained using a Leica TCS SP2 confocal microscope (Wetzlar, Germany).

Membrane fractionation and protein extraction

Total membrane protein extraction and Triton X-100-soluble and -insoluble fractionation were performed as reported by Gnanasekaran et al. 2011 [34]. To ensure equal loading for each cell lysate, protein extracts were quantified with bicinchoninic acid (BCA; Sigma). The amount of loaded proteins was in the 20–50 μg/ml range. Immunoprecipitation of P2X3 receptors from membrane fractions (raft and non-raft) was performed as previously reported [12].

Western blot

Western blot analysis was performed according to the methods previously reported [12, 26]. Cells were lysed in ODG buffer solution (2 % *n*-octyl-beta-D-glucopyranoside, containing 1 % Nonidet P-40, 10 mM Tris pH 7.5, 150 mM NaCl, plus protease inhibitors mixture; Complete, Roche Applied Science, Basel, Switzerland). Proteins were separated in 10 % SDS–polyacrylamide gel and transferred to nitrocellulose membranes. Immunoblotting was performed with the following validated primary antibodies: rabbit anti-P2X3 (1:1000; Santa Cruz Biotechnology, Heidelberg, Germany) rabbit anti-NPR-A (1:1000, Abcam), anti-β-tubulin III (1:2000; Sigma), mouse anti-β-actin (1:3000, Sigma), mouse anti-flotillin 1 (1:250; BD Biosciences), anti-phospho-Serine (1:500, millipore), anti-phospho-Tyrosine (1:500, millipore) [26, 34, 40]. Signals were revealed after incubation with recommended secondary antibodies conjugated with horseradish peroxidase by using ECL detection reagent (Amersham Biosciences, Piscataway, NJ, USA) and recorded by the digital imaging system Alliance 4.7 (UVITEC, Cambridge, UK).

ELISA assay for BNP

Samples from TG cultures and their culture medium were collected 24 h after plating and prepared as described by Vilotti et al. (2013). The BNP levels were assessed using an ELISA kit (Abnova, Hidelberg, Germany), following the instructions of the manufacturer. Sample BNP levels were determined using standard concentration curves and evaluated in duplicate. Data were normalized to sample protein concentration, as determined by the BCA method (Sigma).

Electrophysiology

Electrophysiology experiments were performed using previously reported protocols [39, 51]. Cultured TG neurons were patch-clamped in the whole-cell configuration under continuous perfusion (3 mL/min) with physiological solution containing (in mM): 152 NaCl, 5 KCl, 1 $MgCl_2$, 2 $CaCl_2$, 10 glucose, and 10 HEPES (pH adjusted to 7.4 with NaOH). Patch pipettes were filled with the following solution (in mM): 140 KCl, 0.5 $CaCl_2$, 2 $MgCl_2$, 2 Mg_2ATP3, 2 GTP, 10 HEPES and 10 EGTA (pH adjusted to 7.2 with KOH) and had a resistance of

3–4 MΩ. Recordings were performed from small and medium size trigeminal neurons [39] held at −65 mV after correction for liquid junction potential. Currents were filtered at 1 kHz and acquired by means of a Digi-Data 1200 interface and pClamp8.2 software (Molecular Devices, Sunnyvale, CA, USA). In accordance with our previous studies α,β-methylene-adenosine-5′-triphosphate (α,β-meATP; Sigma), a stable synthetic agonist of P2X3 receptors [33] was applied for 2 s at a standard dose of 10 μM [26, 33, 39] using a fast superfusion system (Rapid Solution Changer RSC-200; BioLogic Science Instruments, Claix, France) to evoke reproducible near-maximal P2X3 responses [13, 77]. Data were collected from at least 4 individual experiments with number of cells equal or greater than 25. Responses were measured as peak amplitudes and presented as current density values (pA/pF) after normalization to the cells' capacity, in order to eliminate differences in currents originated from cell size variation. The only exception were experiments with MβCD, where the data were shown as peak current amplitudes, since MβCD, as a cholesterol depleting agent, is expected to change cell capacitance.

Statistical analysis

Data are expressed as mean ± standard deviation (s.d.) or as mean ± standard error of the mean (SEM), where n indicates the number of independent experiments or the number of investigated cells, as indicated in figure legends. Statistical analysis was performed using nonparametric Mann–Whitney rank sum test, or the Student's t test, after the software-directed choice of non-parametric or parametric data, respectively (Matlab; Sigma Plot and Sigma Stat Software, Chicago, IL, USA), or Kruskal–Wallis test for multiple comparison. A p value of <0.05 was accepted as indicative of a statistically significant difference.

Abbreviations

α,β-meATP: α,β-MethyleneATP; BCA: Bicinchoninic acid; s.d.: Standard deviation; BNP: Brain natriuretic peptide; CaMKII: Calcium calmodulin mediated kinase II; CGRP: Calcitonin gene-related peptide; DRG: Dorsal root ganglia; GTN: Glyceryl trinitrate; MβCD: Methyl-β-cyclodextrin; NO: Nitric oxide; NPR-A: Natriuretic peptide receptor-A; PKG: CGMP-dependent protein kinase; pSer: Serine phosphorylation; pTyr: Tyrosine phosphorylation; sem: Standard error of the mean; TG: Trigeminal ganglion.

Authors' contributions

AM, SV, AN, design of experiments and collection of data; AN, project supervision; AM, SV, EF, AN, joint contribution to MS writing. All authors read and approved the final manuscript.

Author details

[1] Neuroscience Department, International School for Advanced Studies (SISSA), Via Bonomea 265, 34136 Trieste, Italy. [2] Center for Biomedical Sciences and Engineering, University of Nova Gorica, 5000 Nova Gorica, Slovenia.

Acknowledgements

This work was supported by the EU FP7 grant EuroHeadPain (#602633).

Competing interests

The authors declare that they have no competing interests.

Received: 10 September 2015 Accepted: 3 November 2015
Published online: 14 November 2015

References

1. Vulchanova L, Riedl MS, Shuster SJ, Buell G, Surprenant A, North RA, Elde R. Immunohistochemical study of the P2X2 and P2X3 receptor subunits in rat and monkey sensory neurons and their central terminals. Neuropharmacology. 1997;36:1229–42.
2. Llewellyn-Smith IJ, Burnstock G. Ultrastructural localization of P2X3 receptors in rat sensory neurons. NeuroReport. 1998;9:2545–50.
3. Wirkner K, Stanchev D, Köles L, Klebingat M, Dihazi H, Flehmig G, Vial C, Evans RJ, Fürst S, Mager PP, Eschrich K, Illes P. Regulation of human recombinant P2X3 receptors by ecto-protein kinase C. J Neurosci. 2005;25:7734–42.
4. Burnstock G. Purinergic P2 receptors as targets for novel analgesics. Pharmacol Ther. 2006;110:433–54.
5. Giniatullin R, Nistri A, Fabbretti E. Molecular mechanisms of sensitization of pain-transducing P2X3 receptors by the migraine mediators CGRP and NGF. Mol Neurobiol. 2008;37:83–90.
6. Hullugundi SK, Ansuini A, Ferrari MD, van den Maagdenberg AMJM, Nistri A. A hyperexcitability phenotype in mouse trigeminal sensory neurons expressing the R192Q Cacna1a missense mutation of familial hemiplegic migraine type-1. Neuroscience. 2014;266:244–54.
7. Xu G-Y, Huang L-YM. Peripheral inflammation sensitizes P2X receptor-mediated responses in rat dorsal root ganglion neurons. J Neurosci. 2002;22:93–102.
8. Burnstock G. Purinergic signalling: pathophysiology and therapeutic potential. Keio J Med. 2013;62:63–73.
9. Fabbretti E, D'Arco M, Fabbro A, Simonetti M, Nistri A, Giniatullin R. Delayed upregulation of ATP P2X3 receptors of trigeminal sensory neurons by calcitonin gene-related peptide. J Neurosci. 2006;26:6163–71.
10. Ma W, Quirion R. Targeting cell surface trafficking of pain-facilitating receptors to treat chronic pain conditions. Expert Opin Ther Targets. 2014;18:459–72.
11. Chen X-Q, Zhu J-X, Wang Y, Zhang X, Bao L. CaMKIIα and caveolin-1 cooperate to drive ATP-induced membrane delivery of the P2X3 receptor. J Mol Cell Biol. 2014;6:140–53.
12. D'Arco M, Giniatullin R, Leone V, Carloni P, Birsa N, Nair A, Nistri A, Fabbretti E. The C-terminal Src inhibitory kinase (Csk)-mediated tyrosine phosphorylation is a novel molecular mechanism to limit P2X3 receptor function in mouse sensory neurons. J Biol Chem. 2009;284:21393–401.
13. Nair A, Simonetti M, Fabbretti E, Nistri A. The Cdk5 kinase downregulates ATP-gated ionotropic P2X3 receptor function via serine phosphorylation. Cell Mol Neurobiol. 2010;30:505–9.
14. Mo G, Grant R, O'Donnell D, Ragsdale DS, Cao CQ, Séguéla P. Neuropathic Nav1.3-mediated sensitization to P2X activation is regulated by protein kinase C. Mol Pain. 2011;7:14.
15. Giniatullin R, Nistri A. Desensitization properties of P2X3 receptors shaping pain signaling. Front Cell Neurosci. 2013;7:245.
16. Paukert M, Osteroth R, Geisler H-S, Brändle U, Glowatzki E, Ruppersberg JP, Gründer S. Inflammatory Mediators potentiate ATP-gated channels through the P2X3 subunit. J Biol Chem. 2001;276:21077–82.
17. Chen Y, Zhang L, Yang J, Zhang L, Chen Z. LPS-induced dental pulp inflammation increases expression of ionotropic purinergic receptors in rat trigeminal ganglion. NeuroReport. 2014;25:991–7.
18. Schiavuzzo JG, Teixeira JM, Melo B, da Silva Dos Santos DF, Jorge CO, Oliveira-Fusaro MCG, Parada CA. Muscle hyperalgesia induced by peripheral P2X3 receptors is modulated by inflammatory mediators. Neuroscience. 2015;285:24–33.
19. Ellis A, Bennett DLH. Neuroinflammation and the generation of neuropathic pain. Br J Anaesth. 2013;111:26–37.

20. Nakagawa T, Wakamatsu K, Zhang N, Maeda S, Minami M, Satoh M, Kaneko S. Intrathecal administration of ATP produces long-lasting allodynia in rats: differential mechanisms in the phase of the induction and maintenance. Neuroscience. 2007;147:445–55.
21. Fabbretti E. ATP P2X3 receptors and neuronal sensitization. Front Cell Neurosci. 2013;7:236.
22. Yan J, Dussor G. Ion channels and migraine. Headache. 2014;54:619–39.
23. Liu X-Y, Wan L, Huo F-Q, Barry DM, Li H, Zhao Z-Q, Chen Z-F. B-type natriuretic peptide is neither itch-specific nor functions upstream of the GRP-GRPR signaling pathway. Mol Pain. 2014;10:4.
24. Potter LR, Yoder AR, Flora DR, Antos LK, Dickey DM. Natriuretic peptides: their structures, receptors, physiologic functions and therapeutic applications. Handb Exp Pharmacol. 2009:341–366.
25. Misono KS. Natriuretic peptide receptor: structure and signaling. Mol Cell Biochem. 2002;230:49–60.
26. Vilotti S, Marchenkova A, Ntamati N, Nistri A. B-type natriuretic peptide-induced delayed modulation of TRPV1 and P2X3 receptors of mouse trigeminal sensory neurons. PLoS One. 2013;8:e81138.
27. Zhang F-X, Liu X-J, Gong L-Q, Yao J-R, Li K-C, Li Z-Y, Lin L-B, Lu Y-J, Xiao H-S, Bao L, Zhang X-H, Zhang X. Inhibition of inflammatory pain by activating B-type natriuretic peptide signal pathway in nociceptive sensory neurons. J Neurosci. 2010;30:10927–38.
28. Fabbretti E, Nistri A. Regulation of P2X3 receptor structure and function. CNS Neurol Disord. 2012;11:687–98.
29. Vacca F, Amadio S, Sancesario G, Bernardi G, Volonté C. P2X3 receptor localizes into lipid rafts in neuronal cells. J Neurosci Res. 2004;76:653–61.
30. Zajchowski LD, Robbins SM. Lipid rafts and little caves. Compartmentalized signalling in membrane microdomains. Eur J Biochem. 2002;269:737–52.
31. Garcia-Marcos M, Dehaye J-P, Marino A. Membrane compartments and purinergic signalling: the role of plasma membrane microdomains in the modulation of P2XR-mediated signalling. FEBS J. 2009;276:330–40.
32. Allsopp RC, Lalo U, Evans RJ. Lipid raft association and cholesterol sensitivity of P2X1-4 receptors for ATP: chimeras and point mutants identify intracellular amino-terminal residues involved in lipid regulation of P2X1 receptors. J Biol Chem. 2010;285:32770–7.
33. Sokolova E, Skorinkin A, Moiseev I, Agrachev A, Nistri A, Giniatullin R. Experimental and modeling studies of desensitization of P2X3 receptors. Mol Pharmacol. 2006;70:373–82.
34. Gnanasekaran A, Sundukova M, van den Maagdenberg AMJM, Fabbretti E, Nistri A. Lipid rafts control P2X3 receptor distribution and function in trigeminal sensory neurons of a transgenic migraine mouse model. Mol Pain. 2011;7:77.
35. Cady RJ, Glenn JR, Smith KM, Durham PL. Calcitonin gene-related peptide promotes cellular changes in trigeminal neurons and glia implicated in peripheral and central sensitization. Mol Pain. 2011;7:94.
36. Yasuda M, Shinoda M, Kiyomoto M, Honda K, Suzuki A, Tamagawa T, Kaji K, Kimoto S, Iwata K. P2X3 receptor mediates ectopic mechanical allodynia with inflamed lower lip in mice. Neurosci Lett. 2012;528:67–72.
37. Simonetti M, Giniatullin R, Fabbretti E. Mechanisms mediating the enhanced gene transcription of P2X3 receptor by calcitonin gene-related peptide in trigeminal sensory neurons. J Biol Chem. 2008;283:18743–52.
38. Ceruti S, Villa G, Fumagalli M, Colombo L, Magni G, Zanardelli M, Fabbretti E, Verderio C, van den Maagdenberg AMJM, Nistri A, Abbracchio MP. Calcitonin gene-related peptide-mediated enhancement of purinergic Neuron/Glia communication by the algogenic factor Bradykinin in Mouse Trigeminal Ganglia from Wild-Type and R192Q Cav2.1 Knock-In Mice: implications for basic mechanisms of migraine pain. J Neurosci. 2011;31:3638–49.
39. Hullugundi SK, Ferrari MD, van den Maagdenberg AMJM, Nistri A. The mechanism of functional up-regulation of P2X3 receptors of trigeminal sensory neurons in a genetic mouse model of familial hemiplegic migraine type 1 (FHM-1). PLoS One. 2013;8:e60677.
40. Nair A, Simonetti M, Birsa N, Ferrari MD, van den Maagdenberg AMJM, Giniatullin R, Nistri A, Fabbretti E. Familial hemiplegic migraine Ca(v)2.1 channel mutation R192Q enhances ATP-gated P2X3 receptor activity of mouse sensory ganglion neurons mediating trigeminal pain. Mol Pain. 2010;6:48.
41. Xu G-Y, Huang L-YM. Ca^{2+}/calmodulin-dependent protein kinase II potentiates ATP responses by promoting trafficking of P2X receptors. Proc Natl Acad Sci USA. 2004;101:11868–73.
42. Hofmann F, Feil R, Kleppisch T, Schlossmann J. Function of cGMP-dependent protein kinases as revealed by gene deletion. Physiol Rev. 2006;86:1–23.
43. Pandey KN. Guanylyl cyclase/natriuretic peptide receptor-A signaling antagonizes phosphoinositide hydrolysis, Ca^{2+} release, and activation of protein kinase C. Front Mol Neurosci. 2014;7.
44. Reger AS, Yang MP, Koide-Yoshida S, Guo E, Mehta S, Yuasa K, Liu A, Casteel DE, Kim C. Crystal structure of the cGMP-dependent protein kinase II leucine zipper and Rab11b protein complex reveals molecular details of G-kinase-specific interactions. J Biol Chem. 2014;289:25393–403.
45. Potter LR. Regulation and therapeutic targeting of peptide-activated receptor guanylyl cyclases. Pharmacol Ther. 2011;130:71–82.
46. Pasdois P, Quinlan CL, Rissa A, Tariosse L, Vinassa B, Costa ADT, Pierre SV, Dos Santos P, Garlid KD. Ouabain protects rat hearts against ischemia-reperfusion injury via pathway involving src kinase, mitoKATP, and ROS. Am J Physiol Heart Circ Physiol. 2007;292:H1470–8.
47. Hidaka H, Kobayashi R. Pharmacology of protein kinase inhibitors. Annu Rev Pharmacol Toxicol. 1992;32:377–97.
48. Tsuda M, Koizumi S, Kita A, Shigemoto Y, Ueno S, Inoue K. Mechanical allodynia caused by intraplantar injection of P2X receptor agonist in rats: involvement of heteromeric P2X2/3 receptor signaling in capsaicin-sensitive primary afferent neurons. J Neurosci. 2000;20:RC90.
49. Kawashima E, Estoppey D, Virginio C, Fahmi D, Rees S, Surprenant A, North RA. A novel and efficient method for the stable expression of heteromeric ion channels in mammalian cells. Recept Channels. 1998;5:53–60.
50. Chen X, Gebhart GF. Differential purinergic signaling in bladder sensory neurons of naïve and bladder-inflamed mice. Pain. 2010;148:462–72.
51. Simonetti M, Fabbro A, D'Arco M, Zweyer M, Nistri A, Giniatullin R, Fabbretti E. Comparison of P2X and TRPV1 receptors in ganglia or primary culture of trigeminal neurons and their modulation by NGF or serotonin. Mol Pain. 2006;2:11.
52. Pike LJ. Rafts defined: a report on the keystone symposium on lipid rafts and cell function. J Lipid Res. 2006;47:1597–8.
53. Lingwood D, Kaiser H-J, Levental I, Simons K. Lipid rafts as functional heterogeneity in cell membranes. Biochem Soc Trans. 2009;37(Pt 5):955–60.
54. D'Arco M, Giniatullin R, Simonetti M, Fabbro A, Nair A, Nistri A, Fabbretti E. Neutralization of nerve growth factor induces plasticity of ATP-sensitive P2X3 receptors of nociceptive trigeminal ganglion neurons. J Neurosci. 2007;27:8190–201.
55. Gnanasekaran A, Sundukova M, Hullugundi S, Birsa N, Bianchini G, Hsueh Y-P, Nistri A, Fabbretti E. Calcium/calmodulin-dependent serine protein kinase (CASK) is a new intracellular modulator of P2X3 receptors. J Neurochem. 2013;126:102–12.
56. Feil R, Hofmann F, Kleppisch T. Function of cGMP-dependent protein kinases in the nervous system. Rev Neurosci. 2005;16:23–41.
57. Schlossmann J, Desch M. cGK substrates. In: Schmidt HHHW, Hofmann F, Stasch J-P, editors. cGMP: Generators, effectors and therapeutic implications. Berlin, Heidelberg: Springer; 2009. pp. 163–93 **(Handbook of Experimental Pharmacology, vol. 191)**.
58. Hofmann F, Bernhard D, Lukowski R, Weinmeister P. cGMP regulated protein kinases (cGK). Handb Exp Pharmacol. 2009:137–62.
59. Olesen J, Thomsen LL, Iversen H. Nitric oxide is a key molecule in migraine and other vascular headaches. Trends Pharmacol Sci. 1994;15:149–53.
60. Pedersen SH, Ramachandran R, Amrutkar DV, Petersen S, Olesen J, Jansen-Olesen I. Mechanisms of glyceryl trinitrate provoked mast cell degranulation. *Cephalalgia*. 2015.
61. Messlinger K, Lennerz JK, Eberhardt M, Fischer MJM. CGRP and NO in the trigeminal system: mechanisms and role in headache generation. Headache. 2012;52:1411–27.
62. Ramachandran R, Bhatt DK, Ploug KB, Hay-Schmidt A, Jansen-Olesen I, Gupta S, Olesen J. Nitric oxide synthase, calcitonin gene-related peptide and NK-1 receptor mechanisms are involved in GTN-induced neuronal activation. Cephalalgia. 2014;34:136–47.
63. Tvedskov JF, Tfelt-Hansen P, Petersen KA, Jensen LT, Olesen J. CGRP receptor antagonist olcegepant (BIBN4096BS) does not prevent glyceryl trinitrate-induced migraine. Cephalalgia. 2010;30:1346–53.
64. Ohnishi T, Matsumura S, Ito S. Translocation of neuronal nitric oxide synthase to the plasma membrane by ATP is mediated by P2X and P2Y receptors. Mol Pain. 2009;5:40.

65. Tvedskov JF, Iversen HK, Olesen J, Tfelt-Hansen P. Nitroglycerin provocation in normal subjects is not a useful human migraine model? Cephalalgia. 2010;30:928–32.
66. Vulchanova L, Riedl MS, Shuster SJ, Stone LS, Hargreaves KM, Buell G, Surprenant A, North RA, Elde R. P2X3 is expressed by DRG neurons that terminate in inner lamina II. Eur J Neurosci. 1998;10:3470–8.
67. Yu Y-C, Cao L-H, Yang X-L. Modulation by brain natriuretic peptide of GABA receptors on rat retinal ON-type bipolar cells. J Neurosci. 2006;26:696–707.
68. Jansen I, Mortensen A, Edvinsson L. Characterization of calcitonin gene-related peptide receptors in human cerebral vessels. Vasomotor responses and cAMP accumulation. Ann N Y Acad Sci. 1992;657:435–40.
69. Giniatullin R, Di Angelantonio S, Marchetti C, Sokolova E, Khiroug L, Nistri A. Calcitonin gene-related peptide rapidly downregulates nicotinic receptor function and slowly raises intracellular Ca^{2+} in rat chromaffin cells in vitro. J Neurosci. 1999;19:2945–53.
70. Chiba T, Yamaguchi A, Yamatani T, Nakamura A, Morishita T, Inui T, Fukase M, Noda T, Fujita T. Calcitonin gene-related peptide receptor antagonist human CGRP-(8–37). Am J Physiol. 1989;256(2 Pt 1):E331–5.
71. Liu M, Huang W, Wu D, Priestley JV. TRPV1, but not P2X, requires cholesterol for its function and membrane expression in rat nociceptors. Eur J Neurosci. 2006;24:1–6.
72. Szoke E, Börzsei R, Tóth DM, Lengl O, Helyes Z, Sándor Z, Szolcsányi J. Effect of lipid raft disruption on TRPV1 receptor activation of trigeminal sensory neurons and transfected cell line. Eur J Pharmacol. 2010;628:67–74.
73. Ferrari U, Empl M, Kim KS, Sostak P, Förderreuther S, Straube A. Calcineurin inhibitor-induced headache: clinical characteristics and possible mechanisms. Headache. 2005;45:211–4.
74. Grotz WH, Breitenfeldt MK, Braune SW, Allmann KH, Krause TM, Rump JA, Schollmeyer PJ. Calcineurin-inhibitor induced pain syndrome (CIPS): a severe disabling complication after organ transplantation. Transpl Int. 2001;14:16–23.
75. Lyons WE, George EB, Dawson TM, Steiner JP, Snyder SH. Immunosuppressant FK506 promotes neurite outgrowth in cultures of PC12 cells and sensory ganglia. Proc Natl Acad Sci USA. 1994;91:3191–5.
76. Abdelalim EM, Tooyama I. BNP signaling is crucial for embryonic stem cell proliferation. PLoS One. 2009;4:e5341.
77. Franceschini A, Nair A, Bele T, van den Maagdenberg AM, Nistri A, Fabbretti E. Functional crosstalk in culture between macrophages and trigeminal sensory neurons of a mouse genetic model of migraine. BMC Neurosci. 2012;13:143.

3. Inefficient constitutive inhibition of P2X3 receptors by the brain natriuretic peptide system in trigeminal sensory neurons of mouse model of genetic migrain

Inefficient constitutive inhibition of P2X3 receptors by the brain natriuretic peptide system in trigeminal sensory neurons of mouse model of genetic migraine

Anna Marchenkova[1]

[1]Neuroscience Department, International School for Advanced Studies (SISSA), Via Bonomea 265, 34136 Trieste, Italy.

Abstract

Background

On cultured trigeminal ganglion (TG) neurons, pain-sensing P2X3 receptors are constitutively inhibited by brain natriuretic peptide (BNP) via its NPR-A receptor. This inhibitory state is associated with increased P2X3 serine phosphorylation and receptor redistribution to non-lipid raft membrane compartments. The NPR-A antagonist anantin reverses these properties. We studied whether P2X3 inhibition is dysfunctional in a migraine model produced by introducing the R192Q mutation into the mouse *Cacna1a* gene (knock-in (KI) phenotype). This model can replicate certain properties of familial hemiplegic migraine type-1 (FHM1), with gain-of-function of $Ca_V2.1$ Ca^{2+} channels, raised levels of the algogenic peptide CGRP, and enhanced activity of P2X3 receptors.

Results

In KI neurons anantin did not affect P2X3 receptor activity, membrane distribution and serine phosphorylation level, implying ineffective inhibition by the constitutive BNP/NPR-A system. However, expression and functional properties of the BNP/NPR-A pathway remained intact together with its ability to downregulate TRPV1 channels. Reversing the FHM1 phenotype with the $Ca_V2.1$ antagonist ω-agatoxin restored P2X3 activity to WT level and enabled to observe the potentiating effects of anantin again. After blocking CGRP receptors, P2X3 receptors exhibited WT properties and were again potentiated by anantin.

Conclusions

P2X3 receptors of mouse TG neurons are subjected to the contrasting modulation by the inhibitory BNP and the facilitatory CGRP that both operate via complex intracellular signaling. In the FHM1 migraine model the action of CGRP appears to prevail over BNP, thus suggesting that peripheral inhibition of P2X3 receptors becomes insufficient and contributes to trigeminal pain sensitization.

Key words: Trigeminal ganglia; ATP; nociception; purinergic receptor; lipid raft; CGRP; familial hemiplegic migraine type-1

Background

Migraine is a common, disabling, and undertreated episodic brain disorder with incompletely understood pathophysiology [1]. Transgenic mouse models with human monogenic-migraine-syndrome gene mutations are useful to identify and unravel the pathophysiological mechanisms potentially involved in migraine [1, 2]. Familial hemiplegic migraine type-1 (FHM1) is a rare subtype of hereditary migraine [3] caused by missense mutations in the *CACNA1A* gene [4, 5]. This gene encodes the pore-forming α1A subunit of neuronal voltage-gated calcium channel type 2.1 ($Ca_V2.1$, P/Q-type) that triggers neurotransmitter release [6, 7]. Transgenic knock-in (KI) mice with R192Q missense mutation in the orthologous mouse *Cacna1a* gene show gain-of-function of $Ca_V2.1$ channels [5, 7–9] that is expressed as migraine-like pain behavior [10], increased glutamatergic neurotransmission, cerebral hyperexcitability and increased susceptibility to cortical spreading depression [5, 7, 11]. Previous studies show that the R192Q mutation also affects the trigeminovascular system that plays an integral role in migraine pain transduction [2]. In fact, the gain-of-function of $Ca_V2.1$ channels in TG of KI mice leads to increased calcitonin gene-related peptide (CGRP) release [12, 13] and neuronal hyperexcitability [14]. Furthermore, in trigeminal sensory neurons, the R192Q mutation causes sensitization of ATP-gated P2X3 receptors [15], which are considered to play a major role in transducing peripheral nociception, including migraine pain [16, 17]. In KI trigeminal neurons, higher amplitude of P2X3 currents is supported by larger ambient CGRP levels, and it is associated with decreased serine P2X3 phosphorylation and preferential receptor localization to lipid raft membrane compartments [18, 19].

In our search for endogenous mechanisms controlling the function of P2X3 receptors, we have recently observed that, in the TG of wild-type (WT) mice, these receptors are constitutively downregulated by endogenous BNP via activation of its receptor NPR-A [20, 21]. This phenomenon is readily observed by suppressing BNP synthesis or inhibiting its receptors implying that even rather small concentrations of this peptide are sufficient for NPR-A receptor mediated inhibition of P2X3

receptors [21]. Interestingly, sustained inactivation of the BNP/NPR-A pathway in WT TG neurons enhances membrane currents mediated by P2X3 receptors, changes their membrane distribution and decreases their serine phosphorylation, making the WT phenotype of TG neurons close to the KI one [21]. One attractive possibility is that a deficit in the BNP/NPR-A system might account for the sensitization of P2X3 receptors in KI TG. The implication of this hypothesis is that, for at least a genetic type of migraine, pain might originate from lack of intrinsic inhibition of P2X3 receptors, thus paving the way for potentiation by ambient CGRP.

The present study examined this hypothesis by investigating the expression and function of the BNP/NPR-A system in R192Q KI TG, as well as its ability to regulate P2X3 receptor membrane distribution and serine phosphorylation. To this end, we used the selective NPR-A blocker anantin to suppress NPR-A signaling [20, 21] and uncover any constitutive P2X3 inhibition. For the purpose of comparison, we checked if BNP could affect TRPV1 channels that are a less sensitive target for this peptide modulation [20]. Thereafter, we employed the $Ca_V2.1$ antagonist ω-agatoxin or the CGRP receptor antagonist CGRP8-37 to reverse the KI enhancement of P2X3 receptor function [15, 19, 22] and to find out the role (if any) of the NPR-A system.

Results

Untethered P2X3 receptor activity from BNP/NPR-A inhibition in KI neurons

In line with our previous reports on WT cells [20, 21], sustained (3-24 h) block of NPR-A receptors with the selective antagonist anantin (500 nM; [22, 23]) demonstrated significant enhancement of P2X3 receptors activated by the selective agonist α,β-meATP (10 μM) (Fig. 1 A). This facilitation indicates that anantin had reversed the P2X3 downregulation by endogenous BNP [20]. The effect by anantin on WT cells was to bring P2X3 currents up to the amplitude usually observed in KI neurons (Fig. 1 A; [15]). Nevertheless, when applied to KI neurons, anantin failed to further potentiate P2X3

receptor currents after 3 h and 24 h of treatment (Fig.1 A), suggesting loss of modulation by the endogenous BNP/NPR-A pathway.

In TG culture, the BNP/NPR-A pathway increases P2X3 serine phosphorylation (pSer) level and favors P2X3 receptor distribution to non-lipid raft membrane compartments [21]. These two processes are critical regulators of P2X3 receptor function [18, 19]. Figure 1 B compares pSer levels of immunopurified membrane P2X3 receptors from WT or KI cultures in control or anantin-treated condition. In the absence of anantin, P2X3 pSer was low in KI cells compared to WT ones (see also [18]), and was not changed by anantin application (Fig. 1 B). As expected [21], decreased pSer was, however, observed in WT samples treated with anantin (Fig. 1 B).

Figure 1 C shows P2X3 receptor distribution between lipid raft (flotillin-labeled; see methods) and non-raft membrane compartments in control or anantin-treated cultures. Under control conditions, more P2X3 receptors were distributed to the lipid raft compartment in KI TG neurons compared with WT, as previously reported by Gnanasekaran et al [19]. It is noteworthy that, after anantin application to KI cultures, the predominant P2X3 receptor distribution to lipid rafts remained intact (Fig. 1 C). In WT samples, anantin is known to shift a larger fraction of P2X3 receptors to the raft compartment [21]. These data suggested that upregulated function of P2X3 receptors of KI neurons could not be constitutively inhibited by the NPR-A system. We, therefore, looked for any deficit in the expression of BNP and NPR-A receptors.

Efficient BNP and NPR-A expression and function in KI cells

In primary TG cultures from WT mice, NPR-A receptor immunoreactivity was readily detected in 91.7 ± 1.3% of neurons (Fig. 2 A, B) as shown by its co-localization with β-tubulin III in accordance with previous reports [20]. In KI TG cultures, the percentage of β-tubulin III-positive cells expressing NPR-A was somewhat higher ($p<0.05$) than in WT, indicating that almost all KI trigeminal neurons expressed this receptor (98.7 ± 1.3%; Fig. 2 B). Despite this relatively higher

immunoreactivity, Western blot analysis did not show any variation of the NPR-A protein levels between the two genotypes in TG tissue *in situ* from adult (P30) animals (Fig. 2 C, right) or TG primary cultures from young (P12) mice (Fig. 2 C, left).

We sought to find out whether the NPR-A receptor system was functional in KI TG. To this end, since activation of NPR-A by BNP has been shown to increase intracellular cGMP production [24], we investigated if application of BNP to WT and KI cultures could increase intracellular cGMP to comparable levels, as determined by ELISA assay. Figure 2 D shows that basal cGMP was similar in WT and KI samples. Application of 500 ng/ml BNP (vs vehicle control) caused a similar rise in cGMP in WT and KI samples in a time-related fashion. These effects were prevented by 500 nM anantin. It is noteworthy that, in WT and KI TG cultures, anantin per se significantly decreased the basal level of cGMP (Fig.1 D), suggesting constitutive activity of NPR-A receptors.

Consistent with previous findings in TG, that proposed a mainly paracrine BNP action [20], immunocytochemistry revealed scant presence (in TG cultures) of BNP positive cells, in which the peptide staining appeared as cytoplasmic granules (Fig. 1 E). In untreated TG cultures from WT animals, 2% ± 0.2 DAPI-stained cells were identified as BNP-positive, while in KI ganglion culture a slight increase in BNP-immunopositive cells was observed (3.7 % ± 0.7; Fig. 1 F). We measured, with ELISA assay, the concentration of BNP peptide in the culture medium from WT or from KI mice, which was found to be 3.8 ± 1.6 ng/ml and 4.1 ±1.8 ng/ml, respectively, with no significant difference between WT and KI.

KI cultures, thus, possessed an intact (or even slightly enhanced) BNP/NPR-A system, indicating that in these cells the downstream pathway linking NPR-A to P2X3 was perhaps severed. To check if BNP could retain its modulation of other pain-sensing receptors, we explored if inhibition of the TRPV1 receptors by exogenous BNP [20] persisted in KI neurons. Thus, preincubating KI cultures for 24 h with 100 ng/ml BNP significantly depressed currents evoked by the TRPV1 agonist capsaicin (Fig. 3 A), while it did not alter responses mediated by P2X3 receptors (Fig. 3 B). The

inhibitory effect on TRPV1 receptors seen after BNP application was fully prevented by concomitant administration of 500 nM anantin (Fig. 3 A).

Overall, these data indicated rather small differences in the BNP/NPR-A system between the two genotypes, suggesting that loss of constitutive inhibition of P2X3 receptors could not be attributed to deficient agonist or receptor signal of the BNP/NPR-A system.

Reversing the gain-of-function phenotype of KI cells restores NPR-A dependent inhibition of P2X3 receptor activity

The gain-of-function of $Ca_V2.1$ P/Q-type Ca^{2+} channels in KI TG neurons is selectively reversed by ω-agatoxin (200 nM) that also restores P2X3 currents to WT level [15]. Fig. 4 A indicates that overnight pretreatment with ω-agatoxin significantly decreased P2X3 currents in KI neurons [15, 19], and that anantin could then regain its facilitatory action on P2X3 receptors. In addition, ω-agatoxin increased P2X3 pSer (Fig. 4 B) and shifted P2X3 receptors preferentially to the non-raft membrane compartments (Fig. 4 C). When anantin was co-applied with ω-agatoxin, pSer P2X3 levels were significantly reduced (Fig. 4 B). Nonetheless, after ω-agatoxin had decreased P2X3 receptors in the lipid raft compartment of KI samples, anantin could not change this effect (Fig. 4 C).

CGRP receptor antagonism facilitates the action of anantin on KI neurons

CGRP is a powerful positive regulator of P2X3 function [13, 25–27]. In TG neurons, one important action by CGRP is the stimulation of P2X3 receptor trafficking to the membrane [28]. The basal potentiation of P2X3 receptor activity of KI neurons is largely due to higher release of endogenous CGRP from neuronal and non-neuronal sources [29]. We wondered if, in KI TG cultures, BNP-mediated inhibition of P2X3 receptors was swamped by the enhancing action of ambient CGRP. Consistent with previously reported data [29], treatment with the selective CGRP receptor antagonist peptide CGRP8-37 (1 μM, overnight) decreased the mean current density of P2X3 responses in KI

cells (Fig. 5 A). Application of anantin during the last 3 h of CGRP8-37 administration restored α,β-meATP-elicited currents to a level close to control (Fig. 5 A, right). Nonetheless, neither CGRP8-37 alone, nor its combination with anantin, changed pSer P2X3 levels of KI TG (Fig. 5 B). The distribution of P2X3 receptors between raft and non-raft membrane compartments of KI TG is illustrated in Fig. 5 C. Antagonizing CGRP receptors reduced P2X3 protein levels both in the lipid rafts and in the non-rafts. Co-application of CGRP8-37 with anantin increased the fraction of P2X3 receptors in the raft compartment with a corresponding fall in the non-raft domain (Fig. 5 C).

Discussion

The primary finding of the present study is the demonstration that the BNP/NPR-A system, which downregulates P2X3 receptors in WT trigeminal neurons, lost this ability in a transgenic mouse model of FHM1. This novel observation suggests that sensitization of P2X3 receptors may occur not only because of enhancing action of migraine mediators like CGRP [16, 30], but also because an endogenous inhibitor becomes poorly functional. The observation that overwhelming majority of TG neurons expresses NPR-A receptors is compatible with their proposed role in controlling activity of sensory neurons.

Intact BNP/NPR-A system in KI TG

Increased P2X3 activity of KI TG neurons may develop via several mechanisms, like preferential P2X3 receptor redistribution to lipid raft membrane compartments [19], and reduced receptor pSer level [18]. In WT cells, the same parameters are controlled in the opposite direction by the BNP/NPR-A system [20, 21]. The constitutive BNP/NPR-A-induced negative regulation of P2X3 receptor activity in WT trigeminal neurons [20] is indeed due to BNP rather than related peptides because it is prevented by siBNP [21].Thus, it appears that in KI neurons BNP-mediated inhibition could not overcome the P2X3 receptor upregulation. This lack of constitutive inhibition was

apparent when NPR-A receptors of KI neurons were blocked by anantin without any increase in P2X3 function. On the other hand, since TRPV1 receptors in KI trigeminal cultures are not overactive [15, 29], the BNP/NPR-A system could still negatively modulate TRPV1-mediated responses when BNP was exogenously applied. The KI phenotype appeared not to influence the functional state of BNP/NPR-A system, including the expression level of BNP and NPR-A, and their stimulation of cGMP synthesis.

BNP-mediated inhibition of TRPV1 receptors is preserved in KI neurons

Exogenously-applied BNP maintained its ability to inhibit TRPV1 currents of KI neurons in analogy with the effect described for WT cells [20]. We could speculate that, under normal circumstances, the ambient, endogenous BNP concentration is sufficient to modulate P2X3 receptors, but is not high enough for TRPV1 downregulation. The latter observation could also be relevant to migraine pathophysiology, since the plasma level of the BNP peptide precursor is elevated in migraine patients [31]. A multifarious role of endogenous BNP (depending on its extracellular concentration) may, therefore, be exerted on different pain-sensing modalities mediated by P2X3 or TRPV1 receptors. Experiments *in vivo* are necessary to clarify this suggestion.

NPR-A-dependent downregulation of P2X3 receptors is restored by reversing KI phenotype

We investigated what properties made P2X3 receptors of KI neurons apparently disjointed from BNP/NPR-A constitutive inhibition.

Previous studies show that enhanced P2X3 receptor activity in KI sensory neurons could be normalized to the WT level upon prolong inactivation of P/Q-type calcium channels with the selective inhibitor ω-agatoxin [15, 19]. It is noteworthy that this toxin does not change P2X3 receptor activity in WT neurons [15]. When ω-agatoxin was applied to KI cultures, the amplitude of P2X3-mediated responses went back to the WT level and was associated with raised pSer and

membrane redistribution of P2X3 receptors. Over this scenario of reversed functional phenotype, application of anantin could then potentiate P2X3 receptors (unmasking constitutive inhibition) and concomitantly decrease their pSer level. Nevertheless, anantin did not change P2X3 raft membrane distribution. This observation was somewhat unexpected in view of the P2X3 receptor redistribution anantin causes in WT TG [20]. These data thus suggest that low pSer and lipid raft compartmentalization were individual actors in the complex process of P2X3 upregulation, and that they were not mutually exclusive.

Contrasting role of CGRP and BNP on P2X3 receptors

In search for a mechanism regulating P2X3 membrane distribution, one might consider that, in the KI TG, there is increased release of endogenous CGRP leading to constitutive activation of its downstream signaling [12, 13]. This phenomenon targets P2X3 receptors as the CGRP receptor antagonist CGRP8-37 reduces P2X3-mediated responses of KI neurons without affecting WT neurons ([29] see also Fig 5). Following block of CGRP activity, residual inhibition by BNP/NPR-A could be unveiled with anantin without changing P2X3 pSer. Thus, pSer was not dependent on ambient CGRP, implying that this peptide controlled P2X3 receptors via other mechanisms like P2X3 trafficking [28] and lipid raft distribution. In fact, P2X3 receptor expression at membrane level was decreased by CGRP8-37. In KI cultures, in the presence of the CGRP blocker, anantin triggered redistribution of P2X3 receptors preferentially to lipid rafts. This result suggests that, in the dynamic equilibrium between the opposite actions of CGRP and BNP on KI P2X3 receptors, the effect of CGRP was usually predominant in terms of current magnitude and membrane location of the receptors.

It should be noted that, in KI TG in situ and in culture, there is a sterile neuroinflammatory environment [32, 33] with related increase in CGRP release from non-neuronal cells [13]. This condition is not expected to require direct involvement of $Ca_V2.1$ channels that are typically

expressed by neurons. Thus, the present data suggest that there are multiple processes amplifying the function of trigeminal P2X3 receptors in KI ganglia, and that these mechanisms are potent enough to overcome constitutive inhibition by BNP, at least in this genetic model of migraine.

Conclusions

Fig. 6 summarizes our view on the dual regulation of P2X3 receptors by BNP and CGRP. In WT cultures, ambient CGRP is minimal and the NPR-A receptors, highly sensitive even to rather low BNP concentrations, generate (via cGMP and PKG activity) an inhibitory control over P2X3 receptors. This condition is associated with two phenomena: relatively high pSer and significant presence of P2X3 receptors in non-raft compartments.

In KI neurons with enhanced Ca^{2+} influx through P/Q-type channels, the NPR-A and P2X3 receptors became functionally uncoupled for yet unknown reason, as, despite intact cGMP responses to endogenous BNP, the downstream signal could no longer impact the activity of P2X3 receptors. It seems likely that the process of P2X3 upregulation underlying trigeminal sensitization to pain [16, 30] might be triggered because excessive levels of "migraine mediators" like CGRP swamp the negative BNP control that preserves a physiological pain threshold. This notion accords with the observed stronger excitability of KI neurons [14]. While additional experiments are required to clarify the exact molecular mechanisms involved in this process, identifying strategies to enhance intrinsic inhibition, even at peripheral level, may be useful to control pain.

Methods

Animals and TG primary culture preparations

$Ca_V2.1$ R192Q KI and WT littermates were used for the experiments [5]. All animal procedures were conducted in accordance with the guidelines of the Italian Animal Welfare Act and regulations of animal welfare. All treatment protocols were approved by the Scuola Internazionale Superiore di

Studi Avanzati (SISSA) ethics committee and are in accordance with the European Union guidelines and in accordance with the 3 R principles (using cultures and reducing the number of mice). Genotyping was performed by PCR as previously reported [5]. TG primary cultures were obtained from animals at the age of P12-14 as described previously following general anesthesia with slowly raising levels of CO_2 [34] and employed after 24 or 48 h from plating. Ganglion tissue samples and cultures were collected and processed in parallel for WT and R192Q KI mice.

Chemicals and treatments

All reagents were purchased from Sigma-Aldrich (Milan, Italy) except anantin, which was purchased from US Biologicals (Salem, MA, USA); ω-agatoxin, which was purchased from Tocris Bioscience (Bristol, UK); and recombinant mouse BNP, which was purchased from Phoenix Pharmaceuticals (Burlingame, CA, USA). The specific NPR-A receptor antagonist anantin, the CGRP receptor antagonist CGRP8-37, ω-agatoxin and BNP peptide were dissolved in sterile water and freshly diluted from the stock to the desired concentrations before the experiment. Anantin was applied for 30 min up to 24 h at the concentration of 500 nM to fully block NPR-A receptors [35]. CGRP8-37 was applied overnight in 1 μM concentration to effectively block CGRP receptors [29, 36, 37]. BNP was applied at the dose of 100 ng/ml or 500 ng/ml, as previously reported for sensory ganglia [20, 38]. We used ω-agatoxin (200 nM) to selectively inhibit P/Q-type Ca^{2+} channels [39].

Membrane fractionation and Western blot

Total membrane protein extraction and fractionation into lipid raft and non-raft membrane fractions were performed as reported by Gnanasekaran et al. [19]. Immunoprecipitation of P2X3 receptors was described earlier [40]. Equal amount of proteins were separated in 10% SDS-polyacrilamide gel and transferred to nitrocellulose membrane. Immunoblotting was done using the following primary antibodies validated in former studies [18, 20, 21]: anti-NPR-A (1:1000; Abcam, Cambridge, UK), anti-P2X3 (1:1000; Santa Cruz Biotechnology, Heidelberg, Germany), anti-β-actin (1:5000; A5441, Sigma), anti-β-tubulin III (1:2000; T5076, Sigma), anti-flotillin 1 (1:250; BD Biosciences, Milan,

Italy), anti-phospho-Serine (1:500; Millipore, Milan, Italy). Signals were revealed after incubation with secondary antibodies conjugated with horseradish peroxidase by using the ECL detection system (Amersham Biosciences, Piscataway, NJ, USA) and recorded by the Alliance 4.7 (UVITEC, Cambridge, UK) digital imaging.

Immunocytochemistry

Immunocytochemistry was performed as previously described [20] on primary TG cultures prepared from P12-P14 *Cacna1a* R192Q KI and WT mice. Primary antibodies anti-NPR-A (1:1000, Abcam), anti-BNP (1:100, Phoenix Pharmaceuticals) and β-tubulin III (1:2000, Sigma) were used. The specificity of the antibodies used in this study has been previously validated [20, 38]. Secondary antibodies conjugated with Alexa Fluor-488 or Alexa Fluor-594 were purchased from Invitrogen (1:500; Milan, Italy). Nuclei were counterstained with DAPI (Sigma). Cells were mounted with Vectashield (Vector laboratories) and analyzed at confocal microscope (Leica TCS SP2, Wetzlar, Germany).

ELISA assay

Basal and stimulated intracellular cGMP concentrations were evaluated in primary TG cultures after 24 h *in vitro*. A commercial ELISA kit for cGMP (MBL International Corporation, Woburn, MA, USA) was used, following the manufacturer's instructions as previously described [20]. Protein concentrations in cell lysates were determined by the BCA method (Sigma). The cGMP concentrations in pmol/μg of protein were extrapolated from a best-fit line calculated from serial dilutions of a cGMP sample standard.

To determine BNP concentration in medium samples, a commercial ELISA kit for mouse BNP was used (Abnova, Hidelberg, Germany) following the instructions of the manufacturer, as previously reported [20]. After 24 h from plating cells, culture medium was collected. All samples were centrifuged at 1200 rpm for 5 min, and the supernatants immediately processed for BNP

measurement. Protein concentrations in cell lysates were determined by the BCA method (Sigma). All samples were run in triplicate and values averaged.

Electrophysiology

Electrophysiological experiments were performed according to the previously reported protocols [29, 34]. After 24 h incubation, trigeminal cultures were continuously superfused during the experiment (3 mL/min) with physiological solution containing (in mM): 152 NaCl, 5 KCl, 1 $MgCl_2$, 2 $CaCl_2$, 10 glucose, and 10 HEPES (pH adjusted to 7.4 with NaOH). Neurons were patch-clamped in the whole-cell configuration using patch pipettes with 3-4 MΩ resistance and filled with a solution containing (in mM): 140 KCl, 0.5 $CaCl_2$, 2 $MgCl_2$, 2 Mg_2ATP_3, 2 GTP, 10 HEPES and 10 EGTA (pH adjusted to 7.2 with KOH). Recordings were obtained from small and medium size trigeminal neurons [29], with holding potential equal to -65 mV after correction for liquid junction potential. 1 kHz filtering was used during recording; currents were acquired by means of a DigiData 1200 interface and pClamp8.2 software (Molecular Devices, Sunnyvale, CA, USA). To activate P2X3 receptors, the stable synthetic agonist α,β-methylene-adenosine-5'-triphosphate (α,β-meATP; Sigma) [41] was applied for 2 s at a standard concentration of 10 μM [20, 32, 41] to produce near-maximum responses using a fast superfusion system (Rapid Solution Changer RSC-200; BioLogic Science Instruments, Claix, France). Capsaicin (1 μM, 3 s) was used to activate TRPV 1 receptors [15, 29]. For statistical analysis, data from at least 4 individual experiments were collected, with number of cells equal or greater than 25. Capsaicin- and α,β-meATP-induced responses were measured as peak current amplitudes and current density values (pA/pF) were then calculated to normalize current size to the cell capacity and to eliminate differences originated from cell size variation.

Statistical analysis

Data are expressed as mean ± standard deviation (s.d.; for molecular biology experiments) or mean ± standard error of the mean (s.e.m.; for patch clamp experiments), where *n* indicates the number of independent experiments or the number of investigated cells, as indicated in figure legends.

Statistical analysis was performed using nonparametric Mann-Whitney rank sum test, or the Student's *t*-test, after the software directed choice of non-parametric or parametric data, respectively (Matlab; Sigma Plot and Sigma Stat Software, Chicago, IL, USA), or Kruskal-Wallis test for multiple comparison. A p value of < 0.05 was accepted as indicative of a statistically significant difference.

Abbreviations

α,β-meATP: α,β-methyleneATP; BCA: bicinchoninic acid; s.d.: standard deviation; BNP: brain natriuretic peptide; CGRP: calcitonin gene-related peptide; DRG: dorsal root ganglia; NPR-A: natriuretic peptide receptor-A; PKG: cGMP- dependent protein kinase; pSer: serine phosphorylation; s.e.m.: standard error of the mean; TG: trigeminal ganglion

Authors' contributions

All authors read and approved the final manuscript. AM, SV, NN, design of experiments and collection of data; AMJMVDM, mouse genetic model supply; AN, project supervision; AM, SV, AN, AMJMVDM, joint contribution to MS writing.

Authors' information

[1]Neuroscience Department, International School for Advanced Studies (SISSA), Via Bonomea 265, 34136 Trieste, Italy. [2]Department of Neurology, Leiden University Medical Centre, Leiden, Netherlands. [3]Department of Human Genetics, University Medical Centre, Leiden, Netherlands.

Acknowledgements

This work was supported by the EU FP7 grant EuroHeadPain (#602633).

Competing interests

The authors declare that they have no competing interests.

References

1. Ferrari MD, Klever RR, Terwindt GM, Ayata C, van den Maagdenberg AMJM: **Migraine pathophysiology: lessons from mouse models and human genetics**. *Lancet Neurol* 2015, **14**:65–80.

2. Gasparini CF, Sutherland HG, Griffiths LR: **Studies on the Pathophysiology and Genetic Basis of Migraine**. *Curr Genomics* 2013, **14**:300–315.

3. Headache Classification Subcommittee of the International Headache Society: **The International Classification of Headache Disorders: 2nd edition**. *Cephalalgia Int J Headache* 2004, **24 Suppl 1**:9–160.

4. Ophoff RA, Terwindt GM, Vergouwe MN, van Eijk R, Oefner PJ, Hoffman SMG, Lamerdin JE, Mohrenweiser HW, Bulman DE, Ferrari M, Haan J, Lindhout D, van Ommen G-JB, Hofker MH, Ferrari MD, Frants RR: **Familial Hemiplegic Migraine and Episodic Ataxia Type-2 Are Caused by Mutations in the Ca2+ Channel Gene CACNL1A4**. *Cell* 1996, **87**:543–552.

5. van den Maagdenberg AMJM, Pietrobon D, Pizzorusso T, Kaja S, Broos LAM, Cesetti T, van de Ven RCG, Tottene A, van der Kaa J, Plomp JJ, Frants RR, Ferrari MD: **A Cacna1a Knockin Migraine Mouse Model with Increased Susceptibility to Cortical Spreading Depression**. *Neuron* 2004, **41**:701–710.

6. Pietrobon D: **Function and dysfunction of synaptic calcium channels: insights from mouse models**. *Curr Opin Neurobiol* 2005, **15**:257–265. [*Signalling Mechanisms*]

7. Tottene A, Conti R, Fabbro A, Vecchia D, Shapovalova M, Santello M, van den Maagdenberg AMJM, Ferrari MD, Pietrobon D: **Enhanced Excitatory Transmission at Cortical Synapses as the Basis for Facilitated Spreading Depression in CaV2.1 Knockin Migraine Mice**. *Neuron* 2009, **61**:762–773.

8. Gao Z, Todorov B, Barrett CF, Dorp S van, Ferrari MD, Maagdenberg AMJM van den, Zeeuw CID, Hoebeek FE: **Cerebellar Ataxia by Enhanced CaV2.1 Currents Is Alleviated by Ca2+-Dependent K+-Channel Activators in Cacna1aS218L Mutant Mice**. *J Neurosci* 2012, **32**:15533–15546.

9. Uchitel OD, Inchauspe CG, Urbano FJ, Di Guilmi MN: **CaV2.1 voltage activated calcium channels and synaptic transmission in familial hemiplegic migraine pathogenesis**. *J Physiol-Paris* 2012, **106**:12–22. [*Franco-Argentinean Symposium in Neuroscience*]

10. Chanda ML, Tuttle AH, Baran I, Atlin C, Guindi D, Hathaway G, Israelian N, Levenstadt J, Low D, Macrae L, O'Shea L, Silver A, Zendegui E, Mariette Lenselink A, Spijker S, Ferrari MD, van den Maagdenberg AMJM, Mogil JS: **Behavioral evidence for photophobia and stress-related ipsilateral head pain in transgenic Cacna1a mutant mice**. *Pain* 2013, **154**:1254–1262.

11. Eikermann-Haerter K, Dileköz E, Kudo C, Savitz SI, Waeber C, Baum MJ, Ferrari MD, van den Maagdenberg AMJM, Moskowitz MA, Ayata C: **Genetic and hormonal factors modulate spreading depression and transient hemiparesis in mouse models of familial hemiplegic migraine type 1**. *J Clin Invest* 2009, **119**:99–109.

12. Fioretti B, Catacuzzeno L, Sforna L, Gerke-Duncan MB, van den Maagdenberg AMJM, Franciolini F, Connor M, Pietrobon D: **Trigeminal ganglion neuron subtype-specific alterations of CaV2.1 calcium current and excitability in a Cacna1a mouse model of migraine**. *J Physiol* 2011, **589**(Pt 23):5879–5895.

13. Ceruti S, Villa G, Fumagalli M, Colombo L, Magni G, Zanardelli M, Fabbretti E, Verderio C, Maagdenberg AMJM van den, Nistri A, Abbracchio MP: **Calcitonin Gene-Related Peptide-Mediated Enhancement of Purinergic Neuron/Glia Communication by the Algogenic Factor Bradykinin in Mouse Trigeminal Ganglia from Wild-Type and R192Q Cav2.1 Knock-In Mice: Implications for Basic Mechanisms of Migraine Pain**. *J Neurosci* 2011, **31**:3638–3649.

14. Hullugundi SK, Ansuini A, Ferrari MD, van den Maagdenberg AMJM, Nistri A: **A hyperexcitability phenotype in mouse trigeminal sensory neurons expressing the R192Q Cacna1a missense mutation of familial hemiplegic migraine type-1**. *Neuroscience* 2014, **266**:244–254.

15. Nair A, Simonetti M, Birsa N, Ferrari MD, van den Maagdenberg AMJM, Giniatullin R, Nistri A, Fabbretti E: **Familial hemiplegic migraine Ca(v)2.1 channel mutation R192Q enhances ATP-gated P2X3 receptor activity of mouse sensory ganglion neurons mediating trigeminal pain**. *Mol Pain* 2010, **6**:48.

16. Fabbretti E: **ATP P2X3 receptors and neuronal sensitization**. *Front Cell Neurosci* 2013, **7**:236.

17. Yan J, Dussor G: **Ion channels and migraine**. *Headache* 2014, **54**:619–639.

18. Nair A, Simonetti M, Fabbretti E, Nistri A: **The Cdk5 kinase downregulates ATP-gated ionotropic P2X3 receptor function via serine phosphorylation**. *Cell Mol Neurobiol* 2010, **30**:505–509.

19. Gnanasekaran A, Sundukova M, van den Maagdenberg AMJM, Fabbretti E, Nistri A: **Lipid rafts control P2X3 receptor distribution and function in trigeminal sensory neurons of a transgenic migraine mouse model**. *Mol Pain* 2011, **7**:77.

20. Vilotti S, Marchenkova A, Ntamati N, Nistri A: **B-type natriuretic peptide-induced delayed modulation of TRPV1 and P2X3 receptors of mouse trigeminal sensory neurons**. *PloS One* 2013, **8**:e81138.

21. Marchenkova A, Vilotti S, Fabbretti E, Nistri A: **Brain natriuretic peptide constitutively downregulates P2X3 receptors by controlling their phosphorylation state and membrane localization**. *Mol Pain* 2015, **11**:71.

22. Abdelalim EM, Tooyama I: **NPR-A regulates self-renewal and pluripotency of embryonic stem cells**. *Cell Death Dis* 2011, **2**:e127.

23. El-Ayoubi R, Menaouar A, Gutkowska J, Mukaddam-Daher S: **Urinary responses to acute moxonidine are inhibited by natriuretic peptide receptor antagonist**. *Br J Pharmacol* 2005, **145**:50–56.

24. Pandey KN: **Biology of natriuretic peptides and their receptors**. *Peptides* 2005, **26**:901–932. [*Natriuretic Peptides and Receptors*]

25. Cady RJ, Glenn JR, Smith KM, Durham PL: **Calcitonin gene-related peptide promotes cellular changes in trigeminal neurons and glia implicated in peripheral and central sensitization**. *Mol Pain* 2011, **7**:94.

26. Yasuda M, Shinoda M, Kiyomoto M, Honda K, Suzuki A, Tamagawa T, Kaji K, Kimoto S, Iwata K: **P2X3 receptor mediates ectopic mechanical allodynia with inflamed lower lip in mice**. *Neurosci Lett* 2012, **528**:67–72.

27. Simonetti M, Giniatullin R, Fabbretti E: **Mechanisms mediating the enhanced gene transcription of P2X3 receptor by calcitonin gene-related peptide in trigeminal sensory neurons**. *J Biol Chem* 2008, **283**:18743–18752.

28. Fabbretti E, D'Arco M, Fabbro A, Simonetti M, Nistri A, Giniatullin R: **Delayed upregulation of ATP P2X3 receptors of trigeminal sensory neurons by calcitonin gene-related peptide**. *J Neurosci Off J Soc Neurosci* 2006, **26**:6163–6171.

29. Hullugundi SK, Ferrari MD, van den Maagdenberg AMJM, Nistri A: **The mechanism of functional up-regulation of P2X3 receptors of trigeminal sensory neurons in a genetic mouse model of familial hemiplegic migraine type 1 (FHM-1)**. *PloS One* 2013, **8**:e60677.

30. Giniatullin R, Nistri A, Fabbretti E: **Molecular mechanisms of sensitization of pain-transducing P2X3 receptors by the migraine mediators CGRP and NGF**. *Mol Neurobiol* 2008, **37**:83–90.

31. Uzar E, Evliyaoglu O, Yucel Y, Ugur Cevik M, Acar A, Guzel I, Islamoglu Y, Colpan L, Tasdemir N: **Serum cytokine and pro-brain natriuretic peptide (BNP) levels in patients with migraine**. *Eur Rev Med Pharmacol Sci* 2011, **15**:1111–1116.

32. Franceschini A, Nair A, Bele T, van den Maagdenberg AM, Nistri A, Fabbretti E: **Functional crosstalk in culture between macrophages and trigeminal sensory neurons of a mouse genetic model of migraine**. *BMC Neurosci* 2012, **13**:143.

33. Franceschini A, Vilotti S, Ferrari MD, van den Maagdenberg AMJM, Nistri A, Fabbretti E: **TNFα levels and macrophages expression reflect an inflammatory potential of trigeminal ganglia in a mouse model of familial hemiplegic migraine**. *PloS One* 2013, **8**:e52394.

34. Simonetti M, Fabbro A, D'Arco M, Zweyer M, Nistri A, Giniatullin R, Fabbretti E: **Comparison of P2X and TRPV1 receptors in ganglia or primary culture of trigeminal neurons and their modulation by NGF or serotonin**. *Mol Pain* 2006, **2**:11.

35. Yu Y-C, Cao L-H, Yang X-L: **Modulation by brain natriuretic peptide of GABA receptors on rat retinal ON-type bipolar cells**. *J Neurosci Off J Soc Neurosci* 2006, **26**:696–707.

36. Giniatullin R, Di Angelantonio S, Marchetti C, Sokolova E, Khiroug L, Nistri A: **Calcitonin gene-related peptide rapidly downregulates nicotinic receptor function and slowly raises**

intracellular Ca2+ in rat chromaffin cells in vitro. *J Neurosci Off J Soc Neurosci* 1999, **19**:2945–2953.

37. Chiba T, Yamaguchi A, Yamatani T, Nakamura A, Morishita T, Inui T, Fukase M, Noda T, Fujita T: **Calcitonin gene-related peptide receptor antagonist human CGRP-(8-37)**. *Am J Physiol* 1989, **256**(2 Pt 1):E331–335.

38. Zhang F-X, Liu X-J, Gong L-Q, Yao J-R, Li K-C, Li Z-Y, Lin L-B, Lu Y-J, Xiao H-S, Bao L, Zhang X-H, Zhang X: **Inhibition of Inflammatory Pain by Activating B-Type Natriuretic Peptide Signal Pathway in Nociceptive Sensory Neurons**. *J Neurosci* 2010, **30**:10927–10938.

39. Mintz IM, Venema VJ, Swiderek KM, Lee TD, Bean BP, Adams ME: **P-type calcium channels blocked by the spider toxin ω-Aga-IVA**. *Nature* 1992, **355**:827–829.

40. D'Arco M, Giniatullin R, Leone V, Carloni P, Birsa N, Nair A, Nistri A, Fabbretti E: **The C-terminal Src inhibitory kinase (Csk)-mediated tyrosine phosphorylation is a novel molecular mechanism to limit P2X3 receptor function in mouse sensory neurons**. *J Biol Chem* 2009, **284**:21393–21401.

41. Sokolova E, Skorinkin A, Moiseev I, Agrachev A, Nistri A, Giniatullin R: **Experimental and modeling studies of desensitization of P2X3 receptors**. *Mol Pharmacol* 2006, **70**:373–382.

Figures

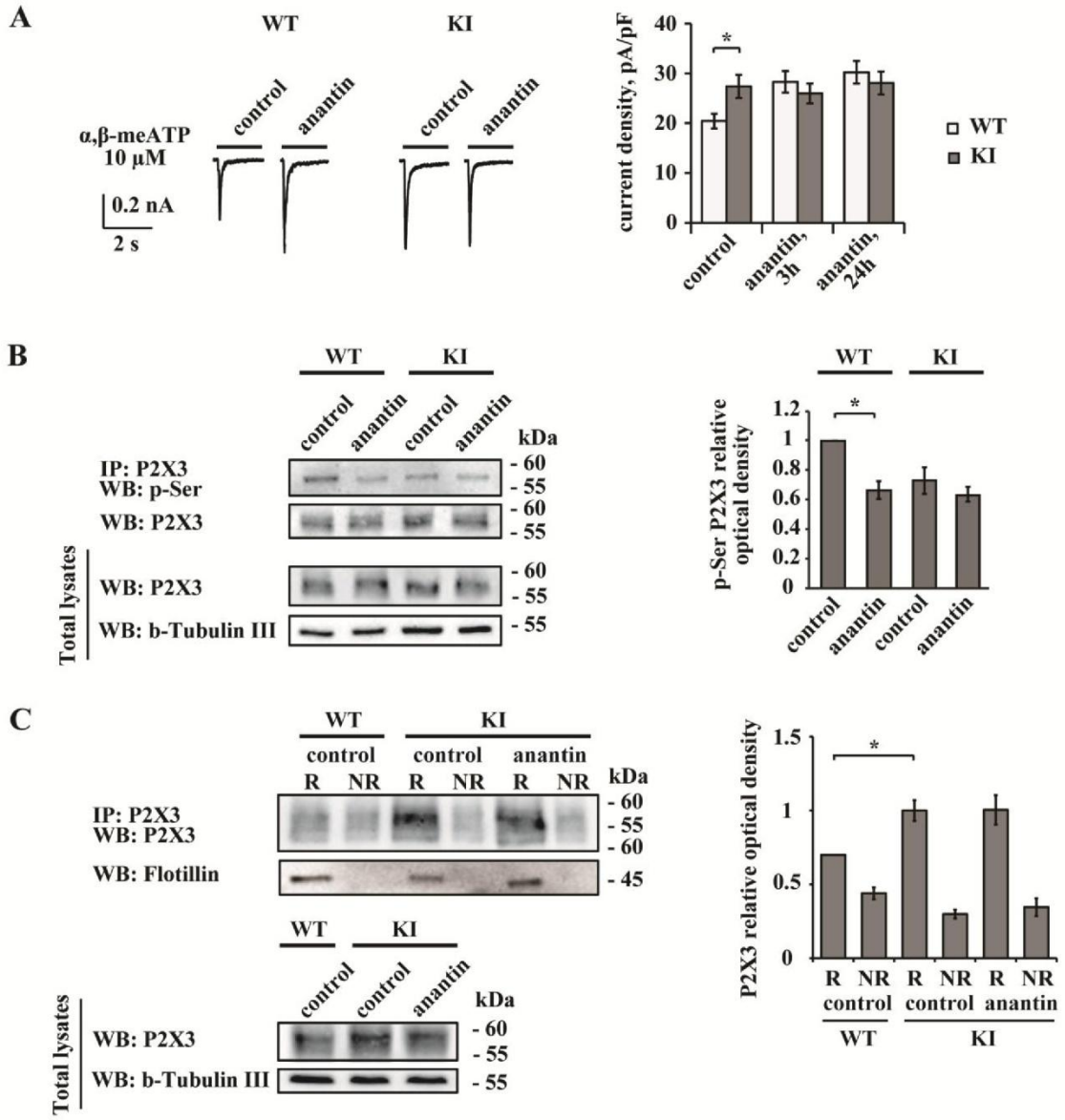

Fig. 1 Anantin effects on WT or KI trigeminal neurons. **A,** Representative traces obtained using α,β-meATP (10 μM, 2 s) show P2X3 current amplitudes in control and after 3 h anantin treatment (500 nM) in WT and KI trigeminal neurons. Histograms show average P2X3 current density values from WT or KI neurons in control or after 3 or 24 h pretreatment with anantin (n = 25, 25, and 26 for WT;

42, 40, 34 for KI cells, respectively; *p < 0.05, Mann-Whitney rank sum test). Note that P2X3 currents in KI control are already potentiated compared to WT and cannot be further enhanced by anantin application. **B,** Western immunoblotting shows the amount of P2X3 pSer and total amount of P2X3 receptors in control and after 24 h anantin (500 nM) application for WT and KI trigeminal cultures. β-Tubulin was used as loading control. Histograms on the right show statistically lower P2X3 pSer (relative optical density value) in WT cultures after anantin application. In KI samples, pSer level is already low and is not altered by anantin (n = 4; *p < 0.05, Mann-Whitney rank sum test). **C,** Top panel is a representative example of Western immunoblotting showing the amount of P2X3 receptors in raft (R) and non-raft (NR) membrane fractions in control or after treatment with anantin (500 nM, 24 h). Flotillin bands indicate lipid raft membrane fractions. Lower panel shows total amount of P2X3 receptors for each experimental condition; β-tubulin was used as loading control. Histograms on the right quantify mean P2X3 relative optical density values in lipid raft and non-raft membrane fractions (n = 4; *p < 0.05, Kruskal-Wallis test).

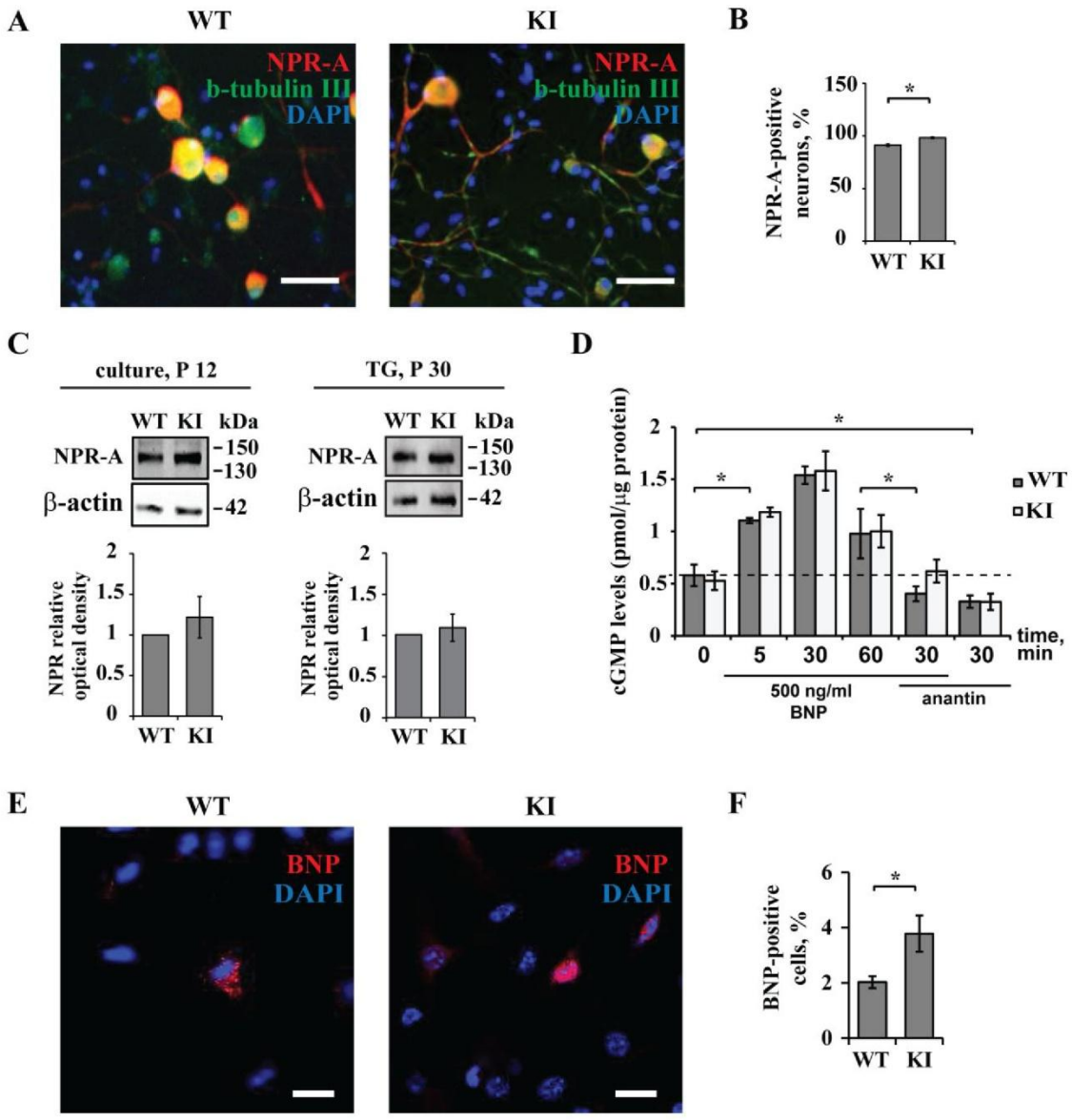

Fig. 2 BNP and NPR-A in WT and KI TG. **A,** Representative immunocytochemical examples of endogenous NPR-A expression in WT (left panel) and KI (right panel) mouse TG cultures. Nuclei are visualized with DAPI (blue); scale bar = 50 μm. Note extensive co-staining of NPR-A (red) and β-tubulin (green). **B,** The histograms quantify percentage of NPR-A-positive cells in WT and KI cultures (n = 4; *$p < 0.05$, Kruskal-Wallis test). **C,** Western blot showing protein expression of NPR-A in TG from P30 mice (right) and TG cultures from P12 mice (left). β-Actin was used as a loading

control. Histograms (bottom) quantify NPR-A relative optical density values for each examined group. **D,** ELISA-based quantification of intracellular cGMP in TG cultures from WT and KI mice. Cultures were treated with BNP (500 ng/ml for 5, 30 or 60 min) and/or anantin (500 nM, 30 min), or vehicle (indicated as 0). Note similar dynamics of cGMP increase after BNP application and similar decrease after treatment with anantin alone (500 nM) throughout. Data were normalized to the total protein content in each sample and are presented as mean value ± s.d. (n = 3 in which samples were run in duplicate; *p < 0.05, Kruskal-Wallis test). **E,** Immunocytochemical analysis of BNP (red) in WT and KI mouse TG culture. Nuclei are visualized with DAPI (blue). Scale bar, 15 µm. **F,** Histograms show percent value of BNP-positive cells in WT and KI populations (DAPI labeled cells).

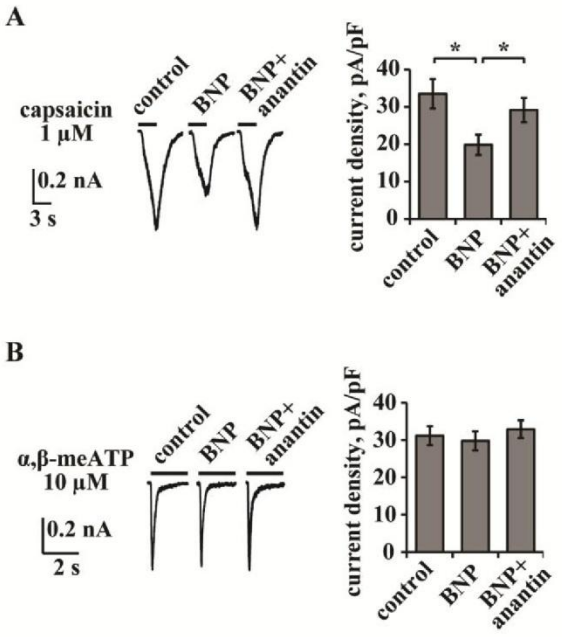

Fig. 3 Effect of exogenous BNP on TRPV1- and P2X3-mediated responses. **A,** Representative traces of capsaicin (1 µM, 3 s)-induced TRPV1 currents of KI trigeminal neurons in control and after application of BNP (100 ng/ml, 24 h) alone or in combination with anantin (500 ng/ml, 24 h). Histograms on the right summarize mean current density values of TRPV1 currents. Note that BNP

suppresses TRPV1 responses and that the effect is fully blocked by anantin (n = 39, 42, 47, *p < 0.05, Mann-Whitney rank sum test). **B,** Representative traces of α,β-meATP (10 μM, 2 s)-evoked P2X3 responses of KI trigeminal neurons in control and after application of BNP (100 ng/ml, 24 h) or BNP together with anantin (500 ng/ml, 24 h). Histograms on the right summarize mean current density values of P2X3 currents. Note that exogenous BNP does not affect P2X3 currents (n = 38, 51, 33, *p ≥ 0.05, Mann-Whitney rank sum test).

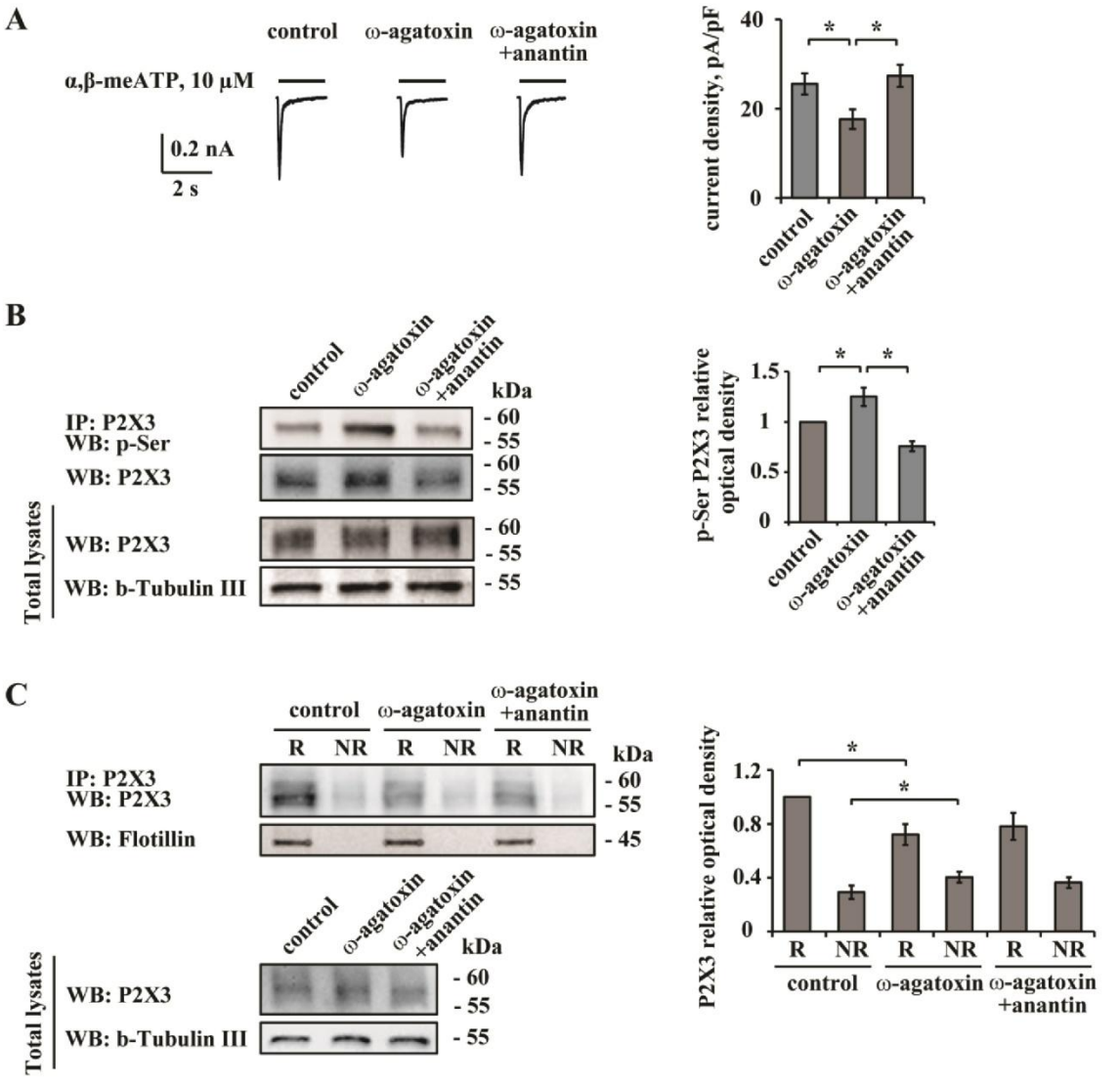

Fig. 4 ω-Agatoxin restores anantin effects on P2X3 receptors in KI neurons. **A,** Representative traces of α,β-meATP (10 μM, 2 s)-evoked P2X3 responses in control and after application of ω-agatoxin (300 nM, 24 h) alone or in a combination with anantin (500 ng/ml; co-applied during the last 3 h of ω-agatoxin treatment). Histograms on the right quantify current density values of P2X3 currents for each condition. Note that ω-agatoxin reduces P2X3 currents and that anantin can upregulate them back to the control level ($n = 23, 24, 25$, $^*p < 0.05$, Mann-Whitney rank sum test). **B,** Western immunoblotting shows the amount of P2X3 pSer and total amount of P2X3 receptors in control, after 24 h ω-agatoxin or ω-agatoxin plus anantin (500 nM, 3 h) treatment. β-Tubulin III was used as loading control. Histograms on the right show statistically higher P2X3 pSer value after ω-agatoxin application compared to control ($n = 4$; $^*p < 0.05$, Mann-Whitney rank sum test) with reversal by anantin application. **C,** Top panel is a representative example of Western immunoblotting showing the amount of P2X3 receptors in raft (R) and non-raft (NR) membrane fractions in control and after treatment with ω-agatoxin (300 nM, 24 h) or a combination of ω-agatoxin and anantin (500 ng/ml; 3 h). Flotillin bands indicate lipid raft membrane fractions. Lower panel shows total amount of P2X3 receptors for each experimental condition; β-tubulin was used as loading control. Histograms on the right quantify mean P2X3 values in lipid raft and non-raft membrane fractions ($n = 4$; $^*p < 0.05$, Kruskal-Wallis test).

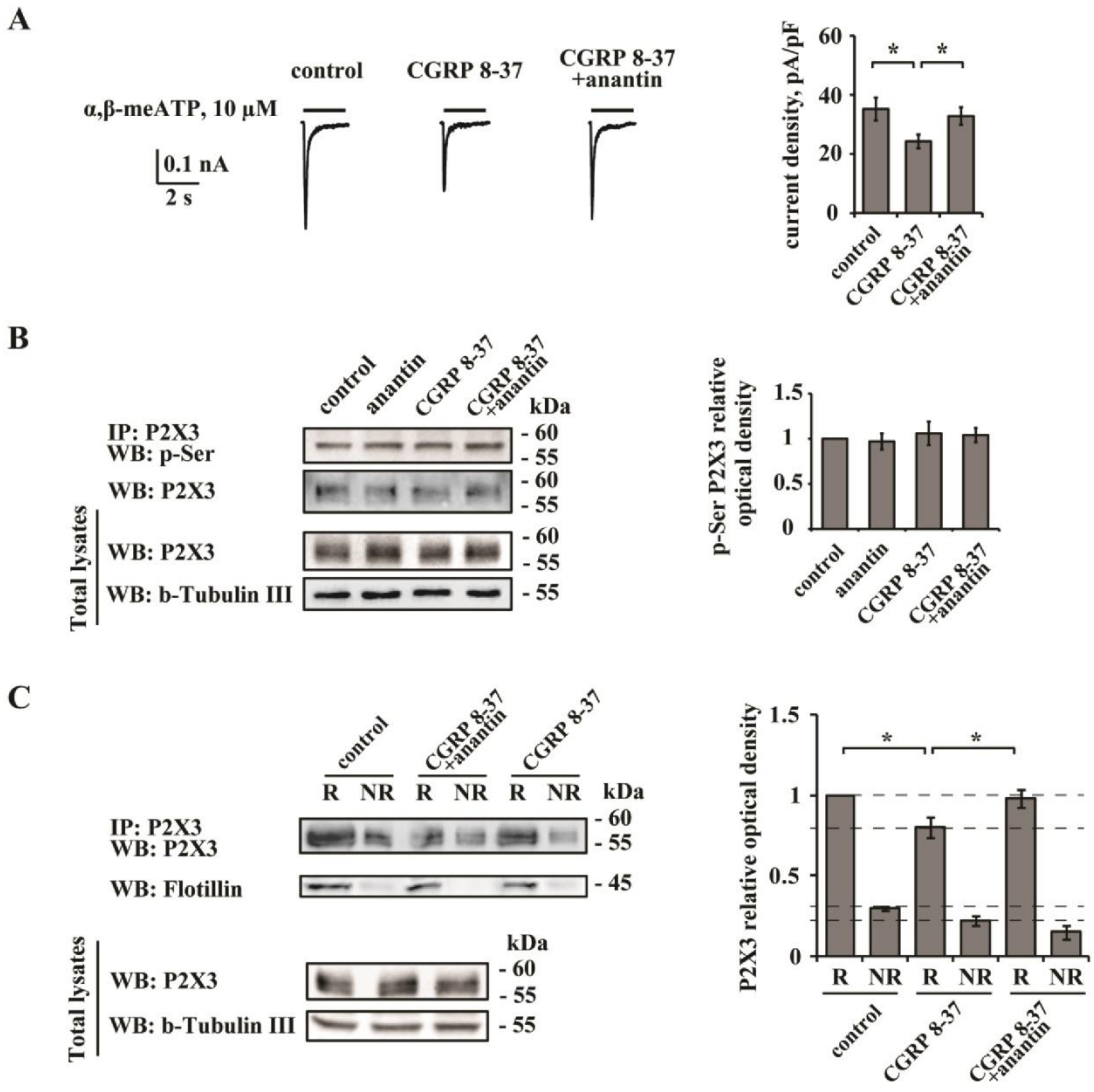

Fig. 5 CGRP receptor antagonist CGRP8-37 restores anantin effects on P2X3 receptors of KI neurons. **A,** Representative traces of P2X3 responses induced by application of α,β-meATP (10 μM, 2 s) in control and after application of CGRP8-37 (1 μM, 24 h) alone or in a combination with anantin (500 ng/ml; co-applied for the last 3 h of CGRP8-37 treatment). Histograms on the right quantify current density values of P2X3 currents for above mentioned conditions. Note that CGRP8-37 reduces P2X3 currents and anantin can reverse them (n = 30, 33, 27, *p < 0.05, Mann-Whitney rank sum test). **B,** Representative example of Western immunoblotting showing the amount of P2X3 pSer and total amount of P2X3 receptors in control, after CGRP8-37 (1 μM, 24 h) or co-application

of CGRP8-37 and anantin (500 nM, 3 h). β-Tubulin was used as loading control. Histograms on the right show P2X3 pSer values for each experimental condition (n = 4). **C,** Top panel is a representative example of Western immunoblotting showing the amount of P2X3 receptors in raft (R) and non-raft (NR) membrane fractions in control and after treatment with CGRP8-37 (1 μM, 24 h) or a combination of CGRP8-37 and anantin (500 ng/ml; 3 h); flotillin bands indicate lipid raft membrane fractions. Lower panel shows total amount of P2X3 receptors for each experimental condition; β-tubulin was used as loading control. Histograms on the right quantify mean P2X3 values in lipid raft and non-raft membrane fractions (n = 3; *p < 0.05, Kruskal-Wallis test). Note a reduction in the amount of P2X3 receptors in R and NR samples after CGRP8-37 application. Anantin relocates P2X3 receptors from non-raft to lipid raft membrane compartments when applied after CGRP8-37 pretreatment.

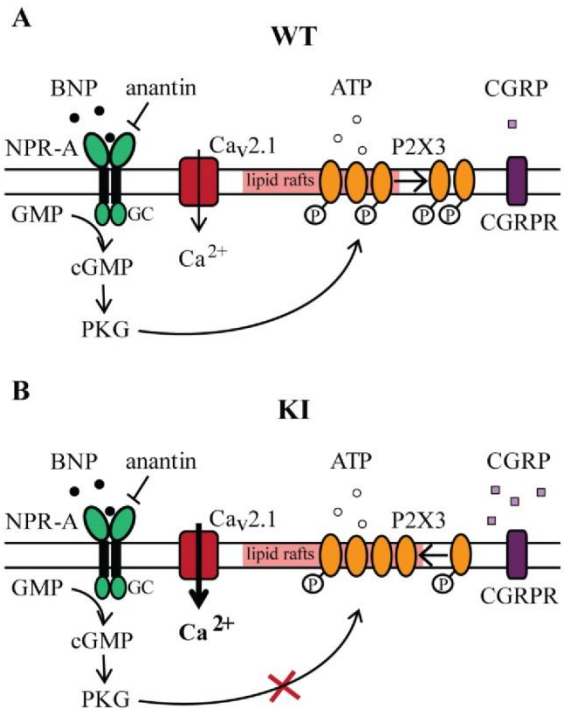

Fig. 6 Scheme of BNP/NPR-A-induced modulation of P2X3 receptors expressed on the membrane of WT and KI trigeminal neurons. **A,** In WT neurons endogenous BNP acting through its receptor

NPR-A constitutively restrains P2X3 receptor activity. This process is cGMP- and PKG-dependent and involves high P2X3 serine phosphorylation and receptor redistribution from lipid rafts to non-raft membrane compartments. Low activity of $Ca_V2.1$ calcium channels and virtually silent CGRP pathway do not generate enough P2X3 stimulation to overcome BNP-mediated inhibition. **B,** In KI trigeminal neurons, elevated concentration of ambient CGRP and gain-of-function of $Ca_V2.1$ extensively enhance P2X3 receptor activity to the level when the inhibitory BNP/NPR-A pathway becomes redundant. This is associated with lower level of P2X3 serine phosphorylation and receptor preferential redistribution to the lipid raft membrane fraction. CGRP-R denotes the CGRP receptor complex. GC = guanylyl cyclase.

4. Loss of selective inhibition by brain natriuretic peptide over P2X3 receptor-mediated excitability of trigeminal ganglion neurons in a mouse model of familial hemiplegic migraine type-1

Loss of selective inhibition by brain natriuretic peptide over P2X3 receptor-mediated excitability of trigeminal ganglion neurons in a mouse model of familial hemiplegic migraine type-1

Anna Marchenkova[1]

[1]Neuroscience Department, International School for Advanced Studies (SISSA), Via Bonomea 265, 34136 Trieste, Italy.

Abstract

P2X3 receptors play an important role in pain pathologies, including migraine. In trigeminal ganglion (TG) P2X3 receptors are constitutively downregulated by endogenous brain natriuretic peptide (BNP) via its receptor NPR-A. Conversely, in a mouse model of familial hemiplegic migraine type-1 (FHM1) lack of BNP-mediated inhibition is associated with gain-of-function of P2X3 receptors. Moreover, KI trigeminal neurons were shown to exhibit a hyperexcitability phenotype. The question remained if BNP-induced changes of P2X3 activity in WT cultures and their absence in KI are reflected in the firing activity of trigeminal neurons.

We used patch-clamp experiments to investigate excitability of WT and KI TG neurons, induced by protocols of depolarizing current injections, and application of P2X3 or TRPV1 agonists. Consistent with the constitutive inhibition of P2X3 by BNP/NPR-A pathway, sustained block of NPR-A selectively enhanced P2X3-mediated excitability of WT neurons without affecting firing modalities evoked by the other protocols. This effect included increased number of action potentials generated in response to P2X3 receptor activation, lower spike threshold and shift of the firing pattern distribution towards higher spiking activity. Thus, inactivation of BNP/NPR-A signaling transformed WT excitability phenotype to the one typical for KI cultures. Noteworthy, the same treatment did not influence excitability of KI neurons, consistent with the lack of BNP-induced P2X3 modulation. Our study suggests that in WT trigeminal neurons negative control over P2X3 receptors by BNP/NPR-A system is translated into tonic suppression of P2X3-mediated excitability with a high degree of selectivity for chemical signaling. Lack of this inhibition in KI cultures results in a hyperexcitability phenotype and might contribute to the pain transduction in migraine pathology.

Key words: purinergic receptor, nociception, sensory neurons, TRPV1

Introduction

The trigeminal ganglion (TG) is a part of trigeminovascular system that plays an integral role in regulating vascular tone and pain transduction in a variety of headache conditions (Gasparini et al., 2013). Trigeminal sensory neurons express on their membrane ATP-gated P2X3 receptors and capsaicin-sensitive transient receptor potential vanilloid-1 (TRPV1) receptors (Vulchanova et al., 1997; Julius and Basbaum, 2001; North, 2003), which mediate nociceptive responses and are considered to play a role in migraine pathophysiology (Yan and Dussor, 2014). Using a knock-in (KI) mouse model replicating the R192Q mutation of CACNA1A gene often detected in familial hemiplegic migraine type-1 (FHM1) (Ophoff et al., 1996), we have observed selective sensitization of P2X3 receptors (Nair et al., 2010) and increased neuronal excitability in response to P2X3 activation (Hullugundi et al., 2014). These results are consistent with the migraine-like pain behavior exhibited by R192Q KI mice (Chanda et al., 2013).

While numerous endogenous modulators upregulate P2X3 receptors, to date only brain natriuretic peptide (BNP) and its receptor NPR-A have recently been reported to induce constitutive downregulation of P2X3-mediated responses in WT TG sensory neurons (Vilotti et al., 2013; Marchenkova et al., 2015). Indeed, inactivation of BNP signaling with the selective NPR-A antagonist anantin or siBNP dramatically enhances P2X3-mediated responses, unmasking background depression of P2X3 receptor activity (Vilotti et al., 2013; Marchenkova et al., 2015). Most interestingly, in mice with the KI R192Q mutation, the BNP-dependent P2X3 modulation appears to be disabled. This phenomenon seemingly contributes to the gain-of-function P2X3 receptor phenotype typical of R192Q KI trigeminal neurons (Marchenkova, unpublished data; Vilotti et al., 2013). These functional data were, however, obtained by recording membrane currents from neurons voltage-clamped far away from their spike threshold. Since trigeminal sensory neurons encode their responses as a series of action potentials, it is critical to understand if the presence of BNP/NPR-A-mediated constitutive inhibition of P2X3 receptors might actually influence their firing properties.

Thus, in order to uncover any constitutive effect of endogenous BNP, we blocked NPR-A receptors with its selective antagonist anantin (Weber et al., 1991; Yu et al., 2006; Abdelalim and Tooyama, 2011; Vilotti et al., 2013) in analogy with the previously reported protocol (Vilotti et al., 2013). Firing of trigeminal sensory neurons from wild type (WT) or R192Q KI mice was investigated in response to current pulses as well as brief application of P2X3 or TRPV1 receptor agonists, α,β-methyl-ATP or capsaicin, respectively.

Experimental procedures

Mouse trigeminal ganglion cultures

Experiments were done on the FHM1 R192Q KI and WT mouse littermates. The colony of KI mice was bred and maintained locally, in accordance with the Italian Animal Welfare Act, after an initial transfer from Leiden University Medical Centre (van den Maagdenberg et al., 2004). All the experimental protocols were approved by the SISSA ethical committee. All efforts were made to minimize the number of animals used for the experiments and their suffering. Genotyping was performed by polymerase chain reaction (PCR), as previously reported (Nair et al., 2010). Primary cultures of P12-P14 mouse trigeminal ganglia were prepared as described previously (Simonetti et al., 2006; Hullugundi et al., 2014) and used 24 h after plating. In short,

trigeminal ganglia were isolated from mice killed by cervical dislocation under general anesthesia by slowly raising levels of CO_2. Ganglia were cut and dissociated for 12 min at 37°C in an enzyme mixture containing 0.25 mg/mL trypsin, 1 mg/mL collagenase, and 0.2 mg/mL DNase (Sigma, Milan, Italy) in F-12 medium (Invitrogen Corp, S.Giuliano Milanese, Italy). Cells were plated on poly-L-lysine-coated petri dishes in F12 medium with 10% fetal calf serum.

Electrophysiology

After 24 h in culture, trigeminal neurons were superfused continuously (2-3 mL/min) with physiological solution containing (in mM): 152 NaCl, 5 KCl, 1 MgCl2, 2 CaCl2, 10 glucose, and 10 HEPES (pH adjusted to 7.4 with NaOH), as previously described (Nair et al., 2010; Hullugundi et al., 2013). Cells were patch-clamped in the whole-cell configuration using glass pipettes with a resistance of 4-5 Mυ filled with the following solution (in mM): 125 K-gluconate, 5 KCl, 2 MgCl2, 2 Mg2ATP3, 10 HEPES, and 10 EGTA (pH adjusted to 7.2 with KOH). K^+ equilibrium potential, calculated with the Nernst equation, was equal to -105 mV, and liquid junction potential was equal to 14.6 mV. Collected data were corrected accordingly.

Recordings were obtained from small and medium size neurons, (capacitance below 25 pF) under current-clamp conditions, using an Axopatch 200B amplifier (Molecular Devices, Sunnyvale, CA, USA). Experimental conditions were very similar to those in our previous study, except for membrane holding potential. Cells were usually held at -70 mV. Electrophysiological responses were filtered at 10 kHz and acquired by means of a DigiData 1200 interface and pClamp 8.2 software (Molecular Devices, Sunnyvale, CA, USA). Input resistance was measured by applying hyperpolarizing pulses of -5 or -2 pA, while cell capacitance was estimated from the whole-cell capacitance facility.

Depolarizing current pulses lasting for 100-300 ms and of amplitude between 45 and 450 pA were used to stimulate neurons. As previously shown (Hullugundi et al., 2014), such stimulus is sufficient to elicit cell-specific firing activity from most small and medium size TG neurons. In accordance with the previous studies, the P2X3 receptor selective agonist α,β-methylene adenosine 5-triphosphate (α,β-meATP; Sigma, Milan, Italy) was applied for 2 s using a fast superfusion system (Rapid Solution Changer RSC-200; BioLogic Science Instruments, Claix, France) at the concentration of 10 μM to produce near-maximal P2X3 receptor activation (Sokolova et al., 2006). Capsaicin (Sigma) was applied for 3–5 s at a concentration of 1 ⊠M to elicit stable TRPV1 receptor-mediated responses (Simonetti et al., 2006; Nair et al., 2010; Hullugundi et al., 2014). The selective NPR-A antagonist anantin (500 nM) was applied to the cultures overnight to block NPR-A receptors (Yu et al., 2006; Vilotti et al., 2013; Marchenkova et al., 2015).

Data analysis

Data are expressed as mean ±sem (standard error of the mean), with n indicating the number of independent experiments or the number of individual cells. Statistical analysis was performed using Student's t-test or the Mann–Whitney rank sum test after the software-directed choice of parametric or nonparametric data, respectively (Matlab; Sigma Plot & Sigma Stat, Chicago, IL, USA). A p-value of 0.05 was accepted as indicative of a statistically significant difference.

Analyzing firing thresholds, we used an algorithm that allowed automated threshold detection based on first and second discrete time derivatives of the voltage timeseries (Matlab) (Platkiewicz and Brette, 2010; Hullugundi et al., 2014). The parameters used for calculating the

exact threshold value were empirically determined and kept constant for all analyzed recordings. The present data were consistent with the values formerly reported (Sekerli et al., 2004; Hullugundi et al., 2014).

Results

Anantin effects on firing patterns of trigeminal sensory neurons

In line with previously reported data, we observed four distinct firing patterns by cultured TG neurons after stimulation with 45, 100, or 200 pA current pulse (Catacuzzeno et al., 2008; Hullugundi et al., 2014). Figure 1 A shows representative examples of neurons with different firing patterns. Single spike (SS) neurons fired only once at the beginning of the stimulus. Fast adaptive (FA) cells stopped firing after generating several spikes. Multiple firing cells (MF) fired during the whole period of stimulation with time-dependent decrease in spike frequency. Rapid firing neurons (RF) showed sustained high-frequency firing and a large after-hyperpolarization (AHP). Finally, in a fraction of neurons 45 pA stimulation did not elicit any firing activity (no spikes, NS cells). The percent distribution of these firing patterns is shown on the Figure 1 B for WT (upper panels) and KI (lower panels) cultures in control and after 24 h treatment with the NPR-A antagonist anantin (500 nM). WT and KI spike patterns were broadly similar (differences are not statistically significant; $p > 0.05$, two-sample proportion t-test). Anantin application did not affect significantly either WT or KI of firing patterns distribution (Fig. 1 B, right panels).

Under physiological conditions, sensory neurons are depolarized by activation of their ionotropic membrane receptors. Thus, TG neurons generate distinct spike activity patterns mediated by ATP-gated P2X3 receptors or TRPV1 receptors (Hullugundi et al., 2014). We investigated how inactivation of the BNP/BPR-A system might affect firing elicited by the P2X3 agonist α,β-meATP (Jarvis and Khakh, 2009; Fabbretti and Nistri, 2012) or the TRPV1 agonist capsaicin (Meents et al., 2010; O'Neill et al., 2012).

Figure 2 A shows representative examples of neuronal responses observed after 2 s pulses of 10 μM α,β-meATP. In view of the fast inactivation of P2X3 currents (North, 2002; Coddou et al., 2011; Giniatullin and Nistri, 2013) that restricts P2X3-induced firing activity to short spike discharges, application of α,β-meATP resulted in SS and MF patterns along with a group of non-firing cells (NS). Unlike responses to current stimulation, in the case of P2X3-mediated firing clear differences appeared between WT and KI cultures, as illustrated in Figure 2 B. In comparison with WT cultures, KI cells showed a much larger number of MF neurons (75 % in KI vs 51 % in WT; $p < 0.01$, two-sample proportion t-test) and correspondingly decreased numbers of NS plus SS neurons (Fig. 2 B, left diagrams; $p < 0.01$, two-sample proportion t-test). It is noteworthy that anantin treatment (500 nM; 24 h) changed the WT distribution profile to the one observed in KI cultures, namely, strongly increased population size of the MF neurons ($p < 0.02$, two-sample proportion t-test), while decreasing the number of non-responsive and single spike cells (Fig. 2 B, upper diagrams; $p < 0.01$, two-sample proportion t-test). Vice versa, the same protocol of anantin application failed to induce significant shifts in the distribution of firing patterns of KI neurons (Fig. 2 B, bottom diagrams).

We next investigated capsaicin (1 μM, 3 s)-induced firing activity of TG neurons as summarized in Figure 3 A, B. Under control conditions, no apparent difference could be detected between WT and KI cultures in control solution (Fig. 3 B, diagrams on the left) or after anantin application (Fig. 3 B, diagrams on the right).

Anantin selectively increases number of spikes during P2X3-dependent firing in WT

The number of spikes generated by a given stimulus is the main parameter to convey activation of brainstem trigeminal nuclei. Thus, we investigated how the average spike number might change in WT and KI neurons in response to 24 h anantin application. Representative α,β-meATP-dependent firing responses are shown in the Figure 4 A. In control Krebs solution, the mean number of spikes across all WT cells was statistically lower than in KI cells, as calculated in Fig. 4B. In particular, this effect was concentrated in MF neurons (Fig. 4 C). Thus, the difference between WT and KI cells regarding the average number of generated action potentials in response to α,β-meATP application most probably originated from the higher percent of MF cells in KI culture and increased number of spikes in the KI MF population.

It is interesting that anantin treatment increased the number of spikes of the WT cell population to the level comparable with KI cultures (Fig. 4 B, D $p < 0.05$, Mann-Whitney rank sum test). In particular, the number of spikes in the WT MF group grew in response to anantin application as shown in Fig. 4 C. The cumulative probability plot (Fig. 4 D) confirmed a rightward shift in the WT firing response after anantin: for instance, there was 80 % probability to observe 5 spikes after anantin vs just 2 in control Krebs solution. This observation is consistent with the enhancement in P2X3 currents detected after anantin application (Vilotti et al., 2013; Marchenkova et al., 2015). In KI cultures, in analogy to the unchanged firing pattern distribution, anantin did not alter the number of evoked spikes as seen from the representative traces (Fig. 4 A, bottom panels), mean number of spikes values (Fig. 4 B, C, open circles) and cumulative probability plot (Fig. 4 E).

The same analysis was performed for capsaicin-mediated or current-evoked firing. Figure 5 summarizes the data for WT and KI cultured neurons in control and after application of anantin. KI and WT cells produced a similar number of spikes in control solution, as well as after anantin application, whether excitation was induced by a depolarizing current pulse (Fig. 5 A) or capsaicin (Fig. 5 B).

Anantin selectively decreases spike threshold for P2X3-dependent firing in WT cells

It has previously been shown that the KI hyperexcitability phenotype is associated with lower threshold for α,β-meATP-evoked firing in KI cultures (Hullugundi et al., 2014). We, therefore, decided to study threshold values of WT and KI neurons to find out if there was any differential change in response to 24 h 500 nM anantin treatment. Threshold values and α,β-meATP-, depolarizing current- or capsaicin-induced firing in each experimental condition are illustrated in Figure 6. In particular, Figure 6 D exempliefies different mean threshold level (see arrows) for neurons stimulated by α,β-meATP. Control threshold values in KI were lower than in WT for α,β-meATP-evoked spikes (Fig. 6 A; $p < 0.05$, Mann-Whitney rank sum test). In line with anantin effects described in this study, we found decrease of threshold in WT neurons after anantin application (Fig. 6 A, closed circles; $p < 0.05$, Mann-Whitney rank sum test). Indeed, spike threshold of treated WT neurons became statistically undistinguishable from the one of KI. It is noteworthy, that anantin showed no influence on KI cells (Fig. 6 A, open circles). In case of current- and capsaicin-evoked action potentials no statistically significant differences in spike threshold values were detected between control and anantin-treated WT and KI trigeminal neurons (Fig. 6 B, C).

Discussion

The principal finding of this study is the observation that sustained inactivation of BNP/NPR-A pathway in WT TG cultures selectively elevated P2X3-dependent neuronal firing up to what was typically seen in TG cultures of the FHMK1 R192Q KI mouse model. We could, therefore, assume that, in WT neurons under basal conditions, the NPR-A pathway, activated by endogenous BNP (Marchenkova et al., 2015), constitutively inhibited neuronal excitability mediated by P2X3 receptors. Furthermore, the present data suggest that the hyperexcitability phenotype typical for trigeminal sensory neurons of KI mice (Hullugundi et al., 2014) could originate at least in part from lack of BNP/NPR-A-mediated regulation.

Differences between WT and KI trigeminal sensory neurons

Considering firing patterns in response to intracellular current pulses injection, four types were distinguished in both WT and KI trigeminal small- to medium-size neurons. Consistent with previous study (Hullugundi et al., 2014), in the case of current and capsaicin stimulation no significant differences were detected between WT and KI cultures in terms of firing pattern distribution, average number of spikes or threshold for generating action potentials. Block of BNP/NPR-A signaling also caused no change in these parameters, implicating that in control conditions the BNP/NPR-A system of TG neurons did not affect voltage-gated ion channels or TRPV1-dependent excitability.

Major differences were, however, observed between P2X3-mediated firing of WT and KI cultures. The hyperexcitability profile of KI neurons (Hullugundi et al., 2014) was expressed as a complex of interrelated parameters: higher percent of MF neurons, increased average number of action potentials, and decreased voltage threshold for α,β-meATP-induced firing. These phenomena could be explained by the fact that P2X3 receptor function is upregulated in KI TG, whereas TRPV1 responses remain at the level of WT ones (Nair et al., 2010). There are many well-known endogenous modulators, like CGRP, NGF, BDNF, and TNFα, which upregulate P2X3 function in normal and pathological conditions (Fabbretti and Nistri, 2012), and therefore may influence neuronal excitability. In particular, elevated levels of CGRP and BDNF are suggested to contribute to P2X3 gain-of-function in KI trigeminal neurons (Ceruti et al., 2011; Hullugundi et al., 2013). More recently, BNP has been reported to be the first negative regulator of P2X3 receptors in TG (Vilotti et al., 2013; Marchenkova et al., 2015). This peptide constitutively suppresses P2X3 currents in WT trigeminal neurons via its receptor NPR-A, via a dual process comprising increased P2X3 serine phosphorylation level and redistribution of these receptors to non-lipid raft membrane compartments (Marchenkova et al., 2015). Ambient concentrations of BNP are sufficient to maximize the P2X3 receptor inhibition that can be readily unveiled by applying the antagonist anantin (Vilotti et al., 2013; Marchenkova et al., 2015). A subsequent study has demonstrated that the BNP/NPR-A control over P2X3 activity is inefficient in KI neurons despite normal expression of NPR-A receptors and the presence of BNP releasing cells (Marchenkova, unpublished data). The main question, therefore, was if these negative modulatory effects were translated into selective changes in firing because P2X3 membrane currents might have been too small to elicit substantial changes in excitability.

Anantin brings WT low excitability profile close to KI hyperexcitability state

Recent studies proposed BNP as a potential endogenous anti-inflammatory and anti-pain modulator, which, acting through its receptor NPR-A, inhibits the excitability of sensory DRG neurons and constantly downregulates P2X3 receptors in TG (Zhang et al., 2010; Vilotti et al., 2013; Marchenkova et al., 2015). In the present study we obtained additional evidence supporting the idea that BNP/NPR-A pathway plays an important role in restraining TG neuronal excitability in response to α,β-meATP application. Being a synthetic analog of the natural P2X3 ligand ATP, α,β-meATP simulates a situation when ATP is released in a pulsatile manner, often together with other neurotransmitters or after mechanical stress (Fabbretti, 2013). Enhanced ATP synthesis in pathological conditions, including migraine (Burnstock et al., 2011), is thought to support the process of neuronal sensitization (Hamilton and McMahon, 2000). Thus, a system that restrains ATP-gated receptors and, in particular, P2X3 receptors expressed by nociceptive neurons, could serve as an intrinsic mechanism to avoid sensitization and prevent overactivation of sensory neurons.

Inhibition of NPR-A receptors with its selective antagonist anantin led to drastic changes in WT α,β-meATP-mediated excitability. Anantin treatment decreased spike threshold, increased the average number of generated action potentials in TG neurons and, as a consequence, changed the distribution of firing types in WT cultures towards prevalence of higher excitability patterns. Altogether, BNP/NPR-A pathway inactivation transformed WT excitability profile to the one usually associated with KI phenotype of FHM1. It is, therefore, possible to argue that under normal conditions in WT TG endogenous BNP acting via NPR-A (Vilotti et al., 2013; Marchenkova et al., 2015) constitutively restrains the activity of P2X3 receptors and, as a consequence, P2X3-mediated neuronal excitability as well. In R192Q KI mouse model, however, BNP/NPR-A system was shown to be active but unable to overcome the upregulation of P2X3 receptors by CGRP (Marchenkova, unpublished data), leading to the increased excitability in response to P2X3 activation.

A striking observation was the highly selective effects evoked by anantin that targeted just P2X3 receptor-mediated spikes. While higher efficiency of P2X3 receptors may be attributed to changed serine phosphorylation and redistribution within the membrane, the issue of negative shift in the value for spike threshold is more complex as there is no apparent difference in passive membrane properties after anantin application (Marchenkova et al., 2015). One hypothesis is that P2X3 receptors might become more closely clustered with voltage gated channels responsible for the subthreshold behavior of sensory neurons. A large number of nociceptive neurons specifically express a certain type of Na^+ channel that increases the probability to reach threshold for firing action potentials by facilitating the voltage trajectory to spike discharge (Dib-Hajj et al., 2013). Hence, the possibility of topographical association between P2X3 receptors and subtypes of Na^+ channels deserves further investigation.

Conclusion

The selective negative modulation by the BNP/NPR-A pathway over P2X3-induced neuronal excitability in WT mouse trigeminal accords with the recent notion that ligand gated receptors can be viewed as biased microprocessors rather than simple voltage switches (Kenakin, 2015). The view of microprocessor function of P2X3 receptors in physiological conditions is consistent

with the selectivity for their chemical signal regulated by an intrinsic inhibitory peptide mechanism based on ambient BNP to determine the neuronal output in terms of action potential number. When this inhibition is swamped by the constitutive hyperexcitability detected in KI neurons of the FHM1 model, migraine-like pain behavior emerges and has specific characteristics conferred by the properties of overactive P2X3 receptors (Fabbretti & Nistri).

Acknowledgements

This work was supported by the EU FP7 grant EuroHeadPain (#602633).

References

Abdelalim EM, Tooyama I (2011) NPR-A regulates self-renewal and pluripotency of embryonic stem cells. Cell Death Dis 2:e127.

Burnstock G, Krügel U, Abbracchio MP, Illes P (2011) Purinergic signalling: from normal behaviour to pathological brain function. Prog Neurobiol 95:229–274.

Catacuzzeno L, Fioretti B, Pietrobon D, Franciolini F (2008) The differential expression of low-threshold K+ currents generates distinct firing patterns in different subtypes of adult mouse trigeminal ganglion neurones. J Physiol 586:5101–5118.

Ceruti S, Villa G, Fumagalli M, Colombo L, Magni G, Zanardelli M, Fabbretti E, Verderio C, Maagdenberg AMJM van den, Nistri A, Abbracchio MP (2011) Calcitonin Gene-Related Peptide-Mediated Enhancement of Purinergic Neuron/Glia Communication by the Algogenic Factor Bradykinin in Mouse Trigeminal Ganglia from Wild-Type and R192Q Cav2.1 Knock-In Mice: Implications for Basic Mechanisms of Migraine Pain. J Neurosci 31:3638–3649.

Chanda ML, Tuttle AH, Baran I, Atlin C, Guindi D, Hathaway G, Israelian N, Levenstadt J, Low D, Macrae L, O'Shea L, Silver A, Zendegui E, Mariette Lenselink A, Spijker S, Ferrari MD, van den Maagdenberg AMJM, Mogil JS (2013) Behavioral evidence for photophobia and stress-related ipsilateral head pain in transgenic Cacna1a mutant mice. Pain 154:1254–1262.

Coddou C, Yan Z, Obsil T, Huidobro-Toro JP, Stojilkovic SS (2011) Activation and regulation of purinergic P2X receptor channels. Pharmacol Rev 63:641–683.

Dib-Hajj SD, Yang Y, Black JA, Waxman SG (2013) The Na(V)1.7 sodium channel: from molecule to man. Nat Rev Neurosci 14:49–62.

Fabbretti E (2013) ATP P2X3 receptors and neuronal sensitization. Front Cell Neurosci 7:236.

Fabbretti E, Nistri A (2012) Regulation of P2X3 receptor structure and function. CNS Neurol Disord Drug Targets 11:687–698.

Gasparini CF, Sutherland HG, Griffiths LR (2013) Studies on the Pathophysiology and Genetic Basis of Migraine. Curr Genomics 14:300–315.

Giniatullin R, Nistri A (2013) Desensitization properties of P2X3 receptors shaping pain signaling. Front Cell Neurosci 7:245.

Hamilton SG, McMahon SB (2000) ATP as a peripheral mediator of pain. J Auton Nerv Syst 81:187–194.

Hullugundi SK, Ansuini A, Ferrari MD, van den Maagdenberg AMJM, Nistri A (2014) A hyperexcitability phenotype in mouse trigeminal sensory neurons expressing the R192Q Cacna1a missense mutation of familial hemiplegic migraine type-1. Neuroscience 266:244–254.

Hullugundi SK, Ferrari MD, van den Maagdenberg AMJM, Nistri A (2013) The mechanism of functional up-regulation of P2X3 receptors of trigeminal sensory neurons in a genetic mouse model of familial hemiplegic migraine type 1 (FHM-1). PloS One 8:e60677.

Jarvis MF, Khakh BS (2009) ATP-gated P2X cation-channels. Neuropharmacology 56:208–215.

Julius D, Basbaum AI (2001) Molecular mechanisms of nociception. Nature 413:203–210.

Kenakin T (2015) Gaddum Memorial Lecture 2014: receptors as an evolving concept: from switches to biased microprocessors. Br J Pharmacol 172:4238–4253.

Marchenkova A (n.d.) Inefficient constitutive inhibition of P2X3 receptors by the brain natriuretic peptide system in trigeminal sensory neurons of mouse model of genetic migrain. Unpubl Data.

Marchenkova A, Vilotti S, Fabbretti E, Nistri A (2015) Brain natriuretic peptide constitutively downregulates P2X3 receptors by controlling their phosphorylation state and membrane localization. Mol Pain 11:71.

Meents JE, Neeb L, Reuter U (2010) TRPV1 in migraine pathophysiology. Trends Mol Med 16:153–159.

Nair A, Simonetti M, Birsa N, Ferrari MD, van den Maagdenberg AMJM, Giniatullin R, Nistri A, Fabbretti E (2010) Familial hemiplegic migraine Ca(v)2.1 channel mutation R192Q enhances ATP-gated P2X3 receptor activity of mouse sensory ganglion neurons mediating trigeminal pain. Mol Pain 6:48.

North RA (2002) Molecular physiology of P2X receptors. Physiol Rev 82:1013–1067.

North RA (2003) The P2X3 subunit: a molecular target in pain therapeutics. Curr Opin Investig Drugs Lond Engl 2000 4:833–840.

O'Neill J, Brock C, Olesen AE, Andresen T, Nilsson M, Dickenson AH (2012) Unravelling the mystery of capsaicin: a tool to understand and treat pain. Pharmacol Rev 64:939–971.

Ophoff RA, Terwindt GM, Vergouwe MN, van Eijk R, Oefner PJ, Hoffman SMG, Lamerdin JE, Mohrenweiser HW, Bulman DE, Ferrari M, Haan J, Lindhout D, van Ommen G-JB, Hofker MH, Ferrari MD, Frants RR (1996) Familial Hemiplegic Migraine and Episodic Ataxia Type-2 Are Caused by Mutations in the Ca2+ Channel Gene CACNL1A4. Cell 87:543–552.

Platkiewicz J, Brette R (2010) A Threshold Equation for Action Potential Initiation. PLoS Comput Biol 6:e1000850.

Sekerli M, Del Negro CA, Lee RH, Butera RJ (2004) Estimating action potential thresholds from neuronal time-series: new metrics and evaluation of methodologies. IEEE Trans Biomed Eng 51:1665–1672.

Simonetti M, Fabbro A, D'Arco M, Zweyer M, Nistri A, Giniatullin R, Fabbretti E (2006) Comparison of P2X and TRPV1 receptors in ganglia or primary culture of trigeminal neurons and their modulation by NGF or serotonin. Mol Pain 2:11.

Sokolova E, Skorinkin A, Moiseev I, Agrachev A, Nistri A, Giniatullin R (2006) Experimental and modeling studies of desensitization of P2X3 receptors. Mol Pharmacol 70:373–382.

van den Maagdenberg AMJM, Pietrobon D, Pizzorusso T, Kaja S, Broos LAM, Cesetti T, van de Ven RCG, Tottene A, van der Kaa J, Plomp JJ, Frants RR, Ferrari MD (2004) A Cacna1a Knockin Migraine Mouse Model with Increased Susceptibility to Cortical Spreading Depression. Neuron 41:701–710.

Vilotti S, Marchenkova A, Ntamati N, Nistri A (2013) B-type natriuretic peptide-induced delayed modulation of TRPV1 and P2X3 receptors of mouse trigeminal sensory neurons. PloS One 8:e81138.

Vulchanova L, Riedl MS, Shuster SJ, Buell G, Surprenant A, North RA, Elde R (1997) Immunohistochemical study of the P2X2 and P2X3 receptor subunits in rat and monkey sensory neurons and their central terminals. Neuropharmacology 36:1229–1242.

Weber W, Fischli W, Hochuli E, Kupfer E, Weibel EK (1991) Anantin--a peptide antagonist of the atrial natriuretic factor (ANF). I. Producing organism, fermentation, isolation and biological activity. J Antibiot (Tokyo) 44:164–171.

Yan J, Dussor G (2014) Ion channels and migraine. Headache 54:619–639.

Yu Y-C, Cao L-H, Yang X-L (2006) Modulation by brain natriuretic peptide of GABA receptors on rat retinal ON-type bipolar cells. J Neurosci Off J Soc Neurosci 26:696–707.

Zhang F-X, Liu X-J, Gong L-Q, Yao J-R, Li K-C, Li Z-Y, Lin L-B, Lu Y-J, Xiao H-S, Bao L, Zhang X-H, Zhang X (2010) Inhibition of Inflammatory Pain by Activating B-Type Natriuretic Peptide Signal Pathway in Nociceptive Sensory Neurons. J Neurosci 30:10927–10938.

Figures

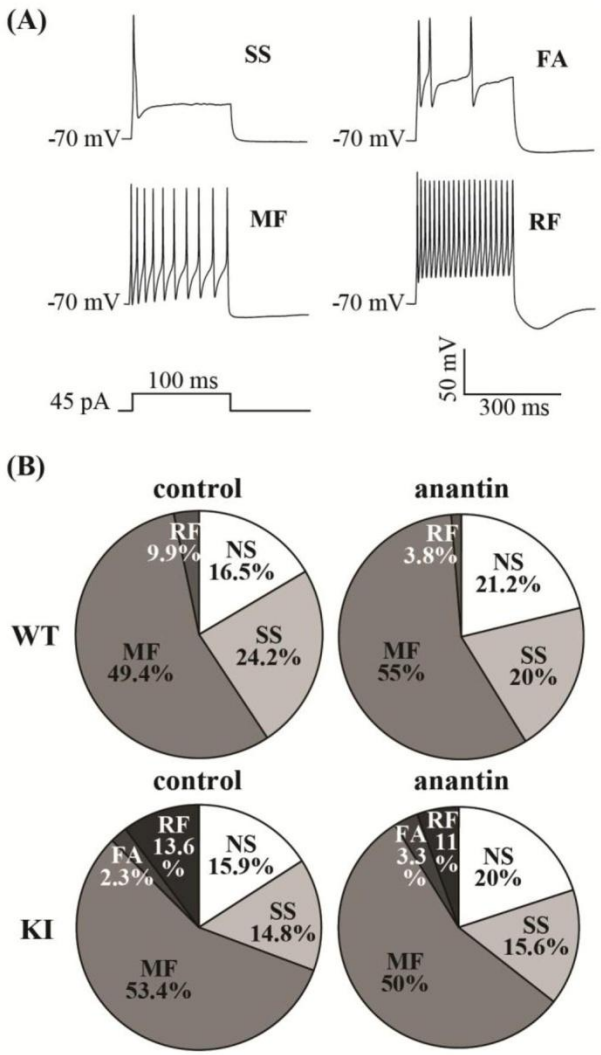

Fig. 1. Firing patterns of trigeminal sensory neurons evoked by intracellular current pulse injections. (A) Representative traces of firing pattern types recorded from WT TG neurons in response to intracellular current pulse injections (45 pA, 300 ms). Similar patterns of firing activity were also found in KI cells. SS – single spiking, FA – fast adaptive, MF – multiple firing and RF – rapid firing neurons. (B) Pie charts showing the percent distribution of neurons with the above mentioned firing patterns plus non-spiking cells (NS) in WT and KI TG cultures in control and after anantin application (500 nM, 24 h). Numbers of cells for NS, SS, MF, FA, RF groups, respectively, are: WT, control, n = 15, 22, 51, 0, 3; WT, after anantin application, n = 17, 16, 46, 0, 1; KI, control, n = 14, 13, 50, 2, 9; KI, after anantin application, n = 18, 14, 50, 3, 5.

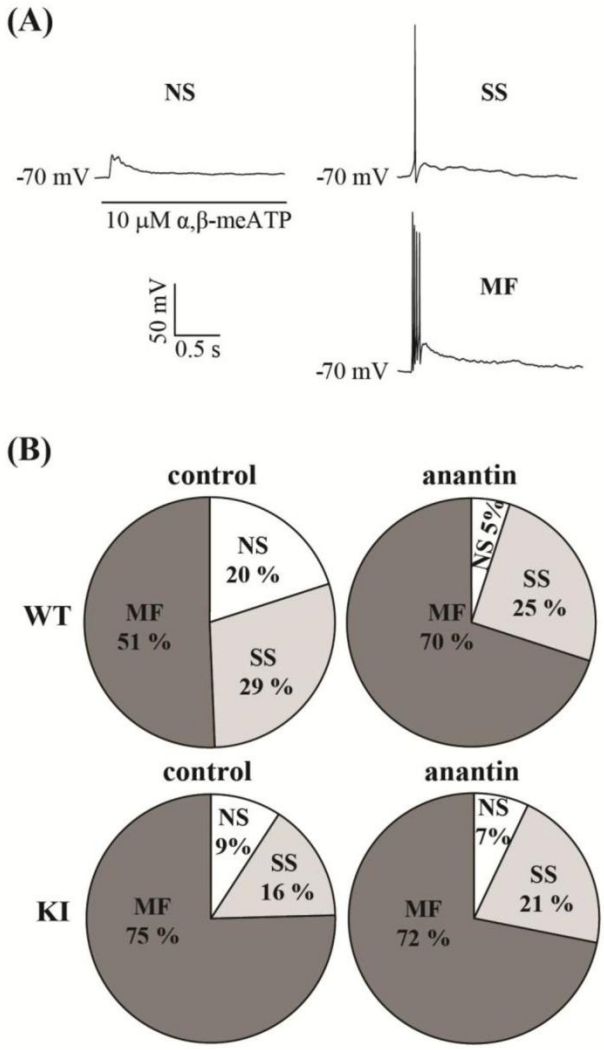

Fig. 2. Firing patterns of trigeminal sensory neurons evoked by α,β-meATP application. (A) Representative traces of firing pattern types recorded from WT TG neurons in response to α,β-meATP pulses (10 μM, 2 s). Similar patterns are also found in KI cells (not shown). NS – neurons that produced no spikes in response to the stimulation, SS – single spiking, MF – multiple firing cells. (B) Pie charts showing the percent distribution of neurons with the above mentioned firing patterns in WT and KI TG cultures in control and after anantin treatment (500 nM, 24 h). Note significantly lower number of SS and higher numbers of RF and FA neurons under control conditions in KI (bottom left chart) versus WT (upper left chart) and the fact that after anantin treatment distribution in WT greatly resembles the one in KI (right diagrams); $p < 0.05$, two-sample proportion t-test. Numbers of cells for NS, SS and MF groups, respectively, are: WT, control, n = 15, 22, 38; WT, after anantin application, n = 4, 20, 56; KI, control, n = 6, 10, 49; KI, after anantin application, n = 5, 15, 51.

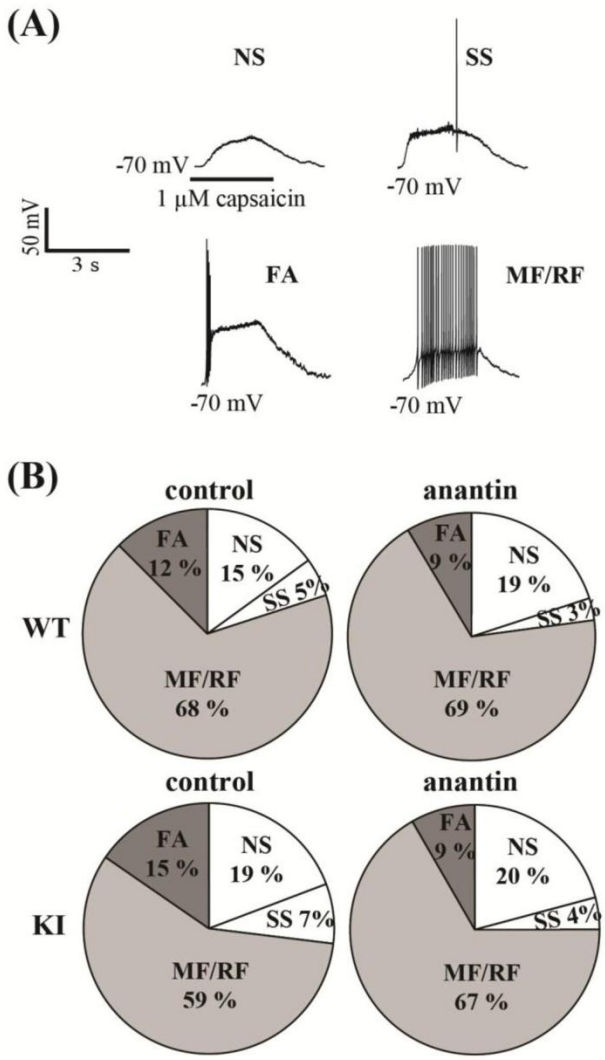

Fig. 3. Firing patterns of trigeminal sensory neurons evoked by capsaicin. (A) Representative traces of firing pattern types recorded from WT TG neurons in response to capsaicin pulses (1 μM, 3 s). Similar patterns of firing were found in KI cells. NS – neurons that produced no spikes in response to the stimulation, SS – single spiking, FA – fast adaptive, MF/RF – multiple firing and rapid firing neurons. (B) Pie charts show percent distribution of neurons with the above mentioned firing patterns in WT and KI TG cultures. Numbers of cells for NS, SS, FA, MF/RF groups, respectively, are: WT, control, n = 6, 2, 5, 27; WT, after anantin application, n = 7, 1, 3, 24; KI, control, n = 5, 2, 4, 15; KI, after anantin application, n = 5, 1, 2, 16.

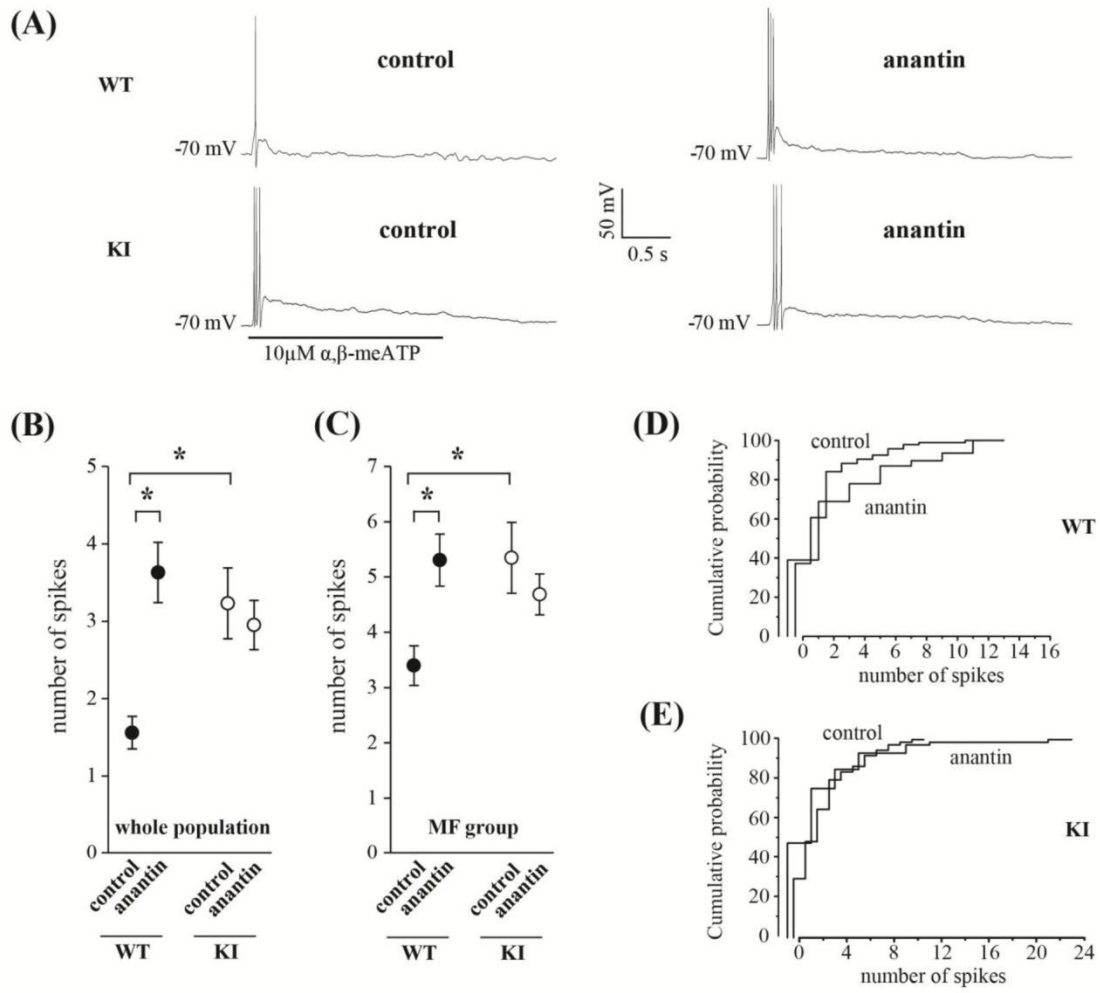

Fig. 4. Anantin increases number of spikes generated by WT neurons in response to α,β-meATP application. (A) Representative traces recorded from WT and KI TG neurons in response to α,β-meATP pulses (10 μM, 2 s) in control and after anantin treatment (24 h, 500 nM). Note how WT firing profile resembles KI one after anantin treatment. (B) Quantification of average number of spikes (mean ± SEM) for WT (closed circles) and KI (opened circles) neurons in control and after anantin application for the whole WT or KI population, including cell with all types of responses (n = 75, WT, control; n = 80, WT, anantin; n = 65, KI, control; n = 71, KI, anantin; $p < 0.05$, Mann–Whitney rank sum test). (C) The diagram quantifies mean number of spikes for MF group only (n = 38, WT, control; n = 56, WT, anantin; n = 49, KI, control; n = 51, KI, anantin; $p < 0.05$, Mann–Whitney rank sum test). Note the similar number of spikes in KI (both control and after anantin) and WT after anantin treatment. (D) Kolmogorov–Smirnov plots of cumulative firing probability for WT neurons in control and after anantin application. (E) Kolmogorov–Smirnov plots of cumulative firing probability for KI neurons in control and after anantin application.

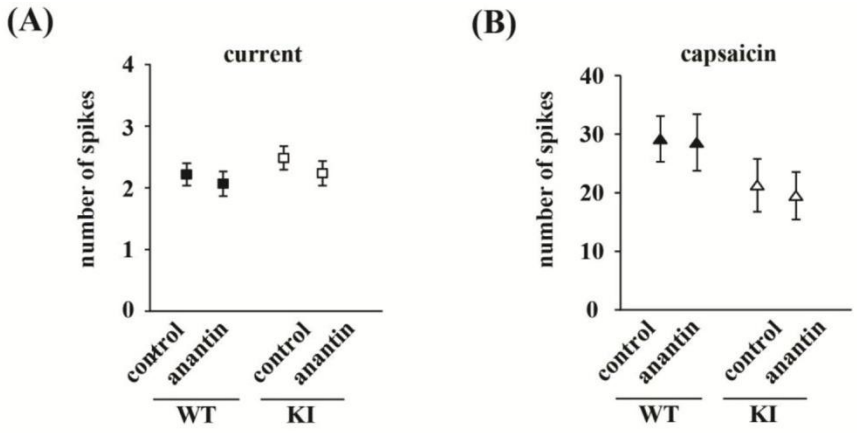

Fig. 5. Anantin does not change number of spikes generated by WT or KI neurons in response to capsaicin or current pulse injections. The graphs compare average number of spikes (mean ± SEM) generated by WT or KI neurons in control and after anantin application in response to current pulse stimulation (45 pA, 300 ms; (A)) or capsaicin (1 μM, 3 s; (B)). Values are quantified for the whole WT or KI population, including cell with all types of responses (current stimulation: n = 91, WT, control; n = 80, WT, anantin; n = 88, KI, control; n = 90, KI, anantin; capsaicin: n = 40, WT, control; n = 35, WT, anantin; n = 26, KI, control; n = 24, KI, anantin).

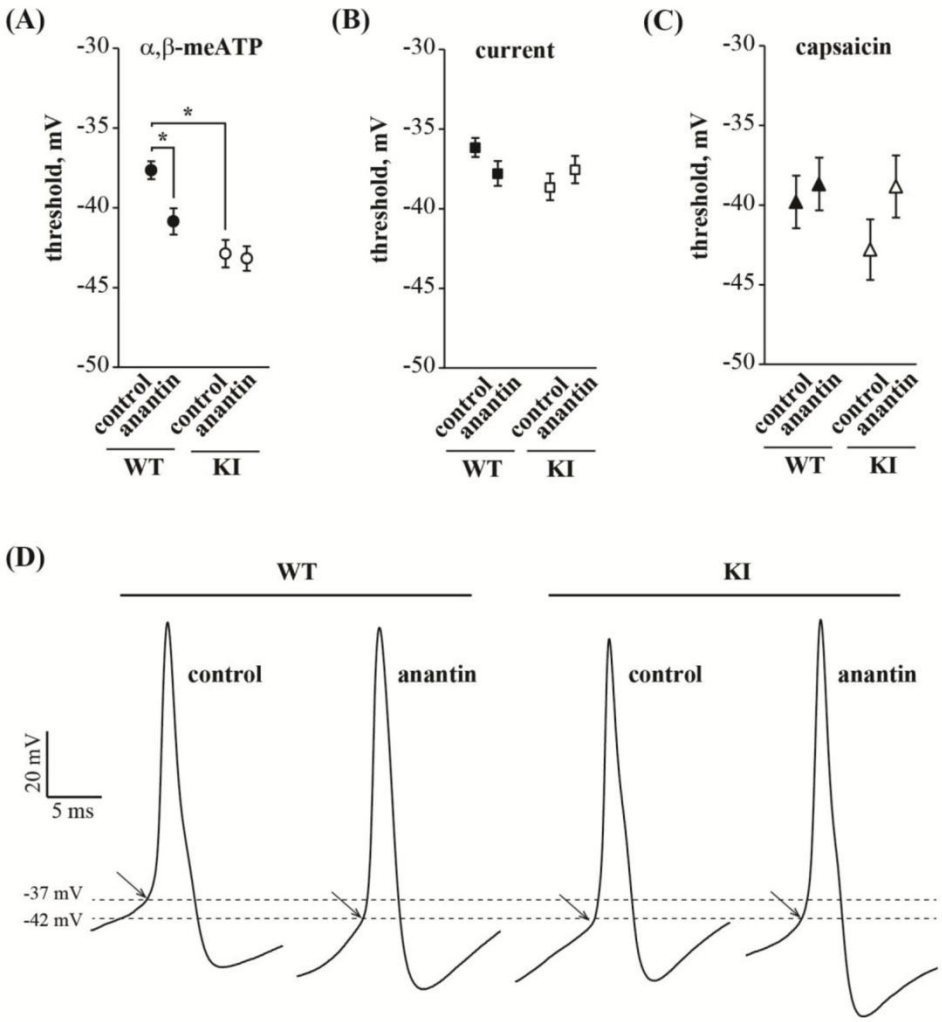

Fig. 6. Anantin decreases threshold for spikes evoked by α,β-meATP in WT neurons. (A) Diagram shows average threshold values (mean ± SEM) for WT and KI neurons in control and after anantin application (500 nm, 24 h) for action potentials evoked by α,β-meATP (10 μM, 2 s). Values are quantified for the whole WT or KI population, including cell with all types of responses. Note how WT threshold value after anantin treatment resembles KI values. *$p < 0.05$, Mann–Whitney rank sum test. Numbers of analyzed neurons are: n = 60, WT, control; n = 76, WT, anantin; n = 59, KI, control; n = 66, KI, anantin). (B), (C), Diagrams show no difference in average threshold values (mean ± SEM) for WT and KI neurons between control and anantin-treated (500 nm, 24 h) neurons for action potentials evoked by 300 ms 45 pA current pulses (B) or capsaicin (1 μM, 3 s; (C)). Numbers of analyzed neurons are: current stimulation: n = 76, WT, control; n = 63, WT, anantin; n = 74, KI, control; n = 72, KI, anantin; capsaicin: n = 34, WT, control; n = 28, WT, anantin; n = 21, KI, control; n = 19, KI, anantin. (D) Representative traces of first generated action potentials in response to α,β-meATP (10 μM, 2 s). Arrows indicate firing threshold. Note how in WT threshold becomes more negative and close to what is observed in KI after anantin treatment.

5. Evaluation of adenine as scaffold for the development of novel P2X3 receptor antagonists

European Journal of Medicinal Chemistry 65 (2013) 41–50

Contents lists available at SciVerse ScienceDirect

European Journal of Medicinal Chemistry

journal homepage: http://www.elsevier.com/locate/ejmech

Original article

Evaluation of adenine as scaffold for the development of novel P2X3 receptor antagonists

Catia Lambertucci [a,1], Mayya Sundukova [b,1], Dhuldeo D. Kachare [a], Deepak S. Panmand [a], Diego Dal Ben [a], Michela Buccioni [a], Gabriella Marucci [a], Anna Marchenkova [b], Ajiroghene Thomas [a], Andrea Nistri [b], Gloria Cristalli [a], Rosaria Volpini [a,*]

[a] School of Pharmacy, Medicinal Chemistry Unit, University of Camerino, Via S. Agostino, 1, 62032 Camerino, MC, Italy
[b] Neuroscience Department, International School for Advanced Studies (SISSA), Via Bonomea, 265, 34136 Trieste, Italy

ARTICLE INFO

Article history:
Received 14 December 2012
Received in revised form
15 April 2013
Accepted 16 April 2013
Available online 24 April 2013

Keywords:
Purinergic receptors
P2X3 receptor
P2X3 receptor antagonists
Adenine derivatives
Purine derivatives
ATP
Purine
Patch clamp

ABSTRACT

Ligands that selectively block P2X3 receptors localized on nociceptive sensory fibres may be useful for the treatment of chronic pain conditions including neuropathic pain, migraine, and inflammatory pain. With the aim at exploring the suitability of adenine moiety as a scaffold for the development of antagonists of this receptor, a series of 9-benzyl-2-aminoadenine derivatives were designed and synthesized. These new compounds were functionally evaluated at rat or human P2X3 receptors expressed in human embryonic kidney (HEK) cells and on native P2X3 receptors from mouse trigeminal ganglion sensory neurons using patch clamp recording under voltage clamp configuration. The new molecules behaved as P2X3 antagonists, as they rapidly and reversibly inhibited (IC_{50} in the low micromolar range) the membrane currents induced via P2X3 receptor activation by the full agonist α,β-methyleneATP. Introduction of a small lipophilic methyl substituent at the 6-amino group enhanced the activity, in comparison to the corresponding unsubstituted derivative, resulting in the 9-(5-iodo-2-isopropyl-4-methoxybenzyl)-N^6-methyl-9*H*-purine-2,6-diamine (**24**), which appears to be a good antagonist on recombinant and native P2X3 receptors with $IC_{50} = 1.74 \pm 0.21$ μM.

1. Introduction

P2X3 receptors belong to the purinergic P2X receptor class of ligand-gated channels activated by extracellular ATP to induce a rapid increase in membrane permeability to mono- and di-valent cations [1–3]. P2X3 receptors were cloned in 1995 [4,5] and shown to be almost exclusively localized on nociceptive sensory neurons and on afferent fibre terminals in lamina two of the spinal cord dorsal horn [6]. They contribute to pain sensation, visceral mechanosensory transduction, and gut peristalsis [7–10]. Extensive activation of such receptors is believed to be involved in a number of chronic pain conditions including neuropathic pain, which is typically resistant to standard pain treatment, migraine, and inflammatory pain [11]. Functional P2X3 receptors are predominantly expressed as homomers (with fastly desensitizing property upon prolonged exposure to ATP), and to a much lesser extent as heteromers with P2X2 (P2X2/3) [4,5,12]. However, the latter can be distinguished by their insensitivity to low concentrations of the reference non-hydrolysable and selective P2X3 agonist α,β-methyleneATP (α,β-meATP) [12–14]. Targeting these receptors with selective, potent antagonists can represent an innovative approach to treat chronic pain conditions of both neuropathic and inflammatory origin when P2X3 receptor function is reported to be enhanced [15,16]. In the last few years considerable effort has been dedicated to the development of potent and selective antagonists at P2X3 receptors; the first identified P2X3 antagonists were negatively charged and/or high molecular weight organic molecules like suramin, pyridoxalphosphate-6-azophenyl-2′,4′-disulfonic acid (PPADS), 2′,3′-*O*-(2,4,6-trinitrophenyl)-ATP (TNP-ATP) [17], and A-317491 (Fig. 1) [18]; on the other hand, some

Abbreviations: α,β-meATP, α,β-methyleneATP; PPADS, pyridoxalphosphate-6-azophenyl-2′,4′-disulfonic acid; TNP-ATP, 2′,3′-*O*-(2,4,6-trinitrophenyl)-ATP; PPP, triphosphate; HTS, high-throughput screening; TG, trigeminal ganglia; DCM, dichloromethane; NOE, nuclear Overhauser effect; TFAA, trifluoroacetic anhydride; TBAN, tetrabutylammonium nitrate; TEA, triethylamine; PTSA, *p*-toluenesulfonic acid; n_H, Hill coefficient; DRG, dorsal root ganglion; τ_{on}, rise time; $\tau_{des1;2}$, time constant of desensitization decay; CPU, central processing unit; MOE, Molecular Operating Environment; TLC, thin-layer chromatography; PTLC, preparative thin-layer chromatography.

* Corresponding author. Tel.: +39 0737 402278; fax: +39 0737 402295.
E-mail address: rosaria.volpini@unicam.it (R. Volpini).

[1] These authors contributed equally to this work.

0223-5234/$ – see front matter © 2013 Elsevier Masson SAS. All rights reserved.
http://dx.doi.org/10.1016/j.ejmech.2013.04.037

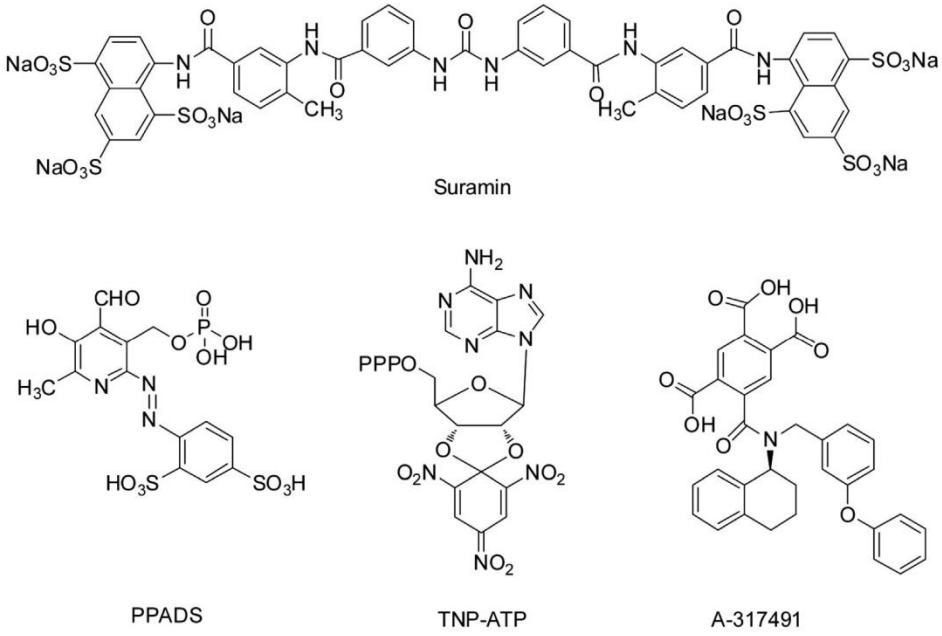

Fig. 1. Structure of some known P2X3 antagonists (PPP = triphosphate).

of them lacked selectivity and potency. The poor pharmacokinetic properties of these molecules (poor oral bioavailability, high protein binding, and uneven tissue distribution) would likely make them unattractive for their development as drugs. More recently, novel antagonists for homomeric P2X3 and heteromeric P2X2/3 receptors, structurally related to the diaminopyrimidine antibacterial drug trimethoprim, have been identified by a high-throughput screening (HTS) campaign [19]. Among them, a compound named RO-3 (Fig. 2A) represents an important step towards discovery of novel drug-like P2X antagonists [20,21] endowed with high affinity and selectivity. Furthermore, new acyclic-nucleotides based on the adenine skeleton and bearing in 9-position a phosphorylated four carbon chain (Fig. 2B) mimicking the ribose function have been described as partial agonists of P2X3 receptors [22].

In the present study, the information coming from the latter two series of above cited compounds was combined with the aim at testing the suitability of the adenine moiety as scaffold for the development of P2X3 antagonists. In detail, a new class of P2X3

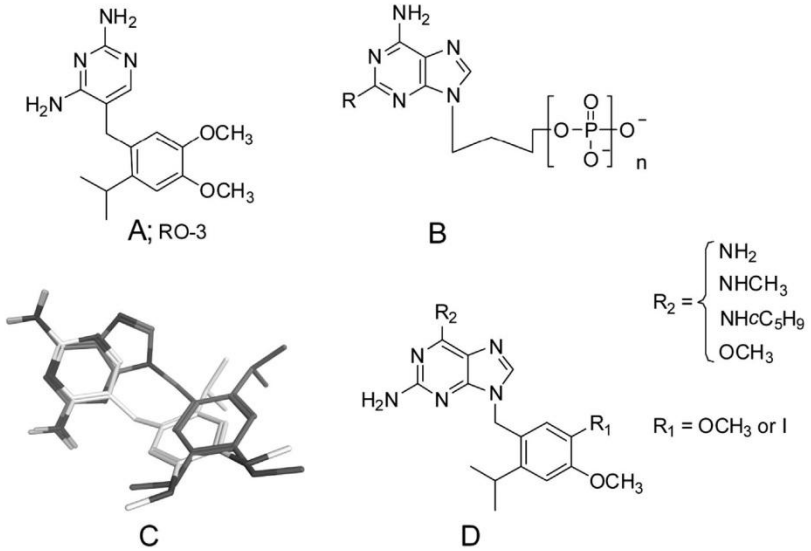

Fig. 2. A and B: known P2X3 ligands; C: 3D alignment of one of the designed purine derivatives (dark grey) with the pyrimidine analogue RO-3 (light grey). Non-polar hydrogen atoms are hidden; D: designed molecules.

ligands was firstly designed by taking into account the structural features of the above mentioned P2X3 receptor antagonists and the adenine scaffold of the partial agonists and by combining this data with the use of molecular modelling tools. A molecular superimposition (Fig. 2C) of the diaminopyrimidine derivative A and the adenine scaffold led to the identification of the 9- and the 2-positions of adenine as possible sites to introduce the substituted aromatic chains and the second amino group observed in diaminopyrimidine series, respectively. As a consequence, 2,6-diaminopurine bearing 2-isopropyl-4,5-dimethoxybenzyl or 5-iodo-2-isopropyl-4-methoxybenzyl chain in 9-position were design ed, synthesized, and tested functionally on P2X3 receptors (Fig. 2D). In order to study the influence of N^6-substitution on P2X3 receptors activity, a methyl and a more sterically hindered cyclopentyl moiety were introduced at N^6-position of these new molecules. Furthermore, the 6-methylamino group was replaced with the isosteric methoxy substituent (Fig. 2D). The new compounds were evaluated for their biological activity on rat and human P2X3 receptors, expressed on human embryonic kidney (HEK) cells and on native P2X3 receptors from mouse trigeminal ganglion (TG) sensory neurons by the patch clamp technique.

2. Results and discussion

2.1. Chemistry

The 9-substituted purine derivatives **21**–**25**, **28** were prepared by alkylating the commercially available 2-amino-6-chloropurine (**16**) with the suitable electrophiles **6** and **15** (Schemes 1–3). For the synthesis of the electrophiles, some intermediates, already reported in literature, were here prepared with different synthetic routes. Experimental details for their synthesis are reported in the Supporting information.

The 2-isopropyl-4,5-dimethoxybenzyl methanesulfonate (**6**) was synthesized starting from the commercially available 3,4-dimethoxy acetophenone (**1**), which was reacted with methyl lithium to give the hydroxy derivative 2-(3,4-dimethoxyphenyl) propan-2-ol (**2**) (Scheme 1). Intermediate alcohol **2** was reduced in the presence of acetic acid, ammonium formate, and a catalytic amount of 10% Pd/C to obtain the corresponding 4-isopropyl-1,2-dimethoxybenzene (**3**).

Formylation of **3** with dichloro(methoxy)methane and tin tetrachloride in dichloromethane (DCM) gave **4**: the synthesis of this compound was also reported in a patent but consisted in a longer route [20]. Compound **4** was then reduced with $NaBH_4$ to (2-isopropyl-4,5-dimethoxyphenyl)methanol (**5**). Mesylation of **5** using methanesulfonyl chloride in the presence of triethylamine gave the desired electrophile **6** (Scheme 1).

The 5-iodo-2-isopropyl-4-methoxybenzyl methanesulfonate (**15**) was synthesized starting from the commercially available 3-methoxyacetophenone (**7**) (Scheme 2). Hence, **7** was reacted with methyl lithium to give the hydroxy derivative 2-(3-methox yphenyl)propan-2-ol (**8**), which was dehydroxylated in the presence of acetic acid, ammonium formate, and catalytic amount of 10% Pd/C, to obtain the corresponding 1-isopropyl-3-methoxy benzene (**9**) [23]. Hence, nitration of compound **9** was performed by reaction with tetrabutylammonium nitrate (TBAN) and trifluoroacetic anhydride (TFAA), in DCM, to obtain the 4-isopropyl-2-methoxy-1-nitrobenzene (**10**). The nitro group of **10** was reduced by hydrogen and 10% Pd/C to furnish the 4-isopropyl-2-methoxyaniline (**11**). 1-Iodo-4-isopropyl-2-methoxybenzene (**12**) was synthesized from **11** by Sandmeyer reaction conditions using *p*-toluenesulfonic acid (PTSA), sodium nitrite, and potassium iodide. Formylation of **12** was achieved by dichloro(methoxy) methane and tin tetrachloride in DCM to furnish **13** (Scheme 2).

The formyl group of **13** was reduced by $NaBH_4$ to give **14**, which was mesylated using the same conditions described for compound **5**, to furnish the desired electrophile **15** (Scheme 2).

After workup, the crude mixtures of mesylates **6** and **15** were reacted with commercially available anhydrous 2-amino-6-chloropurine (**16**) in the presence of K_2CO_3 and 18-crown-6 ether in DMF at 70 °C, to give the desired N9-isomers **17** and **18**, which were obtained as major products along with the N7-regioisomers **19** and **20**, respectively (Scheme 3). The chemical structures of the N9 and N7 isomers were first attributed to compounds **17**, **18** and **19**, **20**, respectively, on the basis of their chemical/physical properties. Firstly, N9-isomers **17** and **18** were obtained in higher yield than the corresponding N7-isomers as it is reported in similar reactions [24]. Secondly, the ^1H NMR spectra of the N9-isomers **17** and **18** showed CH_2–N and H-8 signals at higher magnetic field with respect to the corresponding signals of the N7-isomers, **19** and **20**, as reported in literature for analogous compounds (Fig. 3) [24,25].

The N9-isomers, 6-chloro-9-(2-isopropyl-4,5-dimethoxybenzyl)-9*H*-purin-2-amine (**17**) and 6-chloro-9-(5-iodo-2-isopropyl-4-meth oxybenzyl)-9*H*-purin-2-amine (**18**) were reacted with ammonia to

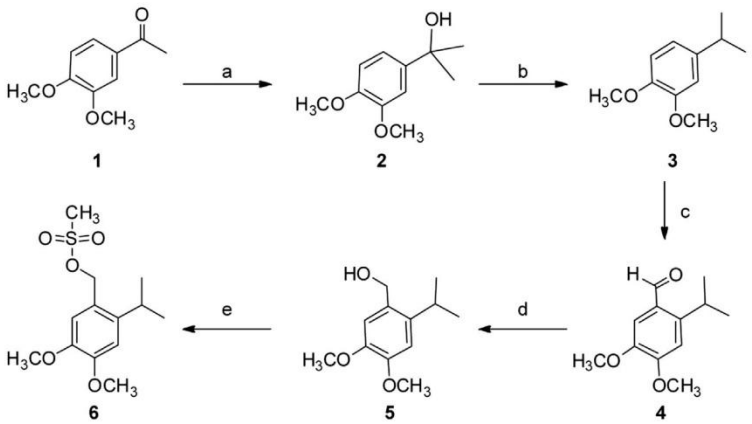

Scheme 1. Reagents and conditions: a. CH_3Li, THF, 69% yield; b. $HCOONH_4$, 10% Pd/C, AcOH, 94% yield; c. Cl_2CHOCH_3, $SnCl_4$, DCM, 92% yield; d. $NaBH_4$, MeOH, 87% yield; e. $MeSO_2Cl$, TEA, DCM, 89% yield.

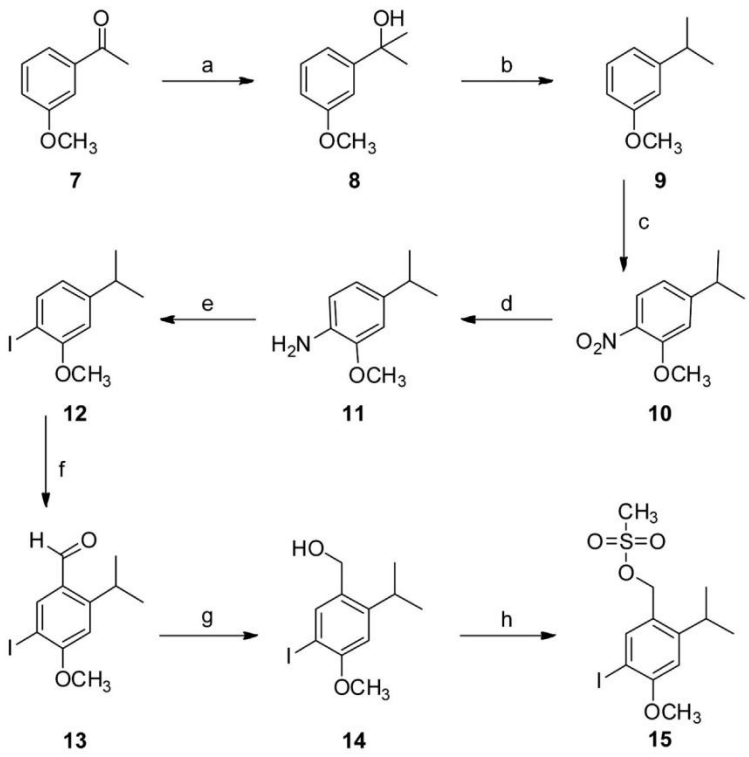

Scheme 2. Reagents and conditions: a. CH_3Li, THF, 77% yield; b. $HCOONH_4$, 10% Pd/C, AcOH, 77% yield; c. TBAN, TFAA, DCM, 77% yield; d. H_2, 10% Pd/C, MeOH, 83% yield; e. PTSA, $NaNO_2$, KI, H_2O/CH_3CN, 65% yield; f. Cl_2CHOCH_3, $SnCl_4$, DCM, 95% yield; g. $NaBH_4$, MeOH, 64% yield; h. $MeSO_2Cl$, TEA, DCM, 92% yield.

obtain compounds **21** and **22**. From the iodomethoxy derivative **18** were also prepared 6-methoxy, 6-methylamino, and 6-cyclopentylamino analogues **23**–**25** by reacting it with sodium methoxide in MeOH, methylamine, and cyclopentylamine, respectively. The two N7-isomers bearing in the 6 position an amino group, **26** and **27**, were prepared from **19** and **20** using the same reaction conditions described above for the corresponding N9-isomers (Scheme 3).

To unequivocally attribute the structure of the N7 and N9-isomers, NOE experiments were performed on 6-amino

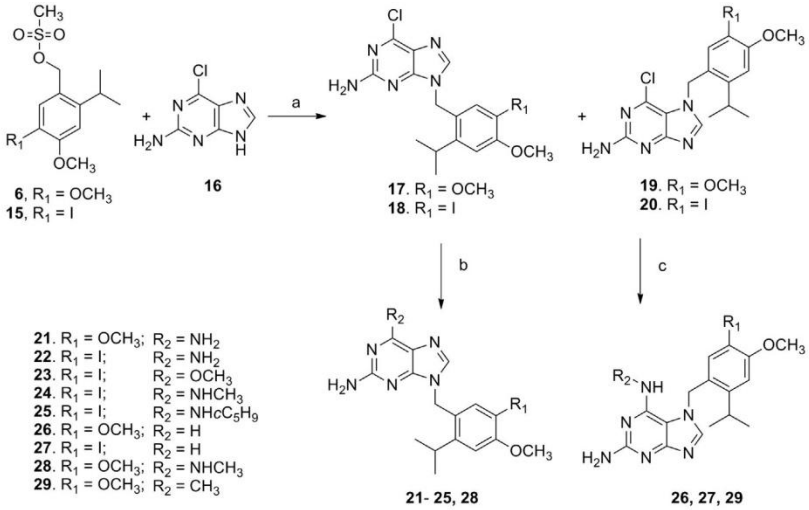

Scheme 3. Reagents and conditions: a. K_2CO_3, 18-crown-6, DMF, yields: **17**–**19** and **20** 51%, 52%, 35%, and 12%, respectively; b. NH_3 liq., or MeONa/MeOH, or CH_3NH_2, or $cC_5H_9NH_2$/THF, yields: **21**–**25** and **28** 54%, 40%, 69%, 76%, 69%, and 40%, respectively; c. NH_3 liq. or CH_3NH_2, yields: **26**, **27**, and **29** 24%, 40%, and 33%, respectively.

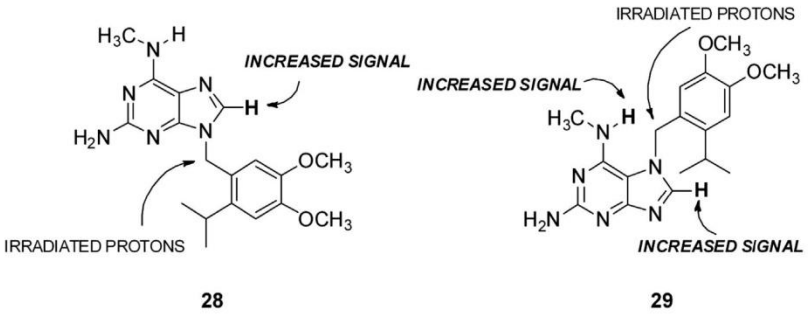

Fig. 3. NOE experiment performed on compound **28** and **29** by irradiation of the signal of CH_2-benzylic group unequivocally permitted to attribute the N9 and N7 isomer structure, respectively.

derivatives **21** and **26** after irradiation of the benzylic CH_2 protons. Results showed increased H-8 signals in ^{1}H NMR spectra of both compounds, but unfortunately no effect was detected at N^6-H_2 hydrogens leaving no possible structure determination. For this reason, the N^6-methylamino derivatives **28** and **29** were prepared from **17** and **19** by reaction with methylamine (Scheme 3). NOE experiments were then performed on **28** and **29** by irradiating the benzylic CH_2 groups. As expected, the intensity of signals for H-8 protons of the two compounds and the N^6-H signal intensity of **29** were increased after irradiation, while no effect was detected on the N^6-H signal of **28**. These data confirmed the structure of the N7-isomer **29**, in which the increased signal intensity of the N^6-H atom was due to the close proximity with the irradiated CH_2 group, which failed to influence the N^6-H signal of **28** owing to its relative distance (Fig. 3).

2.2. Biological assays

2.2.1. Recombinant rat P2X3 receptors expressed in HEK cells

Newly synthesized adenine derivatives **21**–**28**, together with the precursors **17** and **19**, were tested for their biological activity on P2X3 receptors with the patch clamp recording technique. For initial screening, we used rat or human P2X3 receptors transfected into HEK 293T cells, which do not constitutively express them [26,27].

The reference P2X3 agonist α,β-meATP was applied at 100 μM concentration that was reported to elicit maximal effect at this receptor (for full dose–response curve of α,β-meATP at P2X3, see Refs. [26,28,29]; its IC_{50} value is 1.4 μM). All compounds were tested at 100 μM, unless noted, and then the most potent compounds were evaluated also at lower concentrations ranging from 100 to 0.3 μM. Fig. 4 shows the representative trace of the fast desensitizing inward current evoked by α,β-meATP from a HEK 293T cell transfected with rat P2X3 receptors. None of the tested compounds could elicit functional responses even at concentration of 100 μM, except for the rather small and slow current elicited by compound **17** (43 ± 11 pA; 6 ± 2% of control peak of 100 μM α,β-meATP, data not shown). All tested compounds exhibited antagonistic activity on P2X3 receptors, since their continuous application for 20 s blocked subsequent current responses evoked by 2 s pulse of maximal (100 μM) concentration of α,β-meATP with distinct inhibiting potencies. Such inhibition was reversible, as the peak current amplitude fully or partially recovered after 6 min wash out. Inhibition of P2X3-mediated ionic currents induced by compounds **21** and **24** is shown in Fig. 4.

Table 1 shows the calculated percent inhibition of the rat P2X3-mediated currents elicited by tested compounds. At the concentration of 100 μM, the 6-chloro intermediates **17** and **19** showed low inhibition of P2X3 current with a percentage of 27 ± 5% and 19 ± 2%, respectively. The corresponding iodo derivatives **18** and **20** were not tested due to solubility problems. In the series of 6-amino derivatives, the N9-substituted derivatives were more active than the corresponding N7-substituted analogues in all cases. In particular, at 100 μM compound **21** showed 82% inhibition versus compound **26** that showed 23% inhibition, while at 10 μM compound **22** showed higher inhibitory activity versus the corresponding N7 isomer **27** (78% versus 43% inhibition, respectively). Compound **27** was not tested at 100 μM due to solubility problems. Among these compounds the presence of an iodine atom in the benzyl chain instead of a methoxy group favoured the P2X3

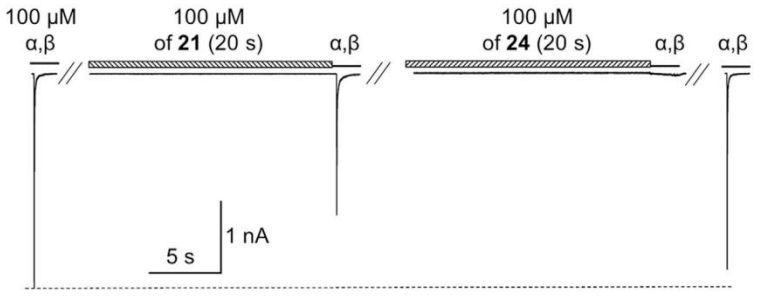

Fig. 4. Effect of **21** and **24** on rat P2X3 receptors expressed by HEK cells. Typical rapidly desensitizing inward current evoked by 100 μM α,β-meATP (α,β in the figure) was taken as control peak current (dashed line). After 20 s application of test compound **21** (100 μM; via fast superperfusion), subsequent application of 100 μM α,β-meATP induced peak current amplitude smaller than the reference one. Application of 100 μM test compound **24** exerted more potent inhibition of P2X3 activity. After 6 min wash out (time necessary for recovery from α,β-meATP-induced desensitization), the current amplitude was almost completely restored.

Table 1
Summary of antagonism activity of novel adenine derivatives.

Compound	Concentration, μM	Inhibition of P2X3 current, %
17	100	27 ± 5
19	100	19 ± 2
21	1	8 ± 4
	10	36 ± 2
	100	82 ± 2
22	0.3	23 ± 7
	1	35 ± 3
	10	78 ± 7
	100	93 ± 2
23	100	50 ± 6
24	0.3	22 ± 4
	1	41 ± 3
	10	76 ± 5
	100	98 ± 1
25	0.3	45 ± 3
	1	51 ± 3
	10	60 ± 10
	100	58 ± 6
26	100	23 ± 7
27	10	43 ± 10
28	100	71 ± 5

Effects of the novel compounds were investigated on P2X3 currents evoked by 100 μM α,β-meATP; inhibition is expressed as % amplitude of control α,β-meATP-evoked current; data are from 5 to 14 experiments.

inhibition activity (see **22**: 78% versus **21**: 82% and **24**: 98% versus **28**: 71%). Replacement in compound **22** of the 6-NH_2 group with the methoxy substituent strongly decreased the activity (compare **22** and **23** at 100 μM: 93% and 50%, respectively). On the other hand, the presence of a small alkyl group at the N^6-position gave a further enhancement of the inhibitory activity (compounds tested at 100 μM), which decreased when a more hindered cyclopentyl was introduced in the same position (at 100 μM **22**: 93% inhibition, **24**: 98% inhibition, and **25**: 58% inhibition). At lower concentration, there was a dose-dependent decrease of the inhibition; although compound **25** produced a relatively strong inhibition (45%) at submicromolar concentration, its antagonism saturated at approximately 60% despite the application of 100 μM. The N^6-methyl derivative **24**, bearing the iodobenzyl chain, resulted in the most potent P2X3 receptors inhibitor of the series with an almost complete inhibition of the full agonist evoked currents and a significant residual 22% inhibition also at the lowest tested concentration of 0.3 μM.

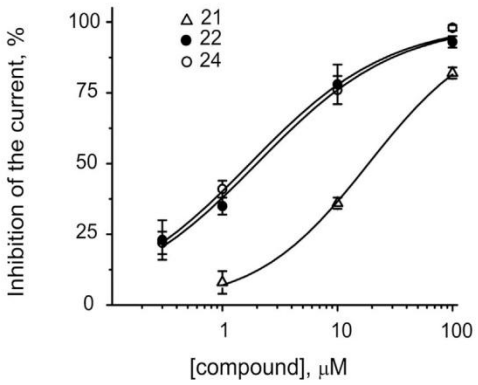

Fig. 5. Dose–inhibition curves of P2X3-mediated currents for compounds **21**, **22**, and **24** built by applying different concentrations of antagonists using the same concentration of agonist (100 μM α,β-meATP). Data points from $n = 6$–14 cells, fitted with Hill equation (Eq. (2)).

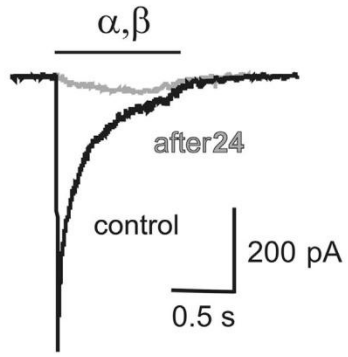

Fig. 6. Representative traces of α,β-meATP evoked P2X3 currents in control (black) and after pre-application of compound **24** (grey) from a TG neuron, superimposed. Note the almost complete suppression of the current after compound application.

Inhibition–response curves were built for the most potent compounds (**21**, **22**, and **24**) as demonstrated in Fig. 5, in which log compound concentration was plotted against the percent depression of the α,β-meATP evoked current. Fitting the data with Hill equation (Eq. (2): see experimental details) yielded for compound **22** a value of $IC_{50} = 2.23 \pm 0.29$ μM with $n_H = 0.6 \pm 0.1$, for compound **24** a value of $IC_{50} = 1.74 \pm 0.21$ μM with $n_H = 0.7 \pm 0.1$, and

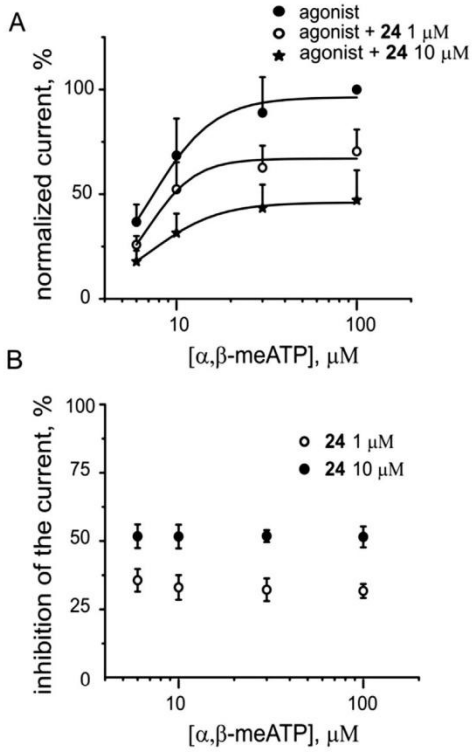

Fig. 7. A. Concentration–response curves for α,β-meATP-evoked rat P2X3 currents in control and with pre-application of increasing concentrations of compound **24** were fitted with empirical Hill equation (Eq. (2) see Experimental section). EC_{50} values for α,β-meATP were 7.2 ± 1.6 μM for control, 6.9 ± 1.0 μM in the presence of 1 μM of **24** and 7.2 ± 2.3 μM in the presence of 10 μM of **24**. B. The data from A re-plotted in terms of inhibition of currents by various concentrations of compound **24** *vs* log concentration of agonist α,β-meATP. Data presented from 5 to 17 cells.

for compound **21** $IC_{50} = 18.6 \pm 0.9$ μM with $n_H = 0.9 \pm 0.1$ ($n = 6$–14 cells, Table 1).

2.2.2. Recombinant human P2X3 receptors

We next enquired if human P2X3 receptors transiently expressed by HEK cells were equi-sensitive to the novel antagonist compound **24** (that was most effective on rat receptors). Human P2X3 currents induced by 100 μM α,β-meATP were almost completely blocked by 20 s pre-application of compound **24** (100 μM). We also tested if compound **24** could block the α,β-meATP current even at the concentrations of 1 μM and 10 μM. Indeed, the percent inhibition of human P2X3 receptor activity was 29 ± 2% (compared with the one of rat P2X3 receptor: 40 ± 3%, $n = 5$), thus, slightly less intense than the blocking action on rodent receptors. Fitting inhibition–response curve with Hill equation yielded for compound **24** a value of $IC_{50} = 2.2 \pm 0.1$ μM with $n_H = 1.1 \pm 0.1$ ($n = 2$–5 cells).

2.2.3. Native receptors in trigeminal ganglion neurons

Since 100 μM of compound **24** produced the strongest inhibition of P2X3 receptors expressed by HEK cells, it was important to test the sensitivity of native P2X3 receptors expressed by TG sensory neurons in culture. Fig. 6 shows an example of α,β-meATP-evoked inward current recorded from a TG neuron and its near-full inhibition by compound **24** (100 μM). At 1 μM the percent inhibition of the current was 37 ± 3% ($n = 7$), hence compound **24** had similar antagonistic potency on recombinant and native P2X3 receptors.

To assess the nature of the mechanism antagonist–receptor interaction, we tested how efficiently compound **24** at different concentrations inhibited the P2X3 currents evoked by different concentrations of the agonist α,β-meATP. As the level of inhibition was similar for the wide range of agonist concentration (low and high concentrations, see Fig. 7), we hypothesize that compound **24** behaves as non-competitive antagonist. However, we cannot exclude that the nature of antagonism is of a mixed type.

3. Conclusions

This study was aimed at testing the adenine moiety as possible new scaffold for the development of P2X3 antagonists. The designed series of 2-aminoadenine derivatives was synthesized and tested on recombinant rat P2X3 receptors expressed in HEK cells, by using patch clamp recording technique. The novel compounds showed to behave as P2X3 receptor antagonists, the N9-isomers being more active than the corresponding N7 analogues. Introduction at the 6-amino group of a small lipophilic substituent increased the potency at least in the series containing the iodo atom within the substituted benzyl chain, resulting in the 9-(5-iodo-2-isopropyl-4-methoxybenzyl)-N^6-methyl-9*H*-purine-2,6-diamine (**24**), which is the most active compound of the presented derivatives (at 100 μM) and appears to be a good antagonist on recombinant and native P2X3 receptors with IC_{50} in the low μM range.

The effect of the introduction of a methyl group in N^6-position was an increase of activity respect to the corresponding unsubstituted compound (at 100 μM; **22**: 93% activity *vs* **24**: 98% activity).

In conclusion, biological results show that the synthesised adenine-based compounds possess antagonist activity at P2X3 receptors, even if with lower potency respect to the corresponding diaminopyrimidines taken as reference compounds. These results are encouraging as the versatility of the adenine scaffold allows the insertion of different substituents in several position of the purine moiety itself. The investigation on the effect of these modifications on P2X3 receptor antagonist activity could help for the development of new agents for the treatment of neuropathic pain, migraine, and inflammatory pain.

4. Experimental section

4.1. Molecular modelling

All molecular modelling studies were performed on a 2 CPU (PIV 2.0–3.0 GHz) Linux PC. Rebuilding of analysed compound structures was carried out using Molecular Operating Environment (MOE, version 2010.10) suite [30]. All ligand structures were optimized using RHF/AM1 semiempirical calculations and the software package MOPAC [31] implemented in MOE was utilized for these calculations. Superimposition of molecules was performed by using the Flexible Alignment tool of MOE.

4.2. Chemistry

Melting points were determined with a Büchi apparatus B-540. ^{1}H NMR spectra were obtained with Varian Mercury 400 MHz spectrometer; δ in ppm, J in Hz. All exchangeable protons were confirmed by addition of D_2O. Thin-layer chromatography (TLC) was carried out on pre-coated TLC plates with silica gel 60 F-254 (Merck) and preparative thin-layer chromatography (PTLC) on pre-coated plates with silica gel 60 Å Analtech. For column chromatography, silica gel 60 (Merck) was used. Mass spectra were recorded on an HP 1100-MSD series instrument. All measurements were performed using electrospray ionization (ESI-MS) on a single quadrupole analyzer. Elemental analyses were determined on a Fisons model EA 1108 CHNS–O model analyser and are within ±0.4% of theoretical values. Purity of the compounds was ≥95% according to elemental analysis data. See the Supporting information for further information.

4.3. General procedure for the preparation of compounds *17*–*20*

K_2CO_3 (0.452 g, 3.27 mmol) was added to stirred solution of mesyl compound **6** or **15** (2.73 mmol) in dry DMF (12 mL). 2-Amino-6-chloropurine (**16**) (0.506 g, 2.73 mmol) and 18-crown-6 (1 mg) were added after 5 min and reaction was left at 65 °C for 12 h. Then reaction mixture was partitioned between EtOAc and water. The combined organics were washed with saturated solution of $NaHCO_3$ and brine, and then they were dried over Na_2SO_4, concentrated under reduced pressure and the residue was chromatographed over flash silica gel column using the appropriate eluent to obtain compounds **17**–**20** as white solids.

*4.3.1. 6-Chloro-9-(2-isopropyl-4,5-dimethoxybenzyl)-9H-purin-2-amine (**17**) and 6-chloro-7-(2-isopropyl-4,5-dimethoxybenzyl)-7H-purin-2-amine (**19**)*

Compounds **17** and **19** were obtained from **6** after flash silica gel column chromatography eluting with $CHCl_3$–MeOH (99.75:0.25–97:3, v/v) as white solids. **17**: Yield 51%; mp 161–163 °C. ^{1}H NMR (DMSO-d_6): δ 1.02 (d, 6H, J = 6.8 Hz, $CH(CH_3)_2$), 3.19 (sept, 1H, J = 6.8 Hz, $CH(CH_3)_2$), 3.68 (s, 3H, OCH_3), 3.74 (s, 3H, OCH_3), 5.19 (s, 2H, NCH_2), 6.84 (s, 1H, H–Ph), 6.91 (s, 1H, H–Ph), 6.93 (brs, 2H, NH_2), 7.95 (s, 1H, H-8). **19**: Yield 35%; mp 193–195 °C. ^{1}H NMR (DMSO-d_6): δ 1.12 (d, 6H, J = 6.8 Hz, $CH(CH_3)_2$), 3.13 (sept, 1H, J = 6.8 Hz, $CH(CH_3)_2$), 3.52 (s, 3H, OCH_3), 3.76 (s, 3H, OCH_3), 5.51 (s, 2H, NCH_2), 6.33 (s, 1H, H–Ph), 6.67 (brs, 2H, NH_2), 6.90 (s, 1H, H–Ph), 8.12 (s, 1H, H-8).

*4.3.2. 6-Chloro-9-(5-iodo-2-isopropyl-4-methoxybenzyl)-9H-purin-2-amine (**18**) and 6-chloro-7-(5-iodo-2-isopropyl-4-methoxybenzyl)-7H-purin-2-amine (**20**)*

Compounds **18** and **20** were obtained from **15** after flash chromatography eluting with CH_2Cl_2–MeCN (98:2, v/v) as white solids. **18**: Yield 52%; mp 120–122 °C. ^{1}H NMR (DMSO-d_6): δ 1.08 (d, 6H, J = 6.8 Hz, CH(CH_3)$_2$), 3.20 (sept, 1H, J = 6.8 Hz, CH(CH_3)$_2$), 3.82 (s, 3H, OCH_3), 5.20 (s, 2H, NCH_2), 6.89 (s, 1H, H–Ph), 6.95 (s, 2H, NH_2), 7.47 (s, 1H, H–Ph), 7.99 (s, 1H, H-8); and CH_2Cl_2–MeCN (96:04, v/v). **20**: Yield 12%; mp 140–142 °C. ^{1}H NMR (DMSO-d_6): δ 1.18 (d, 6H, J = 6.8 Hz, CH(CH_3)$_2$), 3.10 (sept, 1H, J = 6.8 Hz, CH(CH_3)$_2$), 3.83 (s, 3H, OCH_3), 5.52 (s, 2H, NCH_2), 6.71 (brs, 2H, NH_2), 6.88 (s, 1H, H–Ph), 6.94 (s, 1H, H–Ph), 8.27 (s, 1H, H-8).

*4.4. General procedure for the preparation of compounds **21** and **22***

Ammonia gas was condensed at −70 °C in cooled steel vial then starting material **17** or **18** was added and reaction mixture was maintained at room temperature for 16 h. Volatiles were removed and crude mixture was partitioned between EtOAC and H_2O. Then combined organics were washed with saturated solution of NH_4Cl, dried over Na_2SO_4 and concentrated under reduced pressure to obtain crude product **21** or **22**, respectively.

*4.4.1. 9-(2-Isopropyl-4,5-dimethoxybenzyl)-9H-purine-2,6-diamine (**21**)*

Compound **21** was obtained from **17** after crystallization from MeOH, as white solid. Yield 54%; mp 198–200 °C. ^{1}H NMR (DMSO-d_6): δ 1.03 (d, 6H, J = 6.4 Hz, CH(CH_3)$_2$), 3.18 (sept, J = 6.4 Hz, 1H, CH(CH_3)$_2$), 3.66 (s, 3H, OCH_3), 3.74 (s, 3H, OCH_3), 5.08 (s, 2H, NCH_2), 5.78 (brs, 2H, NH_2), 6.64 (brs, 2H, NH_2), 6.84 (s, 1H, H–Ph), 6.89 (s, 1H, H–Ph), 7.46 (s, 1H, H-8); ESI-MS: positive mode m/z 343.1 ([M + H]$^+$), 365.1 ([M + Na]$^+$).

*4.4.2. 9-(5-Iodo-2-isopropyl-4-methoxybenzyl)-9H-purine-2,6-di amine (**22**)*

Compound **22** was obtained from **18** after flash silica gel column chromatography eluting with $CHCl_3$–MeOH (98:2–95:5, v/v) as white solids. Yield 40%; mp 230–232 °C. ^{1}H NMR (DMSO-d_6): δ 1.14 (d, 6H, J = 6.8 Hz, CH(CH_3)$_2$), 3.09 (sept, 1H, J = 6.8 Hz, CH(CH_3)$_2$), 3.82 (s, 3H, OCH_3), 5.46 (s, 2H, NCH_2), 5.55 (s, 2H, NH_2), 6.29 (s, 2H, NH_2), 6.91 (s, 1H, H–Ph), 7.65 (s, 1H, H-8), 7.08 (s, 1H, H–Ph); ESI-MS: positive mode m/z 439.0 ([M + H]$^+$), 461.0 ([M + Na]$^+$), 477.0 ([M + K]$^+$).

*4.4.3. 9-(5-Iodo-2-isopropyl-4-methoxybenzyl)-6-methoxy-9H-purin-2-amine (**23**)*

A suspension of **18** (50 mg, 0.10 mmol) and sodium methoxide (53 mg, 0.98 mmol) in dry CH_3OH (2 mL) was refluxed for 2 h. Then solvent was evaporated and the resulted residue was extracted with EtOAc and water. Combined organics were washed with saturated NH_4Cl solution, dried over anhydrous Na_2SO_4, and evaporated to dryness. The crude was crystallized from MeCN to give **23** as white solid. Yield 69%; mp 212–214 °C. ^{1}H NMR (DMSO-d_6): δ 1.08 (d, 6H, J = 6.8 Hz, CH(CH_3)$_2$), 3.21 (sept, 1H, J = 6.8 Hz, CH(CH_3)$_2$), 3.81 (s, 3H, OCH_3), 3.95 (s, 3H, OCH_3), 5.17 (s, 2H, NCH_2), 6.43 (s, 2H, NH_2), 6.89 (s, 1H, H–Ph), 7.37 (s, 1H, H–Ph), 7.71 (s, 1H, H-8); ESI-MS: positive mode m/z 454.0 ([M + H]$^+$), 492.0 ([M + K]$^+$), 929.0 ([2M + Na]$^+$).

*4.4.4. 9-(5-Iodo-2-isopropyl-4-methoxybenzyl)-N^6-methyl-9H-purine-2,6-diamine (**24**)*

To a suspension of **18** (50 mg, 0.10 mmol) in dry THF (2 mL) was added methylamine (1.5 mL, 33.80 mmol) at −20 °C and reaction mixture was left for 3 h at room temperature, then solvent was evaporated and the resulting residue was extracted with EtOAc. The combined organics were washed with water, dried over anhydrous Na_2SO_4, concentrated and the crude was crystallized from MeCN to give **24** as white solid. Yield 76%; mp 238–240 °C. ^{1}H NMR (DMSO-d_6): δ 1.09 (d, 6H, J = 6.8 Hz, CH(CH_3)$_2$), 2.86 (s, 3H, NHCH$_3$), 3.20 (sept, 1H, J = 7.2 Hz, CH(CH_3)$_2$), 3.81 (s, 3H, OCH_3), 5.10 (s, 2H, NCH_2), 5.85 (s, 2H, NH_2), 6.88 (s, 1H, H–Ph), 7.21 (s, 1H, NHCH$_3$), 7.37 (s, 1H, H–Ph), 7.50 (s, 1H, H-8); ESI-MS: positive mode m/z 453.0 ([M + H]$^+$), 475.0 ([M + Na]$^+$).

*4.4.5. N^6-Cyclopentyl-9-(5-iodo-2-isopropyl-4-methoxybenzyl)-9H-purine-2,6-diamine (**25**)*

A suspension of **18** (0.050 g, 0.10 mmol) and cyclopentylamine (1.02 mL, 10.40 mmol) in dry THF (2 mL) was stirred for 30 h at 60 °C. Then solvent was evaporated and the resulted residue was extracted with EtOAc. The combined organics were washed with water, dried over anhydrous Na_2SO_4, evaporated under vacuo and the crude was chromatographed over flash silica gel column eluting with $CHCl_3$–MeCN (98:2, v/v) to give **25** as white solid. Yield 69%; mp 182–184 °C. ^{1}H NMR (DMSO-d_6): δ 1.09 (d, 6H, J = 6.8 Hz, CH(CH_3)$_2$), 1.50 (m, 4H, *H*-cyclopentyl), 1.68 (m, 2H, H-cyclopentyl), 1.88 (m, 2H, *H*-cyclopentyl), 3.20 (sept, 1H, J = 6.8 Hz, CH(CH_3)$_2$), 3.81 (s, 3H, OCH_3), 4.44 (m, 1H, NHCH), 5.10 (s, 2H, NCH_2), 5.80 (brs, 2H, NH_2), 6.88 (s, 1H, H–Ph), 7.06 (brs, 1H, NH), 7.38 (s, 1H, H–Ph), 7.51 (s, 1H, H-8); ESI-MS: positive mode m/z 507.1 ([M + H]$^+$), 529.0 ([M + Na]$^+$).

*4.5. General procedure for the preparation of compounds (**26** and **27**)*

Ammonia gas was condensed at −70 °C in steel vial then starting material **19** or **20** was added and reaction mixture maintained at 100 °C for 16 h in well packed steel vial. Volatiles were removed and the residue was partitioned between EtOAC and H_2O; the combined organics were washed with saturated solution of NH_4Cl, dried over the Na_2SO_4 and concentrated under reduced pressure. The residue was purified by flash column chromatography.

*4.5.1. 7-(2-Isopropyl-4,5-dimethoxybenzyl)-7H-purine-2,6-diamine (**26**)*

Compound **26** was obtained from **19** after flash silica gel column chromatography eluting with $CHCl_3$–MeOH (98:2–92:8, v/v) as white solid. Yield 24%; mp 245–247 °C. ^{1}H NMR (DMSO-d_6): δ 1.09 (d, 6H, J = 6.8 Hz, CH(CH_3)$_2$), 3.03 (sept, 1H, J = 6.8 Hz, CH(CH_3)$_2$), 3.57 (s, 3H, OCH_3), 3.75 (s, 3H, OCH_3), 5.42 (s, 1H, NCH_2), 5.51 (brs, 2H, NH_2), 6.32 (brs, 2H, NH_2), 6.57 (s, 1H, H–Ph), 6.89 (s, 1H, H–Ph), 7.51 (s, 1H, H-8); ESI-MS: positive mode m/z 343.1 ([M + H]$^+$), 685.3 ([2M + H]$^+$), 707.3 ([2M + Na]$^+$).

*4.5.2. 7-(5-Iodo-2-isopropyl-4-methoxybenzyl)-7H-purine-2,6-diamine (**27**)*

Compound **27** was obtained from **20** after flash silica gel column chromatography eluting with $CHCl_3$–MeOH (98:2–95:5, v/v) as white solid. Yield 40%; mp 240–242 °C. ^{1}H NMR (DMSO-d_6): δ 1.14 (d, 6H, J = 6.8 Hz, CH(CH_3)$_2$), 3.09 (sept, 1H, J = 6.8 Hz, CH(CH_3)$_2$), 3.82 (s, 3H, OCH_3), 5.46 (s, 2H, NCH_2), 5.55 (s, 2H, NH_2), 6.29 (s, 2H, NH_2), 6.91 (s, 1H, H–Ph), 7.08 (s, 1H, H–Ph), 7.65 (s, 1H, H-8); ESI-MS: positive mode m/z 439.0 ([M + H]$^+$), 877.2 ([2M + H]$^+$), 899.0 ([2M + Na]$^+$), 915.0 ([2M + K]$^+$).

*4.6. General procedure for the preparation of compounds (**28** and **29**)*

To compound **17** or **19** (0.22 mmol), taken in steel vessel at −70 °C, methylamine (1.0 mL) was added. The reaction was left for 1 day at room temperature, volatiles were then removed and the crude mixture was purified by silica gel flash column chromatography eluting with the suitable solvent.

*4.6.1. 9-(2-Isopropyl-4,5-dimethoxybenzyl)-N^6-methyl-9H-purine-2,6-diamine (**28**)*

Compound **28** was obtained from **17** after flash silica gel column chromatography eluting with CH_2Cl_2–CH_3OH (97:3, v/v) as white solid. Yield 40%; mp 188–190 °C. ^{1}H NMR (DMSO-d_6): δ 1.02 (d, 6H, J = 7.2 Hz, CH(CH_3)$_2$); 2.85 (br m, 3H, NHCH_3), 3.18 (m, 1H, CH(CH_3)$_2$), 3.65 (s, 3H, OCH_3); 3.73 (s, 3H, OCH_3); 5.08 (s, 2H, CH_2); 5.84 (brs, 2H, NH_2); 6.83 (s, 1H, H–Ph); 6.88 (s, 1H, H–Ph); 7.15 (brs, 1H, NH); 7.44 (s, 1H, H-8); ESI-MS: positive mode m/z 357.4 ([M + H]$^+$), 379.5 ([M + Na]$^+$), 735.8 ([2M + Na]$^+$).

*4.6.2. 7-(2-Isopropyl-4,5-dimethoxybenzyl)-N^6-methyl-7H-purine-2,6-diamine (**29**)*

Compound **29** was obtained from **19** after silica gel flash column chromatography eluting with CH_2Cl_2–CH_3OH (95:5, v/v) as white solid. Yield 33%; mp 254–256 °C. ^{1}H NMR (DMSO-d_6): δ 1.09 (d, 6H, J = 6.8 Hz, CH(CH_3)$_2$); 2.86 (d, 3H, J = 4.4 Hz, NHCH_3), 3.01 (sept, 1H, J = 6.8 Hz, CH(CH_3)$_2$), 3.59 (s, 3H, OCH_3), 3.76 (s, 3H, OCH_3), 5.42 (s, 2H, CH_2), 5.63 (brs, 2H, NH_2), 6.46 (bs, 1H, $NH$$CH_3$), 6.65 (s, 1H, H–Ph), 6.89 (s, 1H, H–Ph), 7.38 (s, 1H, H-8); ESI-MS: positive mode m/z 357.2 ([M + H]$^+$), 713.5 ([2M + H]$^+$), 735.5 ([2M + Na]$^+$).

4.7. Biological assay

4.7.1. Recombinant P2X3 receptors

Experiments were performed in accordance with our recent reports [22,32]. In brief, HEK 293T cells, supplied by the in-house SISSA bank, were cultured in Dulbecco's Modified Eagle Medium (DMEM) supplemented with 10% foetal bovine serum (FBS), Glutamax and antibiotics in an incubator (5% CO_2/95% humidity, 37 °C). Cells were placed on poly-L-lysine coated 35 mm Petri dishes and transiently transfected by the calcium phosphate technique with pEGFP (Clontech, Mountain View, CA) and pcDNA3-P2X3 plasmids (0.5 μg/mL each; 1:1 ratio). Rat and human pcDNA3-P2X3 constructs (NCBI accession numbers CAA62594 and AAH74793, respectively) were kindly provided by Prof. R.A. North (University of Manchester, UK). Twenty four or 48 h later transfected cells were used for experiments, because P2X3 expression was found to be comparable at these time points, probed by immunofluorescence and western blotting.

4.7.2. Trigeminal ganglia culture neurons

Cultures of trigeminal ganglion sensory neurons were prepared from C57Bl/6 wild type mice (P10–14) as previously described [33]. In brief, trigeminal ganglia were rapidly excised and enzymatically dissociated in F12 medium (Invitrogen Corp, Milan, Italy) containing 0.25 mg/mL trypsin, 1 mg/mL collagenase, 0.2 mL DNAse (Sigma, Milan, Italy) at 37 °C for 12 min. Cells were plated on poly-L-lysine coated 35 mm Petri dishes on F12 medium supplemented with 10% foetal bovine serum and antibiotics and incubated for 24 h (5% CO_2/95% humidity, 37 °C).

4.7.3. Patch clamp recordings

Currents were recorded from small/medium size mouse TG neurons (nociceptors that strongly express native P2X3 receptors [33]) or single GFP-positive (visualized by fluorescent microscopy) HEK cells as previously described [32,33] under whole cell voltage clamp mode at a holding potential of −60 mV. Cells were continuously superfused at room temperature with control solution containing (in mM): 152 NaCl, 5 KCl, 1 $MgCl_2$, 2 $CaCl_2$, 10 glucose, 10 HEPES; pH 7.4 adjusted with NaOH. Patch pipettes had a resistance of 3–4 MΩ when filled with (in mM): 140 KCl, 2 $MgCl_2$, 0.5 $CaCl_2$, 2 ATP–Mg, 2 GTP–Li, 20 HEPES, 5 EGTA; pH 7.2 adjusted with KOH (for recordings from TG neurons) and 130 CsCl, 20 HEPES, 1 $MgCl_2$, 3 ATP–Mg, EGTA 5, pH 7.2 adjusted with CsOH (for HEK cells). Data were acquired and analysed with the pCLAMP software Clampex 9.2 (Molecular Devices, Palo Alto, CA, USA). After obtaining whole cell configuration, cell slow capacitance was compensated. Access resistance was never >10 MΩ and was routinely compensated by at least 70%.

4.7.4. Drug application and data analysis

The receptor agonists α,β-meATP (Sigma) and test compounds were applied by rapid solution changer system (Perfusion Fast-Step System SF-77B, Warner Instruments, Hamden, CT, USA). Unless otherwise stated, α,β-meATP was applied at 100 μM concentration that is known to produce a maximal inward current response [26,28,29]. Membrane currents were analysed in terms of their peak amplitude and rise time (10–90% of the peak). Current decay due to receptor desensitization during agonist application was fitted with either a monoexponential or biexponential function using pCLAMP Clampfit 9.2.

Test compounds were kept at +4 °C and dissolved to 10 mM in DMSO or DMSO–H_2O (1:1) or DMSO–HCl (18% 1 N) before experiments and then diluted to necessary concentration in control solution. For routine tests, α,β-meATP was applied at 100 μM concentration (2 s pulse) at least 3 times (at 5 min interval to prevent cumulative receptor desensitization) to obtain an average control response. Since activated P2X3 receptors desensitize rapidly in the sustained presence of agonist, the inward current transient is, of course, too short for the binding equilibrium to be reached when agonist and antagonist are co-applied. Thus, to assess potential receptor blocking activity, each test compound was continuously pre-applied for 20 s before the α,β-meATP application as done previously [22,28]. Antagonist activity was quantified as percent inhibition of the α,β-meATP-induced current:

$$\%\ \text{inhibition} = 100 \times (1 - I_2/I_1), \quad (1)$$

where I_1 is the control peak current, I_2 is the peak amplitude of the current after test compound.

For the most potent compounds, antagonist dose–inhibition curves were constructed by applying for 20 s different concentrations of each test compound using the same maximal concentration (100 μM) of α,β-meATP agonist. Data were plotted and fitted with empirical Hill equation using Origin 6.0 (Microcal, Northampton, MA, USA):

$$\%\ \text{inhibition} = 100/\left(1 + (IC_{50}/[\text{Ant}])^{n_H}\right), \quad (2)$$

where [Ant] is the concentration of the antagonist, n_H is the Hill coefficient, IC_{50} is the concentration of antagonist required to block the maximal current by 50%. Agonist concentration–response curves in terms of normalized currents *vs* log agonist concentration were fitted with the same Hill equation, with corresponding parameters EC_{50} and n_H, where EC_{50} is the concentration of agonist required to produce the half-maximal current. All data are presented as mean ± standard error of the mean (S.E.); n is the number of cells. Statistical significance was evaluated with paired Student's t-test (for parametric data) or Mann–Whitney rank sum test (for nonparametric data), $p < 0.05$ was considered statistically significant.

Acknowledgements

This work was supported by Fondo di Ricerca di Ateneo (University of Camerino). We thank Elena Sokolova for preliminary experiments on biological assay. The financial support of Telethon Foundation – Italy (Grant no. GGP10082) and of Cariplo Foundation to A. N. is gratefully acknowledged.

Appendix A. Supporting information

Supporting information related to this article can be found at http://dx.doi.org/10.1016/j.ejmech.2013.04.037.

References

[1] G. Burnstock, Purinergic mechanosensory transduction and visceral pain, Mol. Pain 5 (2009) 69.
[2] G. Burnstock, Purinergic signalling and disorders of the central nervous system, Nat. Rev. Drug Discov. 7 (2008) 575–590.
[3] T. Nakatsuka, J.G. Gu, P2X purinoceptors and sensory transmission, Pflügers Arch. 452 (2006) 598–607.
[4] C.C. Chen, A.N. Akopian, L. Sivilotti, D. Colquhoun, G. Burnstock, J.N. Wood, A P2X purinoceptor expressed by a subset of sensory neurons, Nature 377 (1995) 428–431.
[5] C. Lewis, S. Neidhart, C. Holy, R.A. North, G. Buell, A. Surprenant, Coexpression of P2X2 and P2X3 receptor subunits can account for ATP-gated currents in sensory neurons, Nature 377 (1995) 432–435.
[6] E.J. Bradbury, G. Burnstock, S.B. McMahon, The expression of P2X3 purinoreceptors in sensory neurons: effects of axotomy and glial-derived neurotrophic factor, Mol. Cell. Neurosci. 12 (1998) 256–268.
[7] B.A. Chizh, P. Illes, P2X receptors and nociception, Pharmacol. Rev. 53 (2001) 553–568.
[8] V. Souslova, P. Cesare, Y. Ding, A.N. Akopian, L. Stanfa, R. Suzuki, K. Carpenter, A. Dickenson, S. Boyce, R. Hill, D. Nebenuis-Oosthuizen, A.J. Smith, E.J. Kidd, J.N. Wood, Warm-coding deficits and aberrant inflammatory pain in mice lacking P2X3 receptors, Nature 407 (2000) 1015–1017.
[9] D.A. Cockayne, S.G. Hamilton, Q.M. Zhu, P.M. Dunn, Y. Zhong, S. Novakovic, A.B. Malmberg, G. Cain, A. Berson, L. Kassotakis, L. Hedley, W.G. Lachnit, G. Burnstock, S.B. McMahon, A.P. Ford, Urinary bladder hyporeflexia and reduced pain-related behaviour in P2X3-deficient mice, Nature 407 (2000) 1011–1015.
[10] X. Bian, J. Ren, M. DeVries, B. Schnegelsberg, D.A. Cockayne, A.P. Ford, J.J. Galligan, Peristalsis is impaired in the small intestine of mice lacking the P2X3 subunit, J. Physiol. 551 (2003) 309–322.
[11] M.F. Jarvis, Contributions of P2X3 homomeric and heteromeric channels to acute and chronic pain, Expert Opin. Ther. Targets 7 (2003) 513–522.
[12] K.J. Lynch, E. Touma, W. Niforatos, K.L. Kage, E.C. Burgard, T. van Biesen, E.A. Kowaluk, M.F. Jarvis, Molecular and functional characterization of human P2X(2) receptors, Mol. Pharmacol. 56 (1999) 1171–1181.
[13] B.R. Bianchi, K.J. Lynch, E. Touma, W. Niforatos, E.C. Burgard, K.M. Alexander, H.S. Park, H. Yu, R. Metzger, E. Kowaluk, M.F. Jarvis, T. van Biesen, Pharmacological characterization of recombinant human and rat P2X receptor subtypes, Eur. J. Pharmacol. 376 (1999) 127–138.
[14] M.F. Jarvis, B.S. Khakh, ATP-gated P2X cation-channels, Neuropharmacology 56 (2009) 208–215.
[15] J.D. Brederson, M.F. Jarvis, Homomeric and heteromeric P2X3 receptors in peripheral sensory neurons, Curr. Opin. Investig. Drugs 9 (2008) 716–725.
[16] K. Wirkner, B. Sperlagh, P. Illes, P2X(3) receptor involvement in pain states, Mol. Neurobiol. 36 (2007) 165–183.
[17] E.C. Burgard, W. Niforatos, T. van Biesen, K.J. Lynch, K.L. Kage, E. Touma, E.A. Kowaluk, M.F. Jarvis, Competitive antagonism of recombinant P2X(2/3) receptors by 2′,3′-*O*-(2,4,6-trinitrophenyl) adenosine 5′-triphosphate (TNP-ATP), Mol. Pharmacol. 58 (2000) 1502–1510.
[18] M.F. Jarvis, E.C. Burgard, S. McGaraughty, P. Honore, K. Lynch, T.J. Brennan, A. Subieta, T. Van Biesen, J. Cartmell, B. Bianchi, W. Niforatos, K. Kage, H. Yu, J. Mikusa, C.T. Wismer, C.Z. Zhu, K. Chu, C.H. Lee, A.O. Stewart, J. Polakowski, B.F. Cox, E. Kowaluk, M. Williams, J. Sullivan, C. Faltynek, A-317491, a novel potent and selective non-nucleotide antagonist of P2X3 and P2X2/3 receptors, reduces chronic inflammatory and neuropathic pain in the rat, Proc. Natl. Acad. Sci. U. S. A. 99 (2002) 17179–17184.
[19] C.E. Muller, Emerging structures and ligands for P2X(3) and P2X(4) receptors-towards novel treatments of neuropathic pain, Purinergic Signal. 6 (2010) 145–148.
[20] D. Carter, M.P. Dillon, R.C. Hawley, C.J.J. Lin, D.W. Parish, C.A. Broka, A. Jahangir, Diaminopyrimidines as P2X3 and P2X2/3 Antagonists, WO 2005/095359 A1, 2005.
[21] A.P. Ford, J.R. Gever, P.A. Nunn, Y. Zhong, J.S. Cefalu, M.P. Dillon, D.A. Cockayne, Purinoceptors as therapeutic targets for lower urinary tract dysfunction, Br. J. Pharmacol. 147 (Suppl. 2) (2006) S132–S143.
[22] R. Volpini, R.C. Mishra, D.D. Kachare, D. Dal Ben, C. Lambertucci, I. Antonini, S. Vittori, G. Marucci, E. Sokolova, A. Nistri, G. Cristalli, Adenine-based acyclic nucleotides as novel $P2X_3$ receptor ligands, J. Med. Chem. 52 (2009) 4596–4603.
[23] S. Calimsiz, M.G. Organ, Negishi cross-coupling of secondary alkylzinc halides with aryl/heteroaryl halides using Pd-PEPPSI-IPent, Chem. Commun. (Camb.) 47 (2011) 5181–5183.
[24] C. Lambertucci, I. Antonini, M. Buccioni, D. Dal Ben, D.D. Kachare, R. Volpini, K.N. Klotz, G. Cristalli, 8-Bromo-9-alkyl adenine derivatives as tools for developing new adenosine A_{2A} and A_{2B} receptors ligands, Bioorg. Med. Chem. 17 (2009) 2812–2822.
[25] G. Langli, L.-L. Gundersen, F. Rise, Regiochemistry in Stille couplings of 2,6-dihalopurines, Tetrahedron 52 (1996) 5625–5638.
[26] E. Fabbretti, E. Sokolova, L. Masten, M. D'Arco, A. Fabbro, A. Nistri, R. Giniatullin, Identification of negative residues in the P2X3 ATP receptor ectodomain as structural determinants for desensitization and the Ca^{2+}-sensing modulatory sites, J. Biol. Chem. 279 (2004) 53109–53115.
[27] D.A. Brown, D.I. Yule, Protein kinase C regulation of P2X3 receptors is unlikely to involve direct receptor phosphorylation, Biochim. Biophys. Acta 1773 (2007) 166–175.
[28] E. Sokolova, A. Skorinkin, E. Fabbretti, L. Masten, A. Nistri, R. Giniatullin, Agonist-dependence of recovery from desensitization of P2X(3) receptors provides a novel and sensitive approach for their rapid up or downregulation, Br. J. Pharmacol. 141 (2004) 1048–1058.
[29] E. Sokolova, A. Skorinkin, I. Moiseev, A. Agrachev, A. Nistri, R. Giniatullin, Experimental and modeling studies of desensitization of P2X3 receptors, Mol. Pharmacol. 70 (2006) 373–382.
[30] Molecular Operating Environment, C.C.G., Inc., 1255 University St., Suite 1600, Montreal, Quebec, Canada H3B 3X3.
[31] J.J. Stewart, MOPAC: a semiempirical molecular orbital program, J. Comput. Aided Mol. Des. 4 (1990) 1–105.
[32] M. Sundukova, S. Vilotti, R. Abbate, E. Fabbretti, A. Nistri, Functional differences between ATP-gated human and rat P2X3 receptors are caused by critical residues of the intracellular C-terminal domain, J. Neurochem. 122 (2012) 557–567.
[33] M. Simonetti, A. Fabbro, M. D'Arco, M. Zweyer, A. Nistri, R. Giniatullin, E. Fabbretti, Comparison of P2X and TRPV1 receptors in ganglia or primary culture of trigeminal neurons and their modulation by NGF or serotonin, Mol. Pain 2 (2006) 11.

6. Ribose blocked ATP derivatives as new potent antagonists for the purinergic P2X3 receptors

Ribose blocked ATP derivatives as new potent antagonists for the purinergic P2X3 receptors

Diego Dal Ben[a], Anna Marchenkova[b], Ajiroghene Thomas[a], Catia Lambertucci[a], Andrea Spinaci[a], Gabriella Marucci[a], Andrea Nistri[b], Rosaria Volpini[a,*].

[a]School of Pharmacy, Medicinal Chemistry Unit, University of Camerino, via S. Agostino 1, 62032 Camerino (MC), Italy.

[b]Sector of Neurobiology and Italian Institute of Technology Unit, International School for Advanced Studies (SISSA), Via Bonomea 265, 34014 Trieste, Italy.

*Corresponding Author:

Prof. Rosaria Volpini

School of Pharmacy, Medicinal Chemistry Unit

University of Camerino

via S. Agostino, 1

62032 Camerino (MC), Italy

Tel: +39-0737-402278

Fax: +39-0737-402295

E-mail: rosaria.volpini@unicam.it

Abstract

Blocking membrane currents evoked by the activation of purinergic P2X3 receptors localized on nociceptive neurons represents a promising strategy for the development of drugs useful for the treatment of chronic pain conditions. 2',3'-*O*-(2,4,6-trinitrophenyl)-ATP (TNP-ATP) is an ATP analogue whose inhibitory activity on P2X receptors has been previously reported. On the basis of the results of molecular modeling studies performed with homology models of the P2X3 receptor, novel adenosine nucleotide analogues bearing cycloalkyl or arylalkyl substituents replacing the trinitrophenyl moiety of TNP-ATP

were designed and synthesized. These new compounds were functionally evaluated on native P2X3 receptors from mouse trigeminal ganglion (TG) sensory neurons using patch clamp recording under voltage clamp configuration. Our data show that some of these molecules are potent (nanomolar range) and reversible inhibitors of P2X3 receptors, with strong selectivity because membrane currents evoked by GABA or 5-HT were unaffected.

Keywords

Purinergic receptors; P2X3 receptor; P2X3 receptor antagonists; ATP derivatives; purine derivatives; ATP; purine; patch clamp; molecular modelling; docking.

1. Introduction

Extracellular adenosine-5′-triphosphate (ATP, **1**, Figure 1) is a key signalling molecule released from healthy or damaged cells and acting through the activation of two different classes of purinergic receptor: the G-protein-coupled P2Y receptors (eight subtypes discovered and cloned to date) and the ionotropic P2X receptors [1-5]. P2X receptors are ion channels assembling as homo- or heterotrimers from seven cloned subunits (P2X1-7) [6,7]. All P2X subunits share a common topology presenting intracellular N- and C- termini, two transmembrane domains (TM1 and TM2), and a large glycosylated and cysteine-rich extracellular domain [8-10]. Binding of ATP to P2X receptors leads to a large conformational change with opening of the transmembrane pore to allow the flow of cations like Na^+, K^+, and Ca^{2+} leading to the depolarization of the cell and action potential signalling [11,12]. The activation process may be followed by receptor desensitization: P2X2, P2X4, and P2X7 receptors show slow desensitization, while P2X1 and P2X3 receptors rapidly desensitize [13]. P2X receptors are of great interest due to their involvement in a wide range of physiological processes like synaptic transmission, cell proliferation and death, smooth muscle contraction and intestinal motility, platelet aggregation, nociception, and inflammation. Consequently, these proteins are considered as therapeutic targets for cancer and inflammatory, neurological, cardiovascular, and endocrine diseases [3,5,14-25]. Among these purinergic receptors, the P2X3 subtype is a subject of a significant number of physiological and pharmacological studies. These proteins were cloned in 1995 [26,27] and shown to be almost exclusively localized to nociceptive sensory ganglion neurons and nodose ganglion neurons [28,29]. Activation of P2X3 receptors is associated to a number of chronic pain conditions including neuropathic pain, which is typically resistant to standard pain treatment, migraine, and inflammatory pain. They contribute also to visceral mechanosensory

transduction, gut peristalsis, and urinary bladder dysfunctions [22,30-38]. As consequence, targeting of P2X3 receptors represents a potential alternative therapeutic strategy to treat chronic pain conditions of both neuropathic and inflammatory origin beyond the analgesic drugs currently available on the market [39,40]. Some recent studies have described a particular property of the P2X3 receptors consisting in its rapid transition to a state of desensitization followed by a relatively slow recovery of sensitivity to ATP [13,41]. The development of long-acting and low efficacy P2X3 agonists could hence represent an approach to generate new agents to block pain via receptor inactivation. An example of such molecules is given by the so-called "acyclic nucleotides" obtained by modifying the sugar moiety of ATP and presenting partial agonist profile at the P2X3 receptor [42].

An alternative strategy to develop analgesic drugs acting on P2X3 receptors is the design and synthesis of antagonists of these proteins. The first identified P2X3 antagonists were negatively charged and/or high molecular weight arylpolysulfonate molecules like the trypanocidal drug suramin, pyridoxalphosphate-6-azophenyl-2',4'-disulfonic acid (PPADS) and its isomer isoPPADS [43]. All these molecules were non selective antagonists at P2X receptors, being able also to antagonize the metabotropic P2YRs [44]. Further studies led to the discovery of a potent and selective P2X3 receptor antagonist, named A-317491 (**2**, Figure 1). This molecule presents nanomolar antagonism at both homomeric P2X3 and heteromeric P2X2/3, with a competitive inhibitory profile and a good selectivity over other P2XRs and a broad panel of membrane receptors, ion channels, and enzymes [45]. The most potent competitive antagonist of P2X3 receptor is the compound 2',3'-*O*-(2,4,6-trinitrophenyl)-ATP (TNP-ATP, **3**, Figure 1) [46], with low nanomolar activity. Several P2X ligands were also discovered through screening studies. For example, a high-throughput screening (HTS) campaign by Roche led to the discovery of a series of diaminopyridine derivatives, like RO-3 or AF-353 (**4** and **5**, respectively Figure 1), bearing a substituted benzyl or phenyloxy chain and acting as allosteric P2X3 antagonists [47-49]. Substitution of the diaminopyridine scaffold with a diaminopurine moiety led to molecules which maintained the antagonistic behavior [50].

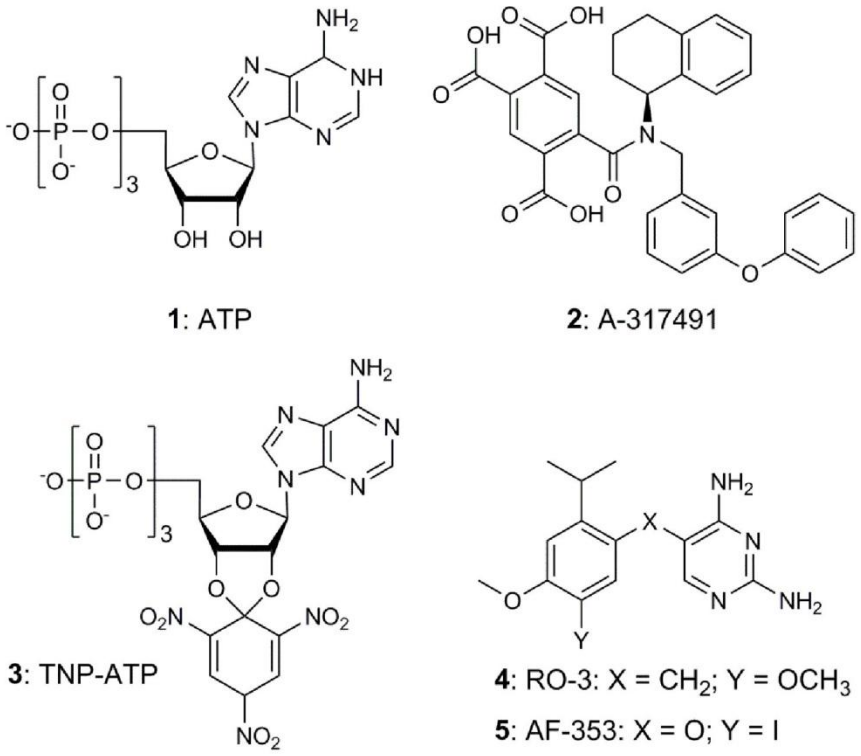

Figure 1. Ligands of the P2X3 receptor

The screening efforts represented for several years the best way to develop P2X ligands due to the lack of reliable structural data of P2X receptors that prevented structure-based design studies of these proteins. The publication of the crystal structure of the zebrafish P2X4 (zP2X4) receptor in the presence and absence of ATP has provided the first structural detail of these membrane proteins [51,52]. These results are very useful for the analysis of the ATP binding mode and of mutagenesis data [12] and for the comparative analysis of the structures underlying the activation mechanism of P2X receptors. We have recently reported a molecular modelling analysis aimed at developing 3D models of the human and rat P2X receptors in both active and inactive state [53]. This study has allowed to analyze the binding mode of the agonist ATP and the antagonist TNP-ATP at the P2X3 receptor. The mechanism of TNP-ATP antagonism, suggested on its ability to prevent the rearrangement of P2X subunits [52], was confirmed by P2X3 modelling studies [53]. The comparison of the binding mode of ATP and TNP-ATP led to an interpretation of the role of the 2',3'-*O*-substituent in the antagonist molecule. We started from these results to design ATP analogues bearing different substituents in 2',3'-*O*-position as new P2X3 antagonists. In the present study we report the design, synthesis, and biological evaluation of three ATP

derivatives presenting in 2',3'-*O*-position a cyclohexyl ring or a benzyl group; the corresponding monophosphate analogues of these compounds were also synthesized as it was observed that the mono- or di-phosphate derivatives of TNP-ATP were able to inhibit the P2X3 receptor [54]. The compounds were evaluated for their biological activity on native P2X3 receptors of mouse TG sensory neurons whose membrane currents were recorded by the patch clamp technique. This method enabled a quantitative investigation into P2X3 agonist/antagonist interaction through the use of dose-response curves in the presence of the reference agonist α,β-methyleneATP (α,β-meATP). This approach also enabled to study changes in receptor desensitization and to test if the new compounds were able to modify membrane currents evoked by activation of other membrane proteins like 5-HT or GABA receptors that are expressed by TG neurons [55-58].

2. Results

2.1 Molecular Modelling Design

We already reported and described the docking conformation of TNP-ATP at the human P2X3 binding site ([53] and Figure 2). In summary, the compound is inserted in the cavity in a similar fashion respect to the ATP binding mode observed from X-ray data (zP2X4) and from ATP-bound homology models of human [53] and mouse (Supporting Material) P2X3 receptors built using the X-ray structure of the zP2X4 receptor in its active state (pdb code: 4DW1; 2.8-Å resolution [52]) as template. The phosphate groups of the ligand are strongly bound to the receptor through an electrostatic/H-bond interaction network with positively charged residues (Lys63, Lys65, Arg281, Lys299) and additional polar interactions with Ser275 and Asn279 (Figure 2). The adenine moiety is inserted between the Lys65 side chain (above) and the hydrophobic Phe174 and Ile215 (below) and provides H-bonding with Thr172 backbone and side chain atoms. The ribose moiety lacks the 2'- and 3'-hydroxy groups of ATP as the two oxygen atoms are bound to the trinitrophenyl function. This group is inserted between two segments of adjacent P2X3 monomers and it is stabilized by the side chains of residues located in its proximity. At the same time, the trinitrophenyl moiety prevents the possible approach of the two monomers observed during the activation process of the receptor [52]. To verify if the role of the trinitrophenyl group is mainly related to its steric hindrance and not to other features given by its chemical structure (i.e. interaction given by the nitro groups), our design process was based on the substitution of the trinitrophenyl function with other groups presenting comparable volume even if with different chemical properties. Hence, we designed ATP derivatives bearing in the 2',3'-*O*-position bulky groups like a cyclohexyl or a benzyl function (2',3'-*O*-cyclohexylATP and 2',3'-*O*-benzylATP, **PF 94**, **PF 95**, and **PF 96**, respectively, see Schemes 1 and 2).

The designed compounds were docked into the binding site of a homology models of the human and mouse P2X3, built using the X-ray structure of the zP2X4 receptor in its apo (inactive) state (pdb code: 4DW0; 2.9-Å resolution [52]) as template. Figure 2 reports a comparison of the binding mode of compounds TNP-ATP and **PF 94** at the human P2X3 binding site, while in the Supporting Material the binding mode of TNP-ATP and the new triphosphate derivatives at the mouse P2X3 and the docking conformations of **PF 95** and **PF 96** at the human receptor are reported. Docking results present the new compound inserted into the binding cavity in a very similar way respect to TNP-ATP, with the phosphate groups positioned close to the cluster of positively charged residues in the depth of the site. The adenine moiety is similarly positioned respect to TNP-ATP (even if slightly reoriented respect to the same group of the latter compound), while the cyclohexyl group is located within the interface of the two subunits in a similar way of the trinitrophenyl function of TNP-ATP. This data suggests that the new compound could provide a similar steric hindrance of the reference molecule and hence could behave as obstacle for the receptor activation mechanism in a similar way of TNP-ATP. The corresponding monophosphate analogues (**PF 91**, **PF 92**, and **PF 93**, respectively) were synthesised as well as it was observed that the mono- or di-phosphate derivatives of TNP-ATP were able to inhibit the P2X3 receptor. In literature we found that the compound **PF 91** was already claimed in a patent describing nucleoside derivatives as P2X7 antagonists [59]; on the other hand the synthesis and the biological activity of this compound at this receptor were not reported. We also found that an analogue of the non-hydrolysable P2X ligand β,γ-meATP, bearing a 2',3'-*O*-benzylidene substituent and hence similar to the compounds **PF 95** and **PF 96** presented in this work, was tested for its biological activity at rabbit ear central artery showing a micromolar agonist activity at this tissue preparation [60].

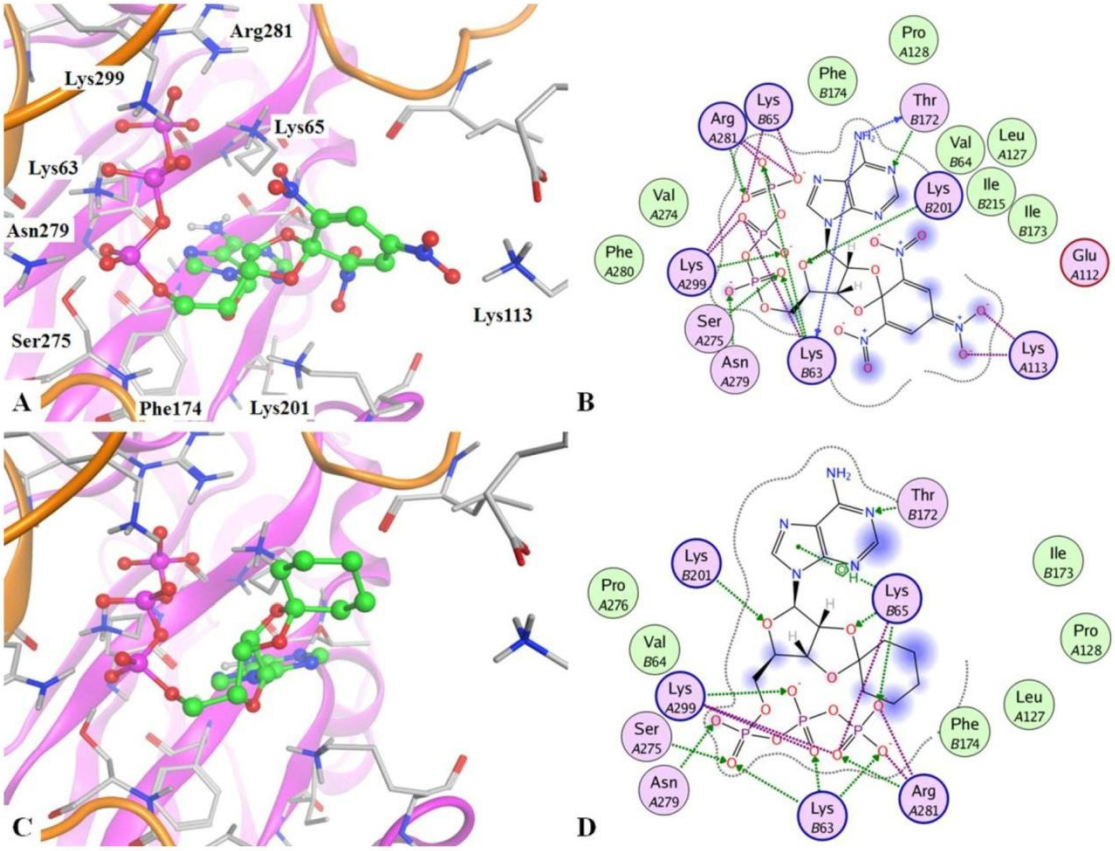

Figure 2. A-B: docking conformation (schematic description in panel B) of TNP-ATP at the human P2X3 binding site. Main residues for the ligand-receptor interaction are indicated. C-D: design of new ligands; docking conformation of the compound **PF 94** (schematic description in panel D).

2.2 Synthesis

The synthesis of new compounds **PF 91** and **PF 94** was performed by reaction of commercially available adenosine (**1**) with freshly distilled cyclohexanone in the presence of *p*-toluenesulfonic acid and 4 Å molecular sieves (Scheme 1), using a modification of a procedure previously reported [59]. The purification of the product of the reaction by silica gel chromatography and crystallization from ethylacetate furnished the intermediate **2** with 33% yield.

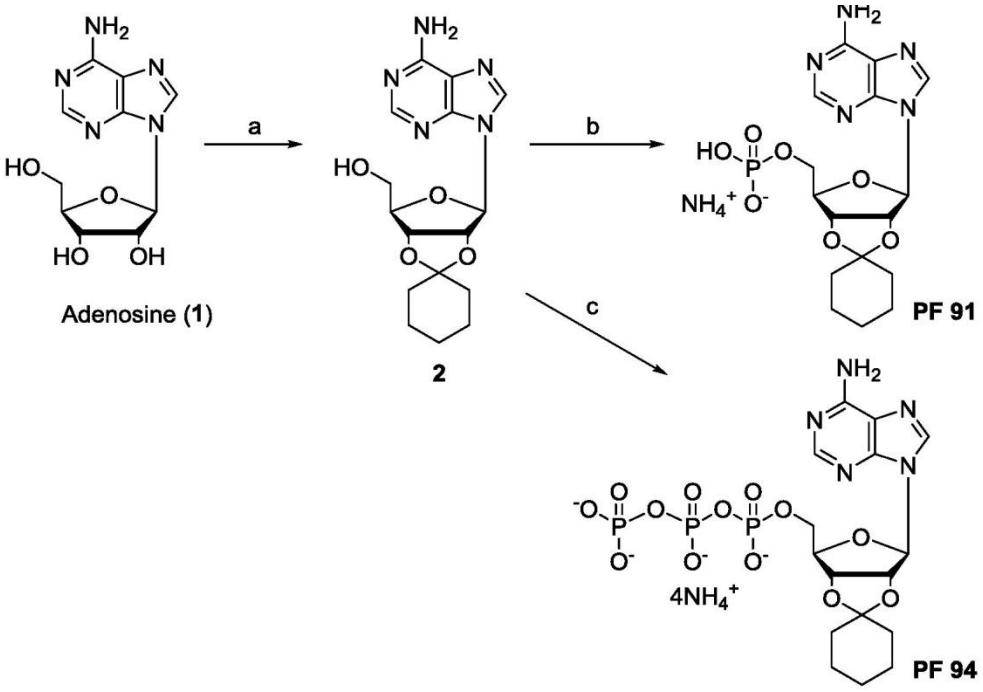

Scheme 1. Reagents and conditions: a. cyclohexanone, p-toluensulfonic acid, 4 Å molecular sieves, 70 °C, 48 h; b. i. phosphorus oxyxhloride, dry trimethyl phosphate, 0 °C, 4 h; ii. 1M TEAB, 0 °C to r. t., 15 min; c. i. phosphorus oxychloride, dry trimethyl phosphate, 0 °C, 4 h; ii. bis-(tri-*n*-butylammonium) pyrophosphate solution in dry DMF, 0 °C, 10 min; iii. 1M TEAB, 0 °C to r. t., 15 min.

On the other hand, the reaction of adenosine with benzaldehyde, using the same reaction conditions described before, furnished the suitable adenosine diastereomer derivatives **3** and **4** (Scheme 2).

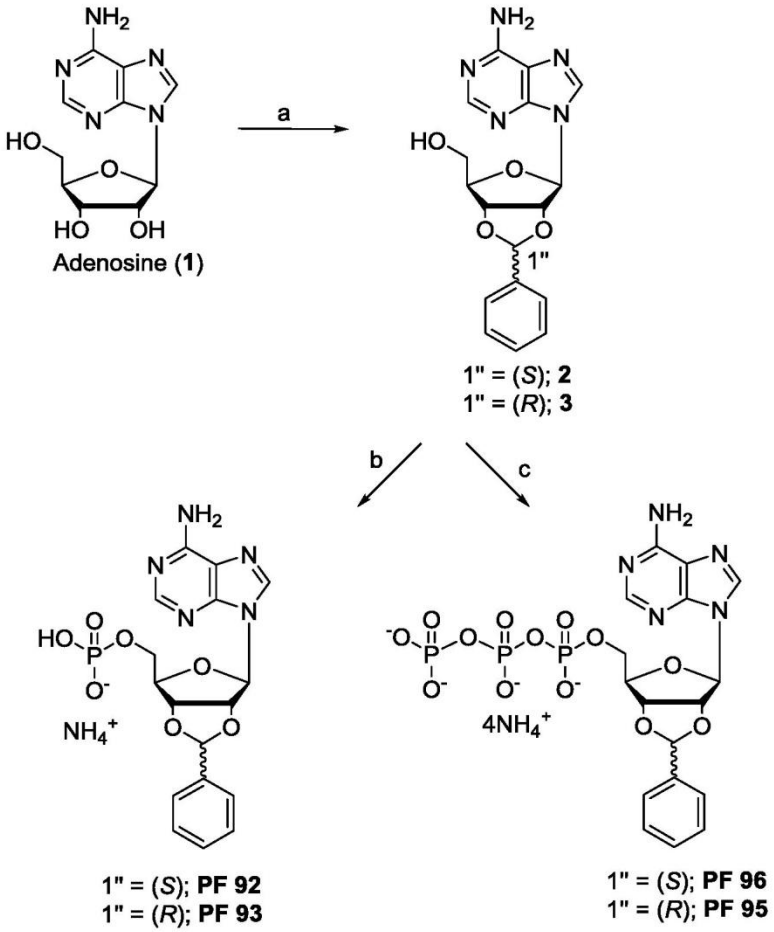

Scheme 2. Reagents and conditions: a. benzaldehyde, p-toluensolfonic acid, 4 Å molecular sieves, 70 °C, 4 h. b. i. phosphorus oxychloride, dry trimethyl phosphate, 0 °C, 4 h; ii. 1M TEAB, 0 °C to r. t., 15 min; c. i. phosphorus oxychloride, dry trimethyl phosphate, 0 °C, 4 h; ii. bis-(tri-*n*-butylammonium) pyrophosphate solution in dry DMF, 0 °C, 10 min; iii. 1M TEAB, 0 °C to r. t., 15 min.

The two epimers formed in the reaction were separated by silica gel chromatography and characterized by NOESY-NMR experiments. In the case of compound 3, a NOESY-2D NMR experiment was performed due to the close vicinity of the signals at 6.24 and 6.28 ppm which did not permitted a selective irradiation of the separate signals. In the obtained spectra, a clear interaction between the signals at 6.24 with 4.28, and at 7.50 ppm was observed. The signal at 4.28 corresponds to the ketal CH (1''-position) of the dioxolane ring, while the other signals belong to the 4' proton of the sugar moiety and to the protons in the orto-position of the phenyl ring.

Then, by a 1D-NOESY experiment (Figure 3), the irradiation of the signal at 6.02 ppm, of compound **4**, induced a signal increase of the peaks at 5.50, 5.08, and 7.56 corresponding to the 2'and 3' proton of the sugar moiety and the hydrogens in the orto-position of the phenyl ring, respectively. Hence, we may ascribe the (*S*) configuration of the ketal chiral center of compound **3**, as only in this case it is possible to have proton magnetic field interaction between the proton in 4'-position of the sugar and the proton of the ketal function. Furthermore, the (*R*) configuration of the corresponding position of compound **4** is confirmed by the observed interaction between the ketal proton and the hydrogens at 2' and 3' position of the sugar moiety.

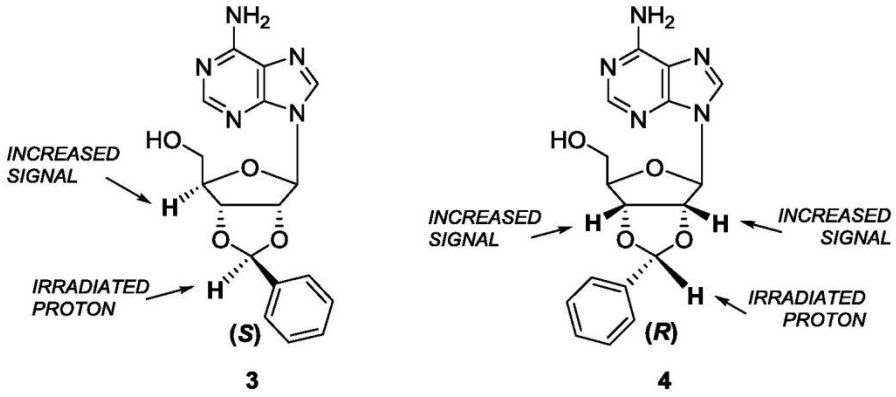

Figure 3. NOESY-1D NMR characterization for the configuration assignment of epimers **3** and **4**.

The synthesis of desired nucleotides (**PF 91**, **PF 92**, and **PF 93**) has been performed by reaction of the suitable intermediates **2**, **3**, and **4** with phosphorus oxychloride in trimethyl phosphate at 0 °C and then, quenching with a cold triethylammonium bicarbonate buffer solution. Compounds **PF 91**, **PF 92**, and **PF 93** were obtained as ammonium salts after ion exchange chromatography on a Sephadex DEAE resin eluted with a solvent gradient of 0 to 0.2 M ammonium bicarbonate buffer (Schemes 1 and 2).

For the synthesis of triphosphate derivatives **PF 94**, **PF 96**, **PF 95**, after a first step reaction with phosphorus oxychloride for 4 h, the reaction mixtures were in turn added of a bis-(tri-*n*-butylammonium) pyrophosphate solution in dry DMF. The reactions were, then, quenched by adding slowly a cold triethylammonium bicarbonate buffer solution and purified on ion exchange chromatography on a Sephadex DEAE resin eluting with a solvent gradient of 0 to 0.4 M ammonium bicarbonate buffer (Schemes 1 and 2).

All nucleotides were characterized by ^{1}H-NMR and ^{31}P-NMR spectra, as usually performed.

2.3 Biological Assays

Newly synthesized derivatives were tested for their biological activity at native mouse P2X3 receptors expressed by TG sensory neurons in culture by using the patch clamp recording technique. As a first approach, all compounds were applied for 5 minutes at 10 μM: the most potent compounds were further evaluated also at lower concentrations ranging from 50 to 0.01 μM. None of the tested compounds could elicit functional responses even at concentration of 10 μM, showing lack of agonist properties. All tested compounds, however, exhibited antagonistic activity on P2X3 receptors, since their application inhibited subsequent current responses evoked by 2 sec pulses of 10 μM α,β-meATP, a selective non-hydrolysable P2X3 agonist. Such inhibition was usually reversible, as the peak current amplitude fully or partially recovered after 5 min wash out. Figure 4 shows representative traces of the fast desensitizing inward currents evoked by 10 μM α,β-meATP and the effect of the synthesized compound **PF 95** applied at 1 and 0.1 μM concentrations.

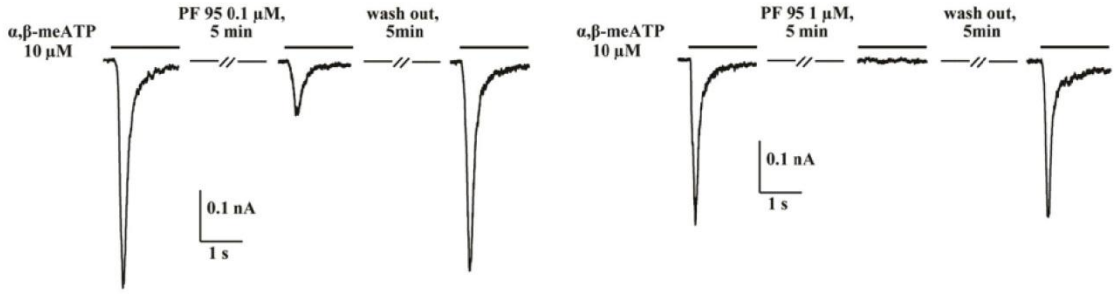

Figure 4. Effect of the application of **PF 95** on currents evoked by α,β-meATP at native mouse P2X3 receptors expressed by TG sensory neurons. The current evoked by 10 μM α,β-meATP was taken as control peak current and corresponds at a near-maximal response [36,41]. After 5 min application of **PF 95** (1 and 0.1 μM concentrations via fast superperfusion), subsequent application of 10 μM α,β-meATP induced smaller peak currents or no response at all. After 5 min washout, the current amplitude was almost completely restored.

Table 1 shows the calculated percent inhibition of the mouse P2X3-mediated currents elicited by tested compounds. The P2X3 inhibitor AF-353 was also tested for comparison. At the concentration of 10 μM, the monophosphate derivatives **PF 91**, **PF 92**, and **PF 93** showed lack or partial inhibition of P2X3 currents with a percent change of -0.9 ± 13%, 27 ± 9%, and 44 ± 8%, respectively. These compounds were, therefore, not tested at lower concentrations. The corresponding triphosphate derivatives **PF 94**, **PF**

95, and **PF 96** showed 100% inhibition of the P2X3 currents at 10 μM concentration. **PF 94** and **PF 95** were able to produce 99% inhibition also at 1 μM. At sub-micromolar level, **PF 94** and **PF 95** elicited a dose dependent inhibition (74% and 71% at 0.5 μM, respectively), while **PF 96** was less potent (34% inhibition at the same concentration). **PF 94** and **PF 95** were partial inhibitors also at nanomolar level (30% and 43% at 50 nM, and 21% and 25% at 10 nM concentrations, respectively).

Table 1. Summary of P2X3 antagonism of novel ATP derivatives.

Compound	Concentration, μM	Inhibition of P2X3 current, %
PF 91	10	-0.9 ± 13
PF 92	10	27 ± 9
PF 93	10	44 ± 8
PF 94	0.01	21 ± 9
	0.05	30 ± 3
	0.1	74 ± 5
	1	99 ± 1
	10	100
PF 95	0.01	25 ± 12
	0.05	43 ± 13
	0.1	71 ± 4
	1	99 ± 1
	10	100
PF 96	0.01	7 ± 11
	0.05	18 ± 7

	0.1 1 10	34 ± 13 86 ± 9 100
AF-353	0.01 0.05 0.1 1 10	69 ± 5 85 ± 12 100 100 100
Effects of the novel compounds were investigated on P2X3 currents evoked by 10 μM α,β-meATP; inhibition is expressed as % amplitude of control α,β-meATP-evoked current; data for each compound concentration are from 5-10 individual cells.		

Dose response curves were built for the most potent compounds (**PF 94**, **PF 95**, and **PF 96**) as shown in Figure 5, in which the log compound concentration was plotted against the percent inhibition of the α,β-meATP (10 μM) evoked current. Fitting the data with the Hill equation (eq. 2; see experimental details) yielded for compound **PF 94** a value of IC_{50} = 82.9 nM, for compound **PF 95** a value of IC_{50} = 80.8 nM, and for compound **PF 96** IC_{50} = 211 nM (n = 5-10 cells).

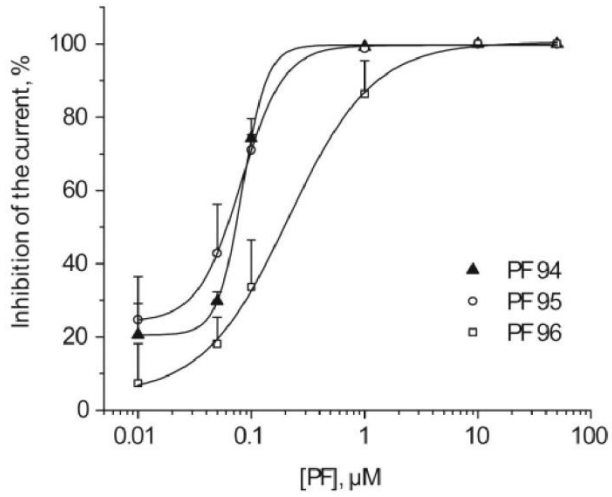

Figure 5. Dose-inhibition curves of P2X3-mediated currents for compounds **PF 94**, **PF 95**, and **PF 96** built by applying different concentrations of antagonists using the same concentration of agonist (10 μM α,β-meATP). Data points from n = 5-10 cells, fitted with Hill equation (eq. 2).

To assess the nature of the antagonist mechanism, we tested the ability of the two most potent compounds **PF 94** and **PF 95** to inhibit the P2X3 currents evoked by different concentrations of the reference agonist α,β-meATP. AF-353 was also tested for comparison. These antagonists were tested at concentrations close to their IC_{50} values (0.05 μM for **PF 94** and **PF 95**; 0.01 μM for AF353) and applied for 5 minutes. The agonist α,β-meATP was applied for 2 sec at 1, 3, 10, 30, and 100 μM concentrations. The dose-response curves are shown in Figure 6. The results indicated that the extent of current inhibition evoked by AF353 did not depend on the α,β-meATP concentration, confirming the non-competitive antagonism of this molecule. The potency of **PF 94** and **PF 95** appeared to decrease with increased agonist concentrations, suggesting a partially surmontable antagonism for these two molecules when the agonist dose was raised (Figure 6A). When analyzing the amplitude of the P2X3 current evoked by the agonist in the presence of the antagonists (Figure 6B), it appears that mixed type of antagonism in which a competitive (surmountable) and non-competitive block emerged.

The ability of **PF 94** and **PF 95** to inhibit responses evoked by high agonist concentrations might be explained by facilitated receptor desensitization in the presence of antagonist. If desensitization develops very rapidly, the response peak would be curtailed, thus summating desensitization-induced depression to any binding antagonism by the novel compounds. To test this possibility, we analyzed P2X3 currents in control and after application of **PF 95** with a two-exponential function [61] that allows calculating the

desensitization time constant τ_1 for both cases. Because τ_1 expresses the rate of current decay, it actually quantifies the speed at which the activated receptor enters into the desensitization state [61]. Since the desensitization constant τ_1 depends on the current amplitude that reflects the number of active receptors [61], to obtain suitable comparisons the currents to be analyzed with or without the antagonist should be approximately of the same size. Thus, we used lower agonist concentrations (5-10 μM) to elicit control currents and higher α,β-meATP concentration (30 μM) after application of **PF 95** (0.03 μM), so that the evoked responses have comparable amplitudes. Figure 7 shows representative examples of superimposed current traces in control and after **PF 95** (0.03 μM), recorded from the same cell. As seen from the bar graph of Figure 7, mean τ_1 values were not significantly different between the experimental conditions ($p = 0.41681$, paired t-test), implicating that **PF 95** did not affect the rate of agonist-induced desensitization.

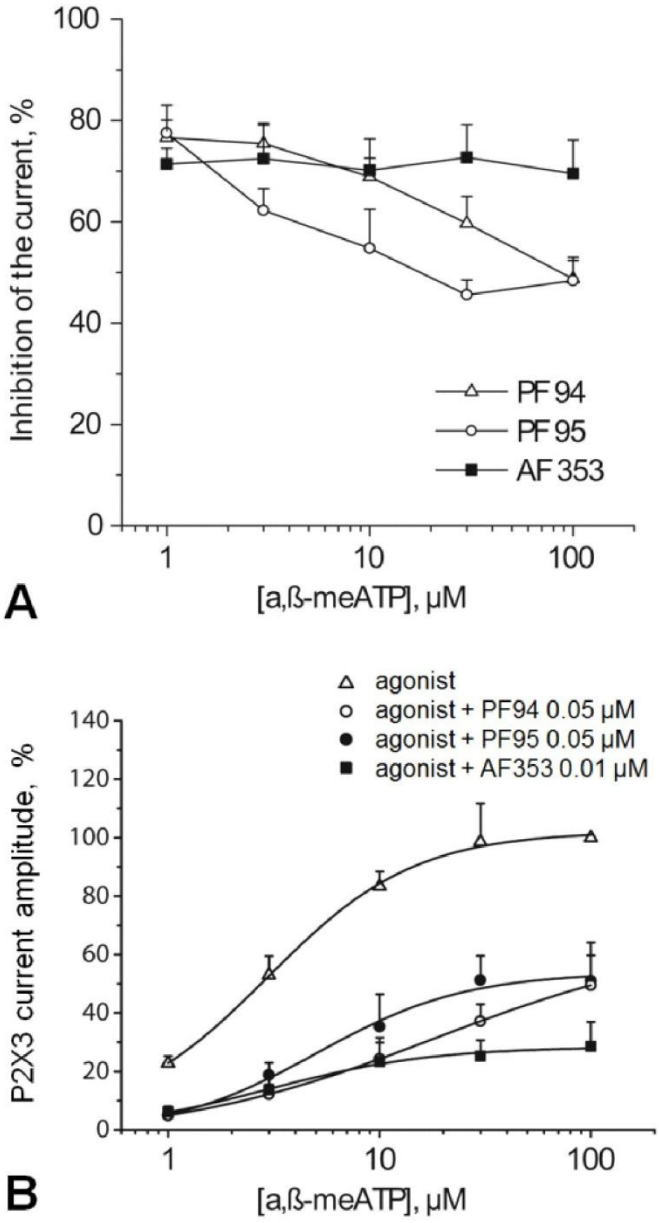

Figure 6. Concentration-response curves for α,β-meATP-evoked P2X3 currents in control and with pre-application of compounds **PF 94**, **PF 95**, and AF353 (0.05 µM for **PF 94** and **PF 95**; 0.01 µM for AF-353). The agonist was applied at 1, 3, 10, 30, and 100 µM concentrations. Data for each point are obtained from 5 to 11 cells.

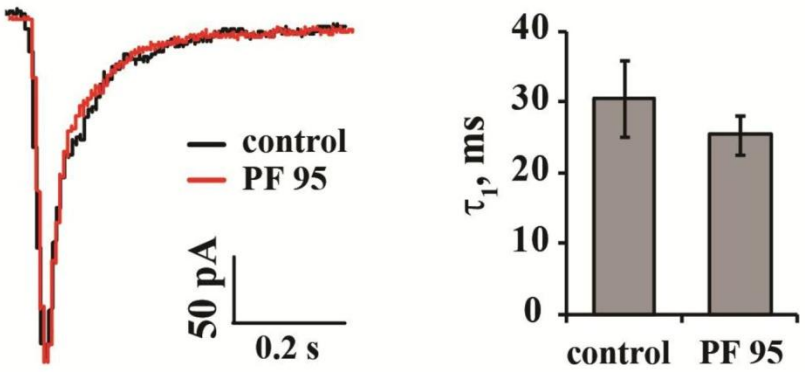

Figure 7. Desensitization of P2X3 currents after application of **PF 95**. Superimposed current traces from the same cell in control and after PF 95 (0.03 μM, 3 min) demonstrate no significant change in current decay time. Control current is induced by 10 μM α,β-meATP, current response after PF 95 treatment is evoked by30 μM α,β-meATP. Histograms on the right show values of desensitization time constant τ_1 (mean ± S.E.); n cells = 7, p = 0.41681, paired t-test.

P2X3 expressing sensory neurons such as DRG and TG are also known to express 5-HT and GABA receptors [55-58]. We used this property to evaluate the receptor selectivity of the newly synthesized antagonists. As expected, the majority of TG neurons responded to GABA (93%) and 5-HT (63%) applied at 10 μM concentration. All these responses had fast rise-time (5-HT: τ_{on} = 65 ± 9 ms, n = 7; GABA: τ_{on} = 107 ± 9 ms, n = 10) and decay (5-HT: τ_{des1} = 145 ± 13 ms, τ_{des2} = 1.44 ± 0.28 s, n=7; GABA: τ_{des} = 1.96 ± 0.39 s, n = 10) indicating that they were mediated by ionotropic receptors (5-HT_3 and $GABA_A$ receptors, respectively). Pre-application of 10 μM **PF 94**, **PF 95**, or **PF 96** did not significantly affected $GABA_A$ and 5-HT_3 currents, indicating that these compounds are selective for the P2X *versus* GABA and 5-HT receptors at TG neurons (Figure 8).

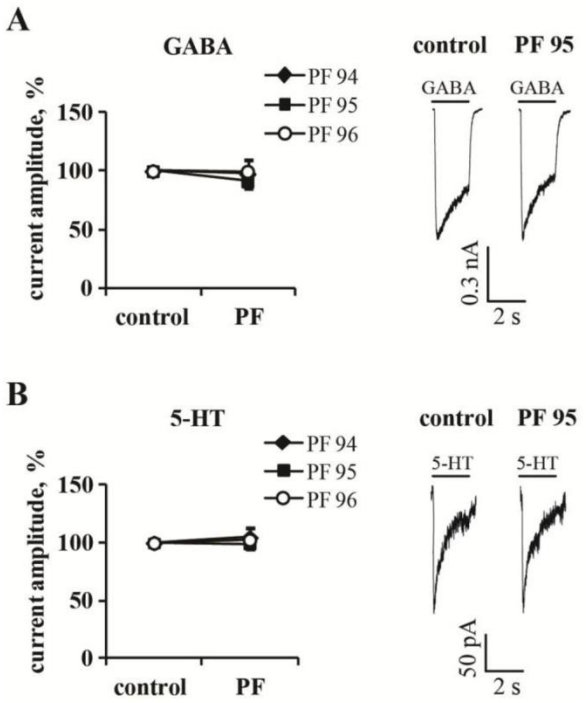

Figure 8. Effect of PF 94-96 on $GABA_A$ and 5-HT receptors. A, Diagram on the left summarizes mean normalized peak amplitude values for currents evoked by 10 μM GABA (2 s pulses) in control and after 5 min application of PF 94, PF 95 or PF 96 (10 μM); n = 4, 6 and 5 for PF 94, PF 95 and PF 96, respectively. Representative traces on the right show GABA-mediated currents in control and after treatment with **PF 95**, recorded from the same cell. B, Diagram on the left shows mean normalized peak amplitudes for currents evoked by 10 μM 5-HT (2 s pulses) in control and after 5 min application of **PF 94**, **PF 95** or **PF 96** (10 μM); n = 4. Examples of 5-HT-mediated current traces (recorded from a single cell) in control and after PF 95 application are presented on the right.

The results of the biological evaluation show that the 2',3'-*O*-substituted ATP analogues developed in this study are antagonists of the P2X3 with nanomolar potency. The corresponding 5'-monophosphate derivatives also showed some antagonism of the same receptor even if at higher concentrations. The comparison with the antagonist potencies of TNP-ATP and its mono- and di-phosphate analogues suggests that the insertion of a 2',3'-*O*-substituent in ATP led to compounds endowed with antagonist profile at the P2X3 receptor. The potency of these derivatives and the corresponding mono- and di-phosphate analogues may be influenced by the chemical-physical profile of the 2',3'-*O*-substituent.

3. Conclusion

Different ATP analogues were developed as ligands of the purinergic P2X receptors, resulting generally agonists or partial agonists of these proteins. The insertion of a 2,4,6-trinitrophenyl moiety in the 2',3'-*O*-position of ATP shifted the agonist profile of the endogenous ligand to the antagonist activity of TNP-ATP. It was also interesting that the removal of one or two phosphate groups of TNP-ATP did not affect the antagonist profile of the molecules, modulating only the antagonist potency at the P2X receptors. The publication of the crystal structure of the zebrafish P2X4 in complex with ATP and the subsequent molecular modelling studies have provided some interpretation of the activity of TNP-ATP at P2X receptors, with the simulation of the interaction of this molecule with the ATP binding site of the protein. The results suggested that the 2,4,6-trinitrophenyl moiety in the 2',3'-*O*-position of TNP-ATP inhibited the rearrangement of the three P2X subunits at the basis of the receptor activation, hence explaining the antagonist profile of the molecule. This work was focused on the evaluation of the effect on the P2X3 antagonist activity of the replacement of the 2,4,6-trinitrophenyl moiety with cycloalkyl or arylalkyl groups, thus roughly maintaining the steric hindrance of the 2',3'-*O*-substituent of TNP-ATP but changing its chemical-physical profile. The new 2',3'-*O*-substituted adenosine derivatives were, therefore, designed and synthesized as both 5'-triphosphate and monophosphate analogues, to test also the impact on the activity of a different number of the phosphate groups. Patch-clamp recording experiments were performed on mouse P2X3 receptors expressed by TG sensory neurons to test the ability of the molecules to inhibit currents evoked by the P2X3 reference agonist α,β-meATP. The results confirm the original hypothesis described as rationale of this work, suggesting that the introduction of a bulky substituent in the 2',3'-*O*-position of ATP, originally occupied by a 2,4,6-trinitrophenyl moiety in TNP-ATP, is responsible of the antagonist profile of the obtained ATP derivatives at the P2X3, while the chemical-physical profile of the 2',3'-*O*-substituent modulates the antagonist potency. These observations could also explain the low activity of the monophosphate analogues developed in this work. On the other hand, further exploration of the chemical-physical properties of the 2',3'-*O*-substituent might lead to the development of novel P2X antagonists with different potency and selectivity profiles at these purinergic receptors.

4. Experimental Section

4.1 Molecular Modelling

All molecular modelling studies were performed on a Core i7 CPU (PIV 2.20 GHZ) PC workstation. Homology modelling, energy minimization, and docking studies were carried out using Molecular Operating Environment (MOE, version 2012.10) suite [62]. All ligand structures were optimized using RHF/AM1 semiempirical calculations and the software package MOPAC [63] implemented in MOE was utilized for these calculations.

4.1.1 Homology modelling of the human and mouse P2X3 receptor

Homology models of the human and mouse P2X3 receptor were built using the X-ray structure of the zP2X4 receptor in its apo (inactive) and ATP-bound (active) states (pdb code: 4DW0; 2.9-Å resolution and pdb code: 4DW1; 2.9-Å resolution as templates [52], respectively). A multiple alignment of the P2X receptor primary sequences was built within MOE as preliminary step. Within the Supporting Material it is reported the alignment of the sequences of human and mouse P2X3 and zP2X4. The boundaries identified from the used X-ray crystal structure of zP2X4 receptor were applied for the sequences of the human and mouse P2X3 receptors. The missing domains were built by the loop search method implemented in MOE. Once modelled the heavy atoms, all hydrogen atoms were added and the protein coordinates were then minimized with MOE using the AMBER99 force field [64] until the Root Mean Square (RMS) gradient of the potential energy was less than 0.05 kJ mol^{-1} $Å^{-1}$. Reliability and quality of the model were checked using the Protein Geometry Monitor application within MOE, which provides a variety of stereochemical measurements for inspection of the structural quality in a given protein, like backbone bond lengths, angles and dihedrals, Ramachandran φ-ψ dihedral plots, and sidechain rotamer and non-bonded contact quality.

4.1.2 Molecular docking analysis

The compound structures were docked into the binding site of the P2X3 receptor models using the MOE Dock tool. This method is divided into a number of stages: *Conformational Analysis of ligands*. The algorithm generated conformations from a single 3D conformation by conducting a systematic search. In this way, all combinations of angles were created for each ligand. *Placement*. A collection of poses was generated from the pool of ligand conformations using Triangle Matcher placement method. Poses were generated by superposition of ligand atom triplets and triplet points in the receptor binding site. The receptor site points are alpha sphere centers which represent locations of tight packing. At each iteration a random conformation was selected, a random triplet of ligand atoms and a random triplet of alpha sphere

centers were used to determine the pose. *Scoring*. Poses generated by the placement methodology were scored using two available methods implemented in MOE, the *London dG* scoring function which estimates the free energy of binding of the ligand from a given pose, and *Affinity dG* scoring which estimates the enthalpy contribution to the free energy of binding. The top 30 poses for each ligand were output in a MOE database.

4.1.3 Post Docking analysis

The docking poses of each compound were then subjected to AMBER99 force field energy minimization until the RMS gradient of the potential energy was less than 0.05 kJ mol^{-1} $Å^{-1}$. Receptor residues within 6 Å distance from the ligand were left free to move, while the remaining receptor coordinates were kept fixed. AMBER99 partial charges of receptor and MOPAC output partial charges of ligands were utilized. Once the compound-binding site energy minimization was completed, receptor coordinates were fixed and a second energy minimization stage was performed leaving free to move only compound atoms. MMFF94 force field [65-71] was applied. For each compound, the minimized docking poses were then rescored using *London dG* and *Affinity dG* scoring functions and the *dock-pK_i* predictor. The latter tool allows estimating the pK_i for each ligand using the "scoring.svl" script retrievable at the SVL exchange service (Chemical Computing Group, Inc. SVL exchange: http://svl.chemcomp.com). The algorithm is based on an empirical scoring function consisting of a directional hydrogen-bonding term, a directional hydrophobic interaction term, and an entropic term (ligand rotatable bonds immobilized in binding). The obtained pK_i values must be considered as docking scores and not as prediction of binding affinity. For each compound, the three top-score docking poses according to at least two out of three scoring functions were selected for final ligand-target interaction analysis.

4.2 Chemistry

Melting points were determined with a Büchi apparatus and are uncorrected. ^{1}H-NMR and ^{31}P-NMR spectra were obtained with Varian Mercury 400 MHz spectrometer; δ in ppm, J in Hz; all exchangeable protons were confirmed by addition of D_2O. Mass spectra were recorded on an HP 1100-MSD series instrument. All measurements were performed using electrospray ionization (ESI-MS) on a single quadrupole analyzer. TLC were carried out on pre-coated TLC plates with silica gel 60 F-254 (Merck). For column chromatography, silica gel 60 (Merck) was used. For ion exchange chromatography, Sephadex DEAE A-25 resin, HCO_3^- form, was used. Elemental analyses were determined on a Fisons model EA 1108 CHNS-O model analyzer and are within ± 0.4% of theoretical values.

2',3'-O-cyclohexylideneadenosine (2): adenosine (**1**, 3 g, 11.23 mmol) and *p*-toluenesulfonic acid (2.564 g, 13.48 mmol) were stirred at 70 °C in freshly distilled cyclohexanone (30 mL) in the presence of 4 Å molecular sieves. The reaction was stirred for 48 h, cooled to room temperature, neutralized with triethylamine, and the molecular sieves were filtered. Water (100 mL) was added and cyclohexanone was extracted with *n*-hexane (70 mL). The product was then extracted from the water phase with ethylacetate (100 mL x 4), dried over anhydrous Na_2SO_4, and evaporated to dryness. The residue was purified by silica gel flash column chromatography eluting with a gradient of 0 to 1.5% MeOH in CH_2Cl_2 to give **2** (1.29 g, 3.70 mmol) in 33% yield as a white powder after recrystallization from ethylacetate. M. p.: 173-175 °C; ^{1}H-NMR (DMSO-d_6, 400 MHz) δ 1.35 (m, 2H, *c*-Hex), 1.47 (m, 2H, *c*-Hex), 1.57 (m, 4H, *c*-Hex), 1.76 (m, 2H, *c*-Hex), 3.52 (m, 2H, H-5'), 4.20 (m, 1H, H-4'), 4.95 (dd, *J*=2.0 Hz, *J*=6.0 Hz, 1H, H-3'), 5.23 (t, *J*=5.2 Hz, 1H, OH), 5.34 (dd, *J*=2.8 Hz, *J*=6.0 Hz, 1H, H-2'), 6.11 (d, *J*=3.2 Hz, 1H, H-1'), 7.36 (s, 2H, NH_2), 8.14 (s, 1H, H-8), 8.33 ppm (s, 1H, H-2). ESI-MS: positive mode *m/z* 348.0 $[M+H]^+$, 370.0 $[M+Na]^+$, 717.0 $[2M+Na]^+$; negative mode *m/z* 346.2 $[M-H]^-$, 382.1 $[M+Cl]^-$.

2',3'-O-(*S*)-benzilideneadenosine (3) and 2',3'-O-(*R*)-benzilideneadenosine (3): adenosine (**1**, 3 g, 11.23 mmol) and *p*-toluenesulfonic acid (2.564 g, 13.48 mmol) were stirred at 70 °C in freshly distilled benzaldehyde (53 mL) in the presence of 4 Å molecular sieves. The reaction was stirred for 4 h, cooled to room temperature, neutralized with triethylamine, and the molecular sieves were filtered. 100 mL of water was added and benzaldehyde was extracted with *n*-hexane (70 mL). The product was then extracted from the water phase with ethylacetate (100 mL x 4), dried over anhydrous Na_2SO_4, and evaporated to dryness. The residue was purified by silica gel normal column chromatography eluting with 4% MeOH in CH_2Cl_2 to give **3** (672 mg, 1.89 mmol), 17% yield, and **4** (1.484 g, 4.18 mmol), 37% yield, as a white powders after recrystallization from ethylacetate. The configuration of the epimers were assigned based on NOESY-NMR experiment data.

3: m. p.: 217-219 °C; ^{1}H-NMR (DMSO-d_6, 400 MHz) δ 3.60 (m, 2H, H-5'), 4.28 (m, 1H, H-4'), 5.08 (m, 1H, H-3'), 5.17 (m, 1H, OH), 5.48 (m, 1H, H-2'), 6.24 (s, 1H, CH), 6.28 (d, *J*=3.2 Hz, 1H, H-1'), 7.36 (s, 2H, NH_2), 7.43 (m, 3H, Ph), 7.50 (m, 2H, Ph), 8.15 (br s, 1H, H-8), 8.37 ppm (s, 1H, H-2). ESI-MS: positive mode *m/z* 355.9, 377.9, 732.9; negative mode *m/z* 354.1, 390.0.

4: m. p.: 229-231 °C ; ^{1}H-NMR (DMSO-d_6, 400 MHz) δ 3.54 (m, 2H, H-5'), 4.36 (m, 1H, H-4'), 5.08 (dd, *J*=2.4 Hz, *J*=2.4 Hz, 1H, H-3'), 5.27 (t, *J*=5.2 Hz, 1H, OH), 5.50 (dd, *J*=2.4 Hz, *J*=2.4 Hz, 1H, H-2'), 6.02 (s, 1H, CH), 6.28 (d, *J*=2.8 Hz, 1H, H-1'), 7.37 (br s, 2H, NH_2), 7.46 (m, 3H, Ph), 7.56 (m, 2H, Ph), 8.15 (s, 1H, H-8), 8.37 ppm (s, 1H, H-2). ESI-MS: positive mode *m/z* 356.0, 377.9, 732.9; negative mode *m/z* 354.1.

General procedure for the synthesis of monophosphates PF 91, PF 92, and PF 93: $POCl_3$ (52 µL, 0.56 mmol) was added dropwise in turn to a solution of **2, 3, or 4** (50 mg, 0.14 mmol) in dry trimethylphosphate (0.7 mL) placed in an ice bath. The reaction was left to stir for 4 h, quenched by slowly adding 3 mL of a cold 1M TEAB solution in an ice bath and then stirred for 15 minutes at r. t. The reaction mixtures were evaporated to dryness and co-evaporated with H_2O (3 x 5 mL). The obtained crude was purified over a Sephadex DEAE A-25 gel (HCO_3^- form) eluting with a solvent gradient of 0 to 0.2 M NH_4HCO_3 buffer. The appropriate fractions were collected, concentrated under vacuum, and co-evaporated several times with H_2O to yield pure monophosphates **PF 91**, **PF 92**, **PF 93** as white solids.

Adenosine-2',3'-cyclohexyl-5'-monophosphate ketal ammonium salt (PF 91): The title compound was obtained from **2** in 93% yield; ^{1}H-NMR (D_2O, 400 MHz) δ 1.26 (m, 2H, *c*-Hex), 1.38 (m, 2H, *c*-Hex), 1.52 (m, 4H, *c*-Hex), 1.73 (m, 2H, *c*-Hex), 3.87 (m, 2H, H-5'), 4.47 (m, 1H, H-4'), 5.00 (dd, *J*=2.0 Hz, *J*=2.0 Hz, 1H, H-3'), 5.23 (dd, *J*=3.6 Hz, *J*=3.6 Hz, 1H, H-2'), 6.09 (d, *J*=3.6 Hz, 1H, H-1'), 8.05 (s, 1H, H-8), 8.24 ppm (s, 1H, H-2). ^{31}P-NMR (D_2O, 162 MHz) δ 1.69 ppm. ESI-MS: negative mode *m/z* 426.0, 853.2.

2',3'-O-(*S*)-benzilideneadenosine-5'-monophosphate ammonium salt (PF 92): The title compound was obtained from **3** in 63% yield; ^{1}H-NMR (D_2O, 400 MHz) δ 3.94 (m, 2H, H-5'), 4.46 (m, 1H, H-4'), 5.08 (dd, *J*=3.6 Hz, *J*=4.0 Hz, 1H, H-3'), 5.33 (dd, *J*=2.8 Hz, *J*=3.2 Hz, 1H, H-2'), 6.08 (s, 1H, CH), 6.17 (d, *J*=3.6 Hz, 1H, H-1'), 7.29 (m, 3H, Ph), 7.36 (m, 2H, Ph), 8.01 (s, 1H, H-8), 8.18 ppm (s, 1H, H-2). ^{31}P-NMR (D_2O, 162 MHz) δ 1.25 ppm. ESI-MS: negative mode *m/z* 433.9, 869.0.

2',3'-O-(*R*)-benzilideneadenosine-5'-monophosphate ammonium salt (PF 93): The title compound was obtained from **4** in 23% yield; ^{1}H-NMR (D_2O, 400 MHz) δ 3.94 (m, 2H, H-5'), 4.63 (m, 1H, H-4'), 5.12 (dd, *J*=1.6 Hz, *J*=1.6 Hz, 1H, H-3'), 5.42 (dd, *J*=2.8 Hz, *J*=2.8 Hz, 1H, H-2'), 5.98 (s, 1H, CH), 6.31 (d, *J*=2.4 Hz, 1H, H-1'), 7.38 (m, 3H, Ph), 7.52 (m, 2H, Ph), 8.12 (s, 1H, H-8), 8.32 ppm (s, 1H, H-2). ^{31}P-NMR (D_2O, 162 MHz) δ 0.98 ppm. ESI-MS: negative mode *m/z* 434.1.

General procedure for the synthesis of triphosphates PF 94, PF 96, and PF 95: $POCl_3$ (108 µL, 1.16 mmol) was added dropwise to a solution of **2**, **3**, **or 4** (100 mg, 0.29 mmol) in dry trimethylphosphate (1.5 mL) placed in an ice bath. The reaction was left to stir for 4 h, after which 5.8 mL (2.90 mmol) of bis-(tri-*n*-butylammonium) pyrophosphate solution in dry DMF was added and stirred for 10 min. The reaction was quenched by slowly adding 5 mL of a cold 1M TEAB solution in an ice bath and then stirred for 15 minutes at r. t. The mixture was extracted with *tert*-butylmethyl ether (3 x 15 mL), and the aqueous solution was evaporated and co-evaporated with H_2O (3 x 10 mL) to yield glassy oils. The obtained crude was purified over a Sephadex DEAE A-25 gel (HCO_3^- form) eluting with a solvent gradient of 0 to 0.4 M NH_4HCO_3 buffer. The appropriate fractions were collected, concentrated under vacuum, co-evaporated several times with H_2O to yield pure triphophate derivatives **PF 94, PF 95, and PF 96** as white powders.

Adenosine-2',3'-cyclohexyl-5'-triphosphate ketal ammonium salt (PF 94): the title compound was obtained from **2** in 25% yield; ^{1}H-NMR (D_2O, 400 MHz) δ 1.29 (m, 2H, *c*-Hex), 1.40 (m, 2H, *c*-Hex), 1.56 (m, 4H, *c*-Hex), 1.77 (m, 2H, *c*-Hex), 4.05 (m, 2H, H-5'), 4.55 (m, 1H, H-4'), 5.09 (m, 1H, H-3'), 5.27 (dd, *J*=3.2 Hz, *J*=3.6 Hz, 1H, H-2'), 6.13 (d, *J*=3.6 Hz, 1H, H-1'), 8.11 (s, 1H, H-8), 8.32 ppm (s, 1H, H-2). ^{31}P-NMR (D_2O, 162 MHz) δ -9.63, -10.65, -22.06 ppm. ESI-MS: negative mode *m/z* 292.5, 586.1.

2',3'-O-(*S*)-benzilideneadenosine-5'-triphosphate ammonium salt (PF 96): the title compound was obtained from **3** in 29% yield; ^{1}H-NMR (D_2O, 400 MHz) δ 4.14 (m, 2H, H-5'), 4.65 (m, 1H, H-4'), 5.22 (m, 1H, H-3'), 5.42 (dd, *J*=3.6 Hz, *J*=3.6 Hz, 1H, H-2'), 6.21 (s, 1H, CH), 6.29 (d, *J*=4.0 Hz, 1H, H-1'), 7.37 (m, 3H, Ph), 7.47 (m, 2H, Ph), 8.12 (s, 1H, H-8), 8.31 ppm (s, 1H, H-2). ^{31}P-NMR (D_2O, 162 MHz) δ -9.22, -10.53, -22.04 ppm. ESI-MS: negative mode *m/z* 296.5, 594.0.

2',3'-O-(*R*)-benzilideneadenosine-5'-triphosphate ammonium salt (PF 95): The title compound was obtained from **4** in 39% yield:. ^{1}H-NMR (D_2O, 400 MHz) δ 4.04 (m, 1H, *H*CH-5'), 4.10 (m, 1H, *H*CH -5'), 4.65 (m, 1H, H-4'), 5.20 (m, 1H, H-3'), 5.40 (dd, *J*=3.2 Hz, *J*=3.2 Hz, 1H, H-2'), 6.00 (s, 1H, CH), 6.28 (d, *J*=3.2 Hz, 1H, H-1'), 7.38 (m, 3H, Ph), 7.53 (m, 2H, Ph), 8.06 (s, 1H, H-8), 8.33 ppm (s, 1H, H-2). ^{31}P-NMR (D_2O, 162 MHz) δ -9.14, -10.66, -21.92 ppm. ESI-MS: negative mode *m/z* 296.6, 593.9.

4.3 Biological Assays

4.3.1 Trigeminal ganglia culture neurons

Cultures of TG sensory neurons were prepared from C57Bl/6 wild type mice (P10–14) as previously described [72]. In brief, TG were rapidly excised and enzymatically dissociated in F12 Medium (Invitrogen Corp, Milan, Italy) containing 0.25 mg/ml trypsin, 1 mg/ml collagenase, 0.2 ml DNAse (Sigma, Milan, Italy) at 37 °C for 12 min. Cells were plated on poly-L-lysine coated 35 mm Petri dishes on F12 medium supplemented with 10% fetal bovine serum and antibiotics and incubated for 24 h (5% CO_2/95% humidity, 37°C).

4.3.2 Patch clamp recordings

Currents were recorded from small/medium size mouse TG neurons (nociceptors that strongly express native P2X3 receptors [72]) as previously described [72,73] under whole cell voltage clamp mode at a holding potential of -65 mV after correction for liquid junction potential. Cells were continuously superfused at room temperature with control solution containing (in mM): 152 NaCl, 5 KCl, 1 $MgCl_2$, 2 $CaCl_2$, 10 glucose, 10 HEPES; pH 7.4 adjusted with NaOH. Patch pipettes had a resistance of 3-4 MΩ

when filled with (in mM): 140 KCl, 2 $MgCl_2$, 0.5 $CaCl_2$, 2 ATP-Mg, 2 GTP-Li, 10 HEPES, 10 EGTA; pH 7.2 adjusted with KOH (for recordings from TG neurons). After obtaining whole cell configuration, cell slow capacitance was compensated. Access resistance was never >10 MΩ and was routinely compensated by at least 70%. 1 kHz filtering was used during recording; currents were acquired by means of a DigiData 1200 interface and pClamp8.2 software (Molecular Devices, Sunnyvale, CA, USA).

4.3.3 Drug application and data analysis

The receptor agonist α,β-methylene-adenosine-5'-triphosphate (α,β-meATP, Sigma) and test compounds were applied by rapid solution changer system ((Rapid Solution Changer RSC-200; BioLogic Science Instruments, Claix, France).). Membrane currents were analyzed in terms of their peak amplitude and rise time (10-90% of the peak). Current decay due to receptor desensitization during agonist application was fitted with either a monoexponential or biexponential function using pCLAMP Clampfit 9.2.

Test compounds were kept at + 4 °C and dissolved to 10 mM in H_2O before experiments and finally diluted to necessary concentration in control solution. For routine tests, the P2X3 selective agonist α,β-meATP was applied at 10 μM concentration (2 s pulse) at least 3 times (at 5 min interval to prevent cumulative receptor desensitization) to obtain an average control response. Since activated P2X3 receptors desensitize rapidly in the sustained presence of agonist, the inward current transient is, of course, too short for the binding equilibrium to be reached when agonist and antagonist are co-applied. Thus, to assess potential receptor blocking activity, each test compound was continuously pre-applied for 5 min before the α,β-meATP application as previously reported [41,42]. Antagonist activity was quantified as percent inhibition of the α,β-meATP-induced current:

$$\% \text{ inhibition} = 100 * (1 - I_2/I_1), \qquad \text{(eq. 1)}$$

where I_1 is the control peak current, I_2 is the peak amplitude of the current after test compound.

For the most potent compounds, antagonist dose-inhibition curves were constructed by applying for 5 min different concentrations of each test compound using the same maximal concentration (10 μM) of α,β-meATP agonist. Data were plotted and fitted with empirical Hill equation using Origin 6.0 (Microcal, Northampton, MA, USA):

$$\% \text{ inhibition} = 100/(1+ (IC_{50}/[Ant])^{nH}), \qquad \text{(eq. 2)}$$

where [Ant] is the concentration of the antagonist, n_H is the Hill coefficient, IC_{50} is the concentration of antagonist required to block the maximal current by 50%. Agonist concentration-response curves in terms of normalized currents vs log agonist concentration were fitted with the same Hill equation, with

corresponding parameters EC_{50} and n_H, where EC_{50} is the concentration of agonist required to produce the half-maximal current. All data are presented as mean ± standard error of the mean (S.E.); n is the number of cells. Statistical significance was evaluated with paired Student's t-test (for parametric data) or Mann−Whitney rank sum test (for nonparametric data), as suggested by the software; $p<0.05$ was considered statistically significant.

Acknowledgement

This work was supported by Fondo di Ricerca di Ateneo (FPI000033 - University of Camerino) and the EU FP7 grant EuroHeadPain (#602633).

Supporting Information

Supporting Information contains the alignment of the sequences of human and mouse P2X3 and zP2X4 (SI1), the binding mode of ATP at the human and mouse P2X3 cavities (SI2), the docking conformation of TNP-ATP (SI3) and the new triphosphate derivatives (SI4) at the mouse P2X3, and the binding mode of the triphosphate derivatives **PF 95** and **PF 96** at the human P2X3 (SI5).

References

1. G. Burnstock, Discovery of purinergic signalling, the initial resistance and current explosion of interest, Br. J. Pharmacol., 167 (2012) 238-255.

2. M.P. Abbracchio, G. Burnstock, A. Verkhratsky, H. Zimmermann, Purinergic signalling in the nervous system: an overview, Trends Neurosci., 32 (2009) 19-29.

3. A. Surprenant, R.A. North, Signaling at purinergic P2X receptors, Annu. Rev. Physiol., 71 (2009) 333-359.

4. G. Burnstock, B.B. Fredholm, R.A. North, A. Verkhratsky, The birth and postnatal development of purinergic signalling, Acta Physiol. (Oxf.), 199 (2010) 93-147.

5. B.S. Khakh, R.A. North, P2X receptors as cell-surface ATP sensors in health and disease, Nature, 442 (2006) 527-532.

6. D. Dal Ben, E. Adinolfi, Editorial: Purinergic P2X receptors: physiological and pathological roles and potential as therapeutic targets, Curr. Med. Chem., 22 (2015) 782.

7. D. Dal Ben, E. Adinolfi, Special Issue: Purinergic P2X receptors: physiological and pathological roles and potential as therapeutic targets, Curr. Med. Chem., 22 (2015) 782-941.

8. M.T. Young, P2X receptors: dawn of the post-structure era, Trends Biochem Sci, 35 (2010) 83-90.

9. L.E. Browne, L.H. Jiang, R.A. North, New structure enlivens interest in P2X receptors, Trends Pharmacol. Sci., 31 (2010) 229-237.

10. R.J. Evans, Structural interpretation of P2X receptor mutagenesis studies on drug action, Br. J. Pharmacol., 161 (2010) 961-971.

11. L. Grimes, M.T. Young, Purinergic P2X receptors: structural and functional features depicted by X-ray and molecular modelling studies, Curr. Med. Chem., 22 (2015) 783-798.

12. R. Hausmann, A. Kless, G. Schmalzing, Key sites for P2X receptor function and multimerization: overview of mutagenesis studies on a structural basis, Curr. Med. Chem., 22 (2015) 799-818.

13. R.A. North, Molecular physiology of P2X receptors, Physiol. Rev., 82 (2002) 1013-1067.

14. G. Burnstock, C. Kennedy, P2X receptors in health and disease, Adv. Pharmacol., 61 (2011) 333-372.

15. G. Burnstock, Purinergic signalling and disorders of the central nervous system, Nat. Rev. Drug Discov., 7 (2008) 575-590.

16. C. Coddou, Z. Yan, T. Obsil, J.P. Huidobro-Toro, S.S. Stojilkovic, Activation and regulation of purinergic P2X receptor channels, Pharmacol. Rev., 63 (2011) 641-683.

17. V. Ralevic, P2X receptors in the cardiovascular system and their potential as therapeutic targets in disease, Curr. Med. Chem., 22 (2015) 851-865.

18. N.R. Jorgensen, S. Syberg, M. Ellegaard, The role of P2X receptors in bone biology, Curr. Med. Chem., 22 (2015) 902-914.

19. C. Fotino, A. Vergani, P. Fiorina, A. Pileggi, P2X receptors and diabetes, Curr. Med. Chem., 22 (2015) 891-901.

20. F. Di Virgilio, P2X receptors and inflammation, Curr. Med. Chem., 22 (2015) 866-877.

21. G. Burnstock, Physiopathological roles of P2X receptors in the central nervous system, Curr. Med. Chem., 22 (2015) 819-844.

22. T. Bele, E. Fabbretti, P2X receptors, sensory neurons and pain, Curr. Med. Chem., 22 (2015) 845-850.

23. E. Adinolfi, M. Capece, F. Amoroso, E. De Marchi, A. Franceschini, Emerging roles of P2X receptors in cancer, Curr. Med. Chem., 22 (2015) 878-890.

24. C.E. Muller, Medicinal chemistry of P2X receptors: allosteric modulators, Curr. Med. Chem., 22 (2015) 929-941.

25. C. Lambertucci, D. Dal Ben, M. Buccioni, G. Marucci, A. Thomas, R. Volpini, Medicinal chemistry of P2X receptors: agonists and orthosteric antagonists, Curr. Med. Chem., 22 (2015) 915-928.

26. C.C. Chen, A.N. Akopian, L. Sivilotti, D. Colquhoun, G. Burnstock, J.N. Wood, A P2X purinoceptor expressed by a subset of sensory neurons, Nature, 377 (1995) 428-431.

27. C. Lewis, S. Neidhart, C. Holy, R.A. North, G. Buell, A. Surprenant, Coexpression of P2X2 and P2X3 receptor subunits can account for ATP-gated currents in sensory neurons, Nature, 377 (1995) 432-435.

28. E.J. Bradbury, G. Burnstock, S.B. McMahon, The expression of P2X3 purinoreceptors in sensory neurons: effects of axotomy and glial-derived neurotrophic factor, Mol. Cell. Neurosci., 12 (1998) 256-268.

29. P.M. Dunn, Y. Zhong, G. Burnstock, P2X receptors in peripheral neurons, Prog. Neurobiol., 65 (2001) 107-134.

30. M.F. Jarvis, Contributions of P2X3 homomeric and heteromeric channels to acute and chronic pain, Expert Opin. Ther. Targets, 7 (2003) 513-522.

31. B.A. Chizh, P. Illes, P2X receptors and nociception, Pharmacol. Rev., 53 (2001) 553-568.

32. V. Souslova, P. Cesare, Y. Ding, A.N. Akopian, L. Stanfa, R. Suzuki, K. Carpenter, A. Dickenson, S. Boyce, R. Hill, D. Nebenuis-Oosthuizen, A.J. Smith, E.J. Kidd, J.N. Wood, Warm-coding deficits and aberrant inflammatory pain in mice lacking P2X3 receptors, Nature, 407 (2000) 1015-1017.

33. D.A. Cockayne, S.G. Hamilton, Q.M. Zhu, P.M. Dunn, Y. Zhong, S. Novakovic, A.B. Malmberg, G. Cain, A. Berson, L. Kassotakis, L. Hedley, W.G. Lachnit, G. Burnstock, S.B. McMahon, A.P. Ford, Urinary bladder hyporeflexia and reduced pain-related behaviour in P2X3-deficient mice, Nature, 407 (2000) 1011-1015.

34. X. Bian, J. Ren, M. DeVries, B. Schnegelsberg, D.A. Cockayne, A.P. Ford, J.J. Galligan, Peristalsis is impaired in the small intestine of mice lacking the P2X3 subunit, J. Physiol., 551 (2003) 309-322.

35. M.G. Rae, E.G. Rowan, C. Kennedy, Pharmacological properties of P2X3-receptors present in neurones of the rat dorsal root ganglia, Br. J. Pharmacol., 124 (1998) 176-180.

36. E. Fabbretti, M. D'Arco, A. Fabbro, M. Simonetti, A. Nistri, R. Giniatullin, Delayed upregulation of ATP P2X3 receptors of trigeminal sensory neurons by calcitonin gene-related peptide, J. Neurosci., 26 (2006) 6163-6171.

37. A.P. Ford, J.R. Gever, P.A. Nunn, Y. Zhong, J.S. Cefalu, M.P. Dillon, D.A. Cockayne, Purinoceptors as therapeutic targets for lower urinary tract dysfunction, Br. J. Pharmacol., 147 Suppl 2 (2006) S132-143.

38. G. Burnstock, Therapeutic potential of purinergic signalling for diseases of the urinary tract, BJU Int., 107 (2011) 192-204.

39. J.D. Brederson, M.F. Jarvis, Homomeric and heteromeric P2X3 receptors in peripheral sensory neurons, Curr. Opin. Investig. Drugs, 9 (2008) 716-725.

40. K. Wirkner, B. Sperlagh, P. Illes, P2X(3) Receptor Involvement in Pain States, Mol. Neurobiol., 36 (2007) 165-183.

41. E. Sokolova, A. Skorinkin, E. Fabbretti, L. Masten, A. Nistri, R. Giniatullin, Agonist-dependence of recovery from desensitization of P2X(3) receptors provides a novel and sensitive approach for their rapid up or downregulation, Br. J. Pharmacol., 141 (2004) 1048-1058.

42. R. Volpini, R.C. Mishra, D.D. Kachare, D. Dal Ben, C. Lambertucci, I. Antonini, S. Vittori, G. Marucci, E. Sokolova, A. Nistri, G. Cristalli, Adenine-Based Acyclic Nucleotides as Novel $P2X_3$ Receptor Ligands, J. Med. Chem., 52 (2009) 4596-4603.

43. S.G. Brown, Y.-C. Kim, S.-A. Kim, K.A. Jacobson, G. Burnstock, K.B. F., Actions of a Series of PPADS Analogs at P2X1 and P2X3 Receptors, Drug Dev. Res. 53 (2001) 281-291.

44. C. Brown, B. Tanna, M.R. Boarder, PPADS: an antagonist at endothelial P2Y-purinoceptors but not P2U-purinoceptors, Br. J. Pharmacol., 116 (1995) 2413-2416.

45. M.F. Jarvis, E.C. Burgard, S. McGaraughty, P. Honore, K. Lynch, T.J. Brennan, A. Subieta, T. Van Biesen, J. Cartmell, B. Bianchi, W. Niforatos, K. Kage, H. Yu, J. Mikusa, C.T. Wismer, C.Z. Zhu, K. Chu, C.H. Lee, A.O. Stewart, J. Polakowski, B.F. Cox, E. Kowaluk, M. Williams, J. Sullivan, C. Faltynek, A-317491, a novel potent and selective non-nucleotide antagonist of P2X3 and P2X2/3

receptors, reduces chronic inflammatory and neuropathic pain in the rat, Proc. Natl. Acad. Sci. U. S. A., 99 (2002) 17179-17184.

46. E.C. Burgard, W. Niforatos, T. van Biesen, K.J. Lynch, K.L. Kage, E. Touma, E.A. Kowaluk, M.F. Jarvis, Competitive antagonism of recombinant P2X(2/3) receptors by 2', 3'-O-(2,4,6-trinitrophenyl) adenosine 5'-triphosphate (TNP-ATP), Mol. Pharmacol., 58 (2000) 1502-1510.

47. D. Carter, M.P. Dillon, R.C. Hawley, C.J.J. Lin, D.W. Parish, C.A. Broka, A. Jahangir, Diaminopyrimidines as $P2X_3$ and $P2X_{2/3}$ antagonists, 2005, WO2005095359.

48. D.S. Carter, M. Alam, H. Cai, M.P. Dillon, A.P. Ford, J.R. Gever, A. Jahangir, C. Lin, A.G. Moore, P.J. Wagner, Y. Zhai, Identification and SAR of novel diaminopyrimidines. Part 1: The discovery of RO-4, a dual P2X(3)/P2X(2/3) antagonist for the treatment of pain, Bioorg. Med. Chem. Lett., 19 (2009) 1628-1631.

49. C.E. Muller, Emerging structures and ligands for P2X(3) and P2X(4) receptors-towards novel treatments of neuropathic pain, Purinergic Signal., 6 (2010) 145-148.

50. C. Lambertucci, M. Sundukova, D.D. Kachare, D.S. Panmand, D. Dal Ben, M. Buccioni, G. Marucci, A. Marchenkova, A. Thomas, A. Nistri, G. Cristalli, R. Volpini, Evaluation of adenine as scaffold for the development of novel P2X3 receptor antagonists, Eur. J. Med. Chem., 65C (2013) 41-50.

51. T. Kawate, J.C. Michel, W.T. Birdsong, E. Gouaux, Crystal structure of the ATP-gated P2X4 ion channel in the closed state, Nature, 460 (2009) 592-598.

52. M. Hattori, E. Gouaux, Molecular mechanism of ATP binding and ion channel activation in P2X receptors, Nature, 485 (2012) 207-212.

53. D. Dal Ben, M. Buccioni, C. Lambertucci, G. Marucci, A. Thomas, R. Volpini, Purinergic P2X receptors: structural models and analysis of ligand-target interaction, Eur. J. Med. Chem., 89 (2015) 561-580.

54. C. Virginio, G. Robertson, A. Surprenant, R.A. North, Trinitrophenyl-substituted nucleotides are potent antagonists selective for P2X1, P2X3, and heteromeric P2X2/3 receptors, Mol. Pharmacol., 53 (1998) 969-973.

55. M. Morales, N. McCollum, E.F. Kirkness, 5-HT(3)-receptor subunits A and B are co-expressed in neurons of the dorsal root ganglion, J. Comp. Neurol., 438 (2001) 163-172.

56. R. Nicholson, J. Small, A.K. Dixon, D. Spanswick, K. Lee, Serotonin receptor mRNA expression in rat dorsal root ganglion neurons, Neurosci. Lett., 337 (2003) 119-122.

57. Stoyanova, II, Gamma-aminobutiric acid immunostaining in trigeminal, nodose and spinal ganglia of the cat, Acta Histochem., 106 (2004) 309-314.

58. W.P. Hu, X.H. You, B.C. Guan, L.Q. Ru, J.G. Chen, Z.W. Li, Substance P potentiates 5-HT3 receptor-mediated current in rat trigeminal ganglion neurons, Neurosci. Lett., 365 (2004) 147-152.

59. J.G. Douglass, S.R. Shaver, T. Navratil, J.L. Boyer, C.A. Samuelson, J.B. DeCamp, Method for treating inflammatory conditions, 2010, WO2010080540A1.

60. P.L. Martin, T.W. Gero, A.A. Potts, N.J. Cusack, Structure-activity studies of analogs of β,γ-methylene-ATP at P2X-purinoceptors in the rabbit ear central artery, Drug Dev. Res., 36 (1995) 153-165.

61. E. Sokolova, A. Skorinkin, I. Moiseev, A. Agrachev, A. Nistri, R. Giniatullin, Experimental and modeling studies of desensitization of P2X3 receptors, Mol. Pharmacol., 70 (2006) 373-382.

62. *Molecular Operating Environment*, C.C.G., Inc., 1255 University St., Suite 1600, Montreal, Quebec, Canada, H3B 3X3.

63. J.J. Stewart, MOPAC: a semiempirical molecular orbital program, J. Comput. Aided Mol. Des., 4 (1990) 1-105.

64. W.D. Cornell, P. Cieplak, C.I. Bayly, I.R. Gould, K.M. Merz, D.M. Ferguson, D.C. Spellmeyer, T. Fox, J.W. Caldwell, P.A. Kollman, A Second Generation Force Field for the Simulation of Proteins, Nucleic Acids, and Organic Molecules, J. Am. Chem. Soc., 117 (1995) 5179-5197.

65. T.A. Halgren, Merck Molecular Force Field. I. Basis, Form, Scope, Parameterization, and Performance of MMFF94, J. Comput. Chem., 17 (1996) 490-519.

66. T.A. Halgren, Merck Molecular Force Field. II. MMFF94 van der Waals and Electrostatic Parameters for Intermolecular Interactions, J. Comput. Chem., 17 (1996) 520-552.

67. T.A. Halgren, Merck Molecular Force Field. III. Molecular Geometries and Vibrational Frequencies for MMFF94, J. Comput. Chem., 17 (1996) 553-586.

68. T.A. Halgren, Merck Molecular Force Field. IV. Conformational Energies and Geometries for MMFF94, J. Comput. Chem., 17 (1996) 587-615.

69. T.A. Halgren, R. Nachbar, Merck Molecular Force Field. V. Extension of MMFF94 Using Experimental Data, Additional Computational Data, and Empirical Rules, J. Comput. Chem., 17 (1996) 616-641.

70. T.A. Halgren, MMFF VI. MMFF94s Option for Energy Minimization Studies, J. Comput. Chem., 20 (1999) 720-729.

71. T.A. Halgren, MMFF VII. Characterization of MMFF94, MMFF94s, and Other Widely Available Force Fields for Conformational Energies and for Intermolecular-Interaction Energies and Geometries, J. Comput. Chem., 20 (1999) 730-748.

72. M. Simonetti, A. Fabbro, M. D'Arco, M. Zweyer, A. Nistri, R. Giniatullin, E. Fabbretti, Comparison of P2X and TRPV1 receptors in ganglia or primary culture of trigeminal neurons and their modulation by NGF or serotonin, Mol. Pain, 2 (2006) 11.

73. M. Sundukova, S. Vilotti, R. Abbate, E. Fabbretti, A. Nistri, Functional differences between ATP-gated human and rat P2X3 receptors are caused by critical residues of the intracellular C-terminal domain, J. Neurochem., 122 (2012) 557-567.

Supporting Information

P2X3 receptor sequence conservation

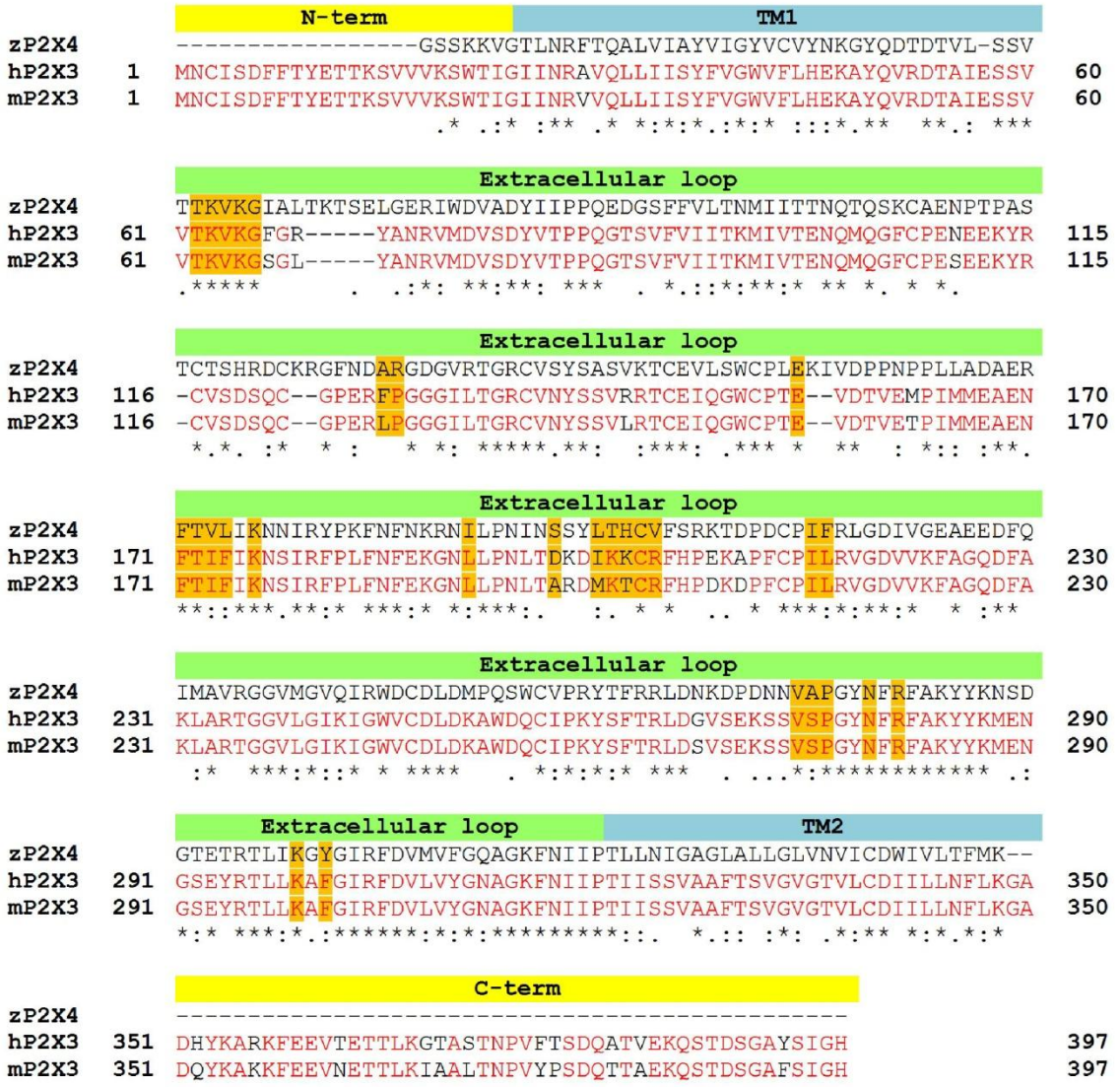

Fig. SI1. Sequence alignment of the human and mouse P2X3 sequences (hP2X3 and mP2X3, respectively). The sequence of zP2X4 has been inserted as belonging to the P2X crystal structure used as template for homology modelling steps. Star (*) symbols indicate identical residues in zP2X4, hP2X3, and mP2X3. Red residues indicate identical aminoacids in hP2X3 and mP2X3. Residues located in the proximity (6Å) of ATP are indicated with orange background.

The human and mouse P2X3 sequences are 93.7% identical; the identity degree considering the residues in the proximity of ATP is 86.2%.

ATP-bound human and mouse P2X3 receptors: the binding cavities in complex with ATP

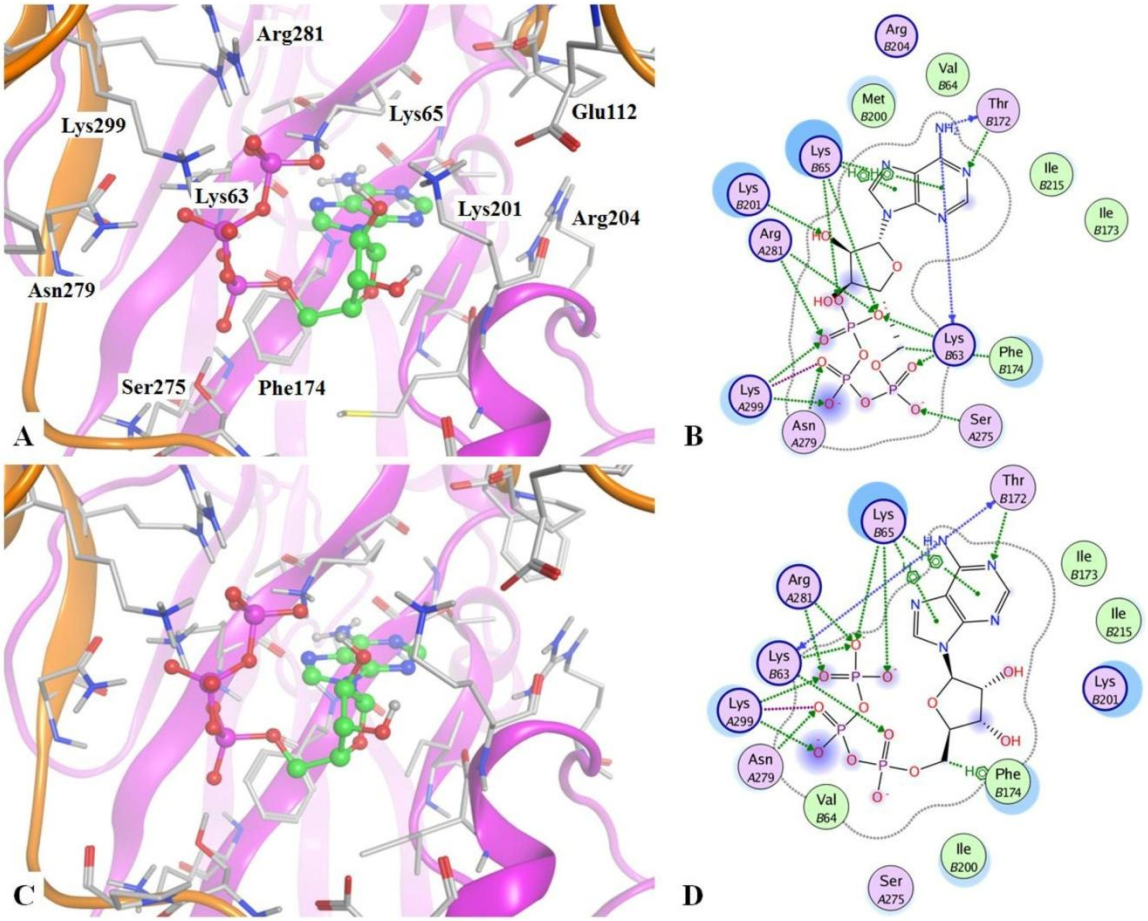

Fig. SI2. Docking conformations of ATP at the human (A-B) and mouse (C-D) P2X3. Residue numbers are indicated only for human ATP cavity as the corresponding region of mP2X3 contains identical residues.

Docking conformation of TNP-ATP at the mouse P2X3 receptor

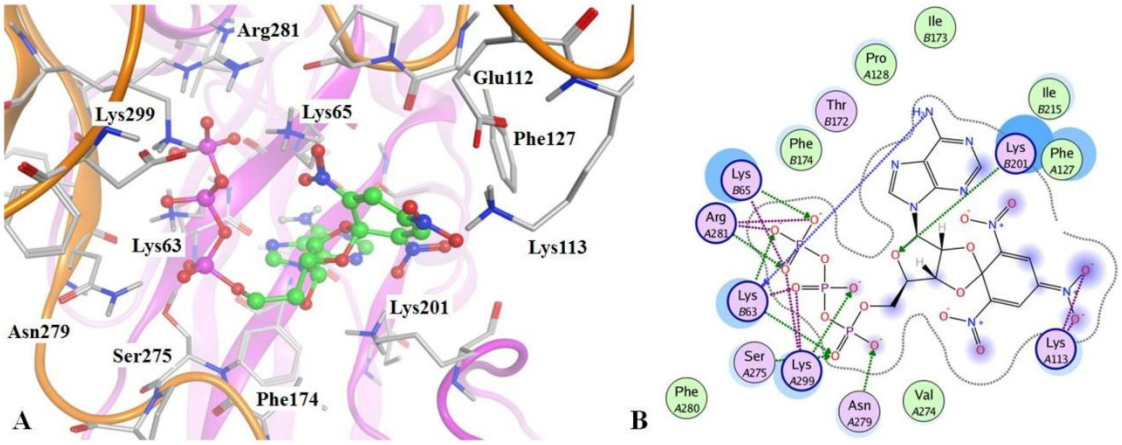

Fig. SI3. Docking conformations of TNP-ATP at the mouse P2X3 binding site.

Docking conformation of synthesised triphosphate derivatives at the mouse P2X3 receptor

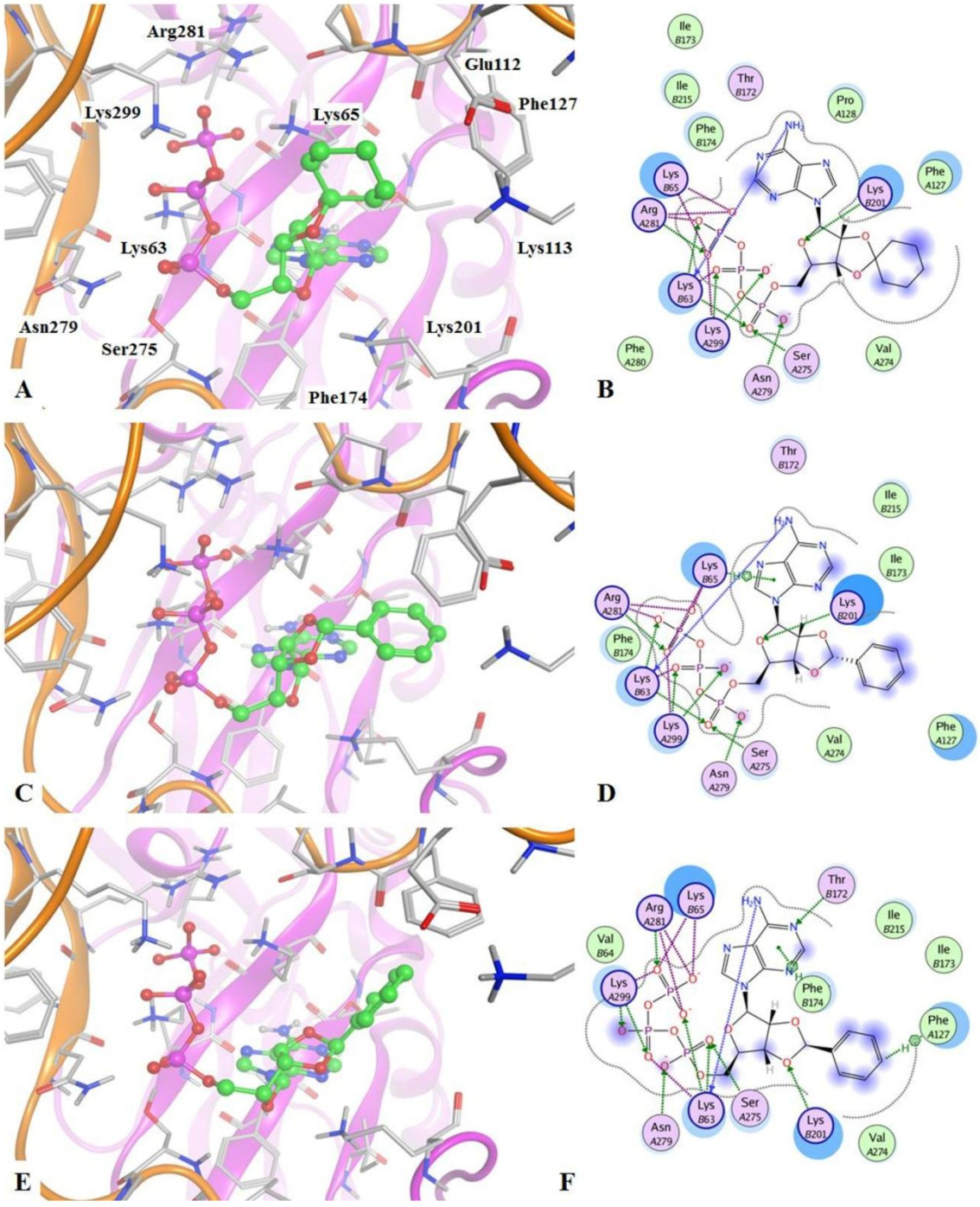

Fig. SI4. Docking conformations of **PF 94** (A-B), **PF 95** (C-D), and **PF 96** (E-F) at the mouse P2X3 binding site.

Docking conformation of synthesised triphosphate derivatives at the human P2X3 receptor

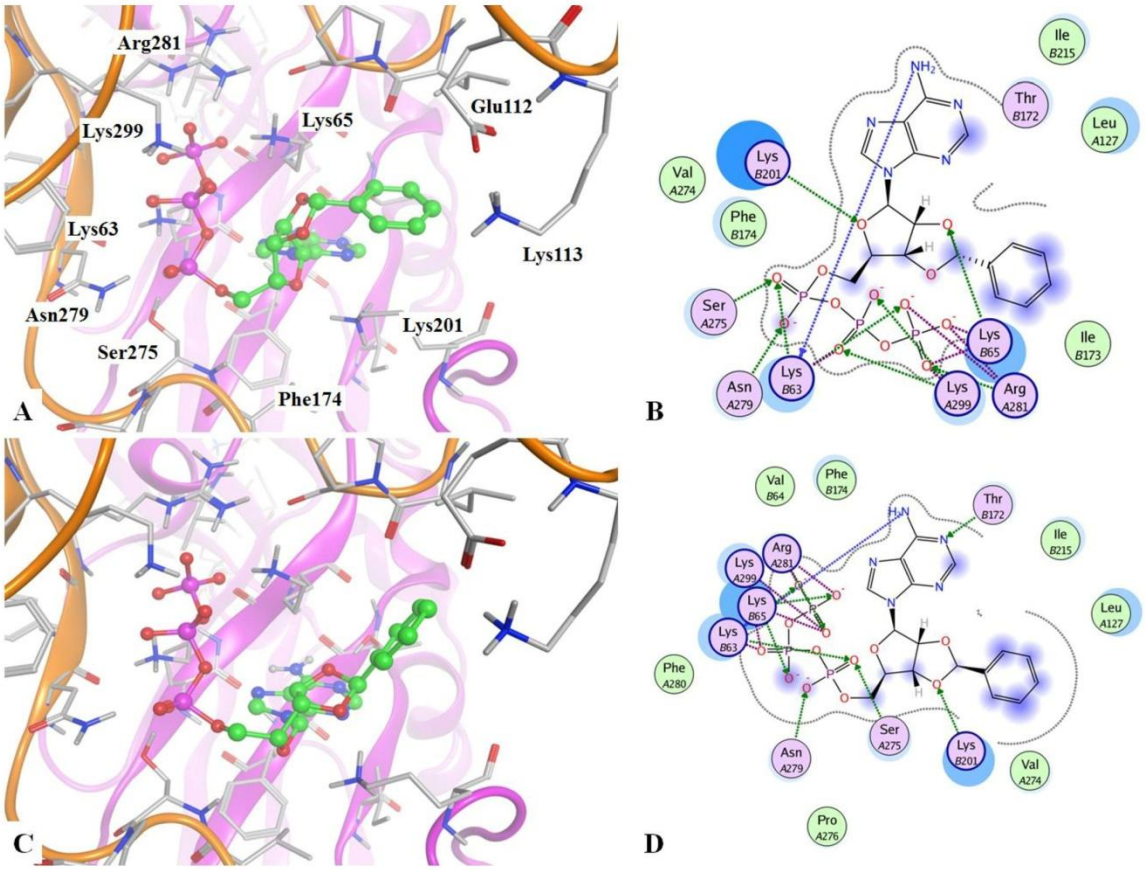

Fig. SI5. Docking conformations of **PF 95** (A-B), and **PF 96** (C-D) at the human P2X3 binding site.

Discussion

Activity of neurons in central and peripheral pain pathways is regulated by a variety of chemical substances that shape pain perception and transduction. Important targets for such modulation are ion channels expressed on the membranes of sensory neurons in trigeminal and dorsal root ganglia (TG and DRG). In particular, ATP-gated P2X3 receptors and capsaicin-sensitive TRPV1 receptors play a critical role in nociception and are proposed to contribute to the development of various pathological pain conditions, including migraine [26,52,65,443,444]. Although many endogenous peptides and trophic factors are reported to upregulate the function of these receptors [76,445,446], much less is known about the potential role of endogenous modulators in restraining the operation of TRPV1 and P2X3 receptors.

BNP/NPR-A pathway in WT and KI trigeminal neurons

Until recently, natriuretic peptides were regarded only in terms of their role in regulating blood pressure and heart function [175,188]. However, growing evidence suggested the importance of natriuretic peptides for nociception, and their ability to exhibit contrasting effects on pain transduction under normal conditions as well as in pathological states [270,272]. In particular, Zhang et al reported BNP and NPR-A expression in the rat DRG, and the fact that their signaling can attenuate inflammatory pain [271].

In the present study our first goal was to characterize the BNP/NPR-A system in trigeminal neurons of WT mice and in a mouse model of FHM1. Experiments on WT and KI mouse TG showed NPR-A expression in the vast majority of neurons *in vivo* and *in vitro*. Moreover, the activity of the NPR-A pathway was similar in these two genotypes and included stimulation of cGMP production, Akt phosphorylation and activation of PKG. Interestingly, like NPR-A, BNP itself both in WT and in KI cultures was produced at rather low level and mostly by non-neuronal cells. Even though KI exhibited a slightly higher percent of BNP-expressing cells, the total BNP concentration in the culture medium was identical to that of WT, suggesting a comparable degree of basal NPR-A activation. Considering the question of the principal endogenous agonist of NPR-A receptors in TG, current evidence supports the idea of BNP serving as the main ligand. Apart from BNP, NPR-A receptors could in theory be activated by atrial natriuretic peptide (ANP) whose RNA was shown to be present in trigeminal ganglion [276,277]. However, the complete similarity between the effects of NPR-A blocker anantin and silencing of BNP RNA suggests that BNP and not ANP is the main peptide for BNP/NPR-A regulation, at least for P2X3 receptors.

Experiments on inactivation of the NPR-A pathway further supported the idea of equal basal BNP/NPR-A activity in WT and KI cultures, showing similar reduction in cGMP levels in WT and KI after siBNP or application of NPR-A antagonist anantin. Thus, the expression and basal activity of the BNP/NPR-A system in KI neurons appear to be very similar to what is observed in WT cultures, implying that any changes in functional properties of this pathway should be explained in terms of more subtle regulatory mechanisms.

Regulation of TRPV1 receptors by exogenous BNP in WT and KI trigeminal neurons

TRPV1 channels, being important transducers of noxious stimuli and potential players in migraine pathophysiology [124,169,444], were the first target for our investigation of BNP/NPR-A functions in TG primary cultures. Our data show that, although the basal activity of the BNP/NPR-A pathway does not alter TRPV1-mediated responses, rather low concentrations of exogenous BNP (100 ng/ml) significantly depressed TRPV1 currents of WT neurons as well as KI. This might indicate the need for additional stimuli, which by raising BNP concentration could control the activity of trigeminal neurons and in particular their TRPV1 receptors. This is consistent with what is known about other neuropeptides, like vasoactive intestinal polypeptide, galanin and NPY, which are normally expressed at low or undetectable levels in sensory neurons and a specific stimulus is required for these peptides to be upregulated [447]. Interestingly, notwithstanding rapid changes in cGMP and pAkt levels following NPR-A activation by BNP, the onset of TRPV1 modulation was delayed by hours, suggesting a complex molecular cascade underneath this regulation that triggers comparatively slow modifications in neuronal activity. A similar phenomenon is also typical of other TRPV1 modulators, such as the growth factors NGF and GDNF [448] or the cytokine TNF-α [449]. The effect of delayed BNP-induced modulation would be compatible with a role of BNP in controlling chronic rather than acute pain. The exact molecular mechanisms underneath BNP-induced TRPV1 modulation remain unclear and require further investigation. However, our data could rule out some potential processes. Thus, no change in total TRPV1 expression level associated with receptor inhibition suggested a subtle mechanism to control TRPV1 activity, like for instance, the level of phosphorylation, trafficking and receptor compartmentalization.

It is worth noting that modulation of TRPV1 receptor function by BNP proved to be reversible, disappearing after NPR-A inactivation with anantin. Thus, BNP/NPR-A influence on TRPV1 receptors appears to be dynamic and sensitive to changes in the environmental conditions, especially the endogenous BNP concentration. Considering possible causes for BNP upregulation, a recent study showed higher concentrations of plasma BNP precursor in migraine patients compared to healthy controls [450]. Thus, we could speculate that, even though under normal conditions, the level of endogenous BNP in TG is not enough to downregulate TRPV1 receptors, in migraine pathology it might become sufficiently high because of elevated levels of BNP in the bloodstream: this phenomenon might serve to prevent exaggerated nociceptive responses. Experiments in vivo are necessary to clarify this suggestion.

Regulation of P2X3 receptors by endogenous BNP in trigeminal neurons of WT and KI mice

ATP-gating P2X3 receptors, which are mostly expressed by sensory neurons, play an important role in nociception under normal as well as pathological conditions [26], including migraine pathology [32,63–65]. In particular, the activity of P2X3 receptors is crucial for trigeminal ganglia. Enhanced functional properties of TG sensory neurons are thought to

underlie neuronal sensitization, facilitating the onset of chronic pain attacks, including migraine [63,303,331,348]. Thus, our next goal was to understand how the BNP/NPR-A system affects P2X3 receptors in WT trigeminal cultures as well as in cultures from KI mice of R192Q FHM1 migraine model.

Unlike TRPV1 receptors, P2X3 receptor activity of WT or KI neurons was not influenced by activation of NPR-A with exogenous BNP. However, in WT cultures suppressing basal BNP/NPR-A signaling with either siBNP or the NPR-A inhibitor anantin greatly enhanced P2X3 receptors. Such findings imply that, under basal conditions, P2X3 receptors in WT trigeminal neurons are constantly inhibited by endogenous BNP. Although the level of endogenous BNP in TG was low, it was apparently sufficient for NPR-A-dependent P2X3 modulation because increasing the BNP concentration did not lead to stronger P2X3 inhibition. Thus, the BNP/NPR-A system in TG can operate on different levels, inhibiting several pain-sensing modalities (P2X3 and TRPV1) depending on the extracellular BNP concentration.

In WT neurons the BNP-dependent P2X3 regulation seemed almost all-or-none, without gradual changes in the size of P2X3 currents. Although the molecular mechanisms involved in this modulation remain incompletely understood, our experiments identified several processes that are employed by the BNP/ NPR-A system to suppress P2X3-mediated responses. Thus, one contribution was likely to originate from the delayed onset of P2X3 receptor desensitization, an important parameter that controls current amplitude and pain signaling [63]. We also showed two distinct mechanisms (downstream of PKG activation) that restrained P2X3 receptors in WT neurons, namely, increased P2X3 serine phosphorylation and receptor redistribution from lipid rafts to non-raft membrane compartments. Interestingly, in KI trigeminal neurons the same P2X3 properties were reversed and associated with enhanced P2X3 activity. Thus, the KI phenotype was characterized by larger P2X3-mediated currents, lower level of P2X3 p-Ser and more P2X3 receptors in the lipid raft membrane fraction. These observations, therefore, suggested loss of NPR-A-dependent downregulation of P2X3 receptors in KI trigeminal neurons. The idea was further supported by the fact that inactivation of BNP/NPR-A pathway in KI cultures did not upregulate P2X3 responses, indicating absence of basal constituitive inhibition typical for P2X3 receptors of WT neurons.

As to the mechanisms that make P2X3 receptors of KI neurons apparently disjointed from BNP/NPR-A constitutive inhibition, our study investigated the influence of CaV2.1 calcium channels and CGRP in this process. In KI trigeminal cultures, the R192Q mutation leads to the gain-of-function of CaV2.1 calcium channels that in turn determine the development of a distinct KI phenotype. In particular, this involves upregulation of P2X3 receptors and activity of the CGRP pathway. We showed that reversing KI phenotype with the inhibitors of CaV 2.1 channels or CGRP receptors could restore the negative control of BNP/NPR-A system over P2X3 activity that was unmasked by blocking NPR-A signaling with anantin. The present data suggest that there are multiple processes impacting on the function of trigeminal P2X3 receptors, and that these mechanisms are potent enough to overcome

constitutive inhibition by BNP, at least in this genetic model of migraine. The process of P2X3 upregulation underlying trigeminal sensitization to pain [52,348] might be triggered because "migraine mediators" like CGRP and other endogenous algogens swamp the normal negative control that maintains a physiological pain threshold. While additional experiments are required to clarify the exact molecular mechanisms involved in this process, identifying strategies to enhance intrinsic inhibition, even at peripheral level, may be useful to control pain.

BNP/NPR-A system negatively regulates P2X3-induced firing of TG neurons in WT but not in KI cultures

Sensory neurons encode their responses to received stimuli as a series of action potentials. The neuronal excitability and firing properties are, therefore, aspects of greatest interest as they are the major determinants to convey activation of brainstem trigeminal nuclei. Trigeminal neurons in culture express diverse voltage gated and ligand gated ion channels and a wide array of metabotropic receptors which collectively control neuronal excitability. Activation of ATP-gated P2X3 channels and capsaicin-sensitive TRPV1 channels can induce firing activity that in higher brain regions is interpreted as pain signals [66,282]. Thus, the next question was if the constitutive modulatory effects of BNP/NPR-A system on P2X3 receptor activity could be reflected in changing the excitability of trigeminal neurons.

In WT and KI neurons similar patterns of firing activity were observed in response to different stimuli, comprising intracellular current pulses, application of α,β-meATP or capsaicin, in analogy with a previous report [66]. However, the distributions of these patterns in the examined WT and KI populations had some significant differences, especially prominent in case of P2X3-dependent firing activity.

Under normal circumstances, trigeminal neurons are relatively quiescent, but they produce highly modulated series of action potentials when stimulated, conveying information about the sensory stimuli to higher brain regions [278]. In some pathological conditions, however, primary sensory neurons can become hyperexcitable and can give rise to unprovoked spontaneous action potential activity or bursting which can contribute to chronic pain [279–281]. A hyperexcitability phenotype had been previously reported for trigeminal neurons of FHM1 mouse migraine model [66]. In line with this notion, in our experiments KI cultures exhibited lower percent of SS and NS cells and higher percent of MF cells when stimulated with α,β-meATP. The discrepancy between WT and KI cultures could probably be explained by upregulated P2X3 receptor currents typical for KI phenotype [64]. Higher-amplitude currents in response to the same agonist concentration may lead to increased firing activity of TG neurons, transforming for example SS cell into FA or MF.

Larger occurrence of MF and RF neurons at the expense of NS and SS cells in KI cultures might also be a consequence of other differences between WT and KI trigeminal sensory neurons, namely the lower spike threshold in KI versus WT cells [66]. Lower threshold for action potentials was understandably associated with a statistically larger number of spikes in KI cultures, averaged for all firing pattern types, as well as increased spike number for MF

group in particular. Thus, lower firing threshold can elevate general level of KI TG neuron excitability. In response to the same extracellular ATP concentration KI neurons are expected to generate, on average, more spikes, meaning at least partial transformation of former NS cells into SS, SS to FA, FA to MF and RF ones.

Anantin brings the WT low excitability profile close to the KI hyperexcitability state

Recent studies proposed BNP as a potential endogenous anti-inflammatory and anti-pain modulator, which, acting through its receptor NPR-A, inhibits excitability of sensory DRG neurons and constantly downregulates P2X3 receptors in TG [271,451] Marchenkova). In the present project, we obtained additional evidence in support of the idea that BNP/NPR-A pathway pays an important role in depressing the excitability of sensory neurons, especially in the case of P2X3-dependent firing. Indeed, negative control over P2X3 receptor activity in trigeminal neurons apparently suppresses their excitability in response to α,β-meATP, which is an analog of the natural ligand ATP and simulates a situation when ATP is released in TG.

It is noteworthy that inactivation of BNP/NPR-A signaling transformed the WT excitability phenotype into the one usually associated with KI. Thus, it decreased spike threshold, increased the average number of action potentials generated in response to α,β-meATP application and, as a consequence, changed the distribution of firing activity types in WT cultures towards the prevalence of higher excitability patterns. This phenomenon mostly concerned trigeminal P2X3-dependent excitability, and did not affect responces to current injections or capsaicin. It is, therefore, possible to argue that, under normal conditions, the WT NPR-A pathway, activated by endogenous BNP [451] dampens neuronal excitability in response to extracellular ATP. In the R192Q KI mouse model, the BNP/NPR-A system activity is unable to overcome the P2X3 upregulation typical for this phenotype. Taken together, our data suggest that hyperexcitability phenotype of trigeminal sensory neurons of FHM1 migraine model could originate from insufficient BNP/NPR-A-mediated negative control over P2X3 receptor activity. The exact mechanisms underlying this modulation remain to be clarified.

New P2X3 antagonists on the basis of diaminopurine and adenosine scaffolds

Nowadays, development of new potent and potentially therapeutic P2X3 antagonists becomes more and more popular among basic scientists and pharmaceutical companies. This is considered as a promising strategy in order to advance research in the area of P2X3 functions in health and disease and, most importantly, to create new drugs for a variety of P2X3-related pathologies. In the current study we aimed at testing the adenine scaffold as possible new basis for the development of P2X3 antagonists. The designed series of 2-aminoadenine derivatives were proved to behave as P2X3 receptor antagonists when tested on recombinant rat P2X3 receptors expressed in HEK cells. The most promising compound 9-(5- iodo-2-isopropyl-4-methoxybenzyl)-N6 -methyl-9H-purine-2,6- diamine (24) appeared to be a good antagonist on both recombinant rat P2X3 receptors as well as on native P2X3 receptors of mouse trigeminal neurons, with IC_{50} in the μM range. Thus, new synthesised

adenine-based compounds exhibited P2X3 antagonist activity, even if with lower potency compared to the corresponding diaminopyrimidines taken as reference compounds. These results are encouraging since the high versatility of the adenine scaffold allows the insertion of different substituents into several positions of the purine moiety.
Further investigation and molecular modeling studies, performed at homology models of the P2X3, proposed several TNP-ATP analogues for the role of P2X3 antagonists. Patch-clamp experiments confirmed antagonistic potency of new compounds. Most potent molecules (2',3'-*O*-cyclohexylATP, 2',3'-*O*-benzylATP) appeared to be potent inhibitors of the P2X3 receptors (IC_{50} in nanomolar range), with selectivity against GABA and 5-HT receptors.
Future investigation into the effect of these modifications on P2X3 antagonism could promote the development of new agents for the treatment of various conditions including neuropathic, inflammatory and migraine pain.

Conclusion

Figure 31 summarises our view on the functional properties of BNP/NPR-A pathway in trigeminal sensory neurons of WT mice and FHM1 mouse migraine model. The primary finding of the present study is the demonstration that in cultures of WT trigeminal ganglion the BNP/NPR-A pathway can efficiently downregulate the activity of pain-sensing P2X3 and TRPV1 receptors (Fig. 31, A). The process of P2X3 inhibition is PKG-dependent and is associated with receptor's serine phosphorylation and redistribution from lipid rafts to non-raft membrane compartments (Fig. 31, A). Consistent with tonic downregulation of P2X3 receptors, NPR-A pathway also negatively controls P2X3-dependent firing activity of trigeminal neurons. In contrast, in KI trigeminal cultures the BNP/NPR-A system loses its ability to effectively supress P2X3 receptor responses or P2X3-dependent neuronal excitability (Fig. 31, B). This phenomenon might be explained by the characteristic KI phenotype that exhibits an elevated Ca^{2+} influx through Cav 2.1 channels and an upregulated CGRP pathway. Other properties of the BNP/NPR-A pathways remain intact, including negative modulation of TRPV1 receptors by exogenous BNP (Fig. 31, B).
A variety of compounds, developed on the basis of diaminopurine and adenosine scaffolds, showed good antagonist activity on recombinant and native P2X3 receptors, with IC_{50} values in micromolar and nanomolar range, respectively. Thus, experimenting with diaminopurine and adenosine moiety could serve as a promising strategy in search for new potent antagonists of P2X3 receptors.

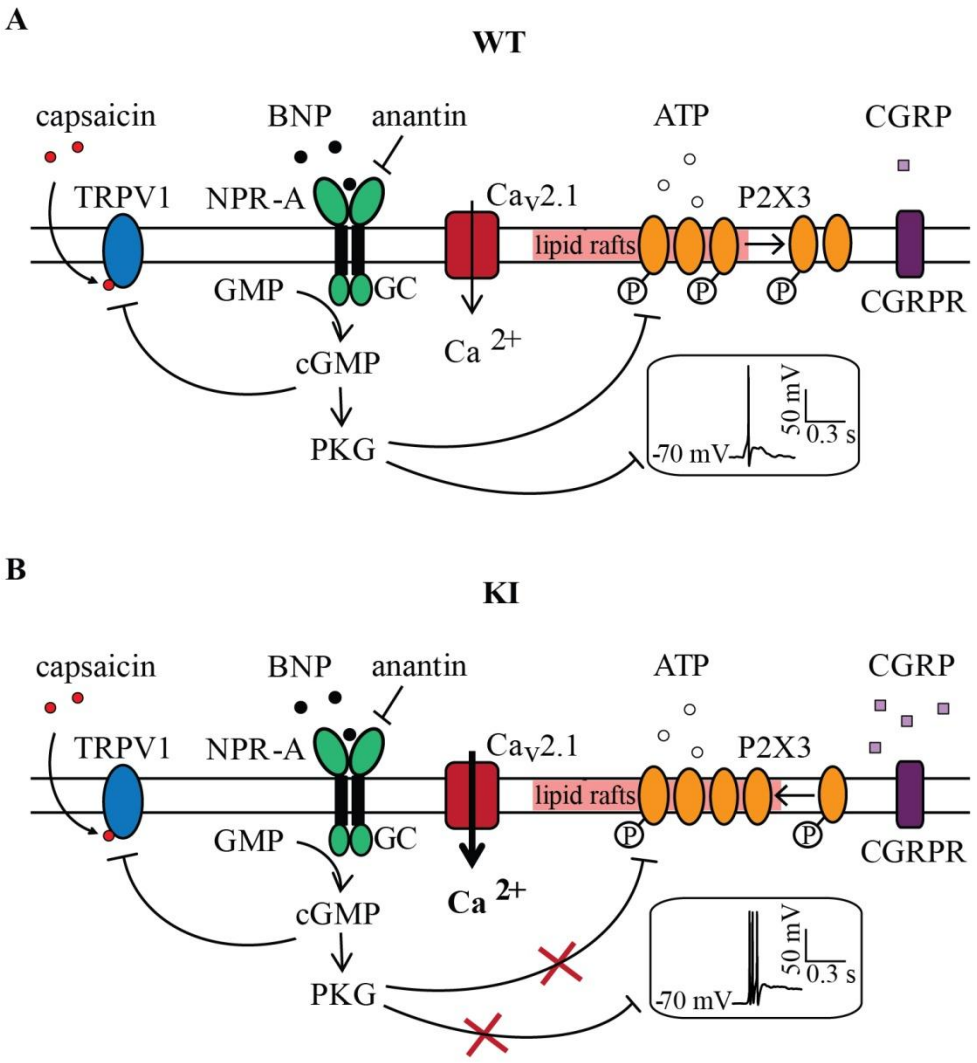

Figure 31. Schematic diagrams for the proposed functions of the BNP/NPR-A system in WT and KI trigeminal neurons. GC –guanylyl cyclase domain of NPR-A receptor; P – P2X3 serine phosphorylation; CGRPR – CGRP receptor.

Future perspectives

In the light of the current findings, several factors emerge which warrant to be extensively studied. The molecular pathways through which BNP is able to negatively regulate P2X3 and TRPV1 receptors require careful investigation. Although some of the intermediate steps and molecular targets have been indicated by current study, many remain still unknown.

The discrepancy between low level of BNP expression in TG and hight – of its receptor NPR-A, raises a question about possible conditions when the BNP production could be upregulated. Considering that BNP is synthesized mostly by non-neuronal cells, a potential crosstalk between neuronal and glia cells might be important for understanding the whole picture of BNP/NPR-A system operation. Thus, the role of non-neuronal cells in regulating the function of trigeminal neurons should be evaluated in detail, especially in relation to the KI phenotype, for which the importance of non-neuronal cells had been already reported [439].

The observed changes in subthreshold properties in the WT trigeminal neurons after inactivation of BNP/NPR-A signaling suggest alterations in voltage-dependent potassium or subthreshold sodium conductances, which have to be carefully studied. Interaction of different voltage- and ligand-gated ion channels and their co-operative behavior further need to be investigated in order to understand how their activity affects excitability of trigeminal sensoty neurons in normal conditions and in pathological models.

The present study presents a perspective which requires a collective approach to tackle the ligand and voltage gated channels for development of therapeutic targets. Further studies are required to evaluate possible targets along BNP/NPR-A pathway to treat chronic pain conditions and migraine pathologies effectively.

Future experiments with diaminopurine and especially adenosine derivatives could provide new copounds with even higher antagonist potency over P2X3 receptors and potentially good pharmacokinetic properties.

Bibliography

1. Bodin, P. & Burnstock, G. Purinergic signalling: ATP release. *Neurochem. Res.* **26,** 959–969 (2001).
2. Holton, P. The liberation of adenosine triphosphate on antidromic stimulation of sensory nerves. *J. Physiol. (Lond.)* **145,** 494–504 (1959).
3. Holton, F. A. & Holton, P. The capillary dilator substances in dry powders of spinal roots; a possible role of adenosine triphosphate in chemical transmission from nerve endings. *J. Physiol. (Lond.)* **126,** 124–140 (1954).
4. Burnstock, G., Cocks, T., Kasakov, L. & Wong, H. K. Direct evidence for ATP release from non-adrenergic, non-cholinergic ('purinergic') nerves in the guinea-pig taenia coli and bladder. *European Journal of Pharmacology* **49,** 145–149 (1978).
5. Jahr, C. E. & Jessell, T. M. ATP excites a subpopulation of rat dorsal horn neurones. *Nature* **304,** 730–733 (1983).
6. Krishtal, O. A., Marchenko, S. M. & Pidoplichko, V. I. Receptor for ATP in the membrane of mammalian sensory neurones. *Neuroscience Letters* **35,** 41–45 (1983).
7. Edwards, F. A., Gibb, A. J. & Colquhoun, D. ATP receptor-mediated synaptic currents in the central nervous system. *Nature* **359,** 144–147 (1992).
8. Evans, R. J., Derkach, V. & Surprenant, A. ATP mediates fast synaptic transmission in mammalian neurons. *Nature* **357,** 503–505 (1992).
9. Silinsky, E. m., Gerzanich, V. & Vanner, S. m. ATP mediates excitatory synaptic transmission in mammalian neurones. *British Journal of Pharmacology* **106,** 762–763 (1992).
10. Lazarowski, E. R., Boucher, R. C. & Harden, T. K. Mechanisms of Release of Nucleotides and Integration of Their Action as P2X- and P2Y-Receptor Activating Molecules. *Mol Pharmacol* **64,** 785–795 (2003).
11. Khakh, B. S. & North, R. A. Neuromodulation by extracellular ATP and P2X receptors in the CNS. *Neuron* **76,** 51–69 (2012).
12. Surprenant, A., Rassendren, F., Kawashima, E., North, R. A. & Buell, G. The Cytolytic P2Z Receptor for Extracellular ATP Identified as a P2X Receptor (P2X7). *Science* **272,** 735–738 (1996).
13. Brake, A. J., Wagenbach, M. J. & Julius, D. New structural motif for ligand-gated ion channels defined by an ionotropic ATP receptor. *Nature* **371,** 519–523 (1994).
14. Valera, S. *et al.* A new class of ligand-gated ion channel defined by P2x receptor for extracellular ATP. *Nature* **371,** 516–519 (1994).
15. Kawate, T., Michel, J. C., Birdsong, W. T. & Gouaux, E. Crystal structure of the ATP-gated P2X4 ion channel in the closed state. *Nature* **460,** 592–598 (2009).
16. Hattori, M. & Gouaux, E. Molecular mechanism of ATP binding and ion channel activation in P2X receptors. *Nature* **485,** 207–212 (2012).
17. Aschrafi, A., Sadtler, S., Niculescu, C., Rettinger, J. & Schmalzing, G. Trimeric architecture of homomeric P2X2 and heteromeric P2X1+2 receptor subtypes. *J. Mol. Biol.* **342,** 333–343 (2004).
18. Chen, C. C. *et al.* A P2X purinoceptor expressed by a subset of sensory neurons. *Nature* **377,** 428–431 (1995).
19. Lewis, C. *et al.* Coexpression of P2X2 and P2X3 receptor subunits can account for ATP-gated currents in sensory neurons. *Nature* **377,** 432–435 (1995).
20. Nicke, A. *et al.* P2X1 and P2X3 receptors form stable trimers: a novel structural motif of ligand-gated ion channels. *EMBO J.* **17,** 3016–3028 (1998).

21. North, R. A. Molecular physiology of P2X receptors. *Physiol. Rev.* **82,** 1013–1067 (2002).
22. Browne, L. E., Jiang, L.-H. & North, R. A. New structure enlivens interest in P2X receptors. *Trends Pharmacol. Sci.* **31,** 229–237 (2010).
23. Egan, T. M. & Khakh, B. S. Contribution of calcium ions to P2X channel responses. *J. Neurosci.* **24,** 3413–3420 (2004).
24. Kaczmarek-Hájek, K., Lörinczi, É., Hausmann, R. & Nicke, A. Molecular and functional properties of P2X receptors—recent progress and persisting challenges. *Purinergic Signal* **8,** 375–417 (2012).
25. Pankratov, Y. V., Lalo, U. V. & Krishtal, O. A. Role for P2X receptors in long-term potentiation. *J. Neurosci.* **22,** 8363–8369 (2002).
26. Burnstock, G. Physiopathological roles of P2X receptors in the central nervous system. *Curr. Med. Chem.* **22,** 819–844 (2015).
27. Burnstock, G. & Kennedy, C. P2X receptors in health and disease. *Adv. Pharmacol.* **61,** 333–372 (2011).
28. Burnstock, G., Fredholm, B. B., North, R. A. & Verkhratsky, A. The birth and postnatal development of purinergic signalling. *Acta Physiol (Oxf)* **199,** 93–147 (2010).
29. Jarvis, M. F. & Khakh, B. S. ATP-gated P2X cation-channels. *Neuropharmacology* **56,** 208–215 (2009).
30. Robertson, S. J., Ennion, S. J., Evans, R. J. & Edwards, F. A. Synaptic P2X receptors. *Current Opinion in Neurobiology* **11,** 378–386 (2001).
31. Fabbretti, E. & Nistri, A. Regulation of P2X3 receptor structure and function. *CNS Neurol Disord Drug Targets* **11,** 687–698 (2012).
32. Wirkner, K., Sperlagh, B. & Illes, P. P2X3 Receptor Involvement in Pain States. *Mol Neurobiol* **36,** 165–183 (2007).
33. Bleehen, T., Hobbiger, F. & Keele, C. A. Identification of algogenic substances in human erythrocytes. *The Journal of Physiology* **262,** 131–149 (1976).
34. Dunn, P. M., Zhong, Y. & Burnstock, G. P2X receptors in peripheral neurons. *Prog. Neurobiol.* **65,** 107–134 (2001).
35. North, R. A. P2X3 receptors and peripheral pain mechanisms. *J. Physiol. (Lond.)* **554,** 301–308 (2004).
36. Vulchanova, L. *et al.* Immunohistochemical study of the P2X2 and P2X3 receptor subunits in rat and monkey sensory neurons and their central terminals. *Neuropharmacology* **36,** 1229–1242 (1997).
37. Vulchanova, L. *et al.* P2X3 is expressed by DRG neurons that terminate in inner lamina II. *Eur. J. Neurosci.* **10,** 3470–3478 (1998).
38. Khakh, B. S. & North, R. A. P2X receptors as cell-surface ATP sensors in health and disease. *Nature* **442,** 527–532 (2006).
39. Guo, A., Vulchanova, L., Wang, J., Li, X. & Elde, R. Immunocytochemical localization of the vanilloid receptor 1 (VR1): relationship to neuropeptides, the P2X3 purinoceptor and IB4 binding sites. *Eur. J. Neurosci.* **11,** 946–958 (1999).
40. Cockayne, D. A. *et al.* Urinary bladder hyporeflexia and reduced pain-related behaviour in P2X 3-deficient mice. *Nature* **407,** 1011–1015 (2000).
41. Souslova, V. *et al.* Warm-coding deficits and aberrant inflammatory pain in mice lacking P2X3 receptors. *Nature* **407,** 1015–1017 (2000).
42. Bodin, P. & Burnstock, G. Increased release of ATP from endothelial cells during acute inflammation. *Inflamm. res.* **47,** 351–354 (1998).
43. Gordon, J. L. Extracellular ATP: effects, sources and fate. *Biochem J* **233,** 309–319 (1986).

44. Ballini, E. *et al.* Characterization of three diaminopyrimidines as potent and selective antagonists of P2X3 and P2X2/3 receptors with in vivo efficacy in a pain model. *British Journal of Pharmacology* **163,** 1315–1325 (2011).
45. Gum, R. J., Wakefield, B. & Jarvis, M. F. P2X receptor antagonists for pain management: examination of binding and physicochemical properties. *Purinergic Signalling* **8,** 41–56 (2011).
46. Jarvis, M. F. *et al.* A-317491, a novel potent and selective non-nucleotide antagonist of P2X3 and P2X2/3 receptors, reduces chronic inflammatory and neuropathic pain in the rat. *PNAS* **99,** 17179–17184 (2002).
47. McGaraughty, S. *et al.* Effects of A-317491, a novel and selective P2X3/P2X2/3 receptor antagonist, on neuropathic, inflammatory and chemogenic nociception following intrathecal and intraplantar administration. *British Journal of Pharmacology* **140,** 1381–1388 (2003).
48. Oliveira, M. C. G., Pelegrini-da-Silva, A., Tambeli, C. H. & Parada, C. A. Peripheral mechanisms underlying the essential role of P2X3,2/3 receptors in the development of inflammatory hyperalgesia. *PAIN®* **141,** 127–134 (2009).
49. Cockayne, D. A. *et al.* P2X2 knockout mice and P2X2/P2X3 double knockout mice reveal a role for the P2X2 receptor subunit in mediating multiple sensory effects of ATP. *J. Physiol. (Lond.)* **567,** 621–639 (2005).
50. Ambalavanar, R., Moritani, M. & Dessem, D. Trigeminal P2X3 receptor expression differs from dorsal root ganglion and is modulated by deep tissue inflammation. *Pain* **117,** 280–291 (2005).
51. Xu, G.-Y. & Huang, L.-Y. M. Peripheral inflammation sensitizes P2X receptor-mediated responses in rat dorsal root ganglion neurons. *J. Neurosci.* **22,** 93–102 (2002).
52. Giniatullin, R., Nistri, A. & Fabbretti, E. Molecular mechanisms of sensitization of pain-transducing P2X3 receptors by the migraine mediators CGRP and NGF. *Mol. Neurobiol.* **37,** 83–90 (2008).
53. Tajti, J. *et al.* Migraine and neuropeptides. *Neuropeptides* (2015). doi:10.1016/j.npep.2015.03.006
54. Mogil, J. S. Animal models of pain: progress and challenges. *Nat. Rev. Neurosci.* **10,** 283–294 (2009).
55. Deiteren, A. *et al.* P2X3 Receptors Mediate Visceral Hypersensitivity during Acute Chemically-Induced Colitis and in the Post-Inflammatory Phase via Different Mechanisms of Sensitization. *PLoS One* **10,** (2015).
56. Wang, Q. *et al.* Sensitization of P2X3 receptors by cystathionine β-synthetase mediates persistent pain hypersensitivity in a rat model of lumbar disc herniation. *Mol Pain* **11,** (2015).
57. Wang, S. *et al.* Adrenergic signaling mediates mechanical hyperalgesia through activation of P2X3 receptors in primary sensory neurons of rats with chronic pancreatitis. *American Journal of Physiology - Gastrointestinal and Liver Physiology* **308,** G710–G719 (2015).
58. Zhang, H.-H. *et al.* Promoted interaction of nuclear factor-kappa B with demethylated purinergic P2X3 receptor gene contributes to neuropathic pain in rats with diabetes. *Diabetes* (2015). doi:10.2337/db15-0138
59. Simonetti, M. *et al.* Comparison of P2X and TRPV1 receptors in ganglia or primary culture of trigeminal neurons and their modulation by NGF or serotonin. *Mol Pain* **2,** 11 (2006).
60. Fabbretti, E. *et al.* Delayed upregulation of ATP P2X3 receptors of trigeminal sensory neurons by calcitonin gene-related peptide. *J. Neurosci.* **26,** 6163–6171 (2006).

61. Hullugundi, S. K., Ferrari, M. D., van den Maagdenberg, A. M. J. M. & Nistri, A. The mechanism of functional up-regulation of P2X3 receptors of trigeminal sensory neurons in a genetic mouse model of familial hemiplegic migraine type 1 (FHM-1). *PLoS ONE* **8,** e60677 (2013).
62. Nair, A., Simonetti, M., Fabbretti, E. & Nistri, A. The Cdk5 kinase downregulates ATP-gated ionotropic P2X3 receptor function via serine phosphorylation. *Cell. Mol. Neurobiol.* **30,** 505–509 (2010).
63. Giniatullin, R. & Nistri, A. Desensitization properties of P2X3 receptors shaping pain signaling. *Front Cell Neurosci* **7,** 245 (2013).
64. Nair, A. *et al.* Familial hemiplegic migraine Ca(v)2.1 channel mutation R192Q enhances ATP-gated P2X3 receptor activity of mouse sensory ganglion neurons mediating trigeminal pain. *Mol Pain* **6,** 48 (2010).
65. Yan, J. & Dussor, G. Ion channels and migraine. *Headache* **54,** 619–639 (2014).
66. Hullugundi, S. K., Ansuini, A., Ferrari, M. D., van den Maagdenberg, A. M. J. M. & Nistri, A. A hyperexcitability phenotype in mouse trigeminal sensory neurons expressing the R192Q Cacna1a missense mutation of familial hemiplegic migraine type-1. *Neuroscience* **266,** 244–254 (2014).
67. Arulmani, U., Maassenvandenbrink, A., Villalón, C. M. & Saxena, P. R. Calcitonin gene-related peptide and its role in migraine pathophysiology. *Eur. J. Pharmacol.* **500,** 315–330 (2004).
68. Ho, T. W., Edvinsson, L. & Goadsby, P. J. CGRP and its receptors provide new insights into migraine pathophysiology. *Nat Rev Neurol* **6,** 573–582 (2010).
69. Russell, F. A., King, R., Smillie, S.-J., Kodji, X. & Brain, S. D. Calcitonin Gene-Related Peptide: Physiology and Pathophysiology. *Physiological Reviews* **94,** 1099–1142 (2014).
70. Sarchielli, P., Alberti, A., Floridi, A. & Gallai, V. Levels of nerve growth factor in cerebrospinal fluid of chronic daily headache patients. *Neurology* **57,** 132–134 (2001).
71. D'Arco, M. *et al.* Neutralization of nerve growth factor induces plasticity of ATP-sensitive P2X3 receptors of nociceptive trigeminal ganglion neurons. *J. Neurosci.* **27,** 8190–8201 (2007).
72. Hautaniemi, T., Petrenko, N., Skorinkin, A. & Giniatullin, R. The inhibitory action of the antimigraine nonsteroidal anti-inflammatory drug naproxen on P2X3 receptor-mediated responses in rat trigeminal neurons. *Neuroscience* **209,** 32–38 (2012).
73. Jang, M.-U., Park, J.-W., Kho, H.-S., Chung, S.-C. & Chung, J.-W. Plasma and saliva levels of nerve growth factor and neuropeptides in chronic migraine patients. *Oral Dis* **17,** 187–193 (2011).
74. Masterson, C. G. & Durham, P. L. DHE repression of ATP-mediated sensitization of trigeminal ganglion neurons. *Headache* **50,** 1424–1439 (2010).
75. Persson, A.-K., Xu, X.-J., Wiesenfeld-Hallin, Z., Devor, M. & Fried, K. Expression of DRG candidate pain molecules after nerve injury--a comparative study among five inbred mouse strains with contrasting pain phenotypes. *J. Peripher. Nerv. Syst.* **15,** 26–39 (2010).
76. Simonetti, M., Giniatullin, R. & Fabbretti, E. Mechanisms mediating the enhanced gene transcription of P2X3 receptor by calcitonin gene-related peptide in trigeminal sensory neurons. *J. Biol. Chem.* **283,** 18743–18752 (2008).
77. Ugarte, G. D., Opazo, T., Leisewitz, F., van Zundert, B. & Montecino, M. Runx1 and C/EBPβ transcription factors directly up-regulate P2X3 gene transcription. *J. Cell. Physiol.* **227,** 1645–1652 (2012).
78. Franck, M. C. M. *et al.* Essential role of Ret for defining non-peptidergic nociceptor phenotypes and functions in the adult mouse. *Eur. J. Neurosci.* **33,** 1385–1400 (2011).

79. Zhou, Y.-L. *et al.* Enhanced Binding Capability of Nuclear Factor-κB with Demethylated P2X3 receptor Gene Contributes to Cancer Pain in Rats. *Pain* (2015). doi:10.1097/j.pain.0000000000000248
80. Xiong, W. *et al.* Effects of intermedin on dorsal root ganglia in the transmission of neuropathic pain in chronic constriction injury rats. *Clin. Exp. Pharmacol. Physiol.* **42,** 780–787 (2015).
81. Chaumont, S., Jiang, L.-H., Penna, A., North, R. A. & Rassendren, F. Identification of a trafficking motif involved in the stabilization and polarization of P2X receptors. *J. Biol. Chem.* **279,** 29628–29638 (2004).
82. Ma, W. & Quirion, R. Targeting cell surface trafficking of pain-facilitating receptors to treat chronic pain conditions. *Expert Opin. Ther. Targets* **18,** 459–472 (2014).
83. Guo, J., Fu, X., Cui, X. & Fan, M. Contributions of purinergic P2X3 receptors within the midbrain periaqueductal gray to diabetes-induced neuropathic pain. *J Physiol Sci* **65,** 99–104 (2014).
84. Chen, Y., Zhang, L., Yang, J., Zhang, L. & Chen, Z. LPS-induced dental pulp inflammation increases expression of ionotropic purinergic receptors in rat trigeminal ganglion. *Neuroreport* **25,** 991–997 (2014).
85. Xu, G.-Y. & Huang, L.-Y. M. Ca2+/calmodulin-dependent protein kinase II potentiates ATP responses by promoting trafficking of P2X receptors. *Proc. Natl. Acad. Sci. U.S.A.* **101,** 11868–11873 (2004).
86. Vacca, F., Giustizieri, M., Ciotti, M. T., Mercuri, N. B. & Volonté, C. Rapid constitutive and ligand-activated endocytic trafficking of P2X receptor. *J. Neurochem.* **109,** 1031–1041 (2009).
87. Gnanasekaran, A. *et al.* Calcium/calmodulin-dependent serine protein kinase (CASK) is a new intracellular modulator of P2X3 receptors. *J. Neurochem.* **126,** 102–112 (2013).
88. Chen, X.-Q. *et al.* Endosome-mediated retrograde axonal transport of P2X3 receptor signals in primary sensory neurons. *Cell Res.* **22,** 677–696 (2012).
89. Chen, X.-Q., Zhu, J.-X., Wang, Y., Zhang, X. & Bao, L. CaMKIIα and caveolin-1 cooperate to drive ATP-induced membrane delivery of the P2X3 receptor. *J Mol Cell Biol* **6,** 140–153 (2014).
90. Dutton, J. L. *et al.* P2X(1) receptor membrane redistribution and down-regulation visualized by using receptor-coupled green fluorescent protein chimeras. *Neuropharmacology* **39,** 2054–2066 (2000).
91. Pato, C. *et al.* Role of lipid rafts in agrin-elicited acetylcholine receptor clustering. *Chem. Biol. Interact.* **175,** 64–67 (2008).
92. Taverna, E. *et al.* Role of lipid microdomains in P/Q-type calcium channel (Cav2.1) clustering and function in presynaptic membranes. *J. Biol. Chem.* **279,** 5127–5134 (2004).
93. Allsopp, R. C., Lalo, U. & Evans, R. J. Lipid raft association and cholesterol sensitivity of P2X1-4 receptors for ATP: chimeras and point mutants identify intracellular amino-terminal residues involved in lipid regulation of P2X1 receptors. *J. Biol. Chem.* **285,** 32770–32777 (2010).
94. Gnanasekaran, A., Sundukova, M., van den Maagdenberg, A. M. J. M., Fabbretti, E. & Nistri, A. Lipid rafts control P2X3 receptor distribution and function in trigeminal sensory neurons of a transgenic migraine mouse model. *Mol Pain* **7,** 77 (2011).
95. Vacca, F., Amadio, S., Sancesario, G., Bernardi, G. & Volonté, C. P2X3 receptor localizes into lipid rafts in neuronal cells. *J. Neurosci. Res.* **76,** 653–661 (2004).
96. Mo, G. *et al.* Subtype-specific regulation of P2X3 and P2X2/3 receptors by phosphoinositides in peripheral nociceptors. *Mol Pain* **5,** 47 (2009).

97. Gnanasekaran, A. *et al.* Mutated CaV2.1 channels dysregulate CASK/P2X3 signaling in mouse trigeminal sensory neurons of R192Q Cacna1a knock-in mice. *Mol Pain* **9,** 62 (2013).
98. Coddou, C., Yan, Z., Obsil, T., Huidobro-Toro, J. P. & Stojilkovic, S. S. Activation and Regulation of Purinergic P2X Receptor Channels. *Pharmacol Rev* **63,** 641–683 (2011).
99. Sokolova, E. *et al.* Experimental and modeling studies of desensitization of P2X3 receptors. *Mol. Pharmacol.* **70,** 373–382 (2006).
100. Khmyz, V., Maximyuk, O., Teslenko, V., Verkhratsky, A. & Krishtal, O. P2X3 receptor gating near normal body temperature. *Pflugers Arch.* **456,** 339–347 (2008).
101. Gerevich, Z. *et al.* Dual Effect of Acid pH on Purinergic P2X3 Receptors Depends on the Histidine 206 Residue. *J. Biol. Chem.* **282,** 33949–33957 (2007).
102. Lambert, G. A. & Michalicek, J. Cortical Spreading Depression Reduces Dural Blood Flow—A Possible Mechanism for Migraine Pain? *Cephalalgia* **14,** 430–436 (1994).
103. Yan, J. *et al.* Dural afferents express acid-sensing ion channels: A role for decreased meningeal pH in migraine headache. *PAIN®* **152,** 106–113 (2011).
104. Paukert, M. *et al.* Inflammatory Mediators Potentiate ATP-gated Channels through the P2X3 Subunit. *J. Biol. Chem.* **276,** 21077–21082 (2001).
105. Alexander, K. *et al.* Allosteric modulation and accelerated resensitization of human P2X(3) receptors by cibacron blue. *J. Pharmacol. Exp. Ther.* **291,** 1135–1142 (1999).
106. Cook, S. P., Rodland, K. D. & McCleskey, E. W. A memory for extracellular Ca2+ by speeding recovery of P2X receptors from desensitization. *J. Neurosci.* **18,** 9238–9244 (1998).
107. Boué-Grabot, E., Archambault, V. & Séguéla, P. A protein kinase C site highly conserved in P2X subunits controls the desensitization kinetics of P2X(2) ATP-gated channels. *J. Biol. Chem.* **275,** 10190–10195 (2000).
108. Brown, D. A. & Yule, D. I. Protein kinase C regulation of P2X3 receptors is unlikely to involve direct receptor phosphorylation. *Biochim. Biophys. Acta* **1773,** 166–175 (2007).
109. Franklin, C., Braam, U., Eisele, T., Schmalzing, G. & Hausmann, R. Lack of evidence for direct phosphorylation of recombinantly expressed P2X(2) and P2X (3) receptors by protein kinase C. *Purinergic Signal.* **3,** 377–388 (2007).
110. D'Arco, M. *et al.* The C-terminal Src inhibitory kinase (Csk)-mediated tyrosine phosphorylation is a novel molecular mechanism to limit P2X3 receptor function in mouse sensory neurons. *J. Biol. Chem.* **284,** 21393–21401 (2009).
111. Utreras, E., Futatsugi, A., Pareek, T. K. & Kulkarni, A. B. Molecular Roles of Cdk5 in Pain Signaling. *Drug Discov Today Ther Strateg* **6,** 105–111 (2009).
112. Wang, C., Gu, Y., Li, G.-W. & Huang, L.-Y. M. A critical role of the cAMP sensor Epac in switching protein kinase signalling in prostaglandin E2-induced potentiation of P2X3 receptor currents in inflamed rats. *J. Physiol. (Lond.)* **584,** 191–203 (2007).
113. Bölcskei, H. & Farkas, B. P2X3 and P2X2/3 receptor antagonists. *Pharm Pat Anal* **3,** 53–64 (2014).
114. Lambertucci, C. *et al.* Medicinal chemistry of P2X receptors: agonists and orthosteric antagonists. *Curr. Med. Chem.* **22,** 915–928 (2015).
115. Finger, T. E. *et al.* ATP signaling is crucial for communication from taste buds to gustatory nerves. *Science* **310,** 1495–1499 (2005).
116. Hansen, R. R. *et al.* Chronic administration of the selective P2X3, P2X2/3 receptor antagonist, A-317491, transiently attenuates cancer-induced bone pain in mice. *Eur. J. Pharmacol.* **688,** 27–34 (2012).
117. Cantin, L.-D. *et al.* Discovery of P2X3 selective antagonists for the treatment of chronic pain. *Bioorg. Med. Chem. Lett.* **22,** 2565–2571 (2012).

118. Carter, D. S. *et al.* Identification and SAR of novel diaminopyrimidines. Part 1: The discovery of RO-4, a dual P2X(3)/P2X(2/3) antagonist for the treatment of pain. *Bioorg. Med. Chem. Lett.* **19,** 1628–1631 (2009).
119. Jahangir, A. *et al.* Identification and SAR of novel diaminopyrimidines. Part 2: The discovery of RO-51, a potent and selective, dual P2X(3)/P2X(2/3) antagonist for the treatment of pain. *Bioorg. Med. Chem. Lett.* **19,** 1632–1635 (2009).
120. Lambertucci, C. *et al.* Evaluation of adenine as scaffold for the development of novel P2X3 receptor antagonists. *European Journal of Medicinal Chemistry* **65,** 41–50 (2013).
121. Brotherton-Pleiss, C. E. *et al.* Discovery and optimization of RO-85, a novel drug-like, potent, and selective P2X3 receptor antagonist. *Bioorg. Med. Chem. Lett.* **20,** 1031–1036 (2010).
122. Nilius, B., Owsianik, G., Voets, T. & Peters, J. A. Transient Receptor Potential Cation Channels in Disease. *Physiological Reviews* **87,** 165–217 (2007).
123. Benemei, S., Patacchini, R., Trevisani, M. & Geppetti, P. TRP channels. *Current Opinion in Pharmacology* **22,** 18–23 (2015).
124. Laing, R. J. & Dhaka, A. ThermoTRPs and Pain. *Neuroscientist* 1073858414567884 (2015). doi:10.1177/1073858414567884
125. Caterina, M. J. & Julius, D. The vanilloid receptor: a molecular gateway to the pain pathway. *Annu. Rev. Neurosci.* **24,** 487–517 (2001).
126. Jordt, S. E., Tominaga, M. & Julius, D. Acid potentiation of the capsaicin receptor determined by a key extracellular site. *Proc. Natl. Acad. Sci. U.S.A.* **97,** 8134–8139 (2000).
127. Caterina, M. J. *et al.* The capsaicin receptor: a heat-activated ion channel in the pain pathway. *Nature* **389,** 816–824 (1997).
128. Ichikawa, H. & Sugimoto, T. VR1-immunoreactive primary sensory neurons in the rat trigeminal ganglion. *Brain Res.* **890,** 184–188 (2001).
129. Tominaga, M. *et al.* The cloned capsaicin receptor integrates multiple pain-producing stimuli. *Neuron* **21,** 531–543 (1998).
130. Lishko, P. V., Procko, E., Jin, X., Phelps, C. B. & Gaudet, R. The ankyrin repeats of TRPV1 bind multiple ligands and modulate channel sensitivity. *Neuron* **54,** 905–918 (2007).
131. Szolcsányi, J. & Sándor, Z. Multisteric TRPV1 nocisensor: a target for analgesics. *Trends in Pharmacological Sciences* **33,** 646–655 (2012).
132. Liao, M., Cao, E., Julius, D. & Cheng, Y. Structure of the TRPV1 ion channel determined by electron cryo-microscopy. *Nature* **504,** 107–112 (2013).
133. Cao, E., Liao, M., Cheng, Y. & Julius, D. TRPV1 structures in distinct conformations reveal activation mechanisms. *Nature* **504,** 113–118 (2013).
134. Ryu, S., Liu, B., Yao, J., Fu, Q. & Qin, F. Uncoupling proton activation of vanilloid receptor TRPV1. *J. Neurosci.* **27,** 12797–12807 (2007).
135. Brauchi, S., Orta, G., Salazar, M., Rosenmann, E. & Latorre, R. A hot-sensing cold receptor: C-terminal domain determines thermosensation in transient receptor potential channels. *J. Neurosci.* **26,** 4835–4840 (2006).
136. Grandl, J. *et al.* Temperature-induced opening of TRPV1 ion channel is stabilized by the pore domain. *Nat. Neurosci.* **13,** 708–714 (2010).
137. Li, L., Hasan, R. & Zhang, X. The basal thermal sensitivity of the TRPV1 ion channel is determined by PKCβII. *J. Neurosci.* **34,** 8246–8258 (2014).
138. Yang, F., Cui, Y., Wang, K. & Zheng, J. Thermosensitive TRP channel pore turret is part of the temperature activation pathway. *Proc. Natl. Acad. Sci. U.S.A.* **107,** 7083–7088 (2010).
139. Yao, J., Liu, B. & Qin, F. Modular thermal sensors in temperature-gated transient receptor potential (TRP) channels. *Proc. Natl. Acad. Sci. U.S.A.* **108,** 11109–11114 (2011).

140. Nilius, B. *et al.* Gating of TRP channels: a voltage connection? *J. Physiol. (Lond.)* **567,** 35–44 (2005).
141. El-Hashim, A. Z. & Jaffal, S. M. Nerve growth factor enhances cough and airway obstruction via TrkA receptor- and TRPV1-dependent mechanisms. *Thorax* **64,** 791–797 (2009).
142. Eskander, M. A. *et al.* Persistent Nociception Triggered by Nerve Growth Factor (NGF) Is Mediated by TRPV1 and Oxidative Mechanisms. *J. Neurosci.* **35,** 8593–8603 (2015).
143. Zhu, W. & Oxford, G. S. Phosphoinositide-3-kinase and mitogen activated protein kinase signaling pathways mediate acute NGF sensitization of TRPV1. *Mol. Cell. Neurosci.* **34,** 689–700 (2007).
144. Stein, A. T., Ufret-Vincenty, C. A., Hua, L., Santana, L. F. & Gordon, S. E. Phosphoinositide 3-kinase binds to TRPV1 and mediates NGF-stimulated TRPV1 trafficking to the plasma membrane. *J. Gen. Physiol.* **128,** 509–522 (2006).
145. Julius, D. TRP Channels and Pain. *Annual Review of Cell and Developmental Biology* **29,** 355–384 (2013).
146. Martins, D., Tavares, I. & Morgado, C. 'Hotheaded': The role OF TRPV1 in brain functions. *Neuropharmacology* **85,** 151–157 (2014).
147. Chizh, B. A. *et al.* The effects of the TRPV1 antagonist SB-705498 on TRPV1 receptor-mediated activity and inflammatory hyperalgesia in humans. *Pain* **132,** 132–141 (2007).
148. Honore, P. *et al.* A-425619 [1-Isoquinolin-5-yl-3-(4-trifluoromethyl-benzyl)-urea], a Novel Transient Receptor Potential Type V1 Receptor Antagonist, Relieves Pathophysiological Pain Associated with Inflammation and Tissue Injury in Rats. *J Pharmacol Exp Ther* **314,** 410–421 (2005).
149. Gopinath, P. *et al.* Increased capsaicin receptor TRPV1 in skin nerve fibres and related vanilloid receptors TRPV3 and TRPV4 in keratinocytes in human breast pain. *BMC Women's Health* **5,** 2 (2005).
150. Akbar, A. *et al.* Increased capsaicin receptor TRPV1-expressing sensory fibres in irritable bowel syndrome and their correlation with abdominal pain. *Gut* **57,** 923–929 (2008).
151. Hutter, M. M. *et al.* Transient receptor potential vanilloid (TRPV-1) promotes neurogenic inflammation in the pancreas via activation of the neurokinin-1 receptor (NK-1R). *Pancreas* **30,** 260–265 (2005).
152. van Wanrooij, S. J. M. *et al.* Sensitivity Testing in Irritable Bowel Syndrome With Rectal Capsaicin Stimulations: Role of TRPV1 Upregulation and Sensitization in Visceral Hypersensitivity? *Am J Gastroenterol* **109,** 99–109 (2014).
153. Xu, G. *et al.* Transient Receptor Potential Vanilloid 1 Mediates Hyperalgesia and Is Up-Regulated in Rats With Chronic Pancreatitis. *Gastroenterology* **133,** 1282–1292 (2007).
154. Urano, H., Ara, T., Fujinami, Y. & Hiraoka, B. Y. Aberrant TRPV1 Expression in Heat Hyperalgesia Associated with Trigeminal Neuropathic Pain. *Int J Med Sci* **9,** 690–697 (2012).
155. Watabiki, T. *et al.* Amelioration of Neuropathic Pain by Novel Transient Receptor Potential Vanilloid 1 Antagonist AS1928370 in Rats without Hyperthermic Effect. *J Pharmacol Exp Ther* **336,** 743–750 (2011).
156. Backonja, M. M., Malan, T. P., Vanhove, G. F. & Tobias, J. K. NGX-4010, a High-Concentration Capsaicin Patch, for the Treatment of Postherpetic Neuralgia: A Randomized, Double-Blind, Controlled Study with an Open-Label Extension. *Pain Medicine* **11,** 600–608 (2010).
157. Forst, T. *et al.* The influence of local capsaicin treatment on small nerve fibre function and neurovascular control in symptomatic diabetic neuropathy. *Acta Diabetol* **39,** 1–6 (2002).

158. King, T. *et al.* Contribution of afferent pathways to nerve injury-induced spontaneous pain and evoked hypersensitivity. *PAIN* **152,** 1997–2005 (2011).
159. R, R. & A, S. Adlea (ALGRX-4975), an injectable capsaicin (TRPV1 receptor agonist) formulation for longlasting pain relief. *IDrugs* **11,** 120–132 (2008).
160. Carreño, O. *et al.* SNP variants within the vanilloid TRPV1 and TRPV3 receptor genes are associated with migraine in the Spanish population. *Am. J. Med. Genet. B Neuropsychiatr. Genet.* **159B,** 94–103 (2012).
161. Shimizu, T. *et al.* Distribution and origin of TRPV1 receptor-containing nerve fibers in the dura mater of rat. *Brain Res.* **1173,** 84–91 (2007).
162. Huang, D., Li, S., Dhaka, A., Story, G. M. & Cao, Y.-Q. Expression of the transient receptor potential channels TRPV1, TRPA1 and TRPM8 in mouse trigeminal primary afferent neurons innervating the dura. *Mol Pain* **8,** 66 (2012).
163. Negri, L. *et al.* Impaired nociception and inflammatory pain sensation in mice lacking the prokineticin receptor PKR1: focus on interaction between PKR1 and the capsaicin receptor TRPV1 in pain behavior. *J. Neurosci.* **26,** 6716–6727 (2006).
164. Tominaga, M., Wada, M. & Masu, M. Potentiation of capsaicin receptor activity by metabotropic ATP receptors as a possible mechanism for ATP-evoked pain and hyperalgesia. *Proc. Natl. Acad. Sci. U.S.A.* **98,** 6951–6956 (2001).
165. Diamond, S., Freitag, F., Phillips, S. B., Bernstein, J. E. & Saper, J. R. Intranasal civamide for the acute treatment of migraine headache. *Cephalalgia* **20,** 597–602 (2000).
166. Anand, P. & Bley, K. Topical capsaicin for pain management: therapeutic potential and mechanisms of action of the new high-concentration capsaicin 8% patch. *Br J Anaesth* **107,** 490–502 (2011).
167. Akerman, S., Kaube, H. & Goadsby, P. J. Vanilloid type 1 receptors (VR1) on trigeminal sensory nerve fibres play a minor role in neurogenic dural vasodilatation, and are involved in capsaicin-induced dural dilation. *Br. J. Pharmacol.* **140,** 718–724 (2003).
168. Nicoletti, P. *et al.* Ethanol causes neurogenic vasodilation by TRPV1 activation and CGRP release in the trigeminovascular system of the guinea pig. *Cephalalgia* **28,** 9–17 (2008).
169. Dussor, G. *et al.* Targeting TRP Channels For Novel Migraine Therapeutics. *ACS Chem. Neurosci.* **5,** 1085–1096 (2014).
170. Hodes, A. & Lichtstein, D. Natriuretic Hormones in Brain Function. *Front Endocrinol (Lausanne)* **5,** (2014).
171. Pandey, K. N. Biology of natriuretic peptides and their receptors. *Peptides* **26,** 901–932 (2005).
172. Potter, L. R., Yoder, A. R., Flora, D. R., Antos, L. K. & Dickey, D. M. Natriuretic peptides: their structures, receptors, physiologic functions and therapeutic applications. *Handb Exp Pharmacol* 341–366 (2009). doi:10.1007/978-3-540-68964-5_15
173. Yang-Feng, T. L., Floyd-Smith, G., Nemer, M., Drouin, J. & Francke, U. The pronatriodilatin gene is located on the distal short arm of human chromosome 1 and on mouse chromosome 4. *Am. J. Hum. Genet.* **37,** 1117–1128 (1985).
174. John, S. W. *et al.* Blood pressure and fluid-electrolyte balance in mice with reduced or absent ANP. *American Journal of Physiology - Regulatory, Integrative and Comparative Physiology* **271,** R109–R114 (1996).
175. Marin-Grez, M., Fleming, J. T. & Steinhausen, M. Atrial natriuretic peptide causes pre-glomerular vasodilatation and post-glomerular vasoconstriction in rat kidney. *Nature* **324,** 473–476 (1986).

176. Klein, R. M., Kelley, K. B. & Merisko-Liversidge, E. M. A Clathrin-Coated Vesicle-Mediated Pathway in Atrial Natriuretic Peptide (ANP) Secretion. *Journal of Molecular and Cellular Cardiology* **25,** 437–452 (1993).
177. Yan, W., Wu, F., Morser, J. & Wu, Q. Corin, a transmembrane cardiac serine protease, acts as a pro-atrial natriuretic peptide-converting enzyme. *PNAS* **97,** 8525–8529 (2000).
178. Chan, J. C. Y. *et al.* Hypertension in mice lacking the proatrial natriuretic peptide convertase corin. *PNAS* **102,** 785–790 (2005).
179. Seidman, C. E., Bloch, K. D., Klein, K. A., Smith, J. A. & Seidman, J. G. Nucleotide sequences of the human and mouse atrial natriuretic factor genes. *Science* **226,** 1206–1209 (1984).
180. Vlasuk, G. P., Miller, J., Bencen, G. H. & Lewicki, J. A. Structure and analysis of the bovine atrial natriuretic peptide precursor gene. *Biochemical and Biophysical Research Communications* **136,** 396–403 (1986).
181. Gardner, D. G., Vlasuk, G. P., Baxter, J. D., Fiddes, J. C. & Lewicki, J. A. Identification of atrial natriuretic factor gene transcripts in the central nervous system of the rat. *PNAS* **84,** 2175–2179 (1987).
182. Potter, L. R., Abbey-Hosch, S. & Dickey, D. M. Natriuretic Peptides, Their Receptors, and Cyclic Guanosine Monophosphate-Dependent Signaling Functions. *Endocrine Reviews* **27,** 47–72 (2006).
183. Sudoh, T., Kangawa, K., Minamino, N. & Matsuo, H. A new natriuretic peptide in porcine brain. *Nature* **332,** 78–81 (1988).
184. Mukoyama, M. *et al.* Brain natriuretic peptide as a novel cardiac hormone in humans. Evidence for an exquisite dual natriuretic peptide system, atrial natriuretic peptide and brain natriuretic peptide. *J Clin Invest* **87,** 1402–1412 (1991).
185. Saito, Y. *et al.* Brain natriuretic peptide is a novel cardiac hormone. *Biochem. Biophys. Res. Commun.* **158,** 360–368 (1989).
186. Tamura, N. *et al.* Two Cardiac Natriuretic Peptide Genes (Atrial Natriuretic Peptide and Brain Natriuretic Peptide) are Organized in Tandem in the Mouse and Human Genomes. *Journal of Molecular and Cellular Cardiology* **28,** 1811–1815 (1996).
187. Tamura, N. *et al.* Cardiac fibrosis in mice lacking brain natriuretic peptide. *PNAS* **97,** 4239–4244 (2000).
188. Nagaya, N. *et al.* Plasma brain natriuretic peptide as a prognostic indicator in patients with primary pulmonary hypertension. *Circulation* **102,** 865–870 (2000).
189. Nakao, K. *et al.* The pharmacokinetics ofα-human atrial natriuretic polypeptide in healthy subjects. *Eur J Clin Pharmacol* **31,** 101–103 (1986).
190. Richards, A. M. *et al.* Brain natriuretic peptide: natriuretic and endocrine effects in essential hypertension. *J. Hypertens.* **11,** 163–170 (1993).
191. Semenov, A. G. *et al.* Processing of Pro–B-Type Natriuretic Peptide: Furin and Corin as Candidate Convertases. *Clinical Chemistry* **56,** 1166–1176 (2010).
192. Ogawa, Y. *et al.* Molecular cloning of the complementary DNA and gene that encode mouse brain natriuretic peptide and generation of transgenic mice that overexpress the brain natriuretic peptide gene. *J Clin Invest* **93,** 1911–1921 (1994).
193. Sudoh, T. *et al.* Cloning and sequence analysis of cDNA encoding a precursor for human brain natriuretic peptide. *Biochemical and Biophysical Research Communications* **159,** 1427–1434 (1989).
194. Nishikimi, T. *et al.* Diversity of molecular forms of plasma brain natriuretic peptide in heart failure—different proBNP-108 to BNP-32 ratios in atrial and ventricular overload. *Heart* **96,** 432–439 (2010).

195. Yasue, H. *et al.* Localization and mechanism of secretion of B-type natriuretic peptide in comparison with those of A-type natriuretic peptide in normal subjects and patients with heart failure. *Circulation* **90,** 195–203 (1994).
196. Gerbes, A. L., Dagnino, L., Nguyen, T. & Nemer, M. Transcription of brain natriuretic peptide and atrial natriuretic peptide genes in human tissues. *The Journal of Clinical Endocrinology & Metabolism* **78,** 1307–1311 (1994).
197. Sudoh, T., Minamino, N., Kangawa, K. & Matsuo, H. C-type natriuretic peptide (CNP): a new member of natriuretic peptide family identified in porcine brain. *Biochem. Biophys. Res. Commun.* **168,** 863–870 (1990).
198. Tawaragi, Y. *et al.* Gene and precursor structures of human C-type natriuretic peptide. *Biochemical and Biophysical Research Communications* **175,** 645–651 (1991).
199. Inoue, K. *et al.* Four functionally distinct C-type natriuretic peptides found in fish reveal evolutionary history of the natriuretic peptide system. *PNAS* **100,** 10079–10084 (2003).
200. Ogawa, Y. *et al.* Molecular Cloning and Chromosomal Assignment of the Mouse C-Type Natriuretic Peptide (CNP) Gene (Nppc): Comparison with the Human CNP Gene (NPPC). *Genomics* **24,** 383–387 (1994).
201. Chusho, H. *et al.* Dwarfism and early death in mice lacking C-type natriuretic peptide. *PNAS* **98,** 4016–4021 (2001).
202. Hagiwara, H. *et al.* Autocrine regulation of rat chondrocyte proliferation by natriuretic peptide C and its receptor, natriuretic peptide receptor-B. *J. Biol. Chem.* **269,** 10729–10733 (1994).
203. Yeung, V. T. F., Ho, S. K. S., Nicholls, M. G. & Cockram, C. S. Binding of CNP-22 and CNP-53 to cultured mouse astrocytes and effects on cyclic GMP. *Peptides* **17,** 101–106 (1996).
204. Stingo, A. J., Clavell, A. L., Aarhus, L. L. & Burnett, J. C. Cardiovascular and renal actions of C-type natriuretic peptide. *American Journal of Physiology-Heart and Circulatory Physiology* **262,** H308–H312 (1992).
205. Togashi, K., Kameya, T., Kurosawa, T., Hasegawa, N. & Kawakami, M. Concentrations and molecular forms of C-type natriuretic peptide in brain and cerebrospinal fluid. *Clinical Chemistry* **38,** 2136–2139 (1992).
206. Totsune, K. *et al.* C-type natriuretic peptide in the human central nervous system: distribution and molecular form. *Peptides* **15,** 37–40 (1994).
207. Garbers, D. L. Guanylyl cyclase receptors and their endocrine, paracrine, and autocrine ligands. *Cell* **71,** 1–4 (1992).
208. Tremblay, J., Desjardins, R., Hum, D., Gutkowska, J. & Hamet, P. Biochemistry and physiology of the natriuretic peptide receptor guanylyl cyclases. *Mol. Cell. Biochem.* **230,** 31–47 (2002).
209. Matsukawa, N. *et al.* The natriuretic peptide clearance receptor locally modulates the physiological effects of the natriuretic peptide system. *Proc. Natl. Acad. Sci. U.S.A.* **96,** 7403–7408 (1999).
210. Potter, L. R. Regulation and therapeutic targeting of peptide-activated receptor guanylyl cyclases. *Pharmacology & Therapeutics* **130,** 71–82 (2011).
211. Oliver, P. M. *et al.* Hypertension, cardiac hypertrophy, and sudden death in mice lacking natriuretic peptide receptor A. *PNAS* **94,** 14730–14735 (1997).
212. Nakayama, T. *et al.* Functional Deletion Mutation of the 5'-Flanking Region of Type A Human Natriuretic Peptide Receptor Gene and Its Association With Essential Hypertension and Left Ventricular Hypertrophy in the Japanese. *Circulation Research* **86,** 841–845 (2000).

213. Chinkers, M. & Wilson, E. M. Ligand-independent oligomerization of natriuretic peptide receptors. Identification of heteromeric receptors and a dominant negative mutant. *J. Biol. Chem.* **267,** 18589–18597 (1992).
214. Lowe, D. G. Human natriuretic peptide receptor-A guanylyl cyclase is self-associated prior to hormone binding. *Biochemistry* **31,** 10421–10425 (1992).
215. Goraczniak, R. M., Duda, T. & Sharma, R. K. A structural motif that defines the ATP-regulatory module of guanylate cyclase in atrial natriuretic factor signalling. *Biochem. J.* **282 (Pt 2),** 533–537 (1992).
216. Burczynska, B., Duda, T. & Sharma, R. K. ATP signaling site in the ARM domain of atrial natriuretic factor receptor guanylate cyclase. *Mol Cell Biochem* **301,** 93–107 (2007).
217. Chinkers, M. Regulation of the atrial natriuretic peptide receptor guanylyl cyclase. *Proc. Soc. Exp. Biol. Med.* **213,** 105–108 (1996).
218. Foster, D. C. & Garbers, D. L. Dual role for adenine nucleotides in the regulation of the atrial natriuretic peptide receptor, guanylyl cyclase-A. *J. Biol. Chem.* **273,** 16311–16318 (1998).
219. Potter, L. R. & Garbers, D. L. Dephosphorylation of the guanylyl cyclase-A receptor causes desensitization. *J. Biol. Chem.* **267,** 14531–14534 (1992).
220. Potter, L. R. & Garbers, D. L. Protein kinase C-dependent desensitization of the atrial natriuretic peptide receptor is mediated by dephosphorylation. *J. Biol. Chem.* **269,** 14636–14642 (1994).
221. Antos, L. K. & Potter, L. R. Adenine nucleotides decrease the apparent Km of endogenous natriuretic peptide receptors for GTP. *Am. J. Physiol. Endocrinol. Metab.* **293,** E1756–1763 (2007).
222. Valli, N., Gobinet, A. & Bordenave, L. Review of 10 years of the clinical use of brain natriuretic peptide in cardiology. *J. Lab. Clin. Med.* **134,** 437–444 (1999).
223. Fan, D., Bryan, P. M., Antos, L. K., Potthast, R. J. & Potter, L. R. Down-regulation does not mediate natriuretic peptide-dependent desensitization of natriuretic peptide receptor (NPR)-A or NPR-B: guanylyl cyclase-linked natriuretic peptide receptors do not internalize. *Mol. Pharmacol.* **67,** 174–183 (2005).
224. Pandey, K. N., Kumar, R., Li, M. & Nguyen, H. Functional domains and expression of truncated atrial natriuretic peptide receptor-A: the carboxyl-terminal regions direct the receptor internalization and sequestration in COS-7 cells. *Mol. Pharmacol.* **57,** 259–267 (2000).
225. Weber, W., Fischli, W., Hochuli, E., Kupfer, E. & Weibel, E. K. Anantin--a peptide antagonist of the atrial natriuretic factor (ANF). I. Producing organism, fermentation, isolation and biological activity. *J. Antibiot.* **44,** 164–171 (1991).
226. Pfeifer, A. Defective smooth muscle regulation in cGMP kinase I-deficient mice. *The EMBO Journal* **17,** 3045–3051 (1998).
227. Ehlert, E. M. E. N-terminal Myristoylation Is Required for Membrane Localization of cGMP-dependent Protein Kinase Type II. *Journal of Biological Chemistry* **271,** 7025–7029 (1996).
228. Chikuda, H. Cyclic GMP-dependent protein kinase II is a molecular switch from proliferation to hypertrophic differentiation of chondrocytes. *Genes & Development* **18,** 2418–2429 (2004).
229. Pfeifer, A. *et al.* Intestinal Secretory Defects and Dwarfism in Mice Lacking cGMP-Dependent Protein Kinase II. *Science* **274,** 2082–2086 (1996).
230. Geahlen, R. L., Allen, S. M. & Krebs, E. G. Effect of phosphorylation on the regulatory subunit of the type I cAMP-dependent protein kinase. *J. Biol. Chem.* **256,** 4536–4540 (1981).

231. Kook, H. *et al.* Physiological concentration of atrial natriuretic peptide induces endothelial regeneration in vitro. *American Journal of Physiology - Heart and Circulatory Physiology* **284,** H1388–H1397 (2003).
232. You, H. & Laychock, S. G. Atrial Natriuretic Peptide Promotes Pancreatic Islet β-Cell Growth and Akt/Foxo1a/Cyclin D2 Signaling. *Endocrinology* **150,** 5455–5465 (2009).
233. Beavo, J. A. Cyclic nucleotide phosphodiesterases: functional implications of multiple isoforms. *Physiol. Rev.* **75,** 725–748 (1995).
234. Corbin, J. D. & Francis, S. H. Cyclic GMP phosphodiesterase-5: target of sildenafil. *J. Biol. Chem.* **274,** 13729–13732 (1999).
235. Kaupp, U. B. & Seifert, R. Cyclic Nucleotide-Gated Ion Channels. *Physiological Reviews* **82,** 769–824 (2002).
236. Bradley, J., Frings, S., Yau, K.-W. & Reed, R. Nomenclature for Ion channel Subunits. *Science* **294,** 2095–2096 (2001).
237. Cao, L.-H. & Yang, X.-L. Natriuretic peptides and their receptors in the central nervous system. *Progress in Neurobiology* **84,** 234–248 (2008).
238. Yamada, T., Matsuda, K. & Uchiyama, M. Atrial natriuretic peptide and cGMP activate sodium transport through PKA-dependent pathway in the urinary bladder of the Japanese tree frog. *J Comp Physiol B* **176,** 203–212 (2005).
239. Imura, H., Nakao, K. & Itoh, H. The natriuretic peptide system in the brain: implications in the central control of cardiovascular and neuroendocrine functions. *Front Neuroendocrinol* **13,** 217–249 (1992).
240. Marei, H. E. S. Fine Structural and Immunohistochemical Localization of Cardiac Hormones (ANP) in the Right Atrium and Hypothalamus of the White Rat. *European Journal of Morphology* **40,** 37–41 (2002).
241. Gonçalves, J., Grove, K. L. & Deschepper, C. F. Generation of cyclic guanosine monophosphate in brain slices incubated with atrial or C-type natriuretic peptides: comparison of the amplitudes and cellular distribution of the responses. *Regulatory Peptides* **57,** 55–63 (1995).
242. Hösli, E. & Hösli, L. Autoradiographic localization of binding sites for arginine vasopressin and atrial natriuretic peptide on astrocytes and neurons of cultured rat central nervous system. *Neuroscience* **51,** 159–166 (1992).
243. Levin, E. R., Frank, H. J., Gelfand, R., Loughlin, S. E. & Kaplan, G. Natriuretic peptide receptors in cultured rat diencephalon. *J. Biol. Chem.* **265,** 10019–10024 (1990).
244. Sumners, C. & Tang, W. Atrial natriuretic peptide receptor subtypes in rat neuronal and astrocyte glial cultures. *American Journal of Physiology - Cell Physiology* **262,** C1134–C1143 (1992).
245. Tang, W., Paulding, W. R. & Sumners, C. ANP receptors in neurons and astrocytes from spontaneously hypertensive rat brain. *American Journal of Physiology - Cell Physiology* **265,** C106–C112 (1993).
246. Yu, Y.-C., Cao, L.-H. & Yang, X.-L. Modulation by brain natriuretic peptide of GABA receptors on rat retinal ON-type bipolar cells. *J. Neurosci.* **26,** 696–707 (2006).
247. Abdelalim, E. M. & Tooyama, I. NPR-A regulates self-renewal and pluripotency of embryonic stem cells. *Cell Death and Dis* **2,** e127 (2011).
248. DiCicco-Bloom, E. *et al.* Embryonic expression and multifunctional actions of the natriuretic peptides and receptors in the developing nervous system. *Developmental Biology* **271,** 161–175 (2004).

249. Levin, E. R. & Frank, H. J. Natriuretic peptides inhibit rat astroglial proliferation: mediation by C receptor. *American Journal of Physiology - Regulatory, Integrative and Comparative Physiology* **261,** R453–R457 (1991).
250. Simpson, P. J. *et al.* Atrial Natriuretic Peptide Type C Induces a Cell-Cycle Switch from Proliferation to Differentiation in Brain-Derived Neurotrophic Factor- or Nerve Growth Factor-Primed Olfactory Receptor Neurons. *J. Neurosci.* **22,** 5536–5551 (2002).
251. Fernández, B. E. *et al.* Atrial natriuretic peptide and angiotensin II interaction on noradrenaline uptake in the central nervous system. *Arch Int Pharmacodyn Ther* **307,** 11–17 (1990).
252. Papouchado, M. L., Vatta, M. S., Bianciotti, L. G. & Fernandez, B. E. Effects of Atrial Natriuretic Factor on Norepinephrine Release Evoked by Angiotensins II and HI in the Rat Adrenal Medulla. *Archives of Physiology and Biochemistry* **103,** 55–58 (1995).
253. Vatta, M. S., Rodríguez-Fermepín, M., Durante, G., Bianciotti, L. G. & Fernández, B. E. Atrial natriuretic factor inhibits norepinephrine biosynthesis and turnover in the rat hypothalamus. *Regulatory Peptides* **85,** 101–107 (1999).
254. Rose, R. A., Anand-Srivastava, M. B., Giles, W. R. & Bains, J. S. C-type Natriuretic Peptide Inhibits L-type Ca2+ Current in Rat Magnocellular Neurosecretory Cells by Activating the NPR-C Receptor. *Journal of Neurophysiology* **94,** 612–621 (2005).
255. Yamamoto, S. *et al.* C-Type natriuretic peptide suppresses arginine-vasopressin secretion from dissociated magnocellular neurons in newborn rat supraoptic nucleus. *Neuroscience Letters* **229,** 97–100 (1997).
256. Richard, D. & Bourque, C. W. Atrial Natriuretic Peptide Modulates Synaptic Transmission from Osmoreceptor Afferents to the Supraoptic Nucleus. *J. Neurosci.* **16,** 7526–7532 (1996).
257. Tian, M. & Yang, X.-L. C-type natriuretic peptide modulates glutamate receptors on cultured rat retinal amacrine cells. *Neuroscience* **139,** 1211–1220 (2006).
258. Hu, F., Ren, J., Zhang, J., Zhong, W. & Luo, M. Natriuretic peptides block synaptic transmission by activating phosphodiesterase 2A and reducing presynaptic PKA activity. *PNAS* **109,** 17681–17686 (2012).
259. Forloni, G., Lucca, E., Angeretti, N., Chiesa, R. & Vezzani, A. Neuroprotective Effect of Somatostatin on Nonapoptotic NMDA-Induced Neuronal Death: Role of Cyclic GMP. *Journal of Neurochemistry* **68,** 319–327 (1997).
260. Moro, M. A., Fernández-Tomé, P., Leza, J. C., Lorenzo, P. & Lizasoain, I. Neuronal death induced by SIN-1 in the presence of superoxide dismutase: protection by cyclic GMP. *Neuropharmacology* **37,** 1071–1079 (1998).
261. Kawahara, N., Ruetzler, C. A. & Klatzo, I. Protective effect of spreading depression against neuronal damage following cardiac arrest cerebral ischaemia. *Neurol. Res.* **17,** 9–16 (1995).
262. Matsushima, K., Hogan, M. J. & Hakim, A. M. Cortical Spreading Depression Protects Against Subsequent Focal Cerebral Ischemia in Rats. *J Cereb Blood Flow Metab* **16,** 221–226 (1996).
263. Wiggins, A. K., Shen, P.-J. & Gundlach, A. L. Atrial natriuretic peptide expression is increased in rat cerebral cortex following spreading depression: possible contribution to sd-induced neuroprotection. *Neuroscience* **118,** 715–726 (2003).
264. Kuribayashi, K. *et al.* Neuroprotective effect of atrial natriuretic peptide against NMDA-induced neurotoxicity in the rat retina. *Brain Research* **1071,** 34–41 (2006).
265. Lang, C. C. & Struthers, A. D. Interactions between atrial natriuretic factor and the autonomic nervous system. *Clinical Autonomic Research* **1,** 329–336 (1991).

266. Herring, N., Zaman, J. A. B. & Paterson, D. J. Natriuretic peptides like NO facilitate cardiac vagal neurotransmission and bradycardia via a cGMP pathway. *American Journal of Physiology - Heart and Circulatory Physiology* **281,** H2318–H2327 (2001).
267. Atchison, D. J. & Ackermann, U. Influence of atrial natriuretic factor on autonomic control of heart rate. *American Journal of Physiology - Regulatory, Integrative and Comparative Physiology* **258,** R718–R723 (1990).
268. Scott, J. N. & Jennes, L. Localization of 125I-atrial natriuretic peptide (ANP) in the rat fetus. *Anat Embryol* **183,** 245–249 (1991).
269. Zhao, Z. & Ma, L. Regulation of axonal development by natriuretic peptide hormones. *PNAS* **106,** 18016–18021 (2009).
270. Kallenborn-Gerhardt, W. & Schmidtko, A. A Novel Signaling Pathway That Modulates Inflammatory Pain. *J. Neurosci.* **31,** 798–800 (2011).
271. Zhang, F.-X. *et al.* Inhibition of Inflammatory Pain by Activating B-Type Natriuretic Peptide Signal Pathway in Nociceptive Sensory Neurons. *J. Neurosci.* **30,** 10927–10938 (2010).
272. Loo, L. *et al.* The C-type natriuretic peptide induces thermal hyperalgesia through a noncanonical Gβγ-dependent modulation of TRPV1 channel. *J. Neurosci.* **32,** 11942–11955 (2012).
273. Abdelalim, E. M., Osman, A. H. K., Takada, T., Torii, R. & Tooyama, I. Immunohistochemical mapping of natriuretic peptide receptor-A in the brainstem of Macaca fascicularis. *Neuroscience* **145,** 1087–1096 (2007).
274. Abdelalim, E. M. *et al.* Distribution of natriuretic peptide receptor-C immunoreactivity in the rat brainstem and its relationship to cholinergic and catecholaminergic neurons. *Neuroscience* **155,** 192–202 (2008).
275. Abdelalim, E. M., Bellier, J.-P. & Tooyama, I. Expression of NPR-B in neurons of the dorsal root ganglia of the rat. *Peptides* **43,** 56–61 (2013).
276. Nohr, D. D., Weihe, E., Zentel, H. J. & Arendt, R. M. Atrial natriuretic factor-like immunoreactivity in spinal cord and in primary sensory neurons of spinal and trigeminal ganglia of guinea-pig: correlation with tachykinin immunoreactivity*. *Cell Tissue Res.* **258,** 387–392 (1989).
277. Puri, V. *et al.* Ovarian steroids regulate neuropeptides in the trigeminal ganglion. *Neuropeptides* **39,** 409–417 (2005).
278. Waxman, S. G., Cummins, T. R., Dib-Hajj, S., Fjell, J. & Black, J. A. Sodium channels, excitability of primary sensory neurons, and the molecular basis of pain. *Muscle Nerve* **22,** 1177–1187 (1999).
279. Nordin, M., Nyström, B., Wallin, U. & Hagbarth, K.-E. Ectopic sensory discharges and paresthesiae in patients with disorders of peripheral nerves, dorsal roots and dorsal columns. *Pain* **20,** 231–245 (1984).
280. Ochoa, J. L. & Torejök, H. E. Paræsthesiæ from Ectopic Impulse Generation in Human Sensory Nerves. *Brain* **103,** 835–853 (1980).
281. Wall, P. D. & Devor, M. The effect of peripheral nerve injury on dorsal root potentials and on transmission of afferent signals into the spinal cord. *Brain Research* **209,** 95–111 (1981).
282. Jarvis, M. F. The neural-glial purinergic receptor ensemble in chronic pain states. *Trends Neurosci.* **33,** 48–57 (2010).
283. Catacuzzeno, L., Fioretti, B., Pietrobon, D. & Franciolini, F. The differential expression of low-threshold K+ currents generates distinct firing patterns in different subtypes of adult mouse trigeminal ganglion neurones. *The Journal of Physiology* **586,** 5101–5118 (2008).
284. Scroggs, R. S. The distribution of low-threshold TTX-resistant Na+ currents in rat trigeminal ganglion cells. *Neuroscience* **222,** 205–214 (2012).

285. Borgland, S. L., Connor, M. & Christie, M. J. Nociceptin inhibits calcium channel currents in a subpopulation of small nociceptive trigeminal ganglion neurons in mouse. *J Physiol* **536,** 35–47 (2001).
286. Ikeda, M. & Matsumoto, S. Classification of voltage-dependent Ca2+ channels in trigeminal ganglion neurons from neonatal rats. *Life Sciences* **73,** 1175–1187 (2003).
287. Morikawa, T., Matsuzawa, Y., Makita, K. & Katayama, Y. Antimigraine drug, zolmitriptan, inhibits high-voltage activated calcium currents in a population of acutely dissociated rat trigeminal sensory neurons. *Molecular Pain* **2,** 10 (2006).
288. Viana, F., de la Peña, E. & Belmonte, C. Specificity of cold thermotransduction is determined by differential ionic channel expression. *Nat Neurosci* **5,** 254–260 (2002).
289. Bean, B. P. The action potential in mammalian central neurons. *Nat Rev Neurosci* **8,** 451–465 (2007).
290. Enoka, R. M. *Neuromechanics of Human Movement*. (Human Kinetics, 2008).
291. Silberstein, S. D. Migraine. *Lancet* **363,** 381–391 (2004).
292. Semenov, I. A. Migraine headaches. *Disease-a-Month* **61,** 218–222 (2015).
293. Weatherall, M. W. The diagnosis and treatment of chronic migraine. *Ther Adv Chronic Dis* **6,** 115–123 (2015).
294. Welch, K. M. A. & Goadsby, P. J. Chronic daily headache: nosology and pathophysiology. *Curr. Opin. Neurol.* **15,** 287–295 (2002).
295. Lipton, R. B. *et al.* The Family Impact of Migraine: Population-Based Studies in the USA and UK. *Cephalalgia* **23,** 429–440 (2003).
296. Stovner, L. J., Zwart, J.-A., Hagen, K., Terwindt, G. M. & Pascual, J. Epidemiology of headache in Europe. *Eur. J. Neurol.* **13,** 333–345 (2006).
297. Lipton, R. B. *et al.* Migraine prevalence, disease burden, and the need for preventive therapy. *Neurology* **68,** 343–349 (2007).
298. Bigal, M. E., Lipton, R. B., Cohen, J. & Silberstein, S. D. Epilepsy and migraine. *Epilepsy & Behavior* **4, Supplement 2,** 13–24 (2003).
299. Gupta, S. N., Gupta, V. S. & Borad, N. Spectrum of migraine variants and beyond: The individual syndromes in children. *Brain Dev.* (2015). doi:10.1016/j.braindev.2015.05.009
300. Silberstein, S. D. & Young, W. B. Migraine aura and prodrome. *Semin Neurol* **15,** 175–182 (1995).
301. Blau, J. N. Migraine prodromes separated from the aura: complete migraine. *Br Med J* **281,** 658–660 (1980).
302. Kaniecki, R. G. Basilar-type migraine. *Curr Pain Headache Rep* **13,** 217–220 (2009).
303. Gasparini, C. F., Sutherland, H. G. & Griffiths, L. R. Studies on the Pathophysiology and Genetic Basis of Migraine. *Curr Genomics* **14,** 300–315 (2013).
304. Tajti, J. *et al.* Migraine is a neuronal disease. *J Neural Transm* **118,** 511–524 (2010).
305. Dalkara, T., Zervas, N. T. & Moskowitz, M. A. From spreading depression to the trigeminovascular system. *Neurol Sci* **27,** s86–s90 (2006).
306. Eadie, M. J. The pathogenesis of migraine – 17th to early 20th Century understandings. *Journal of Clinical Neuroscience* **12,** 383–388 (2005).
307. Wolff, H. G., Tunis, M. M. & Goodell, H. Studies on headache; evidence of damage and changes in pain sensitivity in subjects with vascular headaches of the migraine type. *AMA Arch Intern Med* **92,** 478–484 (1953).
308. Baron, E. P. & Tepper, S. J. Revisiting the Role of Ergots in the Treatment of Migraine and Headache. *Headache: The Journal of Head and Face Pain* **50,** 1353–1361 (2010).
309. Humphrey, P. P. A. The Discovery and Development of the Triptans, a Major Therapeutic Breakthrough. *Headache: The Journal of Head and Face Pain* **48,** 685–687 (2008).

310. Spierings, E. L. H. Migraine: migraine headache pathogenesis in historical perspective. *Rev Neurol Dis* **6,** E77–80 (2009).
311. Moskowitz, M. A. & Macfarlane, R. Neurovascular and molecular mechanisms in migraine headaches. *Cerebrovasc Brain Metab Rev* **5,** 159–177 (1993).
312. Zwetsloot, C. P., Caekebeke, J. F., Odink, J. & Ferrari, M. D. Vascular reactivity during migraine attacks: a transcranial Doppler study. *Headache* **31,** 593–595 (1991).
313. Amin, F. M. *et al.* Magnetic resonance angiography of intracranial and extracranial arteries in patients with spontaneous migraine without aura: a cross-sectional study. *The Lancet Neurology* **12,** 454–461 (2013).
314. Edvinsson, L., Villalón, C. M. & MaassenVanDenBrink, A. Basic mechanisms of migraine and its acute treatment. *Pharmacology & Therapeutics* **136,** 319–333 (2012).
315. PENFIELD W & McNAUGHTON F. DUral headache and innervation of the dura mater. *Arch NeurPsych* **44,** 43–75 (1940).
316. RAY BS & WOLFF HG. Experimental studies on headache: Pain-sensitive structures of the head and their significance in headache. *Arch Surg* **41,** 813–856 (1940).
317. Andres, K. H., Düring, M. von, Muszynski, K. & Schmidt, R. F. Nerve fibres and their terminals of the dura mater encephali of the rat. *Anat Embryol* **175,** 289–301 (1987).
318. Keller, J. T., Saunders, M. C., Beduk, A. & Jollis, J. G. Innervation of the posterior fossa dura of the cat. *Brain Research Bulletin* **14,** 97–102 (1985).
319. Mayberg, M., Langer, R. S., Zervas, N. T. & Moskowitz, M. A. Perivascular meningeal projections from cat trigeminal ganglia: possible pathway for vascular headaches in man. *Science* **213,** 228–230 (1981).
320. Parsons, A. A. & Strijbos, P. J. The neuronal versus vascular hypothesis of migraine and cortical spreading depression. *Current Opinion in Pharmacology* **3,** 73–77 (2003).
321. May, A. & Goadsby, P. J. The Trigeminovascular System in Humans: Pathophysiologic Implications for Primary Headache Syndromes of the Neural Influences on the Cerebral Circulation. *J Cereb Blood Flow Metab* **19,** 115–127 (1999).
322. Messlinger, K., Fischer, M. J. M. & Lennerz, J. K. Neuropeptide Effects in the Trigeminal System: Pathophysiology and Clinical Relevance in Migraine. *The Keio Journal of Medicine* **60,** 82–89 (2011).
323. Akerman, S., Holland, P. R. & Goadsby, P. J. Diencephalic and brainstem mechanisms in migraine. *Nat Rev Neurosci* **12,** 570–584 (2011).
324. Noseda, R. & Burstein, R. Migraine pathophysiology: anatomy of the trigeminovascular pathway and associated neurological symptoms, CSD, sensitization and modulation of pain. *Pain* **154 Suppl 1,** (2013).
325. Goadsby, P. J., Charbit, A. R., Andreou, A. P., Akerman, S. & Holland, P. R. Neurobiology of migraine. *Neuroscience* **161,** 327–341 (2009).
326. Udayasankar Arulmani, MaassenVanDenBrink, A., Villalón, C. M. & Saxena, P. R. Calcitonin gene-related peptide and its role in migraine pathophysiology. *European Journal of Pharmacology* **500,** 315–330 (2004).
327. Holzer, P. Local effector functions of capsaicin-sensitive sensory nerve endings: involvement of tachykinins, calcitonin gene-related peptide and other neuropeptides. *Neuroscience* **24,** 739–768 (1988).
328. Keller, J. T. & Marfurt, C. F. Peptidergic and serotoninergic innervation of the rat dura mater. *J. Comp. Neurol.* **309,** 515–534 (1991).
329. Moskowitz, M. A. Molecular Mechanism of Migraine. *Rinsho Shinkeigaku* **48,** 798–798 (2008).

330. Uddman, R., Edvinsson, L., Ekman, R., Kingman, T. & McCulloch, J. Innervation of the feline cerebral vasculature by nerve fibers containing calcitonin gene-related peptide: trigeminal origin and co-existence with substance P. *Neurosci. Lett.* **62,** 131–136 (1985).
331. Ferrari, M. D., Klever, R. R., Terwindt, G. M., Ayata, C. & van den Maagdenberg, A. M. J. M. Migraine pathophysiology: lessons from mouse models and human genetics. *Lancet Neurol* **14,** 65–80 (2015).
332. Leo, A. A. P. Pial Circulation and Spreading Depression of Activity in the Cerebral Cortex. *Journal of Neurophysiology* **7,** 391–396 (1944).
333. Teive, H. a. G., Kowacs, P. A., Maranhão Filho, P., Piovesan, E. J. & Werneck, L. C. Leao's cortical spreading depression: from experimental 'artifact' to physiological principle. *Neurology* **65,** 1455–1459 (2005).
334. Eikermann-Haerter, K. & Moskowitz, M. A. Animal models of migraine headache and aura. *Curr. Opin. Neurol.* **21,** 294–300 (2008).
335. Moskowitz, M. A. Genes, proteases, cortical spreading depression and migraine: impact on pathophysiology and treatment. *Funct. Neurol.* **22,** 133–136 (2007).
336. Ayata, C. Cortical Spreading Depression Triggers Migraine Attack: Pro. *Headache: The Journal of Head and Face Pain* **50,** 725–730 (2010).
337. Lauritzen, M. Pathophysiology of the migraine aura. *Brain* **117,** 199–210 (1994).
338. Olesen, J. *et al.* Timing and topography of cerebral blood flow, aura, and headache during migraine attacks. *Ann. Neurol.* **28,** 791–798 (1990).
339. Charles, A. Does Cortical Spreading Depression Initiate a Migraine Attack? Maybe Not . . . *Headache: The Journal of Head and Face Pain* **50,** 731–733 (2010).
340. Bolay, H. *et al.* Intrinsic brain activity triggers trigeminal meningeal afferents in a migraine model. *Nat Med* **8,** 136–142 (2002).
341. Zhang, X. *et al.* Activation of meningeal nociceptors by cortical spreading depression: implications to migraine with aura. *J Neurosci* **30,** 8807–8814 (2010).
342. Zhang, X. *et al.* Activation of central trigeminovascular neurons by cortical spreading depression. *Ann Neurol* **69,** 855–865 (2011).
343. Karatas, H. *et al.* Spreading Depression Triggers Headache by Activating Neuronal Panx1 Channels. *Science* **339,** 1092–1095 (2013).
344. Brinley, F. J., Kandel, E. R. & Marshall, W. H. Potassium outflux from rabbit cortex during spreading depression. *J. Neurophysiol.* **23,** 246–256 (1960).
345. James, M. F., Smith, J. M., Boniface, S. J., Huang, C. L. & Leslie, R. A. Cortical spreading depression and migraine: new insights from imaging? *Trends Neurosci.* **24,** 266–271 (2001).
346. Rapoport, S. I. & Marshall, W. H. MEASUREMENT OF CORTICAL PH IN SPREADING CORTICAL DEPRESSION. *Am. J. Physiol.* **206,** 1177–1180 (1964).
347. Andrew, D. & Greenspan, J. D. Mechanical and heat sensitization of cutaneous nociceptors after peripheral inflammation in the rat. *J. Neurophysiol.* **82,** 2649–2656 (1999).
348. Fabbretti, E. ATP P2X3 receptors and neuronal sensitization. *Front Cell Neurosci* **7,** 236 (2013).
349. Levy, D. & Strassman, A. M. Mechanical response properties of A and C primary afferent neurons innervating the rat intracranial dura. *J. Neurophysiol.* **88,** 3021–3031 (2002).
350. Strassman, A. M., Raymond, S. A. & Burstein, R. Sensitization of meningeal sensory neurons and the origin of headaches. *Nature* **384,** 560–564 (1996).
351. Davis, K. D., Meyer, R. A. & Campbell, J. N. Chemosensitivity and sensitization of nociceptive afferents that innervate the hairy skin of monkey. *Journal of Neurophysiology* **69,** 1071–1081 (1993).

352. Martin, H. A., Basbaum, A. I., Kwiat, G. C., Goetzl, E. J. & Levine, J. D. Leukotriene and prostaglandin sensitization of cutaneous high-threshold C- and A-delta mechanonociceptors in the hairy skin of rat hindlimbs. *Neuroscience* **22,** 651–659 (1987).
353. Schaible, H. G. & Schmidt, R. F. Excitation and sensitization of fine articular afferents from cat's knee joint by prostaglandin E2. *The Journal of Physiology* **403,** 91–104 (1988).
354. Waelkens, J. Warning Symptoms in Migraine: Characteristics and Therapeutic Implications. *Cephalalgia* **5,** 223–228 (1985).
355. Cooper, B., Ahlquist, M., Friedman, R. M. & Labanc, J. Properties of high-threshold mechanoreceptors in the goat oral mucosa. II. Dynamic and static reactivity in carrageenan-inflamed mucosa. *Journal of Neurophysiology* **66,** 1280–1290 (1991).
356. Halata, Z., Cooper, B. Y., Baumann, K. I., Schwegmann, C. & Friedman, R. M. Sensory nerve endings in the hard palate and papilla incisiva of the goat. *Exp Brain Res* **129,** 218–228 (1999).
357. Su, X. & Gebhart, G. F. Mechanosensitive Pelvic Nerve Afferent Fibers Innervating the Colon of the Rat are Polymodal in Character. *Journal of Neurophysiology* **80,** 2632–2644 (1998).
358. Blau, J. N. & Dexter, S. L. The Site of Pain Origin during Migraine Attacks*. *Cephalalgia* **1,** 143–147 (1981).
359. Rasmussen, B. K., Jensen, R. & Olesen, J. A Population-Based Analysis of the Diagnostic Criteria of the International Headache Society. *Cephalalgia* **11,** 129–134 (1991).
360. Bardoni, R., Goldstein, P. A., Lee, C. J., Gu, J. G. & MacDermott, A. B. ATP P2X receptors mediate fast synaptic transmission in the dorsal horn of the rat spinal cord. *J. Neurosci.* **17,** 5297–5304 (1997).
361. Steen, K. H., Reeh, P. W., Anton, F. & Handwerker, H. O. Protons selectively induce lasting excitation and sensitization to mechanical stimulation of nociceptors in rat skin, in vitro. *J. Neurosci.* **12,** 86–95 (1992).
362. Obreja, O., Schmelz, M., Poole, S. & Kress, M. Interleukin-6 in combination with its soluble IL-6 receptor sensitises rat skin nociceptors to heat, in vivo. *Pain* **96,** 57–62 (2002).
363. Sachs, D., Cunha, F. Q., Poole, S. & Ferreira, S. H. Tumour necrosis factor-α, interleukin-1β and interleukin-8 induce persistent mechanical nociceptor hypersensitivity. *Pain* **96,** 89–97 (2002).
364. Reuter, U. *et al.* Delayed inflammation in rat meninges: implications for migraine pathophysiology. *Brain* **124,** 2490–2502 (2001).
365. Olesen, J., Thomsen, L. L. & Iversen, H. Nitric oxide is a key molecule in migraine and other vascular headaches. *Trends Pharmacol. Sci.* **15,** 149–153 (1994).
366. Reynier-Rebuffel, A. M. *et al.* Substance P, calcitonin gene-related peptide, and capsaicin release serotonin from cerebrovascular mast cells. *American Journal of Physiology - Regulatory, Integrative and Comparative Physiology* **267,** R1421–R1429 (1994).
367. Suzuki, R. *et al.* Direct Neurite-Mast Cell Communication In Vitro Occurs Via the Neuropeptide Substance P. *J Immunol* **163,** 2410–2415 (1999).
368. Woolf, C. J. & Salter, M. W. Neuronal Plasticity: Increasing the Gain in Pain. *Science* **288,** 1765–1768 (2000).
369. A. Ellis & D. L. H. Bennett. Neuroinflammation and the generation of neuropathic pain. *Br J Anaesth* **111,** 26–37 (2013).
370. Pozo, M. A., Gallego, R., Gallar, J. & Belmonte, C. Blockade by calcium antagonists of chemical excitation and sensitization of polymodal nociceptors in the cat's cornea. *The Journal of Physiology* **450,** 179–189 (1992).

371. Burstein, R., Jakubowski, M. & Rauch, S. D. The science of migraine. *J Vestib Res* **21,** 305–314 (2011).
372. Woolf, C. J. Evidence for a central component of post-injury pain hypersensitivity. *Nature* **306,** 686–688 (1983).
373. Hu, J. W., Sessle, B. J., Raboisson, P., Dallel, R. & Woda, A. Stimulation of craniofacial muscle afferents induces prolonged facilitatory effects in trigeminal nociceptive brain-stem neurones: *Pain* **48,** 53–60 (1992).
374. Koltzenburg, M., Torebjörk, H. E. & Wahren, L. K. Nociceptor modulated central sensitization causes mechanical hyperalgesia in acute chemogenic and chronic neuropathic pain. *Brain* **117,** 579–591 (1994).
375. Magerl, W., Wilk, S. H. & Treede, R.-D. Secondary hyperalgesia and perceptual wind-up following intradermal injection of capsaicin in humans. *Pain* **74,** 257–268 (1998).
376. Ren, K. & Dubner, R. NMDA receptor antagonists attenuate mechanical hyperalgesia in rats with unilateral inflammation of the hindpaw. *Neuroscience Letters* **163,** 22–26 (1993).
377. Simone, D. A. *et al.* Neurogenic hyperalgesia: central neural correlates in responses of spinothalamic tract neurons. *Journal of Neurophysiology* **66,** 228–246 (1991).
378. Torebjörk, H. E., Lundberg, L. E. & LaMotte, R. H. Central changes in processing of mechanoreceptive input in capsaicin-induced secondary hyperalgesia in humans. *J Physiol* **448,** 765–780 (1992).
379. Burstein, R., Cutrer, M. F. & Yarnitsky, D. The development of cutaneous allodynia during a migraine attack Clinical evidence for the sequential recruitment of spinal and supraspinal nociceptive neurons in migraine. *Brain* **123,** 1703–1709 (2000).
380. Drummond, P. D. Scalp tenderness and sensitivity to pain in migraine and tension headache. *Headache* **27,** 45–50 (1987).
381. Göbel, H., Ernst, M., Jeschke, J., Keil, R. & Weigle, L. Acetylsalicylic acid activates antinociceptive brain-stem reflex activity in headache patients and in healthy subjects. *Pain* **48,** 187–195 (1992).
382. Jensen, K., Tuxen, C. & Olesen, J. Pericranial muscle tenderness and pressure-pain threshold in the temporal region during common migraine. *Pain* **35,** 65–70 (1988).
383. Levy, D., Jakubowski, M. & Burstein, R. Disruption of communication between peripheral and central trigeminovascular neurons mediates the antimigraine action of 5HT1B/1D receptor agonists. *PNAS* **101,** 4274–4279 (2004).
384. Burstein, R. Deconstructing migraine headache into peripheral and central sensitization. *Pain* **89,** 107–110 (2001).
385. Burstein, R., Yamamura, H., Malick, A. & Strassman, A. M. Chemical stimulation of the intracranial dura induces enhanced responses to facial stimulation in brain stem trigeminal neurons. *J. Neurophysiol.* **79,** 964–982 (1998).
386. Pietrobon, D. & Striessnig, J. Neurobiology of migraine. *Nat. Rev. Neurosci.* **4,** 386–398 (2003).
387. Ophoff, R. A. *et al.* Familial hemiplegic migraine and episodic ataxia type-2 are caused by mutations in the Ca2+ channel gene CACNL1A4. *Cell* **87,** 543–552 (1996).
388. Ophoff, R. A., Terwindt, G. M., Frants, R. R. & Ferrari, M. D. P/Q-type Ca2+ channel defects in migraine, ataxia and epilepsy. *Trends in Pharmacological Sciences* **19,** 121–127 (1998).
389. Pietrobon, D. Calcium channels and migraine. *Biochimica et Biophysica Acta (BBA) - Biomembranes* **1828,** 1655–1665 (2013).
390. Lafrenière, R. G. & Rouleau, G. A. Migraine: Role of the TRESK two-pore potassium channel. *Int. J. Biochem. Cell Biol.* **43,** 1533–1536 (2011).

391. Lafrenière, R. G. *et al.* A dominant-negative mutation in the TRESK potassium channel is linked to familial migraine with aura. *Nat. Med.* **16,** 1157–1160 (2010).
392. Lingueglia, E. Acid-sensing Ion Channels in Sensory Perception. *J. Biol. Chem.* **282,** 17325–17329 (2007).
393. Wemmie, J. A., Price, M. P. & Welsh, M. J. Acid-sensing ion channels: advances, questions and therapeutic opportunities. *Trends in Neurosciences* **29,** 578–586 (2006).
394. Baron, A., Voilley, N., Lazdunski, M. & Lingueglia, E. Acid Sensing Ion Channels in Dorsal Spinal Cord Neurons. *J. Neurosci.* **28,** 1498–1508 (2008).
395. Wu, L.-J. *et al.* Characterization of Acid-sensing Ion Channels in Dorsal Horn Neurons of Rat Spinal Cord. *J. Biol. Chem.* **279,** 43716–43724 (2004).
396. Mamet, J., Baron, A., Lazdunski, M. & Voilley, N. ProInflammatory Mediators, Stimulators of Sensory Neuron Excitability via the Expression of Acid-Sensing Ion Channels. *J. Neurosci.* **22,** 10662–10670 (2002).
397. Durham, P. L. & Masterson, C. G. Two Mechanisms Involved in Trigeminal CGRP Release: Implications for Migraine Treatment. *Headache: The Journal of Head and Face Pain* **53,** 67–80 (2013).
398. Yan, J., Wei, X., Bischoff, C., Edelmayer, R. M. & Dussor, G. pH-Evoked Dural Afferent Signaling Is Mediated by ASIC3 and Is Sensitized by Mast Cell Mediators. *Headache: The Journal of Head and Face Pain* **53,** 1250–1261 (2013).
399. Holland, P. R. *et al.* Acid-sensing ion channel 1: A novel therapeutic target for migraine with aura. *Ann Neurol.* **72,** 559–563 (2012).
400. Ramsey, I. S., Delling, M. & Clapham, D. E. An Introduction to Trp Channels. *Annual Review of Physiology* **68,** 619–647 (2006).
401. Jordt, S.-E. *et al.* Mustard oils and cannabinoids excite sensory nerve fibres through the TRP channel ANKTM1. *Nature* **427,** 260–265 (2004).
402. Edelmayer, R. M. *et al.* Activation of TRPA1 on dural afferents: A potential mechanism of headache pain. *PAIN®* **153,** 1949–1958 (2012).
403. Basbaum, A. I., Bautista, D. M., Scherrer, G. & Julius, D. Cellular and Molecular Mechanisms of Pain. *Cell* **139,** 267–284 (2009).
404. Nassini, R. *et al.* The 'headache tree' via umbellulone and TRPA1 activates the trigeminovascular system. *Brain* **135,** 376–390 (2012).
405. Irlbacher, K. & Meyer, B.-U. Nasally triggered headache. *Neurology* **58,** 294–294 (2002).
406. Kelman, L. The triggers or precipitants of the acute migraine attack. *Cephalalgia* **27,** 394–402 (2007).
407. Chasman, D. I. *et al.* Genome-wide association study reveals three susceptibility loci for common migraine in the general population. *Nat Genet* **43,** 695–698 (2011).
408. Freilinger, T. *et al.* Genome-wide association analysis identifies susceptibility loci for migraine without aura. *Nat Genet* **44,** 777–782 (2012).
409. Ghosh, J., Pradhan, S. & Mittal, B. Genome-Wide-Associated Variants in Migraine Susceptibility: A Replication Study From North India. *Headache: The Journal of Head and Face Pain* **53,** 1583–1594 (2013).
410. Gribkoff, V. K., Starrett, J. E. & Dworetzky, S. I. Maxi-K Potassium Channels: Form, Function, and Modulation of a Class of Endogenous Regulators of Intracellular Calcium. *Neuroscientist* **7,** 166–177 (2001).
411. Robitaille, R. & Charlton, M. P. Presynaptic calcium signals and transmitter release are modulated by calcium-activated potassium channels. *J. Neurosci.* **12,** 297–305 (1992).

412. Akerman, S., Holland, P. R., Lasalandra, M. P. & Goadsby, P. J. Inhibition of trigeminovascular dural nociceptive afferents by Ca2+-activated K+ (MaxiK/BKCa) channel opening. *PAIN* **151,** 128–136 (2010).
413. Lu, R. *et al.* BKCa channels expressed in sensory neurons modulate inflammatory pain in mice. *PAIN®* **155,** 556–565 (2014).
414. Anttila, V. *et al.* Genome-wide meta-analysis identifies new susceptibility loci for migraine. *Nat Genet* **45,** 912–917 (2013).
415. Carrera, P., Stenirri, S., Ferrari, M. & Battistini, S. Familial hemiplegic migraine: a ion channel disorder. *Brain Res. Bull.* **56,** 239–241 (2001).
416. Russell, M. B. & Ducros, A. Sporadic and familial hemiplegic migraine: pathophysiological mechanisms, clinical characteristics, diagnosis, and management. *The Lancet Neurology* **10,** 457–470 (2011).
417. Thomsen, L. L. *et al.* A population-based study of familial hemiplegic migraine suggests revised diagnostic criteria. *Brain* **125,** 1379–1391 (2002).
418. Thomsen, L. L. *et al.* The genetic spectrum of a population-based sample of familial hemiplegic migraine. *Brain* **130,** 346–356 (2007).
419. Terwindt, G. M. *et al.* Variable clinical expression of mutations in the P/Q-type calcium channel gene in familial hemiplegic migraine. Dutch Migraine Genetics Research Group. *Neurology* **50,** 1105–1110 (1998).
420. Felix, R. Calcium channelopathies. *Neuromolecular Med.* **8,** 307–318 (2006).
421. Pietrobon, D. CaV2.1 channelopathies. *Pflugers Arch.* **460,** 375–393 (2010).
422. Ducros, A. *et al.* The Clinical Spectrum of Familial Hemiplegic Migraine Associated with Mutations in a Neuronal Calcium Channel. *New England Journal of Medicine* **345,** 17–24 (2001).
423. Westenbroek, R. E. *et al.* Immunochemical identification and subcellular distribution of the alpha 1A subunits of brain calcium channels. *J. Neurosci.* **15,** 6403–6418 (1995).
424. Pietrobon, D. Function and dysfunction of synaptic calcium channels: insights from mouse models. *Current Opinion in Neurobiology* **15,** 257–265 (2005).
425. Pineda, J. C., Waters, R. S. & Foehring, R. C. Specificity in the Interaction of HVA Ca2+ Channel Types With Ca2+-Dependent AHPs and Firing Behavior in Neocortical Pyramidal Neurons. *Journal of Neurophysiology* **79,** 2522–2534 (1998).
426. Womack, M. D., Chevez, C. & Khodakhah, K. Calcium-Activated Potassium Channels Are Selectively Coupled to P/Q-Type Calcium Channels in Cerebellar Purkinje Neurons. *J. Neurosci.* **24,** 8818–8822 (2004).
427. Gao, Z. *et al.* Cerebellar Ataxia by Enhanced CaV2.1 Currents Is Alleviated by Ca2+-Dependent K+-Channel Activators in Cacna1aS218L Mutant Mice. *J. Neurosci.* **32,** 15533–15546 (2012).
428. Inchauspe, C. G. *et al.* Gain of Function in FHM-1 Cav2.1 Knock-In Mice Is Related to the Shape of the Action Potential. *J Neurophysiol* **104,** 291–299 (2010).
429. van den Maagdenberg, A. M. J. M. *et al.* A Cacna1a Knockin Migraine Mouse Model with Increased Susceptibility to Cortical Spreading Depression. *Neuron* **41,** 701–710 (2004).
430. van den Maagdenberg, A. M. J. M. *et al.* High cortical spreading depression susceptibility and migraine-associated symptoms in Ca(v)2.1 S218L mice. *Ann. Neurol.* **67,** 85–98 (2010).
431. Tottene, A. *et al.* Familial hemiplegic migraine mutations increase Ca(2+) influx through single human CaV2.1 channels and decrease maximal CaV2.1 current density in neurons. *Proc. Natl. Acad. Sci. U.S.A.* **99,** 13284–13289 (2002).

432. Guilmi, M. N. D. *et al.* Synaptic Gain-of-Function Effects of Mutant Cav2.1 Channels in a Mouse Model of Familial Hemiplegic Migraine Are Due to Increased Basal [Ca2+]i. *J. Neurosci.* **34,** 7047–7058 (2014).
433. Tottene, A. *et al.* Enhanced Excitatory Transmission at Cortical Synapses as the Basis for Facilitated Spreading Depression in CaV2.1 Knockin Migraine Mice. *Neuron* **61,** 762–773 (2009).
434. Eikermann-Haerter, K. *et al.* Genetic and hormonal factors modulate spreading depression and transient hemiparesis in mouse models of familial hemiplegic migraine type 1. *J Clin Invest* **119,** 99–109 (2009).
435. Fioretti, B. *et al.* Trigeminal ganglion neuron subtype-specific alterations of CaV2.1 calcium current and excitability in a Cacna1a mouse model of migraine. *J Physiol* **589,** 5879–5895 (2011).
436. Ceruti, S. *et al.* Calcitonin Gene-Related Peptide-Mediated Enhancement of Purinergic Neuron/Glia Communication by the Algogenic Factor Bradykinin in Mouse Trigeminal Ganglia from Wild-Type and R192Q Cav2.1 Knock-In Mice: Implications for Basic Mechanisms of Migraine Pain. *J. Neurosci.* **31,** 3638–3649 (2011).
437. Vecchia, D. & Pietrobon, D. Migraine: a disorder of brain excitatory–inhibitory balance? *Trends in Neurosciences* **35,** 507–520 (2012).
438. Villalón, C. M. & Olesen, J. The role of CGRP in the pathophysiology of migraine and efficacy of CGRP receptor antagonists as acute antimigraine drugs. *Pharmacology & Therapeutics* **124,** 309–323 (2009).
439. Franceschini, A. *et al.* Functional crosstalk in culture between macrophages and trigeminal sensory neurons of a mouse genetic model of migraine. *BMC Neurosci* **13,** 143 (2012).
440. Franceschini, A. *et al.* TNFα levels and macrophages expression reflect an inflammatory potential of trigeminal ganglia in a mouse model of familial hemiplegic migraine. *PLoS ONE* **8,** e52394 (2013).
441. Kaja, S. *et al.* Severe and Progressive Neurotransmitter Release Aberrations in Familial Hemiplegic Migraine Type 1 Cacna1a S218L Knock-in Mice. *Journal of Neurophysiology* **104,** 1445–1455 (2010).
442. Chanda, M. L. *et al.* Behavioral evidence for photophobia and stress-related ipsilateral head pain in transgenic Cacna1a mutant mice. *Pain* **154,** 1254–1262 (2013).
443. Burnstock, G. Purinergic signalling: pathophysiology and therapeutic potential. *Keio J Med* **62,** 63–73 (2013).
444. Mickle, A. D., Shepherd, A. J. & Mohapatra, D. P. Sensory TRP channels: the key transducers of nociception and pain. *Prog Mol Biol Transl Sci* **131,** 73–118 (2015).
445. Bonnington, J. K. & McNaughton, P. A. Signalling pathways involved in the sensitisation of mouse nociceptive neurones by nerve growth factor. *J. Physiol. (Lond.)* **551,** 433–446 (2003).
446. Premkumar, L. S. & Abooj, M. TRP channels and analgesia. *Life Sciences* **92,** 415–424 (2013).
447. Hökfelt, T. *et al.* Neuropeptides — an overview. *Neuropharmacology* **39,** 1337–1356 (2000).
448. Ciobanu, C., Reid, G. & Babes, A. Acute and chronic effects of neurotrophic factors BDNF and GDNF on responses mediated by thermo-sensitive TRP channels in cultured rat dorsal root ganglion neurons. *Brain Research* **1284,** 54–67 (2009).
449. Spicarova, D. & Palecek, J. Tumor necrosis factor α sensitizes spinal cord TRPV1 receptors to the endogenous agonist N-oleoyldopamine. *Journal of Neuroinflammation* **7,** 49 (2010).

450. Uzar, E. *et al.* Serum cytokine and pro-brain natriuretic peptide (BNP) levels in patients with migraine. *Eur Rev Med Pharmacol Sci* **15,** 1111–1116 (2011).
451. Vilotti, S., Marchenkova, A., Ntamati, N. & Nistri, A. B-type natriuretic peptide-induced delayed modulation of TRPV1 and P2X3 receptors of mouse trigeminal sensory neurons. *PLoS ONE* **8,** e81138 (2013).